2013-01-24

Percolation Properties of Complex Networks

Bizhani, Golnoosh

UNIVERSITY OF CALGARY

Percolation Properties of Complex Networks

by

Golnoosh Bizhani

A THESIS

SUBMITTED TO THE FACULTY OF GRADUATE STUDIES

IN PARTIAL FULFILLMENT OF THE REQUIREMENTS FOR THE

DEGREE OF DOCTOR OF PHILOSOPHY

DEPARTMENT OF PHYSICS AND ASTRONOMY

CALGARY, ALBERTA

January, 2013

Abstract

This dissertation is devoted to the study of connectivity transitions in complex networks via classical and new percolation models. Networks of high complexity appear across many domains; from commerce, telecommunication, infrastructure, and society, to gene regulation, and even evolution. In many cases these networks exhibit a sudden emergence (or breakdown) of long-range connectivity as a result of local microscopic events; this is of particular importance since their proper functioning often relies crucially on connectivity.

One of the well-developed theories that deals with the formation of connected clusters as a result of random microscopic interactions, is percolation theory. This theory has been frequently applied to the study of epidemics and connectivity in complex networks; however details of most spreading phenomena are more involved, and the minimal assumptions of ordinary percolation are not adequate to describe many of their features. Hence it is necessary to design generalized models of percolation to accommodate more layers of complexity in the study of epidemics and connectivity.

In this thesis we try to develop and explore new models of percolation by relaxing the main two assumptions of ordinary percolation, namely independence and locality of interactions. One of the new models we propose is agglomerative percolation, where we let clusters grow along all their boundary instead of a single site. This modification in most cases leads to a novel type of percolation that is in a different universality class than the ordinary type. We study agglomerative transitions on several graphs to extract their scaling properties and critical exponents. We show that agglomerative percolation maps onto random sequential renormalization, a method we developed to study the renormalization group flow of networks, and argue that contrary to previous claims, at least some of the scaling observed in previous renormalization schemes is due to agglomerative percolation rather than an underlying fractality in the structure of networks. In a new class of percolation models called

explosive percolation, we show that the sharp transitions observed in numerical data is an artifact of the finite system sizes in computer simulations, and these transitions are actually continuous. We also contribute to the ongoing challenges in the study of percolation properties of interdependent networks by developing an analytical framework based on epidemic spreading. Finally, we develop cooperative percolation which can be applied to diverse settings, and show that adding cooperative effects to percolation models can change percolation properties dramatically; thus cooperativity — which is in fact present in many social and physical phenomena — needs to be considered in modeling these systems.

Acknowledgments

Over the past four years I have received support and encouragement from a number of individuals to whom I will remain deeply grateful.

First I would like to sincerely thank Maya Paczuski for supervising me through most of my PhD. Her patience and willingness to teach, combined with her kind support, was a great part of what I needed in my path to becoming a scientist. I truly appreciate the friendly, active and highly collaborative working environment she created in the Complexity Science Group.

Having Peter Grassberger as my co-supervisor was a great honor. His knowledge and experience in almost every topic I came across is awe-inspiring, and his wisdom, modesty and generosity have inspired me endlessly. All of my thesis was written in tight collaboration with Peter, and if it were not for his kind consideration, this dissertation would not have been possible. I cannot thank him enough for all I learned from him in science and life.

My special thanks goes to Jörn Davidsen who has always been ready to provide guidance at difficult times during my PhD. He has been my supervisor for the past months, and the last steps in completing this dissertation were taken with his support and help.

A great part of this dissertation was done in collaboration with Seung-Woo Son and Claire Christensen, who were always there for the scientific discussions. Their mentorship helped me tremendously in getting through the challenges in my project. Seung-Woo's brilliance and energy always propelled me to work harder, and the immense amount of encouragement I received from Claire gave me the confidence to pursue my research to a professional level. My valuable friendship with Ghislain St. Yves, Fernando Girotto, Aicko Schumann, Claire and Seung-Woo is something I would definitely wish to continue. The intimate atmosphere of the Complexity Science Group made my time in Calgary memorable and joyful. My transition to this new environment became much easier with the mentorship of Amer Shreim,

and the support of Elliot Martin. I would like to thank them and the others in the CSG: Jacob and David Foster, Orion Penner, Andrew Berdahl, Nicholas Moloney, Chad Gu, Javad Moradpour, Vishal Sood, Hon Wai Lau, and Arsalan Sattari.

Finally, and most importantly, I would like to thank my family. I am indebted to my parents for their faith in me, and their constant support and help throughout my entire life. It was under their watchful eye that I gained the courage to explore new worlds and the strength to tackle challenges head on. My husband, Ali, has been beside me since we came together. Overcoming the difficulties in the past four years would not have been possible without his thoughtful help, patience in listening, and eagerness to find a solution to every problem. I am incredibly grateful to him for all his care and love.

Table of Contents

Abstract . . . i
Acknowledgments . . . iii
Table of Contents . . . v
List of Figures . . . vii
List of Symbols . . . viii
1 **Introduction** . . . 1
1.1 Complex Systems . . . 1
1.2 Complex Networks . . . 2
1.3 Percolation . . . 4
1.4 New Types of Percolation . . . 6
1.5 Overview . . . 9
2 **Mathematical Background** . . . 10
2.1 Network Theory . . . 10
2.1.1 The Erdös Rényi model of networks . . . 12
2.1.2 The Barabási and Albert model of networks . . . 13
2.2 Percolation Theory . . . 14
2.2.1 Percolation in one dimension . . . 16
2.2.2 Percolation in higher dimensions and on the Bethe lattice . . . 17
2.2.3 Fractality of the percolating cluster . . . 19
2.2.4 Finite size scaling analysis and data collapse . . . 21
2.2.5 Mean-field percolation – Erdös Rényi model of networks . . . 22
2.2.6 Real-space renormalization . . . 22
2.2.7 Epidemics and percolation . . . 24
3 **Random Sequential Renormalization and Agglomerative Percolation** 26
3.1 Claims on Fractality of Complex Networks . . . 27
3.1.1 Small-world property and fractality . . . 27
3.1.2 Renormalization of complex networks . . . 28
3.2 Random sequential renormalization and agglomerative percolation . . . 29
3.2.1 Definition and advantages . . . 31
3.2.2 Results for critical trees . . . 33
3.2.3 Results on Erdös-Rényi and scale-free graphs . . . 34
3.2.4 Results on lattices . . . 36
3.3 Publications . . . 39
3.3.1 Random sequential renormalization of networks: Application to critical trees . . . 40
3.3.2 Random sequential renormalization and agglomerative percolation in networks: Application to Erdös Rényi and scale-free graphs . . . 50
3.3.3 Irreversible aggregation and network renormalization . . . 65
3.3.4 Exact solution for mass-dependent irreversible aggregations . . . 70
3.3.5 Agglomerative percolation in two dimensions . . . 74

4 **Other Complex Percolation Models** 84
4.1 Explosive Percolation 85
4.2 Percolation on Interdependent Networks 86
4.3 Generalized Epidemic Processes and Cooperative Percolation 88
4.4 Percolation in Equilibrium Dynamics: Hamiltonian Graphs 89
4.5 Publications 92
4.5.1 Explosive percolation is actually continuous, but with unusual finite size behavior 93
4.5.2 Percolation Theory on interdependent networks based on epidemic spreading 104
4.5.3 Discontinuous percolation transitions in epidemic processes, surface depinning in random media, and Hamiltonian random graphs 110
5 **Conclusions** 119
5.1 Summary 120
5.2 Applications and Outlook 123
Bibliography 126
A On the Inclusion of Previously Published Works 137

List of Figures and Illustrations

1.1 An example of a network with nodes representing agents and links representing interactions between them in the corresponding complex system. This network has $N = 8$ nodes and $L = 9$ links. 2

1.2 A classical example of percolation: a lattice of conducting wires in an electric circuit. In the left panel the lattice is one globally connected cluster and the circuit is closed. In the right panel, wires are cut randomly and after enough wires are cut, the lattice fragments into several *non-percolating* clusters, thus the circuit becomes open. The *phase transition* between the closed circuit phase and the open circuit phase becomes sharper as the lattice size increases. 5

2.1 The Bethe lattice, or the Cayley tree with coordination number $z = 3$. A Bethe lattice is a tree (contains no loops), and can be generated by a branching process with $z - 1$ offspring. Note that an infinite Bethe lattice is completely homogeneous and isotropic, which means that all nodes in the lattice are the same. 17

3.1 One step of RSR with $b = 1$. The randomly chosen target node absorbs all its nearest neighbors. All links to the absorbed neighborhood are then redirected to the target, and repeated links are deleted. RSR with $b > 1$ can be implemented by applying this procedure on the same target b times. Alternatively RSR can be interpreted as a cluster growth process where the supernode is a cluster that grows by eating its neighboring clusters. 32

List of Symbols, Abbreviations and Nomenclature

Symbol	Definition
AP	agglomerative percolation
BA	Barabási and Albert
EP	explosive percolation
ER	Erdös Rényi
GEP	generalized epidemic processes
RG	renormalization group
RSR	random sequential renormalization
$n(s,p)$	percolation theory, section 2.2.1: the number of clusters of size s divided by the system size, when the occupation probability is p
s_ξ	percolation theory, section 2.2.1: characteristic cluster size defined in Eq. (2.3)
σ	percolation theory, section 2.2.1: critical exponent for the divergence of the characteristic cluster size near criticality
χ	percolation theory, section 2.2.1: the average cluster size to which a randomly chosen site belongs
γ	percolation theory, section 2.2.1: the critical exponent for the divergence of the average cluster size near criticality
P_∞	percolation theory, section 2.2.1: percolation probability: the probability that a randomly chosen site belongs to the percolating cluster
τ	percolation theory, section 2.2.2: the critical exponent for cluster size distribution near criticality
β	percolation theory, section 2.2.2: the critical exponent for the order parameter near criticality

Symbol	Definition
D	percolation theory, section 2.2.3: fractal dimension defined in Eqs. (2.16), and (2.18)
R_s	radius of gyration, defined in section 2.2.3
ξ	percolation theory, section 2.2.3: correlation length
ν	percolation theory, section 2.2.3: correlation length exponent defined in Eq. (2.19)

Chapter 1

Introduction

1.1 Complex Systems

Complexity is ubiquitous; from the unexpected cascade of social uprisings in the Middle East and global economic crisis, to the Cambrian explosion of life diversity and mysteries in evolution; from the Internet and complex infrastructural networks to the human brain and neural systems.

The science of complexity is arguably the most interdisciplinary area of contemporary research with threads in engineering, bio-sciences, sociology, economics, medical sciences, geosciences, computer science, mathematics, and physics. It is this diversity that almost prevents complexity scientists to agree on a unified definition of the field. However, despite this heterogeneity, complex systems share common features which suggests that understanding them in one context might help to proceed in others, demanding collaborations across various areas of study.

What characterizes a complex system is usually the large number of interacting components that exhibit as a whole properties that are not obviously predictable from knowing the individual interactions and components. These emergent properties referred to as "collective behavior" in social sciences, mostly stem from strong interactions. Existence of memory and the ability of adaptation are also common features in many complex systems. Strong couplings result in cascades of events that sometimes cause catastrophic failures or explosive revolutions. These properties raise unlimited applicational interest in these systems.

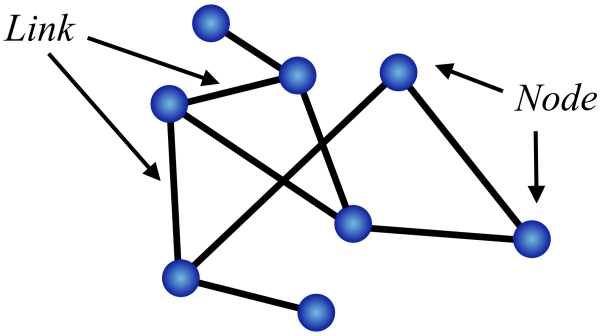

Figure 1.1: An example of a network with nodes representing agents and links representing interactions between them in the corresponding complex system. This network has $N = 8$ nodes and $L = 9$ links.

1.2 Complex Networks

Real-world complex phenomena such as the Internet, social interactions and disease spreading are increasingly being modeled as networks. Providing a simple, yet useful mathematical framework for studying many complex systems, networks capture the most relevant features, namely the agents and the interactions, and discard the details at a certain level. In the simplest picture, the system is mapped to a simple graph (Fig. 1.1) where agents are represented as nodes (or vertices) and the interactions are represented as links (or edges). For example, the Internet is a set of computers (nodes) that are physically connected through cables or optical fibers (links). The World Wide Web is a collection of webpages connected through directional hyper-links, and a social system consists of people with social connections. Similar mapping applies to protein interaction networks, predator-prey networks in food chain, network of financial institutions, et cetera. Usually when a system is reduced to a graph, it spatial structure i.e. the physical locations of its agents, is erased, and only the interactions are kept.

Depending on the system, more features can be added to the graph to make it more realistic. Nodes may have weights associated with them, to show the relative importance of

components. Similarly links can have weights according to the strength of their corresponding interactions [Csermely 09]. Links might be directional as hyperlinks in the World Wide Web are. Networks may be static like a power grid network or evolve dynamically as temporal networks like the network of telephone communications do [Onnela 07, Holme 11]. One could study the structure of the network itself or examine a dynamical process on the network, like epidemics in social networks or data traffic on the Internet. The spatial structure of systems can also be added to the graph representation [Gastner 06].

Complex systems by definition are comprised of various elements with complicated interactions. Networks present a rather simplistic picture of such systems which is not capable of rendering all layers of complexity; yet they can reveal some of the most fundamental properties that many complex systems share. One of these interesting features is *heterogeneity*, which in the language of networks translates into broadness of the distribution of the number of connections (degree) of nodes. Usually complex networks have a few *"hubs"*, nodes with considerably more links than what would be expected from the relatively small link density of the network. In many cases a power-law with an exponential cutoff that accounts for the finite size of the network best fits the extended tail of the degree distribution [Barabási 99][1]. Another important feature is the *small-world* property, which in the context of social systems is known as "six degrees of separation", and states that even in a large society, most people are connected through only a few intermediate nodes. This property is not limited to social networks, and many other systems including metabolic networks, the Internet and the World Wide Web also show small-world properties [Newman 10].

In many real world networks the proper functioning relies crucially on the connectivity of the underlying graph. To give a few examples, damage to a few power stations might result in a global blackout of entire cities or states, as happened in Italy in 2003 [Buldyrev 10b]; failure of submarine cables in Internet bottlenecks can cause continent-wide Internet failure, as damage to Mediterranean cables in 2008 led to a substantial drop in the Internet traffic

[1]This was later challenged for some empirical data by [Clauset 09]

in North Africa and Southwest Asia, with important economic consequences [Desiderio 09]; and an accident on one road might lead to severe traffic jams in the whole network of roads, which is a frequent event in most large cities. However, global connectivity can sometimes be a disadvantage. The main example is the spreading of diseases among humans, or viruses in a computer network, where global connectivity means epidemics, or even pandemics. The study of connectivity in complex networks thus, is crucial in designing, predicting and controlling the corresponding systems.

Our approach to the problem of connectivity is through *percolation theory* which is one of the classical topics in statistical physics, and basically deals with connectivity in graphs, subject to random removal or insertion of either nodes or links. This thesis is devoted to the study of the percolation properties of complex networks via various percolation models.

1.3 Percolation

Percolation theory is the study of the statistical properties of connected clusters formed (annihilated) as a result of random insertion (deletion) of links or nodes in graphs. Most importantly it cares about the largest cluster and whether it is large enough to create macroscopic connectivity in the system. As a simple example, consider a square lattice of conductors in an electric circuit (Fig. 1.2). Now imagine someone starting to cut randomly chosen wires in the lattice. As expected the circuit remains connected for a while, but after enough wires are removed, no connected path through the corners of the lattice survive, and the circuit becomes disconnected. The reverse phenomena happens when water "percolates" through a coffee machine, i.e. a connected stream of water exists through the coffee media. This *phase transition* between the percolating phase and the non-percolating phase becomes sharper as the system size increases. Most of the study of percolation in modern critical phenomena deals with system properties around the percolation threshold, below which there are only small connected patches, and above which a spanning cluster suddenly emerges in the sys-

tem. Interestingly, close to the transition, system properties obey universal features and scaling relations that are independent of the underlying lattice structure and depend only on the dimensionality.

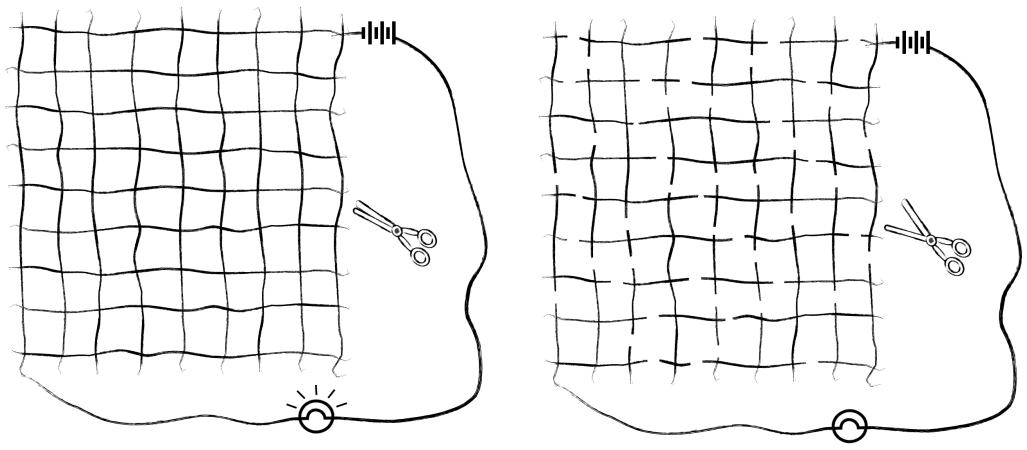

Figure 1.2: A classical example of percolation: a lattice of conducting wires in an electric circuit. In the left panel the lattice is one globally connected cluster and the circuit is closed. In the right panel, wires are cut randomly and after enough wires are cut, the lattice fragments into several *non-percolating* clusters, thus the circuit becomes open. The *phase transition* between the closed circuit phase and the open circuit phase becomes sharper as the lattice size increases.

What has raised a lot of attention to percolation is that it can be adapted to model a variety of systems. Using minimal assumptions it can capture *emergence* which is one of the prominent common features that many complex systems share. Emergence is characterized by simple and *local* interactions leading to large-scale, *global* effects, which are basically the assumptions and outcome of percolation. Some of the famous examples where percolation theory has been successful in modeling are the study of statistical properties of wildfires in forests [Drossel 92, Zinck 10], fluid propagation and interface growth in random media [Barabasi 95], epidemics [Grassberger 83, Cardy 85], and size estimation of oil fields [King 01, King 02]. More recently percolation has been applied to the study of com-

plex contagion on networks [Pastor-Satorras 01, Newman 02], resilience of complex networks with respect to random and targeted removal of nodes [Callaway 00], and cascades of failure in interdependent infrastructural networks [Buldyrev 10b, Vespignani 10].

The latter example is particularly important across various fields, since most of the real-world networks are not isolated but interact at many levels. For example, a cell is an integrated biological system in which the metabolic network interacts with the protein interaction network that affects the network of gene regulation, which in turn controls the production of proteins. The whole cell interacts with vessel and neural networks which are also interdependent. Consideration of the consequences of these interdependencies is particularly important in medicine, diet, and treatment design. Other important examples are the networks of critical infrastructure. Transportation, communication, power grid, and the network of roads are all interdependent on each other. Any malfunction in one of these networks might cause an avalanche of failures in the rest, and finally lead to a global failure of the whole infrastructure [Buldyrev 10b]. Investigating connectivity properties of interdependent networks, is one of the first but fundamental steps in exploring the new challenges brought by interdependencies, and definitely needs further inquiry.

1.4 New Types of Percolation

Ordinary percolation has been successful in capturing the emergence of global connectivity from random interactions in many complex systems. In particular, the study of epidemics on the preexisting structure of networks or lattices is based on percolation and can describe many features in dynamical systems which are embedded on an underlying graph structure. However the details of such processes are usually more intricate, and developing models that can lead to better quantitative explanation of connectivity in complex systems is essential. In the past few years there have been several attempts to generalize percolation to accommodate more layers of complexity in the study of connectivity and robustness.

The classical theory of percolation is based on two fundamental assumptions: events (or interactions) are *local* and *independent*. With such events this theory looks for connected structures across on or off lattice systems consisting of a given number of disconnected elements. The new models of percolation have mostly expanded upon the above concepts.

Some models have looked for the emergence of other substructures where not only the condition of connectivity across the substructure is fulfilled but also additional conditions are imposed to assure the robustness of connectivity. Existence of k-cores — densely connected subgraphs — have been discussed by Goltsev et al. [Goltsev 06] and Baxter et al. [Baxter 11]. These subgraphs were first introduced in the context of social networks [Seidman 83] and later applied to networks of protein interactions [Bader 03]. Another closely related model is the bootstrap percolation with applications in jamming transitions, glassy dynamics and neural activity [Baxter 10]. Others have discussed percolation on systems with different geometries [Bogná 09, Boettcher 09, Boettcher 12], and on growing systems, where the number of elements is dynamically increasing while random connections are being added [Callaway 01].

In most of these alternative percolation models the universal features and scaling laws of classical percolation no longer hold and the transition becomes more abrupt, less predictable and history dependent. Since controlling connectivity transitions is one of the main objectives of percolation studies, detailed study of abruptness and the mechanisms leading to it is notably significant .

Interest in abrupt transitions was initially triggered by attempts to create alternative percolation models with a different motivation. This was in systems where global connectivity is not desirable. Examples are epidemics and systems in which cascading chain of events might lead to breakdown of the whole system. The aim of these alternative percolation models was to suppress the emergence of global connectivity using balanced allocations [Azar 99, D'Souza 07, Achlioptas 09]. In these variants the assumption of locality of interactions has been relaxed, resulting in a delayed, but sharp transition, hence the name

explosive percolation[2].

Another approach in generalizing percolation, which has been given far too little attention in the percolation literature, is to relax the condition of independent interactions. In fact this assumption is one of the main shortcomings of the classical percolation theory in the study of connectivity and epidemics, particularly in social phenomena where "cooperative" effects play an important role in the process of spreading. For example in spreading of a fad, the number of contacts of a given person who are following the spreading fad, highly affects the person's stance towards that fad. In disease spreading sometimes every contact to an infected patient makes the susceptible person weaker (or sometimes stronger in case of partial immunization), and in other words, the infection probability increases (decreases) with the number of previous exposures. Finding methods for incorporating cooperative effects in percolation models, and studying their repercussions in connectivity transitions is essential.

As stated earlier, in most complex systems, the proper performance relies on the global connectivity of the underlying graph. The study of percolation both in its classical and new versions on lattices and on networks (with a more complicated geometry), is pivotal to understanding, prediction, controlling, modeling and design of functional networks.

In this thesis we try to take a step forward in understanding complex phenomena by expanding our knowledge of percolation. We develop agglomerative percolation which naturally applies to the study of aggregation phenomena, we introduce an analytic framework for percolation on interdependent networks based on epidemic processes, we examine some aspects of explosive percolation, and we introduce cooperative percolation and discuss its application in several settings.

[2]Explosive percolation based on local aggregation processes were also suggested as models for graph evolution [D'Souza 10b].

1.5 Overview

This dissertation examines several new percolation models on networks. In chapter 2 we briefly go over basic definitions and methods that are used in network and percolation theories. In chapter 3 we discuss some of the existing challenges in the study of fractality of complex networks, introduce our new method of random sequential renormalization and its connection to a novel type of percolation called agglomerative percolation, and outline our published results which are reprinted in section 3.3 of this thesis. In chapter 4 we discuss some of the other new percolation models including explosive percolation, percolation on interdependent networks, and cooperative percolation, and briefly review our published studies for each model. In chapter 5 we summarize and suggest further avenues that might lead to a better understanding of the structure and function of complex networks using percolation models.

Chapter 2

Mathematical Background

Here we briefly introduce the mathematical formulation for (a) networks and (b) percolation. We give some basic definitions in graph theory and shortly review the methodology and quantities of interest in the study of percolation.

2.1 Network Theory

A *graph* (or network) $\mathcal{G}$ is defined as a set of *nodes* (vertices, sites), $i \in \{1, \dots N\}$ and a set of *links* (edges, bonds), $l_{ij} \in \{1, \dots L\}$, that connect the two nodes i, j (Fig. 1.1). N is the number of nodes and L is the number of links in the network. Usually no spatial structure is assigned to a graph and the position of nodes in any visualization of the network (like the one shown in Fig. 1.1) is arbitrary[1].

A network of size N can be represented by the *adjacency matrix*, $\mathbf{A}$, which is an $N \times N$ matrix with $\mathbf{A}_{ij}$ being one where there is a link between i and j and zero elsewhere. Note that for an undirected network the adjacency matrix is symmetric. Self loops ($A_{ii} = 1$) may be allowed depending on the specific case we study. In a weighted network $\mathbf{A}_{ij}$ is a real number usually in $[0, 1]$. Here we only discuss unweighted undirected networks without self loops. In this case the adjacency matrix is symmetric, with the diagonal elements being zero. Alternatively networks can be represented by their *link list* which is the list of connected pairs of nodes.

In models of epidemics on complex networks usually the "infection" propagates through links, and it is important to know if a *connected path* between two nodes exists. A sequence of nodes $\{i_1, i_2, i_3, ...i_{n-1}, i_n\}$, such that all consecutive pair of nodes are connected by links

[1]For graphs that are embedded in space, additional information about position of nodes is also provided. We do not study such cases here.

$l_{i_1 i_2}, l_{i_2 i_3}, ...l_{i_{n-1} i_n}$ is called a path of length $n-1$ from i_1 to i_n. The length of the shortest path — if it exists at all — is called the *distance* between i and j.

A subset of nodes in a network is called a *connected component* if there is at least one path between every two nodes in the subset, and no links to the rest of the network.

For an undirected and unweighted network the *degree* of a node k_i is the number of links that are connected to it, $k_i = \sum_j \mathbf{A}_{ij}$. The *degree distribution*, p_k, is the relative number of nodes with degree k, which in the limit of large N is the probability distribution function of degrees in the network. As mentioned before the fat tail of the degree distribution of many complex networks can be approximated by a power-law with an exponential cutoff [Barabási 99],

$$p_k = e^{-ck} k^{-\tau} \quad . \tag{2.1}$$

Many network models suggest a pure power-law for the degree distribution in the limit of large network size. One of the main properties of power-law distributions is self affinity, which means scaling the argument by a factor of b, results in the probability distribution to be scaled by a factor of $b^{-\tau}$ [Barabasi 95]. In the continuum limit

$$p(k) = ck^{-\tau}, \quad p(bk) = c(bk)^{-\tau} = b^{-\tau} p(k) \quad . \tag{2.2}$$

The common term "scale-free" networks refers to this feature of the power-law approximation for the degree distribution, and suggests a potential connection between complex networks and the scaling laws associated with phase transitions in critical phenomena. It has inspired models presenting real-world networks as systems in phase transition [Derenyi 04], as well as models seeking fractality in the underlying structure of networks [Song 05, Song 06b, Song 06a, Goh 06, Kim 07c, Kim 07b, Kim 07a, Rozenfeld 10]. We discuss this in more detail in chapter 3.

There has been several attempts to provide models of network formation that can generate ensembles of networks resembling on average some of the properties observed in real-world networks. In the following we introduce two network models that we will use frequently in

this thesis.

2.1.1 The Erdös Rényi model of networks

The Erdös Rényi (ER) model is the simplest random graph model which is generated by a Bernoulli process of link formation among N vertices. It was first studied by Solomonoff and Rapoport [Solomonoff 51] with suggested applications in the study of epidemics, neural nets and mathematical genetics, and later discussed in full detail by Erdös and Rényi [Erdös 60, Erdös 59, Erdös 61]. In an ER ensemble, the connectivity of networks rises rapidly with the number of links added, so that when the link density $L/N \to 1$, the size of the largest connected component reaches 0.8 of the network size. This is particularly important because global connectivity can be interpreted as the maximum expected spread of an epidemics in a network. We discuss the connection between the ER model and percolation (which is related also to epidemics) in section 2.2.5.

There are two methods to generate an ensemble of ER networks. For a set of N nodes, in the first method a fixed number of links, L, connect randomly chosen pairs of nodes. The ensemble of graphs $G(N, L)$ generated this way is a "microcanonical" ensemble. In the second method, any two nodes can be connected with probability p, i.e. every possible link can exist with probability p. In the "canonical" ensemble of graphs $G(N, p)$ generated with the second method, graphs have on average $\bar{L} = pN(N-1)/2$ links. In the large N limit, the distribution of L is Poisson, thus narrow, and the canonical and the microcanonical ensembles are equivalent. For small p the networks are composed of many small disconnected components ($s \ll N$, s being the size of a given component). At larger values of p a giant connected component ($s \sim N$) emerges and expands rapidly, and the system becomes globally connected.

Although the major assumptions of the ER model (links are equally likely and independent) are not realistic for modeling complex networks, it remains the most fundamental and widely studied random graph model. The fact that it is straightforward to perform analyti-

cal calculations on ER graphs makes them the first choice for testing new theories of various network related phenomena.

2.1.2 The Barabási and Albert model of networks

The ER model of networks considers a random and independent process of link formation for networks, and leads to a narrow Poisson degree distribution. This is not the case for many real-world networks with broad degree distributions that can in many cases be estimated by power-laws [Newman 10, Barabási 99].

The model introduced by Barabási and Albert (BA) is an algorithm for generating random scale-free networks using two main mechanisms which are present in the formation of many real networks: growth in size and preferential attachment in connections or "rich gets richer" [Barabási 99]. The model starts with a few nodes that are all linked to each other (a complete graph). Then one new node is added to the network at a time, and becomes connected to a few of the existing nodes, with probability proportional to their degrees. This way over time nodes with higher degrees gain more and more connections, and when the network becomes large enough it develops a power-law degree distribution. The principle of preferential attachment was first studied in the context of economics where Simon showed that such a process in the distribution of benefits can lead to a power-law distribution of wealth [Simon 55]. Later Price applied preferential attachment to suggest a generative model for the network of scientific citations (where scientific papers are nodes and citations are links) [Price 76]. Finally Barabási and Albert suggested their model of network formation in 1999 which became one of the most fundamental generative models of networks [Barabási 99].

2.2 Percolation Theory

As opposed to networks, percolation is mostly defined for lattice systems where position of sites is precisely indicated. In this section we discuss percolation for lattices in different dimensions, and on the Bethe lattice which is infinite dimensional. We also discuss mean-field percolation which is equivalent to the ER model of networks.

Consider a lattice whose sites are occupied randomly and independently with uniform occupation probability p. We are interested in properties of connected clusters, which are groups of nearest neighboring occupied sites, as a function of the occupation probability, or the *control parameter*, p. Quantitatively, usually the size of the largest cluster, average cluster size, number of clusters of a given size, and the probability of existence of a percolating cluster are measured. Since percolation is a stochastic process, and for a given p each realization leads to a different cluster structure, we look for distributions and averages of the quantities of interest. When sites are occupied at random we are talking about *site* percolation. Alternatively one can study *bond* percolation where bonds are turned on at random and clusters of sites that are connected through the "on" bonds are investigated [Stauffer 94, Christensen 05].

In percolation theory we are mostly interested in system behavior in the vicinity of the *phase transition* between the percolating and the non-percolating phases. In the context of thermodynamics when a system goes through a phase transition, the thermodynamic potentials experience sharp changes which, in the thermodynamic limit, correspond to non-analytic behavior. Based on the order of the derivative of the potential which shows discontinuity, phase transitions are categorized into *continuous* or *second order* phase transitions (the potential is continuous but its derivative is not), and *discontinuous* or *first order* phase transitions (the potential itself is not continuous) [Herbut 07]. Usually discontinuous transitions are associated with hysteresis, cooperativity, and latent heat, which are not typically present in continuous transitions. Since phase transitions share various universal features,

a universal language is often used to describe system parameters. The aforementioned potential, or any other quantity that can clearly distinguish the two phases, serves as an *order parameter*. The parameter by tuning which the phase transition can be achieved is called the *control parameter*. For continuous transitions, the non-analytic properties of systems close to transition are referred to as *critical phenomena*, and where the transition takes place in the thermodynamic limit is called a *critical point* [Stanley 71]. Close the critical point, system behavior is usually described by power-laws. The associated exponents are called *critical exponents*, and obey universal scaling relations. Based on their exponents, critical phenomena can be classified into a few universality classes [Herbut 07, Stanley 71, Kardar 07].

Unlike thermodynamical systems, no Hamiltonian governs percolation and no "potential" is assigned to the system. In spite of this fundamental difference, percolation is an example of a continuous phase transition. With a proper choice of an order parameter the non-analytic behavior, divergences, power-laws, critical exponents and universal scaling relations are observed, and the methods and terminology of phase transitions in thermodynamics can be used to discuss percolation transitions.

As an order parameter we are free to choose any quantity that shows a clear difference as percolation happens. Classically, the relative size of the largest cluster is used as an order parameter although other choices are also legitimate [Bizhani 12].

In the following we briefly introduce the quantities of interest for percolation and the exponents associated to their power-law relations, as well as the universal scaling ansatzes and relations. Up to section 2.2.4 the scaling hypotheses are given for infinite systems. In section 2.2.4 we provide corrections to scaling due to finite size effects and introduce the method of finite size scaling analysis to deal with data obtained from finite systems. We start with percolation in one dimension, and expand our discussion by going to higher dimensions and graphs.

2.2.1 Percolation in one dimension

Percolation in one dimension shows some of the main features of percolation and can be fully studied analytically. Therefore, it serves as a pedagogical example in most percolation textbooks [Stauffer 94, Christensen 05]. We follow the same strategy here. Consider an array of size $L \to \infty$, with occupation probability p. The probability that a site belongs to a consecutive group of occupied sites of size s (or a cluster of mass s) is $s(1-p)p^s(1-p)$, so *the number of s-clusters per site*, $n(s)$, — or the cluster number density — is $(1-p)^2p^s$. For $p < 1$, this function clearly falls off for large s. As p approaches one, the decay in $n(s)$ happens at larger values of s. We can define a *characteristic cluster size*, $s_\xi(p)$, to approximate the size of the largest (non-percolating) cluster

$$n(s,p) = (1-p)^2 p^s = (1-p)^2 \exp(-s/s_\xi) \quad , \tag{2.3}$$

with

$$s_\xi = -\frac{1}{\ln p} \quad . \tag{2.4}$$

As we can see the characteristic size diverges as the system approaches the *critical point*, (i.e. the occupation probability approaches to the critical value $p_c = 1$). In this limit, s_ξ can be written as a power-law

$$\lim_{p \to p_c} s_\xi(p) = (p_c - p)^{-1/\sigma}, \quad \sigma = 1 \quad . \tag{2.5}$$

The exponent σ, is one of the *critical exponents* of the percolation transition. These exponents are *universal* (they are independent of many details), and depend only on gross features such as the dimension in the case of lattices. They obey universal *scaling relations* that are valid for any continuous phase transition [Stauffer 94, Christensen 05].

The *percolation probability*, P_∞, is defined as the probability that a randomly chosen site belongs to the percolating cluster. Since by definition P_∞ is zero below p_c, and non-zero above p_c, it is usually the most natural choice for the *order parameter* in the study of the critical behavior near percolation.

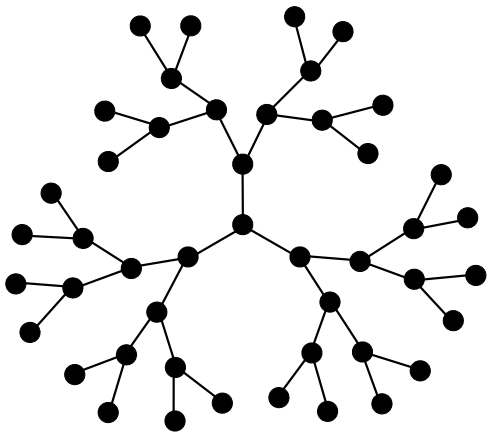

Figure 2.1: The Bethe lattice, or the Cayley tree with coordination number $z = 3$. A Bethe lattice is a tree (contains no loops), and can be generated by a branching process with $z - 1$ offspring. Note that an infinite Bethe lattice is completely homogeneous and isotropic, which means that all nodes in the lattice are the same.

For $p < 1$, the *average cluster size* to which a randomly chosen site belongs, is proportional to the second moment of the cluster mass distribution [2],

$$\chi(p) = \frac{\sum s^2 n(s,p)}{\sum s n(s,p)} \quad . \tag{2.6}$$

In one dimension $\chi(p) = (1+p)/(1-p)$, and in the critical region it obeys a power-law defining the critical exponent γ.

$$\lim_{p \to p_c} \chi(p) = 2(p_c - p)^{-\gamma}, \quad \gamma = 1 \quad . \tag{2.7}$$

Note that the normalization condition for the cluster mass distribution is

$$P_\infty(p) + \sum_{s=1}^{\infty} s n(s,p) = p \tag{2.8}$$

2.2.2 Percolation in higher dimensions and on the Bethe lattice

The above definitions and quantities of interest are used for percolation in higher dimensions and on the Bethe lattice (Cayley tree) as well. A Bethe lattice is a tree (i.e. contains no

[2]The average cluster size, χ, is in correspondence with susceptibility in thermodynamical systems, which diverges at the critical point.

loops) with coordination number z (Fig. 2.1). It can be generated by a branching process with $z-1$ offspring. On a Bethe lattice, with occupation probability, p, a cluster can extend infinitely if each node has in average at least one offspring. Thus the critical occupations probability is $p_c = 1/(z-1)$. It can be shown analytically [Stauffer 94, Christensen 05] that the cluster number density for large s and close to the transition can be written as

$$\begin{aligned} n(s,p) &\propto s^{-\tau}\exp(-s/s_\xi) \qquad \text{for } p \to p_c,\ s \gg 1 \\ s_\xi &\propto |p-p_c|^{-1/\sigma} \qquad \text{for } p \to p_c \quad , \end{aligned} \tag{2.9}$$

with $\tau = 5/2$ and $\sigma = 1/2$. The exponent τ is the third critical exponent of percolation.

To find the percolation probability, P_∞, for $p > p_c$, we use a *consistency condition* for the existence of the percolating cluster, namely the probability that a site belongs to the percolating cluster is equal to the probability that it is occupied and at least one of its neighbors belongs to the percolating cluster, that is

$$P_\infty(p) = p[1 - Q_\infty^z(p)] \quad , \tag{2.10}$$

where $Q_\infty(p)$ is the probability that a site that is connected to a link is not a part of the percolating cluster

$$Q_\infty(p) = (1-p) + pQ_\infty^{z-1}(p) \quad . \tag{2.11}$$

The first term is the probability that the site is not occupied and the second term is the probability that it is occupied, but none of its remaining neighbors belong to the percolating cluster. For $z = 3$, Eqs. (2.10) and (2.11) lead to

$$P_\infty = \begin{cases} 0 & \text{for } p \le p_c \\ p\left[1 - \left(\frac{1-p}{p}\right)^3\right] & \text{for } p > p_c \end{cases} \tag{2.12}$$

The behavior of P_∞ near and above the transition can be obtained by a Taylor expansion of Eq. (2.12)

$$P_\infty(p) \propto (p-p_c)^\beta, \quad \text{for } p > p_c, \quad \text{and } |p-p_c| \to 0 \tag{2.13}$$

with $\beta = 1$. The exponent β is the order parameter exponent and is only defined above the transition. The exponent γ related to the divergence of the average mass near criticality for the Bethe lattice is $\gamma = 1$.

For regular lattices of higher dimensions, the exact functional form of $n(s, p)$ is not known, but numerical evidence suggest that it follows qualitatively similar functional form as the Bethe lattice, but with different exponents.

To obtain a more general form for the cluster number density the following *scaling ansatz* is suggested.

$$n(s, p) = s^{-\tau} f(s/s_\xi) \quad , \tag{2.14}$$

with

$$s_\xi = |p - p_c|^{-1/\sigma}, \quad \text{and} \quad f(0) = const. \neq 0 \quad . \tag{2.15}$$

Analogous ansätze hold for many second order phase transitions. They have not been derived analytically for all systems, but they are consistent with computer simulations and numerical methods. Equation (2.14) basically represents the assumption that there is a single characteristic size, s_ξ, that this size diverges as a power-law when $p \to p_c$, and that $n(s, p)$ is scale-free when $s_\xi \to \infty$.

The precise form of the scaling function, $f(z)$, is to be determined by simulations and other numerical methods in most cases, but the limits for $z \to 0$, and $z \to \infty$ can often be deduced from more general assumptions.

2.2.3 Fractality of the percolating cluster

Critical phenomena are usually tied to the concept of self similarity. As the system approaches its critical point, the correlation length diverges and the systems "looks the same" on all scales. Geometrical self-similarity can be characterized by the fractal dimension. Consider an incipient percolating cluster in an infinite lattice at $p = p_c$. We zoom on a box of size ℓ centered at a site in the cluster. We denote by $M_\infty(p_c, \ell)$, the number of sites in that

box that belong to the incipient percolating cluster. At criticality one finds a power-law relation between $M_\infty(p_c, \ell)$ and the box size

$$M_\infty(p_c, \ell) \propto \ell^D \quad . \tag{2.16}$$

This equation is one of the definitions for the *fractal dimension*, D, of the infinite cluster. Other clusters are finite, but still look fractal on scales smaller than the radius of gyration, R_s. Thus for finite clusters

$$M(s, p_c, \ell) \propto \begin{cases} \ell^D & \text{for } \ell \ll R_s \\ R_s^D & \text{for large } \ell \gg R_s. \end{cases} \tag{2.17}$$

For $p \neq p_c$, we still have the same power-law dependence for typical large clusters. Denoting the characteristic cluster diameter as the correlation length, ξ, we have

$$s_\xi \propto \xi^D \tag{2.18}$$

This, together with Eq. (2.15) leads to

$$\xi \propto |p - p_c|^{-1/D\sigma} \equiv |p - p_c|^{-\nu} \quad . \tag{2.19}$$

The correlation length exponent, ν, is not an independent exponent and is related to D and σ through the *scaling relation*

$$\nu = \frac{1}{D\sigma} \quad . \tag{2.20}$$

Note that the critical exponents are universal, i.e. they only depend on the dimensionality and are independent of the details of the underlying lattice.

The infinite cluster looks fractal for $\ell < \xi$, but has constant density on scales $\ell \gg \xi$. This gives for the part of the mass of the infinite cluster in a box of size $\ell \gg \xi$

$$M_\infty \propto \xi^D (\ell/\xi)^d \quad , \tag{2.21}$$

with d being the dimension of the space. This can be used to relate the order parameter exponent β to other exponents. The density of the percolating cluster in a box of size ℓ can

be written as

$$P_\infty(p,\ell) = \frac{M_\infty(p,\ell)}{\ell^d} \quad , \tag{2.22}$$

The percolation probability can then be written as

$$P_\infty(p) = \lim_{\ell\to\infty} P_\infty(p,\ell) \quad . \tag{2.23}$$

Combining these and Eqs. (2.13), and (2.19) lead to the so called hyper-scaling relation

$$D - d = -\frac{\beta}{\nu} \quad . \tag{2.24}$$

Note that we have assumed that there exists only a single infinite cluster. This is correct for low dimensions, but breaks down at the upper critical dimension $d = d_c = 6$ [Stauffer 94].

2.2.4 Finite size scaling analysis and data collapse

Our discussion up to this point was based on the assumption that the system size is infinitely large. For systems with finite size, several corrections to the scaling form of Eq.(2.14) must be considered. This is particularly important when the critical behavior and the exponents are to be found with computer simulations. At the phase transition, the correlation length diverges, so all the clusters including the percolating one are bound to a size of L^D instead of ξ^D. So in the vicinity of the phase transition, the ratio L/ξ is a relevant factor to be included in our scaling assumption. We update the scaling ansatz of Eq. (2.14) to

$$n(s,p) = s^{-\tau} f(s/s_\xi, L/\xi) \quad , \tag{2.25}$$

with

$$s_\xi \sim |p - p_c|^{-1/\sigma} \quad \text{and} \quad \xi \sim |p - p_c|^{-\nu}. \tag{2.26}$$

This suggests that in the graph of $n(s,p)$ *vs.* s at p_c, by properly rescaling the axes, graphs obtained from different system sizes will collapse on top of each other. So for finding the critical exponent D from numerical data, one needs to tune D such that the best data collapse is achieved. In this thesis extracting the critical exponents from the computer simulations is mostly done by this method.

2.2.5 Mean-field percolation – Erdös Rényi model of networks

The Erdös Rényi model of networks is the mean-field version of bond percolation, where the lattice structure is completely erased, and no space dimension is attached to sites (nodes). Bonds (links) are then randomly and independently placed between nodes, and the statistics of clusters of connected nodes are studied as a function of p, the probability of each link to exist. Like percolation on lattices p is chosen as the control parameter, and the order parameter is the relative size of the largest cluster, $S_{\max}/N$. At $p = p_c = 1/(N-1)$, a percolating cluster emerges and the network becomes globally connected. Since no length scale is defined for a network, the exponent D should be redefined as

$$s_\xi \sim N^D \quad . \tag{2.27}$$

The scaling ansatz will then change to

$$n(s, p; N) = s^{-\tau} f(s/s_\xi,\ N^D/s_\xi) \quad , \tag{2.28}$$

with

$$s_\xi \sim |p - p_c|^{-1/\sigma} \quad . \tag{2.29}$$

As before, the average cluster size scales as $\chi \sim |p - p_c|^{-\gamma}$, and the percolation probability scales as $P_\infty \sim \frac{S_{\max}}{N} \sim |p - p_c|^\beta$. The exponent ν is defined as $\nu = 1/D\sigma$, and other scaling relations hold between the critical exponents.

2.2.6 Real-space renormalization

At the critical point the correlation length of the system diverges and the system becomes self-similar with no characteristic scale. Self-similarity can be identified with the fixed points of a rescaling transformation that reduces all the length scales of the system, including the correlation length, by a fixed factor. For systems slightly above and slightly below the critical point the correlation length reduces to zero after repeated rescaling steps, but at the critical

point it remains infinite. So the critical point is an unstable fixed point of the rescaling transformation [Amit 05, Zinn-Justin 02].

Renormalization group (RG) is a mathematical tool to probe how a system is observed differently at different scales. Originally it was developed in quantum electrodynamics, and quantum field theory [Bellac 92], and was later applied to critical phenomena and phase transitions in statistical physics [Wilson 71a, Wilson 71b]. In the RG picture, the symmetry (scale invariance) of the system is broken when the control parameter is even slightly off its critical value. The critical exponents represent how the system goes away from its symmetric state as the symmetry breaking parameter is increased (the control parameter goes off its critical value) [Stauffer 94, Christensen 05].

In RG, system properties are probed under successive steps of coarse graining and rescaling. At each step of real-space renormalization, the lattice is regularly tiled with blocks of linear size b. Each block of sites is replaced by a super-site, disregarding the fluctuations inside the block, and all length scales are rescaled by a factor of b to restore the lattice spacing. Critical exponents can then be found by studying how a system close to the critical point moves away from criticality under the RG flow.

While RG techniques are well developed for lattice models, the situation becomes complicated when dealing with networks. The method of coarse graining and rescaling regular lattices with homogeneous geometry is a common sense procedure, but it is not at all trivial for the heterogeneous structure of complex networks. Some methods of renormalization for complex networks were suggested in the past decade, and were used to determine the fractal properties of networks [Song 05, Song 06b, Song 06a]. In the next chapter we discuss these methods and their limitations and difficulties, and introduce our method of random sequential renormalization and its connection to agglomerative percolation.

2.2.7 Epidemics and percolation

One of the main applications of percolation theory is in the study of epidemics. Epidemics can refer to a variety of spreading phenomena. From disease spreading in a social network [Newman 02] or spreading of a computer virus in a network of computers [Balthrop 04], to innovation diffusion, spreading of a rumor [Watts 02] and consensus formation [Shao 09], global spreading can be translated into a percolation transition.

To model epidemics on a graph (lattice or network) using percolation, we start with a seed infected node. The seed attacks (i.e. tries to infect) its immediate neighbors. Each attack can be successful with probability p. Any node in the graph, once infected, makes an attempt to infect its uninfected neighbors, and this way — if p is large enough — the infection spreads throughout the system.

Note that in the original form of bond percolation for a given p the system contains many clusters of different sizes. On the other hand in every run of an epidemic process there is only one cluster whose size depends on p and the specific stochastic process leading to it. An ensemble of several runs of the epidemics process is then statistically equivalent to bond percolation.

For a network, epidemics can be formulated mathematically by writing a consistency equation for the existence of a percolating cluster. Let S be the probability that a node at the end of a random link belongs to the percolating cluster. Then $1 - S$ is the probability that it does not belong to the percolating cluster, which equals to the probability that it does not get the infection from any of its neighbors. If the node has k neighbors, the latter is $(1 - pS)^{k-1}$, and averaging over all nodes gives

$$1 - S = \frac{1}{z} \sum_k \left[k P_k (1 - pS)^{k-1} \right] \quad , \tag{2.30}$$

where P_k is the degree distribution, and z is the average degree of the network. Note that the degree distribution of a node at the end of a randomly chosen link is kP_k/z instead of just P_k. This equation can be solved for S as function of p, and the percolation threshold and

transition properties can be determined by checking for the existence of non trivial solutions for S.

The above model might be the simplest model of epidemics which can be applied to spreading of diseases with short infection period, and immunity (or death) after infection such as measles and mumps. In epidemiology it is equivalent to the SIR (susceptible, infected, recovered or removed) model [Newman 02]. Other models such as the SEIR (susceptible, exposed, infectious, recovered), the MSIR (maternally-derived immunity, susceptible, infected, recovered), the SIS (susceptible, infected susceptible), the SEIS, the MSIS, etc. models are also suggested to match different features of spreading of various diseases. These models help to predict the future course of outbreaks and to find strategies to control an epidemic [Daley 99, Brauer 10].

The application of percolation models in the study of innovation diffusion, opinion dynamics and consensus formation has been discussed in several references including [Watts 02, Shao 09, Dodds 04, Sattari 12]

Chapter 3

Random Sequential Renormalization and Agglomerative Percolation

As mentioned before, one of the fundamental properties of most complex networks is the heterogeneity of connectivity which leads to broad degree distributions usually estimated by power-laws. This "scale-free"-ness of the degree distribution suggests the existence of repeating patterns in the structure of these networks at different scales. Finding these patterns might lead to an understanding of the fundamental mechanisms in the formation and evolution of complex networks that result in the structural and behavioral properties they share. The potential connection between scale-free degree distribution and scale-free-ness and fractality near phase transitions in critical phenomena might give a deeper insight to the origins of emergence and collective behavior in complex systems [Cohen 10]. This idea was the motivation for a number of papers trying to find the fractal properties of the underlying structure of networks using coarse graining and RG methods, as well as papers suggesting evolution mechanisms that would lead to these structures [Song 05, Goh 06, Kim 07c, Rozenfeld 10]. In this chapter we briefly review some of the results of these studies, discuss a sequential renormalization scheme that we developed for complex networks and its connection to a novel type of percolation called agglomerative percolation, and summarize our related publications which are reprinted in section .3.3.

3.1 Claims on Fractality of Complex Networks

3.1.1 Small-world property and fractality

In many naturally occurring networks, any node can be reached from any other node by following a path that passes through only a few links and nodes. This "small-world" property was first revealed by Milgram's experiment in the 60s [Milgram 67] in the context of social networks, and later studied in more detail by Watts and Strogatz [Watts 98]. It states that even in a large society, most people are connected through only a few intermediate nodes. The small-world effect is not limited to social networks. Many other systems including metabolic networks, the Internet and the World Wide Web also show small-world properties [Newman 10]. For many systems (for instance ER networks), the small-world property is expressed mathematically by the logarithmic increase in the average distances in the network, ℓ, with the network size N

$$\ell \sim \log N \quad , \tag{3.1}$$

or equivalently

$$N \sim e^{\ell/\ell_0} \quad . \tag{3.2}$$

Comparing this with the definition of the fractal dimension in (Eq. (2.18)), one can easily deduce that the fractal dimension of small-world networks is infinite. Yet, there have been claims on finding a finite fractal dimension for networks with broad degree distribution using box counting algorithms [Song 05]. There are several methods to measure the fractal dimension of spatially embedded objects. Two of the most popular ones are the cluster growth method and the box covering method [Falconer 03]. In the first method which was used in section 2.2.3, the mass of the nodes belonging to the fractal object in a box of size ℓ, centered at a random point in the fractal object, is measured as a function of the box size. Basically we grow a cluster centered at a point in the object and measure its mass as the linear size of the cluster increases. In the second method, the whole object is covered with

boxes of linear size ℓ, and the fractal dimension is obtained by the scaling relation (if any) between the number of boxes needed to cover the object and the box size

$$N_B \sim \ell^{-D} \quad . \tag{3.3}$$

The object must be covered with the *minimum* number of boxes such that the distance between any two points in a given box is less than ℓ. In most cases, these two methods result in the same fractal dimension. For random networks, if the degree distribution is narrow (i.e. the network is homogeneous), the two methods lead to the same infinite dimension. The reason is that different parts of a homogeneous network "look the same", so if a cluster is grown up to size ℓ, its mass is statistically the same as the mass contained in each box in the box covering method with box size ℓ. However in networks with broad degree distributions, one should be very careful in finding the proper box covering algorithm, to get the tiling with minimum number of boxes. Various methods were introduced by several authors [Song 05, Song 06a, Goh 06, Kim 07c, Kim 07b], and it was argued that they reveal the fractal nature of many real-world networks and their associated self-similarity exponents. Although the conflict between the exponential growth of mass in small-world networks and the power-law growth of fractals was never solved, later works suggested that this fractality stems from self organization in the formation and growth of complex networks [Song 06b], and is related to fractality of the skeleton [Goh 06, Kim 07c], and assortativity of the network [Yook 05].

3.1.2 Renormalization of complex networks

For models on a lattice, fractality and self-similarity are closely related to the notion of renormalization group (RG) and its fixed points. RG analysis is basically the study of invariant properties of systems under coarse graining. During a renormalization process the degrees of freedom of a system are eliminated successively by coarse-graining, and the system parameters are rescaled to compensate for the decimation. The critical point is usually a fixed point of the RG flow, and the scaling behavior of the system close to the RG fixed

point gives the critical exponents, based on which systems are classified into a few universality classes [Christensen 05, Stanley 71, Herbut 07]. A typical real-space renormalization is implemented by covering the embedding lattice with a regular grid of boxes, reducing each box with a "super-site", and rescaling all length scales by the reverse box size. Complex networks however, have no spacial structure, and it is not clear whether the RG technique can be applied to them. Nevertheless a renormalization scheme based on the box covering method used for finding the fractal dimension was proposed [Song 05], where each box is replaced by a super-node. In the renormalized network, (super)nodes are connected if there is at least one link between the nodes contained in them. This method is intended to be a parallel renormalization scheme since at each step the whole network is renormalized, but all realizations proposed in previous literature [Song 05, Song 06a, Goh 06, Kim 07c, Kim 07b] are partially sequential.

Avoiding the small-world/fractal paradox, Radicchi et al. examined the RG flow itself and its fixed points for several network models, without making any claims about fractality [Radicchi 08, Radicchi 09]. Critical exponents were derived and used to suggest universality classes for networks. The scaling behavior of some real-world networks were also studied under this renormalization scheme [Radicchi 09].

In the next section, we discuss in more detail the inherent difficulties with the box covering method and the (quasi)parallel renormalization scheme. We argue that the scaling of the RG flow observed in previous works is actually related to a novel type of percolation called *agglomerative percolation*.

3.2 Random sequential renormalization and agglomerative percolation

There are a number of technical concerns and inherent difficulties with the previous works on the renormalization of networks, which make it difficult to interpret the results, and might

lead to erroneous conclusions about the fractal dimension of the underlying graph.

According to the original idea of Hausdorff [Falconer 03], every element of the partitioning should have an individually optimized size up to some largest distance ℓ, so that the number of elements multiplied by a power of their sizes, is minimized. For homogeneous systems, since the number of points per box (the mass of each box) has small fluctuations, this optimization is not actually needed. But, for small-world networks with broad degree distribution, these fluctuations are considerable and indeed most of boxes end up having only a few nodes.

Even with a fixed box size, the covering has to be optimized with the exact placement of the boxes which is an NP hard problem. Methods of optimization were claimed to overcome this problem [Song 05, Song 06a] but they still depend on the order of which the boxes are placed, and thus they are not completely parallel renormalization schemes but quasi-parallel, in the sense that every step of renormalization is implemented as a sequence of non-commuting local coarse grainings.

Another problem with this renormalization scheme is that at every step, it dramatically decreases the number of nodes in the network, so the RG flow contains only a few points and limited statistics. In particular for small-world networks this is a serious problem as they collapse to one node in a few renormalization steps, even when the network size is large. To avoid this problem Rosenfeld et al. renormalized in every step only parts of the network [Rozenfeld 10], at the cost of adding more parameters and making the results more difficult to interpret.

In this thesis, we introduce a *random sequential renormalization* (RSR) scheme for unweighted and undirected networks using a purely sequential algorithm, where at each step of renormalization one node is selected at random and all nodes within a fixed distance of it are replaced with a supernode [Bizhani 11b]. The supernode has links to every node that had at least one link to an absorbed node. We show that this renormalization scheme is

mapped to an aggregation process called *agglomerative percolation* (AP), which is a new type of percolation we study in this chapter. This method can be applied to any graph including regular lattices and random networks.

Another application of RSR and AP is in the study of irreversible aggregation processes, where a number of particles coalesce to form clusters of larger sizes, a phenomenon observed in several settings including gelation, nucleation, and formation of rain [Zangwill 01].

We apply RSR and AP on several graphs including lattices that are patently non-fractal, and observe scaling properties similar to those observed under the parallel renormalization scheme. Our detailed results show that at least some of the results of [Song 05, Song 06b, Song 06a, Rozenfeld 10, Goh 06, Kim 07c] are due to the AP phase transition rather than an underlying fractal structure.

In the rest of this section, we discuss RSR in more detail, point out its advantages over the previous graph renormalization schemes, and relate it to AP. We briefly discuss the the behavior of several types of graphs under RSR and their AP transitions. Detailed results are published in several papers and are included at the end of this chapter [Bizhani 11b, Bizhani 11a, Son 11a, Son 11b, Christensen 12].

3.2.1 Definition and advantages

In RSR a local coarse-graining process is consecutively applied to a given graph G, and generates a series of graphs G_t, with $t \in \{0, 1, 2, ...T\}$, and strictly decreasing sizes N_t (t is called the time). The initial graphs at $t = 0$ has N_0 nodes and the final graph at $t = T$ has only one node. We also assign masses to the nodes (initially $m_i = 1; \forall\ i \in G_0$).
For a graph G_t with N_t nodes of masses m_i, each step of RSR (see Fig. 3.1) with arbitrary radius b ($b = 1, 2, ...$) is implemented as follows:

- Choose randomly one of the nodes in the graph as the target.

- Define the neighborhood $\mathcal{N}$ around the target to include all nodes within the distance

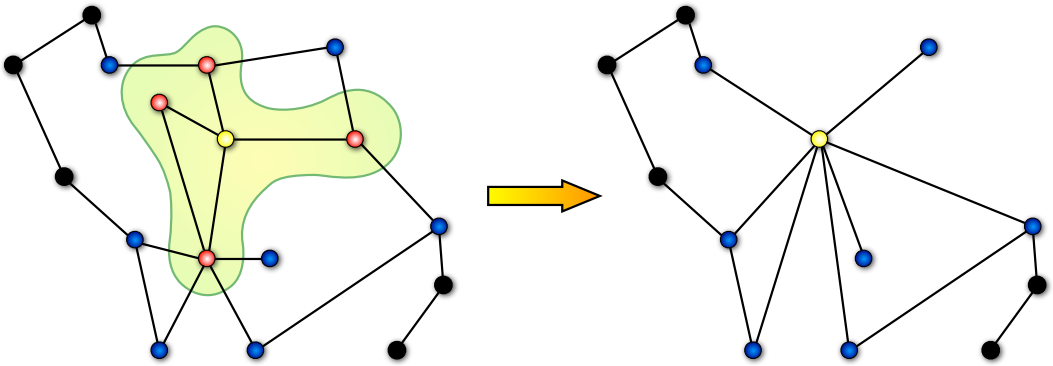

Figure 3.1: One step of RSR with $b = 1$. The randomly chosen target node absorbs all its nearest neighbors. All links to the absorbed neighborhood are then redirected to the target, and repeated links are deleted. RSR with $b > 1$ can be implemented by applying this procedure on the same target b times. Alternatively RSR can be interpreted as a cluster growth process where the supernode is a cluster that grows by eating its neighboring clusters.

$d < b$ from the target.

- Delete all the nodes in $\mathcal{N}$, except for the target.

- Delete all internal links of $\mathcal{N}$.

- Redirect to the target all links that connect any node in $\mathcal{N}$ to the rest of the network.

- If a multiple link appears, replace it by a single link.

- Update the mass of the target to $m = \sum_i m_i$, with $i \in \mathcal{N}$.

Analogous to coarse graining in real-space renormalization, the target node and its neighbors up to distance b are replaced with a supernode, so that all the links to the outside are preserved while the internal details have been discarded.

Alternatively this process can be viewed as a cluster growth process where at each step a random cluster grows by amalgamating to its neighboring clusters. In this mapping initially every node is a cluster of mass one. As time increases clusters of higher mass appear in the

system until a giant percolating cluster emerges. We show that AP is a continuous phase transition, and find its corresponding scaling laws and critical exponents for several graphs.

RSR eliminates the problem of finding an optimum tiling of the network, and is very easy to implement and understand. It avoids the problem of mostly empty boxes. In addition, at each step of RSR the network is decimated only locally and the small effect of each decimation gives a much more detailed statistical picture of the renormalization flow.

Another advantage of RSR is that it can be mapped onto AP, and graph behavior under renormalization can be understood in the view of percolation. Methods and algorithms of percolation can also be applied here. By using the fast Monte Carlo algorithm of Newman and Ziff [Newman 00, Newman 01b] we were able to easily implement RSR on graphs with millions of nodes. In this algorithm initially every node is a root and has a root value of -1. To make a cluster, a node A joins a node B, by being rerooted to B. The root of a cluster is the node with root value of -1 (node B in this case). Every time a cluster joins another one, its root gets rerooted to the first one. The number of nodes that are remained at root value of -1 determines the number of clusters in the graph.

One can define other aggregation rules. For example the target cluster can be chosen with probability proportional to its mass. This is equivalent to picking sites at random and targeting the cluster to which they belong rather than picking a cluster at random. Such *weighted* AP is discussed in [Son 11b] and in [Christensen 12].

3.2.2 Results for critical trees

Here we give a brief summary of our study of RSR on critical trees. The details of our work is published in [Bizhani 11b] and reprinted in section 3.3 of this chapter.

Our critical trees are critical branching processes on a Bethe lattice, where each node can have 0, 1, or 2 offspring with probabilities 1/4, 1/2 and 1/4. The branching process runs until it dies due to fluctuations and thus the size of trees is a stochastic quantity following $p(N) \sim N^{-3/2}$. We take an ensemble of trees with the desired size $N_0(\pm 10\%)$, and discard

the rest. Note that this construction of trees leaves an imprint of the direction of growth on them, so that for a tree of outdegree distribution p_k, the outdegree of the mother of a given node is distributed $\propto kp_k$, and the outdegree of its offspring is $\propto p_k$. This makes these networks different from ER graphs, where the degree distribution of all neighbors of a node is $\propto kp_k$.

As a critical tree of size N_0 evolves under RSR with $b = 1$, it typically experiences three regimes; The first regime extends over $N_0^\nu \lesssim N < N_0$, where N is the size of the tree at a given renormalization step and $\nu = 1/2$. In this regime, the behavior of the tree is described by a mean-field theory which we developed by writing master equations for the evolution of the degree distribution, and by using the generating function methods discussed in [Newman 01a]. When the system size is $N \sim N_0^\nu$, the tree undergoes a continuous AP transition from the mean-field regime to a second regime where it turns into a short fat tree with average radius of $\mathcal{O}(1)$. In the transition region, the degree distribution is approximately a power-law, and quantities like the variance of the degree distribution, the maximum degree in the network, and the ratio of the largest to the second largest degree diverge. We derived the corresponding exponents both by computer simulations and analytically. Our numerical results show that the tree then evolves into a third regime for $N \lesssim N_0^{\nu_{\rm star}}$ where it becomes a pure star, waiting to be reduced to a single node by the renormalization process.

3.2.3 Results on Erdös-Rényi and scale-free graphs

A substantial part of our study on RSR and AP was focused on ER graphs with average degree $\langle k \rangle = 2$ under RSR with $b = 1$. We also studied ER graphs with other link densities as well as scale-free networks and annealed graphs. Detailed results are given in [Bizhani 11a] and reprinted in section 3.3 of this chapter.

In ER graphs with $\langle k \rangle = 2$ under RSR with $b = 1$ we located a continuous AP transition at $x \equiv N/N_0 = c$ with c being a nonzero constant, where both the mass of the largest cluster and the largest degree in the network diverge. In contrast to the critical trees where

the transition was driven to zero, here it happens at a finite value of x, which makes it easier to obtain sufficient statistics from numerical simulations. We examined the degree distribution of nodes (for RSR interpretation), and the mass distribution of clusters (for AP interpretation) and showed that in the vicinity of the phase transition, they both obey power-laws and lead to similar conclusion about the scaling properties and the critical exponents.

In the AP interpretation, we were able to adapt the fast Monte Carlo algorithm of Newman and Ziff for percolation [Newman 00, Newman 01b], to obtain numerical results for networks with millions of nodes on a normal work station. These results were consistent with a scaling ansatz for the mass distribution. Using finite size scaling analysis methods, we extracted the critical exponents, and checked them against the scaling relations of the scaling theory of percolation. Within error, these exponents were the same for all sparse ER graphs regardless of their initial average degree, but different from the exponents of mean-field ordinary percolation.

We also studied in detail the behavior of ER graphs above percolation where a giant hub dominates the behavior of networks. In this regime the size of network shows large fluctuations and leads to an asymmetric relaxation time distribution (relaxation time is the number of RSR steps before the network reduces to a single node). Here again, like critical trees, networks experience a star phase in the latest stage of their evolution under RSR.

We checked a mean-field version of AP by studying an annealed model, were we took the ER graphs studied above and kept their degree sequence, discarding the network structure. At each step of RSR we took a random node (of a random degree k), and merged it with k other nodes which were also chosen randomly, but this time with probabilities proportional to their degrees, k_i. The degree of the resulting supernode was then updated to $(\sum_{i=1}^{k} k_i) - k$, consistent with the renormalization process. We developed a mean-field theory based on generating functions [Newman 01a] for the behavior of the annealed model under RSR. We derived the critical exponents of the phase transition analytically and showed that even at

the mean-field level, AP is in a different universality class than ordinary percolation. These results were consistent with our simulations.

For the scale-free model of Barabasi and Albert (BA) [Barabási 99], we also obtained an AP transition when $x \to 1$, in the thermodynamic limit. Since the transition here happens at the very beginning of the renormalization flow, it is more difficult to perform finite size scaling analysis to obtain the critical exponents. The estimated errors for the exponents were large compared to the ones for ER networks, but it seems that AP for BA graphs belongs to a different universality class.

RSR with $b > 1$ is fundamentally different from RSR with $b = 1$. As mentioned before, RSR with any $b > 1$ can be implemented by applying one step of RSR with $b = 1$ on the same node for b successive times. In RSR the target is chosen at random, so it is more likely that is has a low degree (mass), but there is a high chance that this target is connected to a high degree (mass) node, and as a result, it will be replaced by a supernode of high degree (mass). Choosing the same node as the target again will enhance the decimation and percolation process dramatically. Thus RSR with $b > 1$ is more like a runaway nucleation process, were the rate of growth is proportional to the mass of clusters. For ER graphs under RSR with $b > 1$, we see evidence of a phase transition in the early stages of the renormalization flow, but it is not possible to extract the critical point and the exponents with precision.

3.2.4 Results on lattices

The process of agglomeration of clusters can be viewed as the irreversible aggregation problem, where a group of neighboring particles coalesce to make larger structures. We studied this process on one and two dimensional lattices. Here we review our results that are published in [Son 11a, Son 11b, Christensen 12] and reprinted at the end of this chapter.

In one dimension, RSR with box size b is equivalent to an aggregation process of $(k + 1)X \to X$, where a particle coalesces with k neighbors, and $k = 2b$. In the well-mixed aggregation process with constant kernel [Leyvraz 03], a randomly chosen particle coalesces with

k other randomly chosen particles. This is the mean-field version of the same model. We find the exact solution for the mass distribution of clusters at a given time, using combinatorics where we count the number of possible histories that can lead to a given configuration. The resulting probabilities are represented in a compact way using the Pochhammer k-symbols. Interestingly, the results for the mean-field case is exactly the same as the results for particles on a ring and particles on a loop. In the limit of large system size, the mass distribution of clusters follows power-laws and scaling relations consistent with previous results given in [Krapivski 91].

We applied the same methodology to a *mass dependent* aggregation process (or the sum kernel [Leyvraz 03]), where the target cluster is chosen with probability proportional to its mass. Here as well, we found similar combinatorial exact solutions which are again the same for the probability of any given configuration of particles on a ring, particles on a line and in the well mixed case.

We studied the mass dependent aggregation process on two dimensional lattices as well. In this case the resulting clusters are compact, and the emergence of the incipient giant cluster happens when $N/N_0 \to 1$.

On two dimensional lattices AP exhibits interesting features. On triangular lattices, AP has a finite critical point and exactly the same critical exponents as ordinary bond percolation. On square lattices with helical boundary conditions, we see a completely different behavior. The transitions seems to be driven to zero, and strong logarithmic corrections to scaling are observed. The exponents are very hard to obtain numerically, but we can argue that asymptotically, the Fisher exponent $\tau = 2$, and the fractal dimension of the percolating cluster $D = 2$. The correlation length exponent ν is argued to be infinite. Thus on a square lattice, AP is not in the same universality class as ordinary percolation.

The breakdown of universality in two dimensional lattices was later studied in more detail in [Lau 12]. They showed that this nonuniversal behavior is a result of the bipartite structure

of the square lattice, and leads to a spontaneous symmetry breaking at the percolation threshold. They also examined AP on bipartite graphs of higher dimension and bipartite random networks.

We developed the method of RSR for complex networks as an equivalent to real-space renormalization for lattices, in order to study the behavior of networks under renormalization. We showed that in several graphs including ones that are patently nonfractal, RSR leads to scaling behavior and power-laws that are related to a new type of percolation transition. This suggests that at least some of scaling observed in previous works on network renormalization is due to AP rather than the supposed fractality of the underlying graphs.

RSR and AP have application in the study of growth mechanisms in which a cluster grows by invading its neighboring clusters. Alternative models, where only a fraction of the invaded neighbors agglomerate with the invading cluster, could be more relevant to many real problems. Such models were briefly discussed in [Lau 12], and can also be used to delay the AP transition in networks especially in cases where the transition is pushed to the beginning of the renormalization flow. This is particularly important in the study of RSR and AP on real-world complex networks, and might help us to extract the scaling properties and the critical exponents with more accuracy. It remains an open question whether this method can be useful in identifying universality classes in networks, if they exist.

3.3 Publications

This section includes reprints of the publication mentioned in this chapter. These publications include:

1 – [Bizhani 11b]

Random sequential renormalization of networks: Application to critical trees,

G. Bizhani, V. Sood, M. Paczuski, and P. Grassberger, *Phys. Rev. E*, **83**, 036110 (2011).

2 – [Bizhani 11a]

Random sequential renormalization and agglomerative percolation in networks: Application to Erdös Rényi and scale-free graphs

G. Bizhani, P. Grassberger, and M. Paczuski, *Phys. Rev. E*, **84**, 066111 (2011).

3 – [Son 11a]

Irreversible aggregation and network renormalization

S-W. Son, G. Bizhani, C. Christensen, P. Grassberger, and M. Paczuski, *Euro Phys. Lett.*, **95**, 58007 (2011).

4 – [Son 11b]

Exact solution for mass-dependent irreversible aggregations

S-W. Son, C. Christensen, G. Bizhani, P. Grassberger, and M. Paczuski, *Phys. Rev. E*, **84**, 040102(R) (2011)

5 – [Christensen 12]

Agglomerative percolation in two dimensions

C. Christensen, G. Bizhani, S-W. Son, M. Paczuski, and P. Grassberger, *Euro. Phys. Lett.*, **97**, 16004 (2012)

Random sequential renormalization of networks: Application to critical trees

Golnoosh Bizhani,[1] Vishal Sood,[2] Maya Paczuski,[1] and Peter Grassberger[1,3]
[1]*Complexity Science Group, University of Calgary, Calgary, Canada*
[2]*Niels Bohr Institute, Copenhagen, Denmark*
[3]*NIC, Forschungszentrum Jülich, D-52425 Jülich, Germany*
(Received 20 September 2010; revised manuscript received 11 January 2011; published 22 March 2011)

We introduce the concept of random sequential renormalization (RSR) for arbitrary networks. RSR is a graph renormalization procedure that locally aggregates nodes to produce a coarse grained network. It is analogous to the (quasi)parallel renormalization schemes introduced by C. Song *et al*. [C. Song *et al*., Nature (London) **433**, 392 (2005)] and studied by F. Radicchi *et al*. [F. Radicchi *et al*., Phys. Rev. Lett. **101**, 148701 (2008)], but much simpler and easier to implement. Here we apply RSR to critical trees and derive analytical results consistent with numerical simulations. Critical trees exhibit three regimes in their evolution under RSR. (i) For $N_0^{\nu} \lesssim N < N_0$, where N is the number of nodes at some step in the renormalization and N_0 is the initial size of the tree, RSR is described by a mean-field theory, and fluctuations from one realization to another are small. The exponent $\nu = 1/2$ is derived using random walk and other arguments. The degree distribution becomes broader under successive steps, reaching a power law $p_k \sim 1/k^{\gamma}$ with $\gamma = 2$ and a variance that diverges as $N_0^{1/2}$ at the end of this regime. Both of these latter results are obtained from a scaling theory. (ii) For $N_0^{\nu_{\rm star}} \lesssim N \lesssim N_0^{1/2}$, with $\nu_{\rm star} \approx 1/4$ hubs develop, and fluctuations between different realizations of the RSR are large. Trees are short and fat with an average radius that is $\mathcal{O}(1)$. Crossover functions exhibiting finite-size scaling in the critical region $N \sim N_0^{1/2} \to \infty$ connect the behaviors in the first two regimes. (iii) For $N \lesssim N_0^{\nu_{\rm star}}$, star configurations appear with a central hub surrounded by many leaves. The distribution of stars is broadly distributed over this range. The scaling behaviors found under RSR are identified with a continuous transition in a process called "agglomerative percolation" (AP), with the coarse-grained nodes in RSR corresponding to clusters in AP that grow by simultaneously attaching to all their neighboring clusters.

DOI: 10.1103/PhysRevE.83.036110 PACS number(s): 89.75.Hc, 02.70.Rr, 05.10.Cc, 89.75.Da

I. INTRODUCTION

Renormalization is a basic concept in statistical physics. It is a process whereby degrees of freedom in a system are successively eliminated by coarse graining. At the same time system parameters are rescaled to compensate for the decimation, and the smallest scale is reset to its original value [1]. Since a series of such transformations is itself a transformation, the transformations $\{\mathcal{R}\}$ form a semi-group: the "renormalization group" (RG).

If the system is statistically invariant under $\{\mathcal{R}\}$, one speaks of RG invariance. An invariant system exhibits an asymptotic fixed point under the RG flow with scaling described by homogeneous functions. Prototypical RG fixed points are critical phenomena displayed at continuous phase transitions as for the Ising model, by a-thermal systems like directed [2] or ordinary [3] percolation, relativistic quantum field theories [4], or the Feigenbaum (period doubling) cascade in one-dimensional dynamical systems [5]. Systems with the same fixed point under RG are in the same universality class and share the same critical exponents.

It is natural to ask if similar concepts can be applied to glean meaningful information about complex networks. A positive answer was suggested in Ref. [6] and has stirred much interest. In the present paper we start an investigation to further explore whether and in what sense this can be true.

For models on a lattice, coarse graining can be accomplished either in Fourier space or in real space. A typical real space RG proceeds heuristically by covering a spin lattice with a regular grid of boxes, and replacing the degrees of freedom in each box by a "superspin" [3]. Interactions between spins in neighboring boxes are used to specify the couplings between superspins.

However, many real-world phenomena are better represented as complex networks rather than regular lattices. Although research in this area has exploded in recent years (for reviews see, e.g., Refs. [7–9]), our understanding of the statistical physics of complex networks has not caught up with the vast body of knowledge accrued over decades for lattice systems. Some phase transitions on networks (e.g., in the spreading of epidemics [10,11]) are straightforward generalizations of critical phenomena on lattices. Yet it is not clear whether the RG, and real-space renormalization, in particular, can be applied systematically to complex networks.

Closely related to renormalization is the notion of fractal dimensions [1,4]. Many complex networks are *small world* networks [12,13], where the number of nodes within reach of any node via paths of length r increases exponentially with r. Via any standard definition, this gives infinite fractal dimensions. However Song *et al*. [6] made claims to the contrary, finding finite fractal dimensions for several real-world networks based on a quasiparallel renormalization scheme. A real-space RG for networks that is *not based* on the concept of fractal dimensions, but studied in terms of the flow under renormalization, was proposed by Radicchi *et al*. [14,15].

A fundamental issue pertinent to all the work up to now on renormalization of networks (see, for instance, Refs. [6, 14–20]) is that completely covering a network with equal size

boxes leads to a number of unavoidable dilemmas that could lead to erroneous conclusions. Conceptually, covering the system with boxes of equal sizes is a flagrant violation of the original idea of Hausdorff [21], where the system ought to be covered with a partitioning whose elements have individually optimized sizes up to some largest size r. In most applications this is not a serious impediment, and a covering with equal size elements gives equivalent results. Thus most estimates of fractal dimensions in physics use fixed box sizes, although there are well known cases where this leads to erroneous results. The most famous one is given by any infinite but countable set of points, which according to Hausdorff, but not according to any covering algorithm with fixed box size, has zero dimension.

One reason why this problem can be neglected in many physical systems is that the number of points per box (or, more precisely, the weight of each box) has small fluctuations, in particular, relative to a distribution whose width increases exponentially with box size. For small world networks, where, indeed, the *maximum* number of nodes increases exponentially, the schemes of Refs. [6,16–20] may give misleading results because *most* boxes have only a few nodes. Then the problems associated with fixed box size become acute and there is no reason to believe that the results obtained are related to genuine fractal dimensions of the underlying graph.

Even with fixed box size, the covering should also be optimized with respect to the exact placement or tiling of the boxes, which is an NP hard problem [17]. Heuristic methods for this optimization have been claimed to work [6,16,20], but as a matter of fact they depend on the order in which boxes are laid down. Thus they are not true *parallel* substitutions of nodes by supernodes, but quasiparallel since the single step of tiling the whole network is implemented as a sequence of partial tilings. Combined with the problem of almost empty boxes, this means that the efficiency of the box covering algorithm changes both within each renormalization step (the boxes put down first contain in general more vertices than later boxes) and from one step to the next.

Another problem with the (quasi)parallel renormalization scheme is that each step of renormalization dramatically reduces the number of nodes in the network. Therefore few points and less statistics are obtained for analyzing renormalization flow. This becomes particularly serious in the case of small world networks which collapse to one node in a few steps, even when the initial network size is huge. This has been overcome to some extent in Ref. [22] by performing a renormalization where only parts of the network are coarse-grained at each step, at the cost of adding more parameters and making the results harder to interpret.

In view of these problems, we decided to study graph renormalization for unweighted, undirected networks by means of a purely *sequential* algorithm: At each step one node is selected at random, and all nodes within a fixed distance of it (including itself) are replaced by a single supernode. The supernode has links to all other nodes that were connected to the original subset absorbed into the supernode. This is repeated until the network collapses to a single node.

Our method avoids the problem of finding an optimum tiling as well as problems with almost empty boxes. A further advantage of our random sequential renormalization (RSR) procedure is that each step has a much smaller effect on the network, and thus the whole renormalization flow consists of many more single steps for a finite system and allows for a more fine grained analysis.

If there are fixed points underlying this RG flow, then they will manifest themselves in terms of (finite-size) scaling laws, which hold for large initial networks at intermediate times. Here time is measured by the number of steps in the RSR. At intermediate times, the system is far from both the initial network and the non-invariant final network composed of a single super node.

On any graph, including networks or lattices, the supernodes can be viewed as clusters that grow by attaching to all of their neighboring clusters, up to a distance b in the network of clusters. This process, called "agglomerative percolation," has been solved exactly in one dimension and shown to exhibit scaling laws with exponents that depend on b [23]. On a square lattice in two dimensions, critical behavior is seen which is in a different universality class [24] than ordinary percolation. Thus the scaling behavior seen in RSR occurs as a result of a type of percolation transition and is not restricted to cases where the underlying graph is fractal.

Here we apply our RSR methodology to critical trees and also find evidence for a critical point (which is, however, *not* a fixed point of the RSR) where the number of links attached to any node (i.e., its degree) follows a power law and divergences appear for a number of quantities, including the variance of the degree distribution. The size of the networks at the transition point diverges as $N_0^{1/2}$, slower than the initial network size (N_0) in the limit of infinite system size. Below this transition, renormalized trees are short and fat with an average depth (or radius) which is $\mathcal{O}(1)$. We determine some critical exponents using random walk and other arguments, as well as a mean-field theory for the initial, uncorrelated phase. We use, in addition, the observation that all renormalized networks for $b = 1$ eventually reach a star dominated by a central hub before they collapse to a single node. Our results are confirmed by means of finite-size scaling analyses of results from numerical simulations. These simulations also reveal scaling behavior for the probability distribution for the sizes of networks that first reach a star configuration. This turns out to be equivalent to the distribution of sizes one step before the network collapses to a single node. Stars first appear for renormalized networks when the size of the network is $N \lesssim N_0^{\nu_{\text{star}}}$ with $\nu_{\text{star}} \approx 1/4$.

In Sec. II, we define the general RSR procedure for any network as well as the specific ensemble of networks we analyze in this paper. Section III presents our theoretical and numerical results for RSR of critical trees. Finally, we end with with conclusions and outlook for future work in Sec. IV.

II. THE MODEL

A. Random sequential renormalization

For any undirected, unweighted graph, RSR with *radius* b ($b = 1,2,\ldots$) is defined as follows: Starting with a graph with N_0 nodes, we produce a sequence of graphs of strictly decreasing sizes N_t with $0 < t \leqslant T$ and $N_T = 1$. For each step

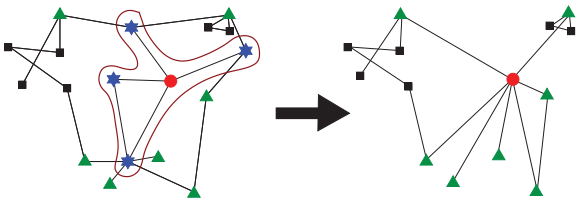

FIG. 1. (Color online) One step of RSR with $b = 1$. The randomly chosen target node (red circle), absorbs all its nearest neighbors (blue stars). All links to the absorbed nodes (from green triangular nodes) are then redirected to the target. Alternatively one can view the supernode as a cluster (bounded by the red curve) that subsequently grows by invading its neighboring clusters.

$t \to t + 1$ (t is called "time" in the following).

(i) We choose randomly a *target node* $i \in [1, \ldots, N_t]$.

(ii) We delete all nodes that can be reached from i by at least one path of length $1 \leqslant \ell \leqslant b$.

(iii) We also delete all links *between* these chosen nodes, and all links connecting them to i.

(iv) Each link connecting any node outside this neighborhood to a deleted node is redirected toward the target.

(v) If this creates a multiple link between any two nodes, it is replaced by a single link.

Hence the target node i is replaced by a supernode that maintains all links to the outside. Its internal features, however, are erased from the network; consistent with coarse graining. Figure 1 shows an example of one step of RSR for $b = 1$. After absorbing its neighbors the supernode is treated like any other node and the process repeats until the network collapses into a single node. One could also vary the probability of choosing a target node by a function of its mass (the number of nodes absorbed into it), or its degree (the number of links attached to it), but these aspects are not explored here.

When $b = 1$, only nearest neighbors of the target node are deleted. For $b > 1$ each step can be implemented by performing b successive decimations with radius one on the same target. Although this method is slightly slower than an optimal coding where all nodes within distance $\leqslant b$ of the target are found and deleted in a single step, it reduces code complexity and potential sources of errors.

For any radius $b \geqslant 1$, RSR exhibits two trivial fixed points: a graph consisting of a single node, and an infinitely long chain. For a long but finite chain, the time until a single node is reached is $T = \lceil N_0/2b \rceil$. In one dimension, the exact probability to find any consecutive sequence of node masses for any N_0 and at any time has been determined [23]. At late times, and for large N_0, the mass distribution of the nodes exhibits scaling both at small and large sizes with (different) exponents that depend on b. For $b = 1$ another fixed point exists, which is a star with infinitely many leaves. In that limit, the probability to choose the central hub of the star as the target vanishes. With probability one, a single leaf is removed during each RSR step. For a finite number $N_{\text{star}} - 1$ of leaves, a star has an average lifetime $\bar{T} = \mathcal{O}(N_{\text{star}})$ before it collapses into a single node. Notice that simple stars are not fixed points for $b > 1$, as any star reduces to a single node in one step with probability one. In this paper we study only the case of RSR with $b = 1$.

B. Initial graph ensemble

The ensemble of critical trees is generated as follows: Starting with a single node, each node can have 0, 1, or 2 offspring with probabilities 1/4, 1/2, and 1/4. (Hence the mean number of offspring is 1.) The process runs until it dies due to fluctuations. The sizes of trees obtained in this way are distributed according to an inverse power law $P(N_0) \sim N_0^{-3/2}$ [3]. From these we pick a large ($\approx 10^2$–10^3) ensemble of trees with the desired (large) $N_0(\pm 10\%)$, and discard all others. Note that simply truncating trees that survive up to N_0 would give a biased sampling of the ensemble.

This construction generates a rooted tree, with important consequences for joint degree distributions of adjacent nodes. The direction of growth leaves its imprint on them. For ordinary undirected random graphs (Erdös-Renyi graphs), it is well known that the degree distribution for pairs of nodes obtained by randomly choosing a link is different from that obtained by choosing any two nodes at random. If the degree distribution is p_k, the distribution of degree pairs for linked nodes is not $p_k p_{k'}$, but $kk' p_k p_{k'}/\langle k \rangle^2$ because higher-degree nodes have a greater chance of being attached to a randomly chosen link. For the present model, two connected nodes are always in a mother-daughter relationship. In particular, all nodes have in-degree one; that is, they have one mother (except for the root). If k is the *out*-degree of the mother and k' the *out*-degree of the daughter, then the distribution of degree pairs obtained by randomly choosing links is

$$\frac{k p_k p_{k'}}{\sum_{l,l'} l p_l p_{l'}} = \frac{k p_k p_{k'}}{\langle k \rangle}. \tag{1}$$

While high-degree mothers have a greater chance of appearing in a pair than low-degree mothers, no such bias holds for daughters. Otherwise said, if we pick a random node, the out-degrees of its daughters will be distributed according to $p_{k'}$, while the out-degree of its mother is distributed $\propto k p_k$. Notice that this implies that our ensemble of critical trees is *not* equivalent to the ensemble of critical Erdös-Renyi graphs.

In the following, we shall always denote by p_k the distribution of out-degrees, and we will, for simplicity, always call k the "degree" (even though the real degree is $k + 1$).

III. ANALYTICAL CALCULATIONS AND SIMULATION RESULTS

A. Evolution of the tree size N

Let n_k be the number of nodes with degree k, and $N = \Sigma_k n_k$ the total number of nodes in the tree (i.e., its size, at a given step). Both N and n_k are fluctuating functions of time t. Since target nodes are picked randomly, the average degree of the target is $\langle k \rangle \equiv N^{-1} \Sigma_k k n_k = 1 - 1/N$, where the last equality follows from the fact that the total number of links in a tree is always $N - 1$. Since all the target's neighbors (both its mother, unless it is the root, and any daughters) are deleted in the subsequent renormalization step, we get the exact result

$$\overline{\frac{\Delta N}{\Delta t}} = -\langle k \rangle - 1 + \frac{1}{N} = -2 + \frac{2}{N}. \tag{2}$$

Here the overline denotes an average over the randomness of the last step only, while brackets denote ensemble averages

(except for $\langle k\rangle$) including also the randomness from previous RSR steps. Approximating t by a continuous variable and performing such an ensemble average gives

$$\langle N\rangle = N_0 - 2t + \ln\left(\frac{N_0-1}{\langle N\rangle - 1}\right). \tag{3}$$

(The integration can only be performed for $N > 1$.) We have replaced $\langle 1/N\rangle$ on the right-hand side of Eq. (3) by $1/\langle N\rangle$, which is a mean-field approximation. We show in Sec. III E that this mean-field regime extends up to a time when $N \sim \mathcal{O}(N_0^{1/2})$.

B. Evolution of the degree distribution

The probability that a randomly chosen node in a network has degree k is $p_k = n_k/N$. The change of n_k in one step of renormalization has three contributions

$$\overline{\frac{\Delta n_k}{\Delta t}} = r_k + s_k + q_k, \tag{4}$$

where r_k is a loss term associated with the possibility that the target had the (old) degree k before the considered renormalization step. It is

$$r_k = -p_k. \tag{5}$$

s_k is a loss term from (old) neighbors of the target having degree k. Assuming no degree correlations, which is also a mean-field approximation, and summing over all (old) degrees k' of the target gives

$$\begin{aligned} s_k &= -\sum_{k'} k' p_{k'} p_k - \sum_{k'} p_{k'}\left(\frac{k p_k}{\sum_l l p_l}\right) \\ &= -\langle k\rangle p_k - \frac{k p_k}{\langle k\rangle} \\ &\approx -(1+k)p_k. \end{aligned} \tag{6}$$

Here the first term is the contribution of the daughters, while the second is due to the mother. This assumes that the target is not the root. For simplicity we shall neglect that possibility in the following, which makes errors of $\mathcal{O}(1/N)$. These are negligible for large N. The last line follows from $\langle k\rangle = 1 - 1/N \approx 1$, which is a good approximation for the same reason.

q_k is a gain term arising from the possibility that the target acquires new degree k. Assume that the old degree of the target was m, that the degrees of its daughters were $k_1,\ldots,k_m$, and that the degree of its mother was k_0 and that all degrees are uncorrelated. Then

$$q_k = \sum_m p_m \sum_{k_0,\ldots,k_m} \frac{k_0 p_{k_0}}{\langle k\rangle} \prod_{i=1}^{m} p_{k_i}\ \delta_{k_0+\ldots,k_m-1,k}. \tag{7}$$

This term is not very transparent. For a more tractable formulation we use the generating function methods discussed next.

C. Generating functions

The generating function for p_k is

$$G(x) = \sum_k p_k x^k, \tag{8}$$

and moments of the distribution are given by

$$\langle k^m\rangle = \left[\left(x\frac{d}{dx}\right)^m G(x)\right]_{x=1}. \tag{9}$$

Similarly, the generating function for the gain term is

$$Q(x) = \sum_k q_k x^k. \tag{10}$$

If a variable has a given generating function, then the generating function for the sum of that variable over m-independent realizations is given by the mth power of that generating function [25]. Hence, if the target node has degree m, the generating function for the sum of degrees of all its daughters is $[G(x)]^m$. Using the above definitions and $G'(1) = \langle k\rangle \approx 1$, we get

$$Q(x) = \sum_m p_m G'(x) G^m(x) = G'(x)G[G(x)]. \tag{11}$$

This, together with Eqs. (2) through (6), leads to

$$\overline{\frac{\Delta G(x)}{\Delta t}} = \frac{1}{N}\{G'(x)G[G(x)] - xG'(x)\} + \mathcal{O}(1/N^2). \tag{12}$$

A more tedious calculation, which requires generating functions for the root of the tree, arrives at the neglected $\mathcal{O}(1/N^2)$ terms. The exact result (assuming no correlations) is

$$\begin{aligned} \overline{\frac{\Delta G(x)}{\Delta t}} &= \frac{1}{N}\{G'(x)G[G(x)] - xG'(x)\} \\ &\quad + \frac{1}{N^2}\{G[G(x)] - G(x)\}. \end{aligned} \tag{13}$$

One checks easily that this satisfies the conditions that $G(1)$ is constant and $G'(1) = 1 - 1/N$ for all t.

D. Variance of the degree distribution

Obtaining the time evolution of the variance of the degree distribution requires an expression for the time evolution of the second derivative of G. From Eq. (12) it follows that

$$\overline{\frac{\Delta G''(1)}{\Delta t}} = \frac{2G''(1)}{N} + \mathcal{O}(1/N^2). \tag{14}$$

Making the same steps and approximations as in Sec. III A gives

$$\begin{aligned} \frac{dG''(x)}{dt} &= \frac{d\langle k^2 - k\rangle}{dt} \\ &= \frac{2\langle k^2 - k\rangle}{\langle N\rangle} + \mathcal{O}(1/\langle N\rangle^2) \\ &\approx \frac{2\langle k^2 - k\rangle}{N_0 - 2t}. \end{aligned} \tag{15}$$

Integrating, fixing the integration constant by the condition $\langle k^2\rangle_0 = 3/2 + \mathcal{O}(1/N_0)$, and rewriting the result in terms of the variance of the degree distribution σ^2 gives

$$\sigma^2 \equiv \langle k^2\rangle - \langle k\rangle^2 \approx \frac{N_0}{2(N_0-2t)} \approx \frac{N_0}{2N}. \tag{16}$$

In Fig. 2 we compare Eq. (16) for the variance of the degree distribution with numerical simulations of RSR for different initial sizes of critical trees. We see perfect agreement at early

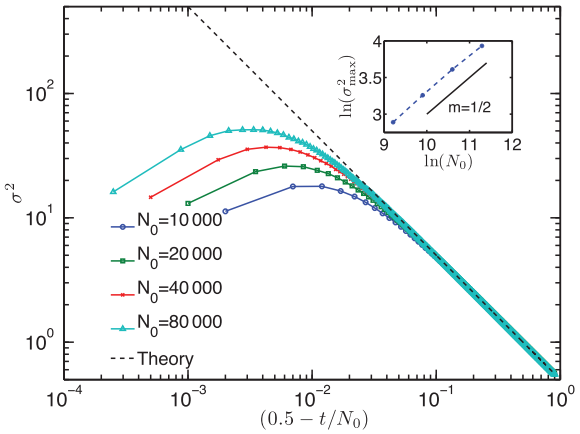

FIG. 2. (Color online) Comparison between the variance of the degree distribution obtained from Eq. (16) and simulations for different system sizes, N_0. The mean-field theory extends over a larger range for increasing N_0. The inset shows that the maximum variance in RSR observed numerically scales as $N_0^{1/2}$, in agreement with our scaling ansatz Eq. (17).

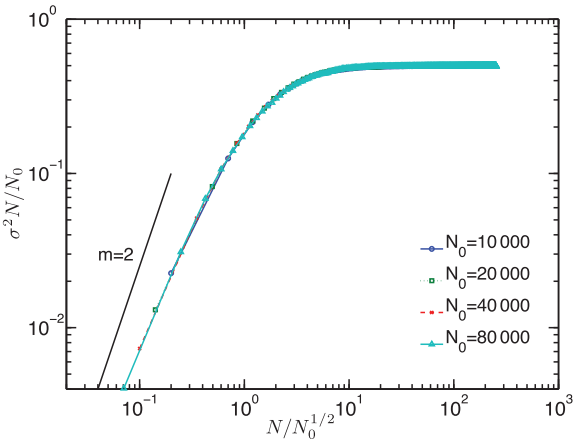

FIG. 3. (Color online) Scaling of the variance of the degree distribution obtained from RSR. The data are the same as in Fig. 2, but the axes are different. They are chosen according to the scaling ansatz Eq. (17), and give excellent data collapse. The straight line has slope $m = 2$.

times, but increasingly larger disagreement at later times. This is only, in part, due to the neglected higher-order terms in $1/N$. Another source of error at late times is that N exhibits large fluctuations compared to its average. Also, degree correlations develop. Hence, the mean-field approximation breaks down for large t. But we also see from Fig. 2 that agreement between theory and numerical results extends over a broader range for increasing system size N_0.

To understand better the behavior at late times (small N/N_0), we replot the same data using a finite-size scaling (FSS) method in Fig. 3. This plot demonstrates that the scaling ansatz

$$\sigma^2 = \frac{N_0}{N} g\left(\frac{N}{N_0^{\nu}}\right), \tag{17}$$

with scaling exponent $\nu = 1/2$ gives excellent data collapse. We derive the result $\nu = 1/2$ in the next section. The scaling function $g(x)$ satisfies $g(x) \to 1/2$ for $x \to \infty$, in agreement with Eq. (16). In addition, the network must, by definition, end up as a star before it collapses. Assuming that the star consists of a central hub surrounded by low-degree nodes (which is verified numerically), its variance will scale with its size as $\sigma^2 \sim N$. Also, the variance of the degree distribution of the star must be independent of the initial size N_0. These considerations lead to the conclusion that $g(x) \to x^2$ as $x \to 0$. Finally, in the scaling ansatz, g and its derivative are continuous functions. As a result the maximum variance occurs when $N \sim N_0^{1/2}$ so that the maximum value of $\sigma^2 \sim N_0^{1/2}$, in agreement with the inset of Fig. 2. Scaling laws like Eq. (17) in terms of homogeneous functions are well known from critical phenomena [1,4], where they describe FSS with several control parameters such as temperature and magnetic field.

E. Fluctuations of the system size and the relaxation time

In this section we derive the result $\nu = 1/2$ by considering fluctuations around the average value of $\Delta N/\Delta t$, and the resulting fluctuations both of N_t and of the relaxation time T. (Recall that the latter is defined as the time when the tree is first reduced to a single node.) Here we explicitly label the fluctuating number of nodes with its time dependence N_t.

Generalizing Eq. (2) and neglecting the $\mathcal{O}(1/N)$ term, we make the ansatz

$$\frac{\Delta N_t}{\Delta t} = -2 + \epsilon_t. \tag{18}$$

Here ϵ is a random variable with zero mean and with variance equal to the variance of the degree distribution σ_t^2, which, on average, increases with time t. Assuming no degree correlations, the random variables ϵ_t at different times are also uncorrelated, and

$$\langle \epsilon_t \epsilon_{t'} \rangle = \delta_{t,t'} \sigma_t^2 \, . \tag{19}$$

Thus the fluctuations of N_t are given by

$$\delta N_t \equiv N_t - \langle N_t \rangle = \sum_{t'=0}^{t-1} \epsilon_{t'}. \tag{20}$$

Since σ_t is finite for all t, the central limit theorem implies that δN_t is Gaussian for large t with variance

$$\begin{aligned} \mathrm{Var}[\delta N_t] &= \sum_{t'=0}^{t-1} \sigma_{t'}^2 \approx \sum_{t'=0}^{t-1} \frac{N_0}{2(N_0 - 2t')} \\ &\approx \frac{N_0}{4} \ln \frac{N_0}{\langle N_t \rangle}. \end{aligned} \tag{21}$$

This estimate has to break down when typical fluctuations of N_t are as big as its average, or when $\mathrm{Var}[\delta N_t] \approx \langle N_t \rangle^2$. We claim that this happens at a time when $\langle N_t \rangle \sim N_0^{1/2}$, explaining the fact that $\nu = 1/2$. Indeed, when $\langle N_t \rangle \sim N_0^{\nu}$ with some positive exponent ν, then $\mathrm{Var}[\delta N_t] \sim N_0 \ln N_0 > N_0$ for large N_0, implying that it is larger than $\langle N_t \rangle^2$ for any $\nu < 1/2$. On the other hand, $\mathrm{Var}[\delta N_t]$ increases less quickly than $\langle N_t \rangle^2$ for

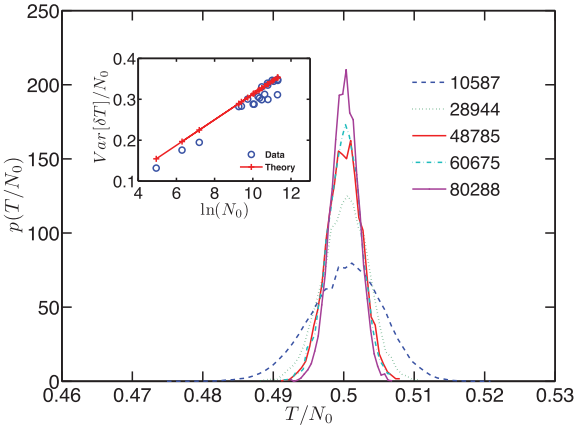

FIG. 4. (Color online) Distributions of relaxation times for various values of N_0. The inset compares the variance of these distributions to Eq. (23) finding good agreement.

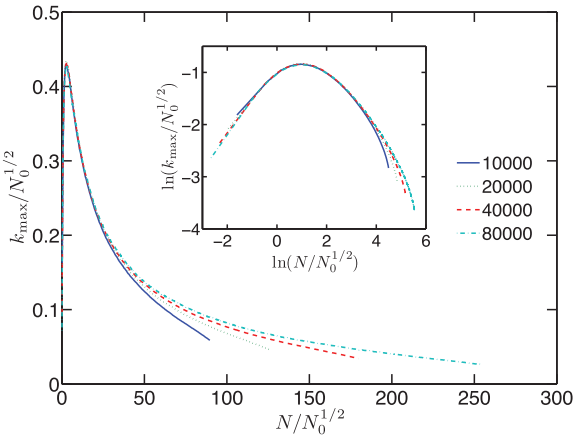

FIG. 5. (Color online) FSS analysis of k_{max} using Eq. (24). There is perfect data collapse in the region $N \sim N_0^{1/2}$.

any $\nu > 1/2$, showing that the initial scaling regime breaks down when $\langle N_t \rangle \sim N_0^{\nu}$ with $\nu = 1/2$.

Fluctuations of the relaxation time T are obtained by demanding that $N_T = 1$, which gives

$$2T - \sum_{t'=0}^{T-1} \epsilon_{t'} = N_0. \tag{22}$$

Hence, for large N_0, T is distributed as an inverse Gaussian variate, which is well approximated in the large N_0 limit by an ordinary Gaussian. Strictly, its variance cannot be calculated exactly since the summation extends beyond the limit of applicability of our theory. To take this into account, we first convert the summation over t' to an integral over N and truncate the integral at $N_0^{1/2}$, where the mean-field theory breaks down. Integration gives

$$\mathrm{Var}[\delta T] = \tfrac{1}{32} N_0 \ln N_0, \tag{23}$$

plus lower-order terms. This is compared with the simulation results shown in the inset of Fig. 4, finding good agreement.

F. Scaling of maximum degree

A simple way to track the formation of hubs under RSR is to measure the maximum degree in the network k_{max}. A naive scaling assumption is that when a few large hubs together with many low-degree nodes dominate, $\sigma^2 \sim k_{max}^2/N$. Using Eq. (17) gives

$$k_{max} \sim N_0^{1/2} f\left(\frac{N}{N_0^{1/2}}\right). \tag{24}$$

Figure 5 compares this equation to results from numerical simulations. While there are clear (and expected) deviations for $N/N_0^{1/2} \to \infty$, the collapse in the intermediate region $N \sim N_0^{1/2}$, where σ^2 achieves its maximum, is perfect. As before, assuming that the tree evolves to a star with a hub at its center suggests that $f(x) \sim x$ as $x \to 0$. However in Fig. 5 we do not observe this behavior as the fitting region is small and there is still some curvature in the scaling function. As for σ^2, our theory predicts that the largest value of k_{max} observed under RSR scales as $N_0^{1/2}$ and agrees with the data seen in the inset of Fig. 5.

G. Ratio of the largest degree to the second largest degree

The ratio of k_{max} to the second largest degree $k_{max,2}$ (provided that $k_{max,2} > 0$) is shown in Fig. 6. It agrees with an FSS analysis using the same exponent $\nu = 1/2$

$$\frac{k_{max}}{k_{max,2}} = h\left(\frac{N}{N_0^{1/2}}\right). \tag{25}$$

Once again the extreme limits of the scaling function h can be determined. For the initial network the largest and second largest degree are equal, so $h(x \to \infty) \to 1$. For a pure star

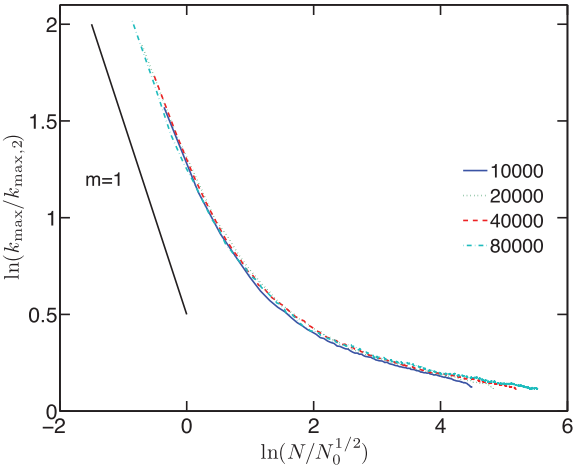

FIG. 6. (Color online) FSS analysis of $k_{max}/k_{max,2}$. This ratio increases as one large hub separates from the rest of the degree distribution. The data show good agreement with the scaling ansatz Eq. (25). The line with slope -1 indicates the theoretical prediction as the network approaches a star.

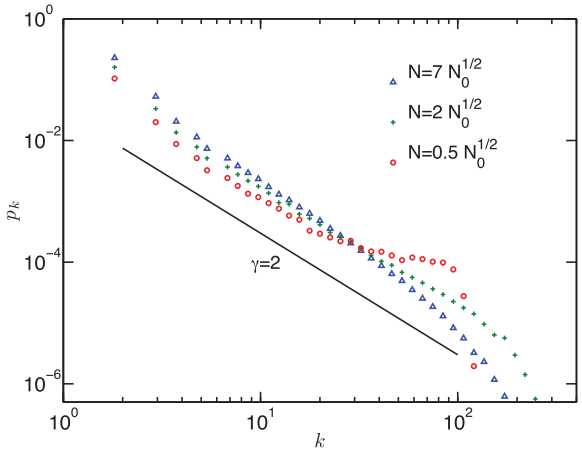

FIG. 7. (Color online) Log-log plot of the degree distribution p_k for trees with $N_0 = 8 \times 10^4$ at three values of N: $N = 7N_0^{1/2}$, $N = 2N_0^{1/2}$, and $N = 0.5N_0^{1/2}$. These distributions are obtained by averaging over different initial networks and different realizations of RSR. The distribution widens and then becomes more narrow on decreasing N as hubs separate from the rest of the nodes during the transition. The data are consistent with our theoretical prediction that at the critical point $p_k \sim k^{-\gamma}$ with $\gamma = 2$.

of size N, $k_{\max}/k_{\max,2} = N$. As shown in Sec. III J, stars first appear when $N \sim N_0^{\nu_{\text{star}}}$ with $\nu_{\text{star}} \approx 1/4$. In that case $k_{\max}/k_{\max,2} \sim N_0^{1/4}$. Hence $h(N_0^{-1/4}) \sim N_0^{1/4}$, or $h(x \to 0) \sim 1/x$. Figure 6 shows that h is increasing in this limit, although the asymptotic regime is not yet reached for the system sizes studied.

H. Degree distribution

Degree distributions for large initial trees at three points in the evolution are shown in Fig. 7. Critical trees start with a narrow degree distribution, which becomes broader and broader under RSR. The degree distribution gradually transforms into a power-law distribution as N approaches $\sim N_0^{1/2}$. For a power-law degree distribution $p(k) \sim k^{-\gamma}$, the variance obeys

$$\sigma^2 \sim \int^{k_{\max}} k^{2-\gamma} dk \sim k_{\max}^{3-\gamma}. \tag{26}$$

From the scaling result at the transition, $\sigma^2 \sim k_{\max} \sim N_0^{1/2}$, we get $\gamma = 2$, consistent with the data shown.

With the formation of a giant hub at the transition, a bump appears at large k in p_k. This is clearly visible for $N = 0.5N_0^{1/2}$ in Fig. 7. Note that the distributions shown in this figure are obtained by averaging over many initial networks and many realizations of RSR. In the degree distribution of a single network a gap emerges between the largest hub and the rest of the nodes for $N \sim N_0^{1/2}$ as demonstrated in Fig. 6.

I. Mean-field theory for average radius of trees

The sum of the distances of nodes from the root in a tree of size N can be written as

$$R = \sum_{x=1}^{N-1} g_x, \tag{27}$$

where g_x is the distance of node x from the root. It is simplest to consider that (except for the root) the mother of a target node absorbs her (target) daughter plus all of that daughter's daughters. Consider node x at distance $g_x > 1$. If the root is the target in the next RSR step, g_x is reduced by 1. If an ancestor of $x's$ mother is hit, which is not the root, then g_x is reduced by 2. If either x or her mother is the target, then x disappears, contributing zero to R. Hence the position of x evolves in the continuous time approximation on average as

$$N \frac{\partial g_x}{\partial t} = -1 - 2(g_x - 2) - 2g_x = -4g_x + 3, \tag{28}$$

for $x > 1$. For $x = 1$

$$N \frac{\partial g_x}{\partial t} = -2. \tag{29}$$

We can write the evolution in terms of the average number of nodes instead of time. As before, in mean field we ignore fluctuations in N about its average $\langle N \rangle$, in R about its average $\langle R \rangle$, and in the number of nodes at distance 1 in the tree S_1 about its average $\langle S_1 \rangle$. This gives, after dropping all angular brackets,

$$\frac{dR}{dN} = \frac{2R}{N} - \frac{3}{2}\left(1 - \frac{1}{N}\right) + \frac{S_1}{2N}. \tag{30}$$

Defining the average radius $r = R/N$ with initial value $r_0 = \alpha N_0^{1/2}$ for large N_0, the constant $\alpha \sim \mathcal{O}(1)$ depends on the precise rule for constructing critical trees. Equation (30) can be solved to get

$$r(N) = \frac{3}{2}\left(1 - \frac{N}{N_0}\right) + \alpha \frac{N}{N_0^{1/2}} - \frac{N}{2}\int_N^{N_0} dy \left(\frac{S_1}{y^3}\right). \tag{31}$$

Bounds on $r(N)$ can be placed based on the fact that $1 \leqslant S_1 < N$ to get

$$1 + \alpha\left(\frac{N}{N_0^{1/2}}\right) - \frac{N}{2N_0} < r \leqslant \frac{3}{2}\left(1 - \frac{N}{N_0}\right) + \alpha\left(\frac{N}{N_0^{1/2}}\right) - \frac{1}{4N} + \frac{N}{4N_0^2}. \tag{32}$$

These bounds are tested against numerical data in Fig. 8 showing excellent agreement, up until the regime where N becomes small compared to $N_0^{1/2}$. At that point mean-field theory breaks down. As the trees start to exit the mean-field regime, their average radius becomes order unity even for $N \sim N_0^{1/2} \to \infty$. Figure 9 shows the evolution of the average number of nodes at distances 1, 2, 3, and 4 from the root, (S_1, S_2, S_3, and S_4, respectively). At $N = N_0^{1/2}$, S_1 becomes the largest shell, and S_2 seems to be exactly equal to S_1 at that point. All other shells vanish compared to S_1 for smaller N. This is the origin of the finite radius of renormalized trees near the end of the mean-field regime.

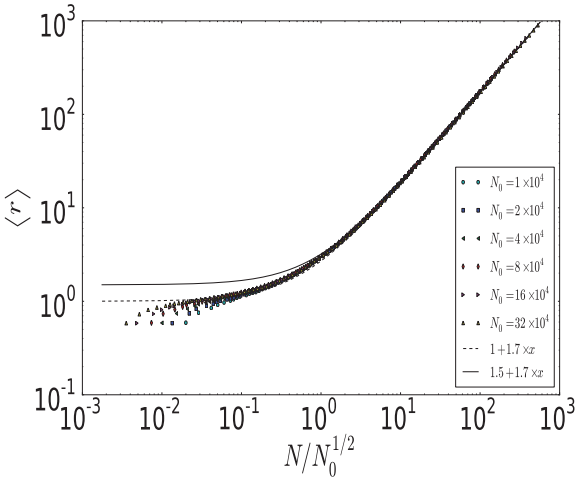

FIG. 8. (Color online) Mean radius r of trees as a function of $N/N_0^{1/2}$. Agreement with Eq. (32) is excellent with $\alpha = 1.7$ as indicated. Fluctuations cannot be ignored for small $N/N_0^{1/2}$ when mean-field theory breaks down and the bounds are no longer valid.

J. Distribution of last sizes and the star regime

Before the network reaches the trivial fixed point at $N = 1$ it must first turn into a star. The star eventually collapses into a single node when the central node is hit as the target.

We define the quantity N_ℓ to be the size of the network one step before it dies. Figure 10 shows an FSS plot for the probability distribution of N_ℓ. More precisely, it shows $N_\ell^{1.4}\ p(N_\ell)$ against $N_\ell/N_0^{1/4}$. The data collapse seen suggests a scaling form

$$p(N_\ell) \sim \frac{1}{N_\ell^{\tau}} \Phi\left(N_\ell / N_0^{D}\right), \tag{33}$$

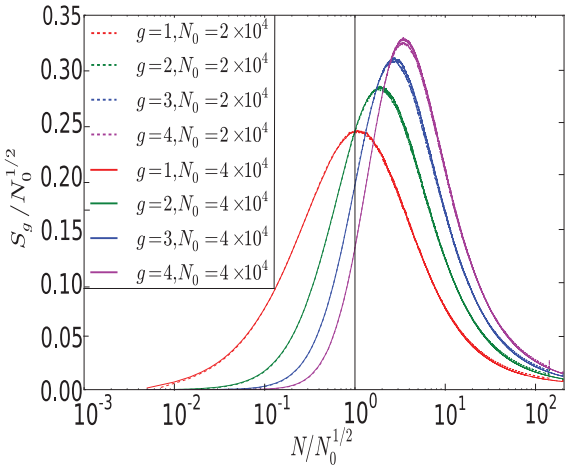

FIG. 9. (Color online) The evolution of the number of nodes in the first four shells as a function of $N/N_0^{1/2}$ for two different system sizes. Note that S_1 crosses S_2 to become the largest shell at $N = N_0^{1/2}$. The other shells vanish increasingly faster as N decreases further.

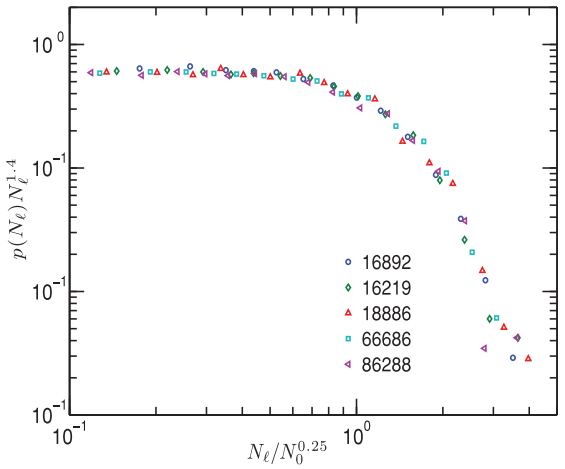

FIG. 10. (Color online) FSS analysis for the distribution of last sizes based on Eqs. (34)–(36) with $\tau = 1.4 \pm 0.1$ and $D = 0.25 \pm 0.07$. In view of the comment after Eq. (34), $p(N_\ell)$ is replaced with $p(N_\ell)/2$ for $N_\ell = 2$.

with $\tau = 1.4 \pm 0.1$, $D = 0.25 \pm 0.05$. The scaling function $\Phi(x)$ seems to approach a constant for $x \to 0$, suggesting that $p(N_\ell)$ tends to a power law, $p(N_\ell) \sim N_\ell^{-\tau}$, for $N_\ell \ll N_0^{1/4}$.

From the distribution of N_ℓ we can determine the distribution of sizes when the tree first turns into a star. Let us call s the size when the renormalized tree first reaches a star configuration, and $p_s(s)$ its distribution. In each subsequent time step the star can either shrink by exactly one node (probability $1 - 1/N$), or it can be reduced immediately to a single node (probability $1/N$). Starting with a star of size s, the conditional probability to end up at final size N_ℓ is

$$p(N_\ell|s) = \begin{cases} \frac{1}{s}, & N_\ell = s, \\ \prod_{t=1}^{s-N_\ell} \frac{s-t}{s-t+1} \frac{1}{N_\ell} = \frac{1}{s}, & 2 < N_\ell < s, \\ \frac{2}{s}, & N_\ell = 2, \end{cases} \tag{34}$$

where the last line comes from the degeneracy of a star with two nodes and is required for proper normalization. Assuming that $p_s(s)$ has a scaling form with possibly new exponents and a new scaling function ϕ

$$p_s(s) \sim \frac{1}{s^{\alpha}} \phi\left(s / N_0^{\beta}\right), \tag{35}$$

we obtain

$$\begin{aligned} p(N_\ell) &= \sum_{s \geqslant N_\ell} p(N_\ell|s) p_s(s) \\ &\approx \int_{N_\ell}^{\infty} ds \frac{\phi\left(s/N_0^{\beta}\right)}{s^{1+\alpha}} \\ &= \frac{1}{N_\ell^{\alpha}} \Psi\left(N_\ell / N_0^{\beta}\right), \end{aligned} \tag{36}$$

with $\Psi(x) = x^{\alpha} \int_x^{\infty} dx'\ \phi(x')/x'^{1+\alpha}$. This agrees with Eq. (33), if we identify $\alpha = \tau$, $\beta = D$, and $\Psi(x) = \Phi(x)$.

Thus the distributions of s and of N_ℓ have the same exponents, if they obey FSS, which we verified numerically.

IV. CONCLUSION

To study invariant properties of graphs under coarse graining, we have introduced the RSR method, where in each step only a part of the network within a fixed distance b from a randomly chosen node collapses into one node. RSR is easy to implement and eliminates the problem of finding an optimum tiling of the network. In addition, the small effect of each decimation gives a much more detailed statistical picture of the renormalization flow. We applied the RSR with $b = 1$ to critical trees and derived results analytically, finding good agreement with numerical simulations.

Under renormalization a critical regime appears when the size of the tree $N \sim N_0^\nu$ with $\nu = 1/2$. The behavior of the tree before this regime is reached is described using a mean-field theory based on generating functions. There is a constant $c \simeq 1$ such that the degree distribution of the network is scale free, $p_k \sim k^{-\gamma}$ with $\gamma = 2$, in the limit $N_0 \to \infty$ and $N/N_0^{1/2} = c$. Both the variance of the degree distribution σ^2 and the maximum degree in the network $k_{\max}$ diverge as $N_0^{1/2}$ in this limit. Both of these quantities are described by crossover functions exhibiting FSS that connect the mean-field regime to a regime for $N_0^{1/4} \lesssim N \lesssim N_0^{1/2}$ when hubs start to emerge. Results from numerical simulations agree with a scaling theory we develop to describe this fixed point. Trees are short and fat near this point with an average depth $\mathcal{O}(1)$. As RSR proceeds further, star configurations start to appear for $N \sim N_0^{\nu_{\text{star}}}$ with $\nu_{\text{star}} \approx 1/4$. The distribution of star sizes seems to obey FSS, characterized by its own critical exponents, which we were not able to derive analytically.

We began this investigation to study in a more controlled way claims made in the literature about real-space renormalization of complex networks [6,14,15]. In the most detailed previous study [14,15] many of the findings are similar to ours, with the caveat that unlike previous works, the results presented here are for critical trees rather than for general networks. The most striking and robust agreement is the emergence of hubs under renormalization, which leads to a final star regime. Associated with the emergence of hubs is a fixed point that gives rise to a power-law degree distribution.

An alternative way to describe RSR is the following: Instead of removing nodes in each coarse-graining step and replacing them by a new "super" node, we keep them and join them into a cluster. At each subsequent RSR step, entire clusters are joined into new "superclusters." This process, where clusters grow by attaching to all the neighbors is an aggregation process [23] is called "agglomerative percolation" (AP) in Ref. [24]. The original network has only clusters of size 1, but larger and larger clusters appear as the RG flow goes on. At the critical point, an infinite cluster (in the limit $N_0 \to \infty$) appears. In this interpretation, the critical behavior seen in this paper (and in Refs. [14,15]) is just a novel type of percolation.

If the original network is a simple chain, the probability distribution to find any sequence of masses for any b, initial size N_0, and time t have been derived exactly. In this case, AP exhibits critical exponents different from ordinary percolation. These exponents depend on b [23]. In two dimensions on a square lattice, AP is in a different universality class than ordinary percolation [24].

In future work [26] we plan to study RSR on networks that are more complex than trees. For Erdös-Renyi graphs we have found a fixed point at finite ratio N/N_0 associated with the emergence of hubs, which in the case of critical trees and of simple chains is driven to zero. This difference between trees and Erdös-Renyi graphs is intuitively most easily understood in the percolation picture discussed above. Trees having topological dimension 1, any percolation transition on them can only happen when the probabilities for establishing bonds goes to 1.

It remains to be seen whether RSR (or equivalently AP) can be used as a generic tool to uncover universality classes in large networks (in the usual RG sense) by eliminating irrelevant degrees of freedom. On a more speculative note, our results point to another way to create scale-free networks that is not based on an explicit generative mechanism for power-law behavior at the microscopic scale, but result from hubs being aggregates of many microscopic nodes. That would suggest the view that networks are emergent collections of smaller networks made up of even smaller ones down to the lowest scales.

ACKNOWLEDGEMENT

We thank Claire Christensen for very helpful discussions, in particular, for pointing out the connection with percolation processes.

[1] D. J. Amit, *Field Theory, the Renormalization Group, and Critical Phenomena*, 2nd ed. (World Scientific, Singapore, 2005).
[2] H. Hinrichsen, Adv. Phys. **49**, 815 (2000).
[3] D. Stauffer and A. Aharony, *Introduction to Percolation Theory*, 2nd ed. (Taylor & Francis, London, 1994).
[4] J. Zinn-Justin, *Quantum Field Theory and Critical Phenomena*, 4th ed. (Oxford University Press, New York, 2002).
[5] M. J. Feigenbaum, J. Stat. Phys. **19**, 25 (1978).
[6] C. Song, S. Havlin, and H. A. Makse, Nature (London) **433**, 392 (2005).
[7] M. J. E. Newman, SIAM Rev. **45**, 167 (2003).
[8] A.-L. Barabsi and R. Albert, Science **286**, 509 (1999).
[9] S. Boccaletti, V. Latora, Y. Moreno, M. Chavez, and D. U. Hwang, Phys. Rep. **424**, 175 (2006).
[10] M. E. J. Newman, Phys. Rev. E **66**, 016128 (2002).
[11] R. Pastor-Satorras and A. Vespignani, Phys. Rev. E **63**, 066117 (2001).
[12] S. Milgram, Psychology Today **1**, 61 (1967).
[13] D. J. Watts and S. H. Strogatz, Nature (London) **393**, 440 (1998).
[14] F. Radicchi, J. J. Ramasco, A. Barrat, and S. Fortunato, Phys. Rev. Lett. **101**, 148701 (2008).

[15] F. Radicchi, A. Barrat, S. Fortunato, and J. J. Ramasco, Phys. Rev. E **79**, 026104 (2009).
[16] C. Song, S. Havlin, and H. A. Makse, Nature Physics **2**, 275 (2006).
[17] C. Song, L. K. Gallos, S. Havlin, and H. A. Makse, J. Stat. Mech.: Theory Exp. (**2007**) P03006.
[18] J. S. Kim, K. I. Goh, G. Salvi, E. Oh, B. Kahng, and D. Kim, Phys. Rev. E **75**, 016110 (2007).
[19] J. S. Kim, K. I. Goh, B. Kahng, and D. Kim, New J. Phys. **9**, 177 (2007).
[20] J. S. Kim, K. I. Goh, B. Kahng, and D. Kim, Chaos **17**, 026116 (2007).
[21] K. J. Falconer, *The Geometry of Fractal Sets* (Cambridge University Press, Cambridge, England, 1985).
[22] H. D. Rozenfeld, C. Song, and H. A. Makse, Phys. Rev. Lett. **104**, 025701 (2010).
[23] S.-W. Son, G. Bizhani, P. Grassberger, and M. Paczuski, e-print arXiv:1011.0944.
[24] C. Christensen, G. Bizhani, S.-W. Son, M. Paczuski, and P. Grassberger, e-print arXiv:1012.1070v1.
[25] M. E. J. Newman, S. H. Strogatz, and D. J. Watts, Phys. Rev. E **64**, 026118 (2001).
[26] G. Bizhani *et al.* (unpublished).

Random sequential renormalization and agglomerative percolation in networks: Application to Erdös-Rényi and scale-free graphs

Golnoosh Bizhani, Peter Grassberger, and Maya Paczuski
Complexity Science Group, University of Calgary, Calgary, Canada T2N 1N4
(Received 23 September 2011; published 15 December 2011)

We study the statistical behavior under random sequential renormalization (RSR) of several network models including Erdös-Rényi (ER) graphs, scale-free networks, and an annealed model related to ER graphs. In RSR the network is locally coarse grained by choosing at each renormalization step a node at random and joining it to all its neighbors. Compared to previous (quasi-)parallel renormalization methods [Song *et al.*, Nature (London) **433**, 392 (2005)], RSR allows a more fine-grained analysis of the renormalization group (RG) flow and unravels new features that were not discussed in the previous analyses. In particular, we find that all networks exhibit a second-order transition in their RG flow. This phase transition is associated with the emergence of a giant hub and can be viewed as a new variant of percolation, called agglomerative percolation. We claim that this transition exists also in previous graph renormalization schemes and explains some of the scaling behavior seen there. For critical trees it happens as $N/N_0 \to 0$ in the limit of large systems (where N_0 is the initial size of the graph and N its size at a given RSR step). In contrast, it happens at finite N/N_0 in sparse ER graphs and in the annealed model, while it happens for $N/N_0 \to 1$ on scale-free networks. Critical exponents seem to depend on the type of the graph but not on the average degree and obey usual scaling relations for percolation phenomena. For the annealed model they agree with the exponents obtained from a mean-field theory. At late times, the networks exhibit a starlike structure in agreement with the results of Radicchi *et al.* [Phys. Rev. Lett. **101**, 148701 (2008)]. While degree distributions are of main interest when regarding the scheme as network renormalization, mass distributions (which are more relevant when considering "supernodes" as clusters) are much easier to study using the fast Newman-Ziff algorithm for percolation, allowing us to obtain very high statistics.

DOI: 10.1103/PhysRevE.84.066111 PACS number(s): 89.75.Da, 64.60.aq, 64.60.ah, 05.10.Cc

I. INTRODUCTION

Complex networks provide a useful representation for complex phenomena in a variety of settings including social, biological, and technological systems and have been studied extensively in the past decade [1–3]. A common property of many complex real world networks is the heterogeneity of nodes leading to wide (power-law, "scale-free") degree distributions [4].

For systems embedded in Euclidean space, scale-free statistics is often related to the notion of self-similarity. In statistical physics and critical phenomena this is usually studied by using the renormalization group (RG) technique, where degrees of freedom of the system are eliminated successively by coarse graining. The scaling behavior of the systems close to the fixed point of the RG flow is then examined and systems with similar scaling behavior are classified into universality classes [5,6].

While renormalization is well defined and extensively studied for spatially extended systems (including regular lattices and disordered systems), it is not clear whether it can be applied to complex networks that have no spatial structure, where the topology is given only by the network itself. Naively one would expect that the "small-world" property displayed by many real networks [7,8] means that they cannot be embedded in any finite dimensional space, and thus renormalization schemes should be less useful. Nevertheless, a real space renormalization transformation for such networks was introduced by Song *et al.* [9,10]. In this scheme, the entire network is covered in each RG step by a set of boxes, and each box is considered as a "supernode" in the next RG step. Several complex networks were claimed to have a finite self-similar or fractal dimension; that is, the number of boxes needed to cover the network seemed to show a power-law relation with the diameter of the box, in blatant contradiction to their small-world property. Although this issue was never solved, it was suggested that the fractality of real world networks depends on self-organization in the growth mechanism [11], assortativity of fractal networks [12], and fractality of their underlying structure [13–17].

This conflict between the "small-world" property and any fractality of complex networks was avoided by Radicchi *et al.* [18,19] by using an RG analysis based on the same box covering idea, but studying carefully the RG flow itself, without using any length scale dependence for making claims about fractality.

There are some technical concerns in these previous box covering methods for renormalizing networks. First, according to the original idea of Hausdorff [20], the sizes of boxes should be individually optimized, whereas in the suggested methods all boxes are of equal size. This is a particularly severe problem due to the heterogeneous connectivity in complex networks that leads also to very wide distributions of nodes per box, most of them being nearly empty. Second, even when boxes of the same size are used, the precise placement of boxes strongly affects the result, and optimizing their positions is not practically feasible. Although the suggested methods in Refs. [9–11,13] are claimed to overcome this problem, their results still depend on the order in which the boxes are laid down, making these schemes quasisequential. In particular, the number of nodes per box decreases strongly with the number of boxes already put down. Finally, during each RG step the size of the network decreases dramatically, which results in a

small number of data points in the RG flow. For networks with small-world property this is particularly serious, as the diameter of the networks scales only with $\log(N)$ (N being the size of the network). To compensate for this, only parts of the network have been coarse grained in Ref. [17] at each step of renormalization, which adds more complexity to the process and makes the results even more difficult to interpret.

In our previous work [21], we suggested a completely sequential renormalization scheme for undirected and unweighted graphs called random sequential renormalization (RSR). In RSR at each step of renormalization one node is chosen randomly, and all nodes within a given distance b are replaced by a single supernode. All links from the outside to the (removed) neighborhood are redirected to the supernode, and the supernode is then treated like any other node in the network. The parameter b is called the box radius.

RSR has the advantage that it does not involve any optimum tiling and is very easy to code and understand. It avoids the problem of mostly empty boxes. Furthermore, as the network is affected only locally and the decimation is considerably less at each step of RSR, the whole flow generates much more statistics, which allows a more detailed analysis.

Another advantage of RSR is that it can be interpreted as a cluster growth process, where initially all nodes are considered to be clusters of mass one. At each step of RSR a randomly chosen cluster grows by agglomerating with all its neighboring clusters. Using the fast Monte Carlo algorithm for percolation introduced by Newman and Ziff (NZ) [22,23], RSR can be easily implemented on networks with millions of nodes.

In our first paper on RSR [21], we applied this method to critical trees. Their simple structure makes it possible to study the renormalization flow analytically, giving perfect agreement with results from numerical simulations. We found three regimes in the evolution of critical trees under RSR. (i) First is an initial regime with small fluctuations in the region $N_0^{1/2} \lesssim N < N_0$ (with N_0 being the initial size of the network and N its size at a given renormalization step). (ii) The second is an intermediate regime for $N_0^{1/4} \lesssim N \lesssim N_0^{1/2}$ where the network is a fat, short tree whose structure is dominated by a giant hub. The transition between these two regimes is associated with emergence of a power-law degree distribution and is described by crossover functions exhibiting finite-size scaling. (iii) A third regime extends down to $N = 1$ where the network is a star with a central hub and many leaves.

The appearance of power-law distributions and scaling is associated with a continuous transition, called "agglomerative percolation" (AP) [24]. In one dimension (i.e., graphs consisting of a simple 1D chain), AP has been solved exactly [25,26]. There it shows nontrivial scaling with exponents that depend on the box size [25]. In two dimensions, AP is for triangular lattices in the same universality class as ordinary percolation (OP), whereas it shows different critical behavior for square lattices [24]. This is related to the bipartite structure of the square lattice as every site on the boundary of any cluster is on the same sublattice [27]. The fact that patently nonfractal structures like 1D and 2D lattices also exhibit scaling under RSR suggests that some of the scaling laws previously found in small-world networks are due to AP transition, rather than any underlying fractality of most networks.

In the present paper we study the behavior of sparse Erdös-Rényi (ER) graphs and of the scale-free model of Barabási and Albert (BA) [4] under RSR. For sparse ER graphs under RSR with $b = 1$, we find a continuous percolation transition at finite $x = N/N_0$. Using finite size scaling methods, we show that the corresponding critical exponents are consistent with a scaling theory based on two independent exponents. Within our error estimates, these exponents appear to be independent of the initial average degree of the ER graphs. For the BA model the transition seems to be pushed to $x = 1$, which makes it more difficult to obtain precise numerical results.

We also study RSR analytically using a mean-field theory based on generating functions. The behavior of graphs before the AP transition is consistent with this theory. After the transition the theory fails due to large fluctuations, as well as due to the effect of loops that are negligible before the transition. The predictions of the theory are in agreement with our simulations of an annealed model.

We introduce our model and simulation method in Sec. II, where we also define the graphs and the sizes of the ensembles under study. Section III presents our simulation results for ER graphs. We show evidence of a continuous percolation transition, find the scaling properties and the corresponding critical exponents numerically, and show that they obey the common scaling relations of OP. In Sec. IV we develop a mean-field theory for the evolution of ER graphs under RSR and compare its results with our simulations of an annealed model. We discuss the behavior of graphs beyond the percolation transition in Sec. V. Sections VI and VII are devoted to the results of simulations on ER graphs with different average degrees as well as RSR with larger box sizes. Finally, in Sec. VIII we examine BA networks, and we conclude our study in Sec. IX.

II. THE MODEL

A. Random sequential renormalization

Random sequential renormalization with radius $b (b = 1,2,\ldots)$ is the process of consecutively applying a local coarse graining (one step of RSR), on a given network G_0, which leads to a series of graphs $G_t (0 \leqslant t \leqslant T)$ with strictly decreasing sizes N_t. In the following, t is called *time*. The initial graph at $t = 0$ has N_0 nodes, and the final graph at $t = T$ is just a single node. We also assign masses to the nodes (initially $m_i = 1; \forall\, i \in G_0$). For any undirected and unweighted graph with N nodes of masses m_i, one step of RSR (as shown in Fig. 1) proceeds as follows.

(i) Choose randomly one of the nodes in the graph as the target.

(ii) Define the neighborhood $\mathcal{N}$ around the target to include all nodes within a distance $d \leqslant b$ from the target. Distance is measured by the number of links that make the shortest path between two nodes.

(iii) Delete all the nodes in $\mathcal{N}$, except for the target.

(iv) Delete all the internal links of $\mathcal{N}$.

(v) Redirect to the target all links that connect nodes in $\mathcal{N}$ to the rest of the network.

(vi) If a multiple link appears, replace it with a single link.

(vii) Update the mass of the target to $m = \sum_i m_i$, with $i \in \mathcal{N}$.

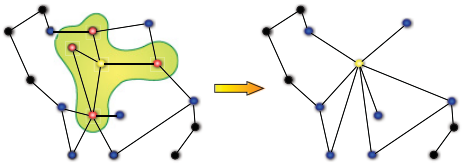

FIG. 1. (Color online) One step of RSR with radius $b = 1$. The randomly chosen target node [yellow (white)] absorbs all its nearest neighbors [red (light gray)]. All links to the absorbed nodes [blue (dark gray)] are then redirected to the target. Alternatively, one can view the supernode as a cluster that grows by eating all its neighboring clusters. RSR with any $b > 1$ can be performed by applying the above procedure on the same target b times.

Hence, the target node and all its neighbors up to distance b in the network are replaced by a supernode. This process preserves all the links to the outside but discards the internal details in the target's neighborhood, analog to course graining in real space renormalization. The supernode is then treated like any other node in the network. We consecutively repeat this procedure until the graph is reduced to a single node. Alternatively, one can also define RSR such that the target node is chosen with probability proportional to its mass [24,26] or degree, but we only discuss the unweighted form here.

For $b = 1$ the target absorbs only its nearest neighbors. The easiest way to implement RSR with any $b > 1$ is to apply RSR with $b = 1$ on the same target for b successive steps. Although this is slightly slower than an optimal coding, we use it in our simulations to reduce code complexity and potential sources of errors.

As indicated in Fig. 1 RSR can also be interpreted as a cluster growth process on the graph. The target cluster is chosen at random and grows by absorbing all clusters within distance b of it. Hence, the fast NZ algorithm for growth of percolation clusters can be easily adapted to this problem, and it makes sense to speak of a percolation transition beyond which one of the clusters occupies a finite fraction of the nodes.

B. The graph ensembles under discussion

We mainly focus on connected ER graphs with average degree $\langle k\rangle$ slightly larger than 2. The ensemble is produced in the following way: For each graph size N_0 we make several ER graphs with fixed size $N^* > N_0$ and a fixed number of links such that the average degree $\langle k\rangle^* = 2$ and determine their giant component (which contains about 80% of the nodes for this value of $\langle k\rangle^*$). If the size of the giant component is $N_0 \pm 1\%$—corresponding to $N_0 = (0.80 \pm 0.01)N^*$—we add the giant component to the ensemble; otherwise it is discarded. Notice that this leads to a slight scatter of N_0 and of the average degree of the graphs at the start of RSR. The latter is $\approx\langle k\rangle_0 = 2.4$. For each N^* the ensembles typically contain $\approx 10^4$ networks, and we apply several realizations of RSR on each of them.

We also examine RSR on ER graphs with $\langle k\rangle^* \neq 2$, as well as the scale-free model of Barabási and Albert [4]. In each case, the ensemble of connected graphs is generated in a similar manner.

C. Algorithms and quantities of interest

In network studies much attention has focused on the statistics of the number of links (degree) of nodes in a network. The degree distribution, the maximum degree, the average, and higher moments of the distribution are also often considered. However, keeping track of the degrees of all nodes under RSR is time consuming and seriously confines the system sizes and statistics of numerical studies. In this paper we have performed numerical simulations with degree measurements for networks up to $N^* = 2.4 \times 10^5$ nodes.

As mentioned previously, the NZ algorithm can be adapted to keep track of cluster masses rather than their degrees. With the NZ algorithm large network sizes with high statistics can be simulated in a reasonable time. We have performed RSR with mass analyses on networks up to $N^* = 10^7$ nodes. Unfortunately, all our efforts to track the degrees of the nodes using the NZ or other algorithms have led to extremely long running times; thus, we restrict our analysis to degrees of smaller networks and measure only masses for larger ones. As far as critical behavior is concerned, we show that mass and degree distributions lead to similar conclusions.

D. Averaging over the ensemble

When discussing ensemble averages, one can use different quantities as independent control parameters. In particular, one can average over RSR trajectories at fixed N or at fixed t. As shown in Fig. 2, these two ways of averaging give different results at late times (and hence small N), due to large fluctuations in the number of nodes eliminated per RSR step in the hub dominant phase. In the same figure we also show the result of a mean-field theory (MFT) discussed in Sec. IV.

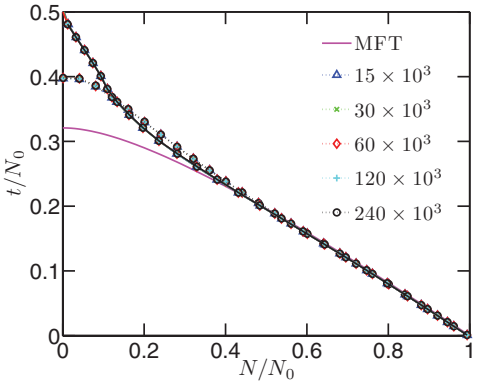

FIG. 2. (Color online) Time dependence of network size, N, in rescaled units. The size decreases monotonically under RSR. Data is obtained from ER graphs with $\langle k\rangle^* = 2$ under RSR with $b = 1$. The curves with dashed lines are obtained by averaging t values corresponding to fixed N, and the curves with solid lines are obtained by averaging N for fixed t. The magenta (gray) solid line shows the mean-field theory prediction (see Sec. IV). The two averages differ when mean-field theory breaks down due to fluctuations. In the rest of the paper we choose N as the independent variable and average all other quantities at fixed N. Numbers in the legend show the initial size of the ER graph, N^*, from which the initial giant components are obtained.

During the initial stages of the flow, MFT gives an accurate description of RSR, but breaks down when different ensembles lead to different results. Some RSR flows last a much longer time than others and since we want to keep the number of members in the ensemble more or less fixed to obtain each data point, we choose to average at fixed N (rather than t) in the rest of this paper.

III. SIMULATION RESULTS FOR ER GRAPHS WITH INITIAL $\langle k\rangle^*=2$

We focus in detail on the behavior of the giant component of ER graphs with $\langle k\rangle^* = 2$ under RSR with $b = 1$. For these graphs the average degree of the giant component is $\langle k\rangle_0 = 2.4$. We find evidence for a continuous AP transition in the evolution of these networks under RSR. The transition is associated with the emergence of a giant hub or the percolation of a giant cluster on the network. We study scaling properties at this transition and measure the corresponding critical exponents numerically. We show that these exponents obey scaling relations associated with percolation, although RSR represents a different universality class than OP, even in the mean-field limit.

A. Evidence for a phase transition

We begin by studying the behavior of the maximum degree $k_{\max}$, as a function of N/N_0, for various initial system sizes, as shown in Fig. 3. Note that the direction of the renormalization flow—or *time*—is from right to left. The initial ER graph has a narrow Poisson degree distribution with no hubs and $k_{\max}/N_0$ is $\mathcal{O}(1/N_0)$. As RSR aggregates nodes locally, although higher degree nodes appear in the system, $k_{\max}/N_0$ remains small. However, as shown in Fig. 3, $k_{\max}/N_0$, suddenly at $N/N_0 \sim 0.7$, starts to increase more rapidly. This implies the existence of at least two regimes in the evolution of ER graphs under RSR: first, a *no-hub* (or mean-field; see Sec. IV) regime, where the degree distribution is narrow, fluctuations are negligible, and a mean-field theory describes the evolution of the system; second, a *hub* regime where a growing hub exists and our mean-field theory breaks down. This is due to large fluctuations as well as the effect of loops in the network. Loops are present in the networks initially, but they typically are large and the graphs are locally treelike. As RSR proceeds, these loops become shorter and the graphs no longer remain locally treelike. As indicated in Fig. 3, the transition between these two regimes becomes sharper on increasing system size N_0.

The same behavior can be observed for the mass of the larger cluster, $M_{\max}$, as shown in the inset of Fig. 3. Initially $m = 1$ for all nodes. Although clusters grow under the renormalization flow in the mean-field regime, the maximum mass remains $\mathcal{O}(1)$. In the critical region a node with the largest mass percolates and separates itself from the rest of the distribution in terms of both size and degree.

This is also indicated in Fig. 4, where both $k_{\max}$ and the second largest degree $k_{\max,2}$ are plotted vs N/N_0. While the two largest degrees are about the same size in the mean-field regime, after the transition the largest hub grows and the second largest degree shrinks, which is another indication of a percolation transition. Similar behavior for $M_{\max}$ and the second largest mass, $M_{\max,2}$, is shown in the inset.

The detailed relation between mass and degree is discussed in the Appendix. No singular behavior in $k_{\max}$ vs $M_{\max}$ appears in the critical region, and this smoothness holds statistically for the mass and degree of other nodes as well. Thus, either variable can be used to extract the critical properties of the phase transition. Since RSR with mass measurement is much

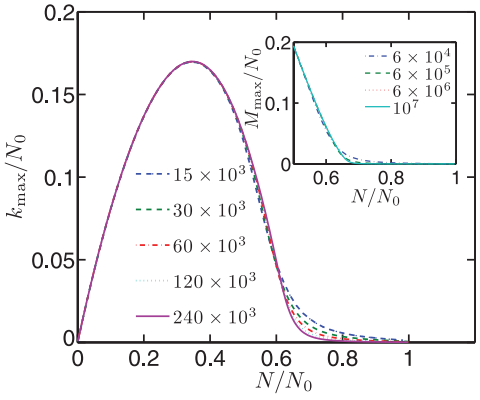

FIG. 3. (Color online) Plot of $k_{\max}/N_0$ vs N/N_0 for ER graphs with $\langle k\rangle^* = 2$ and several initial sizes. Note that the direction of the RSR flow is from right to left. While $k_{\max}/N_0$ is close to zero in the mean-field regime, the hub at late times absorbs a finite and increasing fraction of the nodes. The transition gets sharper with increased system size. (Inset) Similar behavior for the rescaled maximal cluster mass $M_{\max}/N_0$. Note that $M_{\max}$ always increases monotonically under RSR, whereas $k_{\max}$ has to finally decrease. Using the Newman-Ziff algorithm mass related properties can be measured on much larger systems than degree related properties.

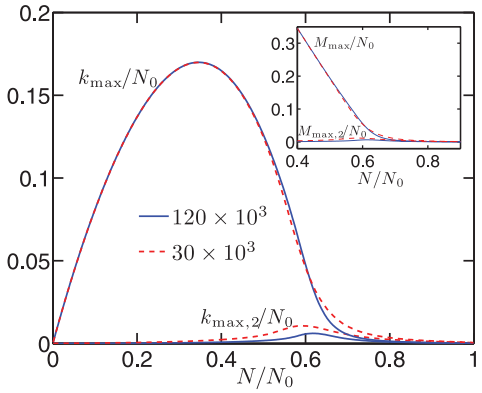

FIG. 4. (Color online) The largest degree $k_{\max}$ and the second largest degree, $k_{\max,2}$, are of comparable size in the mean-field regime, but in the hub regime a giant hub takes over and the second largest degree shrinks. This behavior is also consistent with a continuous percolation transition and shows that there is only one outstanding hub (cluster) in every network. The inset shows the same behavior for the largest and the second largest mass. The data are obtained from ER graphs with $\langle k\rangle^* = 2$.

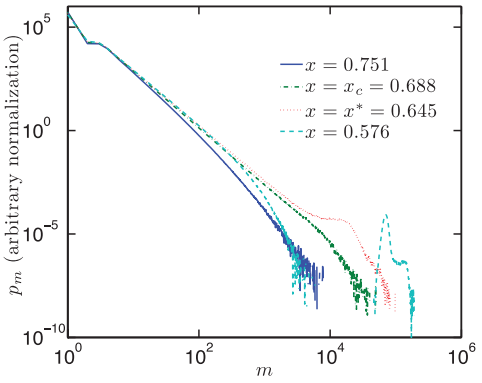

FIG. 5. (Color online) Cluster mass distribution at different stages of the RSR flow for ER graphs of $N^* = 10^6$ nodes, and $\langle k \rangle^* = 2$. This distribution broadens and approaches a power law $p_m \sim m^{-\tau}$ as $x = N/N_0$ decreases. The power law is broadest at $x^*(N_0) = 0.645$, for this system size. For $N_0 \to \infty$, the critical point converges to $x^* \to x_c = 0.688$ (the green dashed-dotted curve). For $x < x^*$ a giant cluster emerges and a gap expands between this cluster and the rest of the distribution. Note that the size distribution of the giant cluster has a shoulder on the right (unlike OP). This is due to the possibility of selecting the hub as a target node and is discussed in more detail in Sec. V.

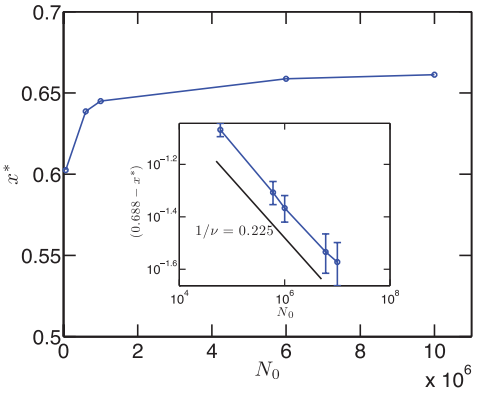

FIG. 6. (Color online) Convergence of the effective critical point, $x^*(N_0)$, to $x_c = 0.688$ as the system size increases. (Inset) The critical point x_c and the exponent $1/\nu$ are consistent with the values $x_c = 0.688$ and $-1/\nu = -0.225$, as indicated by the slope of the straight line.

faster using the NZ algorithm, we mostly base our discussions on the masses of nodes.

B. Finite size scaling analysis

In order to analyze the RG flow in the critical region, we perform a finite size scaling (FSS) analysis on a number of quantities and their distributions. Initially, all the nodes have mass $m = 1$. As shown in Fig. 5, the mass distribution broadens with the number of RSR steps, until a power-law distribution $p_m \sim m^{-\tau}$ emerges in the critical region. As the RSR flow continues, an expanding gap appears between the giant cluster and the rest of the clusters. As shown by the curve for $x \equiv N/N_0 = 0.576$ (below the transition), the peak corresponding to the giant cluster has a pronounced shoulder on the right. This is different from OP, where the peak is featureless. As discussed in more detail in Sec. V, this shoulder results from the giant cluster being chosen repeatedly as the target of RSR. These are rare events, but they have dramatic effects on the flow.

Setting $x = N/N_0$, the effective critical point for a finite system, $x^*(N_0)$, is defined as the value at which the system has the broadest power law in its mass distribution. In Fig. 6, we illustrate the convergence of x^* as the system size increases. The limiting value for infinite system size, x_c, is consistent with $x_c = 0.688$, as shown in the inset.

To proceed further, we make a conventional scaling ansatz for the mass distribution of a finite system in terms of a homogeneous scaling function [6],

$$p_m = m^{-\tau} g\left(n N_0^{1/\nu}, m/N_0^D\right), \tag{1}$$

where

$$n = (x - x_c)/x_c. \tag{2}$$

Note that such an ansatz is never perfect, and all critical parameters discussed in the following are obtained by compromises to get the best overall data collapses for all quantities of interest and by assuming the scaling relations between critical exponents implied by the FSS ansatz. A summary of all critical exponents, the equations defining them and the figures demonstrating numerical evidence, is given in Table I.

Our best estimate for the critical point—mainly from Fig. 6, but also taking into account the consistency checks in Sec. III C—is

$$x_c = 0.688 \pm 0.002. \tag{3}$$

The exponent $1/\nu$ in Eq. (1), describing the convergence of x^* to x_c with increase of system size, is determined to be

$$1/\nu = 0.225 \pm 0.005. \tag{4}$$

The exponent D, giving the scaling of the maximum mass with system size (see Fig. 7), is

$$D = 0.60 \pm 0.01. \tag{5}$$

It is related to the Fisher exponent τ by demanding that there is $O(1)$ cluster of size $\geqslant N_0^D$ and using Eq. (1) [6]:

$$\tau = \frac{1 + D}{D} = 2.67 \pm 0.03. \tag{6}$$

Degree distributions behave similar to the mass distributions. The initial ER graph has a Poisson degree distribution. As RSR proceeds, higher degree nodes appear and the degree distribution broadens. At the phase transition local hubs join together to make a single hub much larger than all others. Just before the giant hub emerges, the degree distribution is approximately a power law with a power τ_k that is consistent with the power τ of the mass distribution. Afterward, the hub continues to grow, but not forever. Figure 8 shows the degree distribution at different values of $x = N/N_0$. At $x \approx 0.7$ the distribution resembles a power law; at $x \approx 0.6$ a bump appears at the rightmost end of the distribution. Later, when $x < 0.6$, a growing gap forms between the giant hub and the rest of the

TABLE I. Summary of critical exponents for ER graphs with $\langle k\rangle^* = 2$ under RSR with $b = 1$. All exponents are obtained by best compromise for the data collapses shown in the figures listed in column 5 and by requiring the scaling relations in column 3 to hold, except for the exponent α (last line). The critical exponents are clearly different from those of mean-field OP (column 6) and for mean-field AP(last column).

Exponent	Value (RSR)	Scaling relation	Eq(s).	Fig(s).	Mean-field OP	Mean-field AP
D	0.60 ± 0.01		(1)	7	2/3	
ν	4.44 ± 0.10		(1)	6, 7	3	4.4 ± 0.3
τ	2.67 ± 0.03	$(1 + D)/D$	(1), (6)	7	5/2	3
β	1.78 ± 0.08	$(1 - D)\nu$	(7), (8), (9)	9	1	
σ	0.375 ± 0.015	$1/(D\nu)$	(11), (12), (13)	10	1/2	
γ	0.88 ± 0.10	$2D\nu - \nu$	(15), (16), (17)	11	1	1/2
α	6.8 ± 0.3	See text	(18)	12	4	

nodes. This continues until the shrinking system size forces the degree of the giant hub to decrease.

C. Consistency checks

In this section we check for consistency of our simulations with the scaling theory based on the FSS ansatz in Eq. (1) by showing data collapses for different quantities of interest. Notice that the well known scaling relations between critical exponents [6] follow from Eq. (1) by considering appropriate limits.

1. The order parameter

An order parameter is any property of a system that can unravel the singularity at the critical point, which is nonzero only on one side of the transition. Typically, P_∞, the probability that a given site belongs to the percolating cluster, is considered as an order parameter for percolation. For RSR on graphs both $k_{\max}/N_0$ and $M_{\max}/N_0$ can be used as order parameters. Notice that the latter is equal to P_∞.

An FSS ansatz for $M_{\max}$ follows by multiplying Eq. (1) by m^y, integrating over m, and taking the limit $y \to \infty$. Using also Eq. (6) gives

$$\frac{M_{\max}}{N_0^D} = h\left(nN_0^{1/\nu}\right). \tag{7}$$

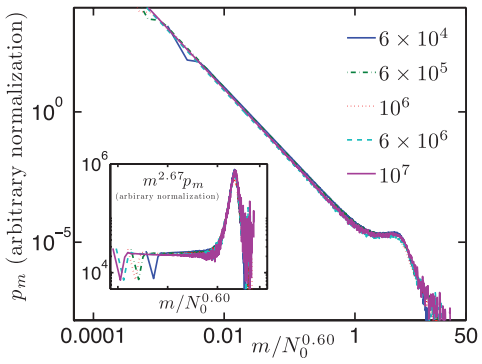

FIG. 7. (Color online) Data collapse using the FSS ansatz in Eq. (1) for the mass distribution at $x^*(N_0)$. The exponent $D = 0.6$ gives the best data collapse, and $\tau = 2.67$ fits the power law (see the inset). These values are consistent with Eq. (6).

Assume now that $h(z)$ satisfies a power law, $h(z) \sim z^\beta$ for $z \to 0$. Equation (7) gives then in the supercritical case $n < 0$ (where we expect $M_{\max} \propto N_0$),

$$D = 1 - \frac{\beta}{\nu} \tag{8}$$

and

$$\frac{M_{\max}}{N_0} \sim |n|^\beta. \tag{9}$$

Figure 9 shows a data collapse according to Eq. (7), with $x_c = 0.688$ and critical exponents as given in Table I. The analogous FSS ansatz for $k_{\max}$,

$$\frac{k_{\max}}{N_0^{1-\beta_k/\nu_k}} = h_k\left(nN_0^{1/\nu_k}\right), \tag{10}$$

with $\nu_k = \nu$ and $\beta_k = \beta$ is shown in the inset of Fig. 9. The exponents for maximal mass and degree are equal within our errors.

2. The cutoff scale for the cluster size distribution

The size of the second large cluster, $M_{\max,2}$ (resp. $k_{\max,2}$), determines the cutoff for the finite clusters (excluding the hub).

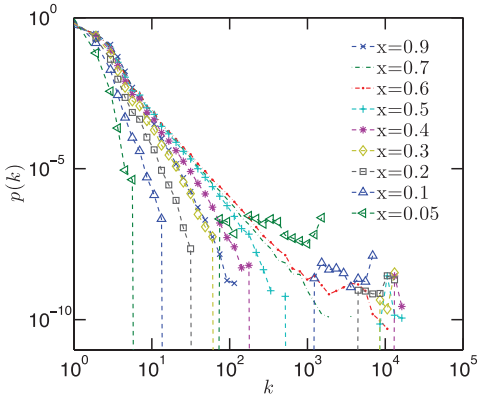

FIG. 8. (Color online) Degree distributions for $N^* = 1.2 \times 10^5$ at different stages of the RSR flow. The initial, narrow distribution gets broader and approaches a power law $p_k = k^{-\tau_k}$ close to the transition. Then a giant hub stands out and a gap opens between the hub and the rest of the nodes.

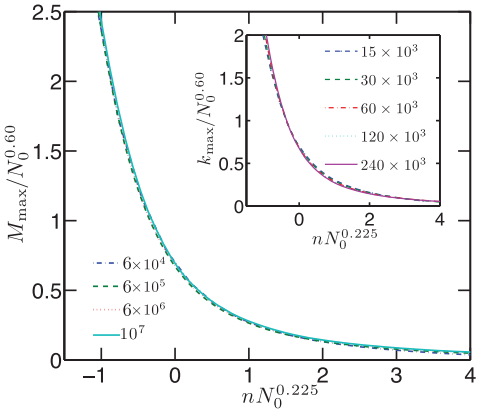

FIG. 9. (Color online) Scaling plot of $M_{\max}$ in the critical region. The value of $x_c = 0.688$ in here and the following figures is the same as in Fig. 6, and the critical exponents are those given in Table I. The inset shows that the exponents ν_k and β_k for the maximum degree are the same as those for the maximum mass within error.

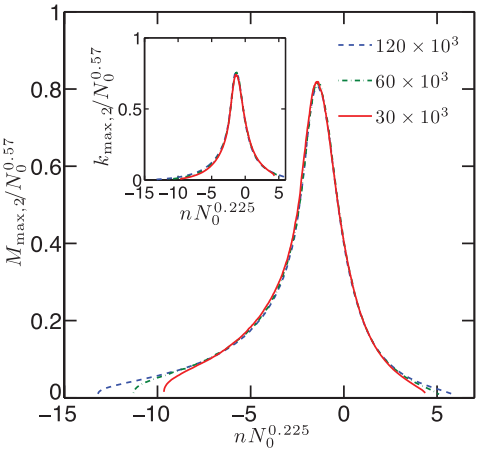

FIG. 10. (Color online) Data collapse for the second largest mass and the second largest degree. Again ν is taken from Table I, while σ is fitted for optimal collapse. The value of σ_k used in the inset is equal to σ, which is here $\sigma = 0.395$.

An FSS ansatz based on Eq. (1) gives

$$\frac{M_{\max,2}}{N_0^{1/\sigma\nu}} = h_2\left(nN_0^{1/\nu}\right), \tag{11}$$

and for the infinite system limit

$$M_{\max,2} \sim n^{-1/\sigma}. \tag{12}$$

The exponent σ is related to other exponents by

$$\sigma = \frac{1}{D\nu} = 0.375 \pm 0.015. \tag{13}$$

One can write similar equations for $k_{\max,2}$. Figure 10 shows data collapse plots with $1/\sigma\nu = 1/\sigma_k\nu = 0.57$ for the second largest mass and degree. This leads to

$$\sigma = \sigma_k = 0.395. \tag{14}$$

This estimate was chosen as it gives the best data collapse. It is consistent with the value obtained in Eq. (13), within error.

3. Average cluster size

The average size of the cluster to which a randomly chosen node of the original network belongs is equal to the second moment of the mass distribution. An FSS ansatz for the average cluster size can be written as

$$\frac{\langle m^2\rangle}{N_0^{\gamma/\nu}} = J\left(nN_0^{1/\nu}\right), \tag{15}$$

and in the limit of $N_0 \to \infty$

$$\langle m^2\rangle = n^{-\gamma}. \tag{16}$$

The exponent γ obeys the scaling relation

$$\gamma = (2D-1)\nu = 0.88 \pm 0.10. \tag{17}$$

Figure 11 shows the corresponding FSS analysis, with $\gamma/\nu = 0.17$ chosen for an optimal data collapse. Within errors, this is consistent with the value $\gamma/\nu = 0.20 \pm 0.20$ obtained in Eq. (17). In the inset we show the second moment of the mass distribution excluding the largest cluster, $\langle m^2\rangle_{ex}$, with the same scaling exponents. The exponent γ_k for the degree moment is found to be the same as that for the mass moment within error (data not shown).

4. Variance of the maximal cluster size

The variance of $k_{\max}$ and $M_{\max}$ also diverge at the critical point. Because of technical problems we do not have precise values of the latter, and we concentrate on the variance of $k_{\max}$. It should scale as

$$\frac{Var[k_{\max}]}{N_0^{\alpha_k/\nu_k}} = J'\left(nN_0^{1/\nu_k}\right). \tag{18}$$

Figure 12 shows the corresponding scaling plot. In OP the standard deviation of the order parameter has the same

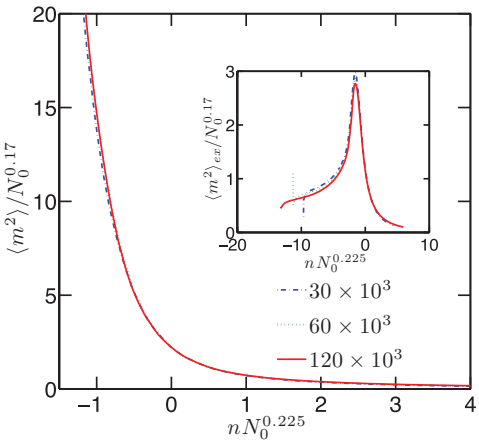

FIG. 11. (Color online) Scaling plot of the second moment of the mass distribution, $\langle m^2\rangle$, for ER graphs, with $\gamma/\nu = 0.17 \pm 0.03$. The inset shows the same plot for $\langle m^2\rangle_{ex}$. The same exponents are obtained.

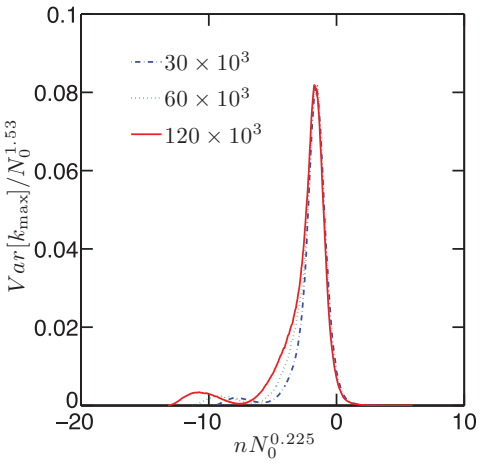

FIG. 12. (Color online) Scaling plot for the variance of the maximum degree, with $x_c = 0.688$, $1/\nu = 0.225$, and $\alpha_k/\nu = 1.53 \pm 0.02$.

critical exponent as the order parameter itself [28], implying $\nu - \beta = \alpha/2$. This is not what we find for RSR on ER graphs, if we assume $\alpha = \alpha_k$. To clarify this we directly looked at the distribution of $k_{\max}$ at x^* for each of the system sizes shown in Fig. 12 (data not shown). The distribution is flat on the left side, but has an approximate power-law tail on the right. The fluctuations in this case grow faster than the average, unlike in OP. We thus believe that the observed violation of the scaling relation is not due to $\alpha \neq \alpha_k$, but shows that the relation $\nu - \beta = \alpha/2$ is violated in AP.

This stems from the difference in the growth process in agglomerative and OP. Adding a bond (or site) in OP might merge only a few clusters into the giant cluster, leading to an additive growth of its size (and degree). In contrast, if the hub is chosen as the RSR target, it absorbs all its neighboring clusters. This leads to multiplicative growth. Thus, in RSR we expect to see larger relative fluctuations in the hub size near the transition comparing to OP (see also Sec. V).

IV. MEAN-FIELD THEORY AND AN ANNEALED MODEL

We now approach the problem analytically using a mean-field theory (MFT) based on generating functions [29]. We show that the critical exponents for mean-field RSR do not agree with the ones for ordinary mean-field percolation.

A. General formalism

Let n_k be the number of nodes with degree k. The total number of nodes in the network is $N = \sum_k n_k$ and the probability of picking a node with degree k is $p_k = n_k/N$. The change of n_k in one step of RSR can be written as the sum of a loss term r_k associated with eliminating a k-degree node and a gain term q_k associated with creating one,

$$\frac{dn_k}{dt} = r_k + q_k. \tag{19}$$

The loss term r_k is

$$r_k = -p_k - \sum_{k'} k' \frac{kp_k}{\sum_l l p_l} p_{k'} = -(k+1)p_k. \tag{20}$$

The first term in the central expression is the probability of targeting a k-degree node, and the second term is the probability that any of the neighbors of the target have degree k. Note that the mean-field assumption is to ignore any potential correlations between the degrees of neighboring nodes.

In order to obtain an equation for dN/dt one does not need to know q_k in detail; one just has to know that exactly one new node is created, whence $\sum_k q_k = 1$. Summing Eq. (19) over k leads then, indeed, to

$$\frac{dN}{dt} = -\langle k \rangle, \tag{21}$$

as expected from the fact that all neighbors of a randomly chosen node are eliminated in one RSR step.

To get q_k, assume that the target has m neighbors with degrees $k_1, k_2, \ldots, k_m$. The new degree of the target will be the number of its second nearest neighbors. If all degrees are uncorrelated and the target's neighbors are not connected among themselves,

$$q_k = \sum_m p_m \sum_{k_1,k_2,\ldots,k_m} \prod_{i=1}^{m} \frac{k_i p_{k_i}}{\langle k \rangle} \delta_{k_1+\cdots+k_m,k+m}. \tag{22}$$

We use generating functions to proceed. The degree distribution is generated by

$$G(x) = \sum_k p_k x^k, \tag{23}$$

and q_k by

$$Q(x) = \sum_k q_k x^k. \tag{24}$$

The degree distribution of the neighbors of the target is proportional to kp_k; thus, their remaining degree is generated by

$$\frac{\sum_k k p_k x^{k-1}}{\sum_k k p_k} = \frac{G'(x)}{\langle k \rangle}. \tag{25}$$

Equation (22) gives then

$$Q(x) = \sum_m p_m \left(\frac{G'(x)}{\langle k \rangle} \right)^m = G\left(\frac{G'(x)}{\langle k \rangle} \right). \tag{26}$$

Using Eqs. (19) through (26) one can write the master equation for the generating function of the degree distribution as

$$\frac{d}{dt} G(x) = \frac{1}{N} \left[G\left(\frac{G'(x)}{\langle k \rangle} \right) + \langle k - 1 \rangle G(x) - x G'(x) \right]. \tag{27}$$

B. The average degree

The moments of the distribution can be obtained from

$$\langle k^m \rangle = \left[\left(x \frac{d}{dx} \right)^m G(x) \right]_{x=1}. \tag{28}$$

One can check that the time derivative of the zeroth moment is zero, that is, normalization is correct. The time derivative of the first moment is given by

$$\frac{d\langle k\rangle}{dt} = \frac{1}{N}[\langle k\rangle^2 - 2\langle k\rangle]. \tag{29}$$

Using Eq. (21) to convert to the derivative with respect to N (for subtleties in this, see [21]) and integrating gives

$$\langle k\rangle = \frac{aN_0}{N} + 2, \tag{30}$$

where $a = \langle k\rangle_0 - 2$ and the subscript zero refers to the initial value.

To test the results of MFT we have simulated RSR for an *annealed random graph model* (AM) in the following way: We start with the degree sequence of the giant component of the ER graphs studied in the previous section, remembering for each of the N_0 nodes its degree, but remove all links. During each RSR step we first pick a random target node and read its degree k. Then we pick k other random nodes $i = 1, \ldots, k$, this time with probabilities proportional to their degrees k_i. Finally, we update the degree of the target to $k' = (\sum_1^k k_i) - k$ and discard the other k nodes.

Figure 13 compares Eq. (30) to the simulation results of the AM and of the model discussed in the last section starting with ER graphs. In all three cases we used $\langle k\rangle^* = 2$. Due to loops in the ER graphs, the average degree of the ER graphs is always less than or equal to that of the AM or MFT. Note that ER graphs are locally treelike and the effect of loops can be ignored initially. Thus, before the transition—in the mean-field regime—there is complete agreement between the results of MFT, the AM, and the ER graphs. However, after the transition, the effect of loops as well as fluctuations (which we discuss later) results in a breakdown of the mean-field assumptions and the average degree of the ER graphs no longer agrees with the other two cases.

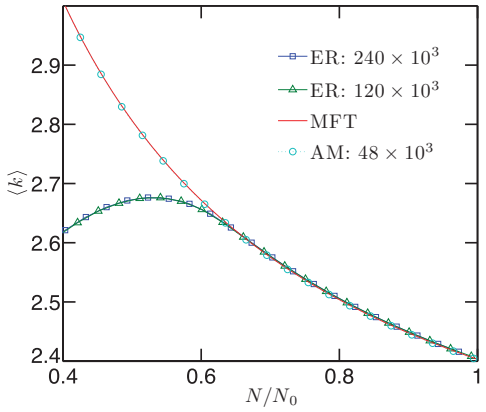

FIG. 13. (Color online) Comparison between the annealed model (AM), mean-field theory (MFT), and ER graphs with $\langle k\rangle^* = 2$. There is good agreement between theory and data in the mean-field regime $x \geqslant x_c$. After the transition the effect of loops in ER graphs can no longer be ignored and results in smaller $\langle k\rangle$ for ER graphs.

In the mean-field regime the system size, N, can be found as an implicit function of t by using Eqs. (21) and (30) to get

$$t = -\frac{1}{2}\left\{N - N_0 - \frac{aN_0}{2}\ln\left[\frac{a + 2N/N_0}{a+2}\right]\right\}. \tag{31}$$

This result is shown in Fig. 2 and is in good agreement with simulation results in the mean-field regime.

C. Divergence of degree fluctuations

Also within MFT, the variance of the degree distribution diverges at the transition point. For ease of calculations we switch to factorial moments of the degree distribution obtained by consecutive derivatives of the generating function,

$$\langle k_-^m\rangle = \langle k(k-1)\cdots(k-m+1)\rangle = \left[\left(\frac{d}{dx}\right)^m G(x)\right]_{x=1}. \tag{32}$$

Using Eq. (27), the time derivative of the second factorial moment is

$$\frac{d}{dt}\langle k_-^2\rangle = \frac{\langle k_-^2\rangle}{N}\left[\frac{\langle k_-^2\rangle^2}{\langle k\rangle^2} + \langle k\rangle - 3\right]. \tag{33}$$

We next define a variable $u = \langle k_-^2\rangle/\langle k\rangle$ and use Eqs. (21), (29), and (30) to get

$$\frac{du}{u^3 - u} = -\frac{dN}{aN_0 + 2N} = -\frac{dx}{a + 2x}, \tag{34}$$

with $x = N/N_0$. Integrating this equation leads to

$$u^2 = \frac{a + 2x}{a - c + 2x}, \tag{35}$$

where

$$c = \frac{u_0^2 - 1}{u_0^2}(a+2), \tag{36}$$

and u_0 is the initial value of u. Since the average degree $\langle k\rangle$ does not diverge at the transition, the divergence of u is the same as the divergence of the variance of the degree distribution. The quantity u diverges when the denominator of Eq. (35) vanishes, so the critical point is at

$$x_c = \frac{N_c}{N_0} = \frac{1}{2}[c - (\langle k\rangle_0 - 2)]. \tag{37}$$

Equations (36) and (37) result in $x_c = 0.718\ldots$ for the AM model with $\langle k\rangle_0 = 2.4$ we study here (notice that the initial degree distribution is not strictly Poissonian due to the restriction to the giant component of the original ER graph). Substituting $n = (x - x_c)/x_c$ into Eq. (35) we get

$$\langle k^2\rangle \sim u \sim n^{-\gamma} \quad \text{with} \quad \gamma = 1/2. \tag{38}$$

For a finite system, we make the FSS ansatz

$$\frac{\langle k^2\rangle}{N_0^{\gamma/\nu}} = f\left(nN_0^{1/\nu}\right). \tag{39}$$

Figure 14 shows an FSS analysis of $\langle k^2\rangle$ for the annealed model, close to criticality, and for several system sizes. The values of $x_c = 0.718$ and $\gamma = 0.112/0.225 = 0.5$ used in

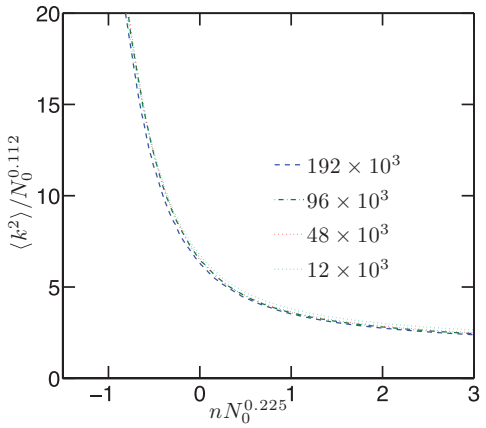

FIG. 14. (Color online) FSS analysis of the second moment of the degree distribution, $\langle k^2\rangle$, close to criticality for the AM. The values of $x_c = 0.718$ and $\gamma = 0.5$ used in the plot are those obtained from the MFT. While the exponent $1/\nu = 0.225 \pm 0.015$, obtained from the FSS data collapse, is similar to ER graphs, the exponent γ is different from $\gamma = 0.88$ in ER graphs.

the FSS analysis are taken from MFT and give excellent agreement.

D. Other critical exponents

To get all other exponents in MFT we use Eqs. (27) and (32) to find the time derivative of the third factorial moment, $h = \langle k_-^3\rangle$,

$$\frac{dh}{dt} = \frac{hu^3}{N} + \cdots, \tag{40}$$

where the dots stand for terms that are less divergent for $x \to x_c$. Together with $du/dt \sim u^3/N + \cdots$ this gives near the critical point

$$\ln h \sim u \sim n^{-1/2} \Rightarrow h \sim e^{1/n^{1/2}}, \tag{41}$$

suggesting that the third moment has an essential singularity. The latter seems to be contradictory to scaling theory, but it really is not, and there exists a consistent solution showing these features. Assume the scaling ansatz

$$p_k = k^{-\tau} f(k/k_{\text{cutoff}}) \tag{42}$$

for the degree distribution near the critical point, with k_{cutoff} diverging at $x \to x_c$. For u to diverge, τ must be $\leqslant 3$. If τ were strictly <3, we would have $u \sim k_{\text{cutoff}}^{3-\tau}$ and $h \sim k_{\text{cutoff}}^{4-\tau}$; that is, there would be a power relation between them: $h \sim u^{(4-\tau)/(3-\tau)}$. The only way to obtain $u \sim \ln h$ is by having a logarithmic divergence of the sum $\sum_k k^2 p_k$, that is,

$$\tau = 3. \tag{43}$$

In order to have $\gamma = 1/2$, one needs furthermore $k_{\text{cutoff}} \sim e^{1/n^{1/2}} \sim N_0$, giving then also Eq. (41). The fact that k_{cutoff} diverges faster than a power for $x \to x_c$ means that there is no simple scaling theory near the transition due to the singularity.

E. Limiting behavior for $\langle k\rangle^* \to 1$

In the limit $\langle k\rangle^* = 1$, the giant components of ER networks become trees with $\langle k\rangle_0 = 2$. Since trees remain trees during RSR, $\langle k\rangle = 2$ during the entire RSR flow, consistent with Eq. (29). On the other hand, $\langle k^2\rangle$ does increase with t. Equation (35) leads to

$$u^2 = \frac{2x}{2x - c}, \tag{44}$$

and Eq. (37) gives

$$x_c = \frac{u_0^2 - 1}{u_0^2} > 0. \tag{45}$$

This is in contrast to the result of [21], where we found $x_c = 0$ for critical trees. Indeed, the limit $\langle k\rangle^* \to 1$ of the present model is *not* the model of critical trees that was treated in [21].

This follows from how the critical trees of [21] and critical ER graphs are generated. In ER graphs links are distributed among nodes completely at random. If a node is picked at random, the degrees of all its neighbors are distributed according to

$$kp_k \Big/ \sum_l l p_l, \tag{46}$$

and there is no further structure. In contrast, the critical trees of [21] are generated by a critical random branching process that starts from one particular node and imprints on them a *rooted* structure. Therefore, if a node is picked randomly, there are relations that hold seperately for its mother and its daughters. While the degree distribution for the mother satisfies Eq. (46) with k replaced by $k-1$, the degree distribution of the daughters is simply p_k. One might think that this subtle difference can be neglected in a mean-field approximation, but this is not true: Since each RSR step affects three generations of nodes, a consistent grandmother-mother-daughter relationship has an effect on the RSR flow. However, it is not intuitively clear why this small difference has such a strong influence on the threshold for AP. Notice that an even more surprising dependence on minor details, leading indeed to a violation of universality, is seen also in AP on 2D lattices [24].

We did not study the case $\langle k\rangle^* = 1$ numerically, because the size of the largest component in critical ER graphs of size N_0 is $\sim N_0^{2/3}$, making it very difficult to create large initial connected graphs.

V. FLUCTUATIONS IN THE HUB PHASE

If the giant cluster (or hub) is itself a target of RSR, the size of the network decreases significantly in that time step. This gives rise to large fluctuations in the size of the network.

Figure 15 shows a scatter plot of t vs N in rescaled units for an ensemble of ER networks with $N^* = 1.2 \times 10^5$ and $\langle k\rangle^* = 2$. The x and y axes in this plot are coarse grained into 500 and 200 bins, respectively, giving 100 000 pixels. The color of each pixel represents the frequency of this (N,t) pair relative to the frequency of the most populated pixel. As one can see, an envelope exists corresponding to the largest N at a given time (and biggest time for a given N). There is also a second band (of high probability) which corresponds to

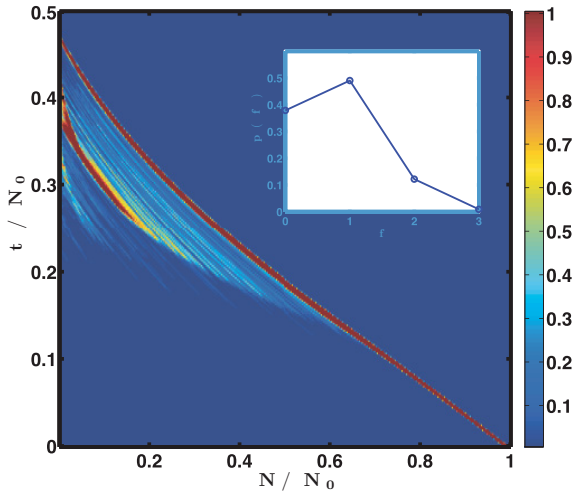

FIG. 15. (Color online) Scatter plot of t vs N in rescaled units for ER graphs with $\langle k\rangle^* = 2$ and $N^* = 120 \times 10^3$. The color map shows the relative frequency of each (N,t) pair in the ensemble. The main, intermediate, and weak bands correspond to realizations where the giant hub has been hit zero, one, or two times, respectively. The inset shows the probability that the giant hub is targeted f times by RSR.

intermediate N. A third but weak band also appears at smaller system sizes, which is more difficult to distinguish due to the considerable fluctuations.

The inset of Fig. 15 shows the fraction of realizations in which the giant hub is hit f times, conditioned on $k_{\max}/N_0 > 0.1$. Most often the hub is hit only once and never more than three times. Evidently, the envelope (the uppermost band) comes from the realizations in which the giant hub was not hit at all, the intermediate band results from cases where the giant hub is hit once, and the third weak band is due to rare cases where the giant hub is hit twice.

The slopes of the main bands are also informative. The uppermost band starts with slope $\frac{-1}{\langle k\rangle_0}$, in agreement with Eq. (21). At the final stages, where the structure is starlike (as discussed in the following section), the bands have slope -1, which means that in most cases a leaf is targeted and thus one node is removed in one time step. The wide range of values for realizations as shown in Fig. 15 explains why in Fig. 2 averaging over t at fixed N gave a different result than averaging over N at fixed t.

The distribution of times T for the networks to reach $N = 1$ corresponds to the leftmost column in Fig. 15. This distribution has a shoulder where the uppermost band hits the y axis, (at $t/N_0 \approx 0.47$) and a peak where the second one hits it ($t/N_0 \approx 0.38$). These distributions show perfect data collapses for different system sizes (data not shown). For networks with $\langle k\rangle^* > 2$ the shoulder turns into a second peak which grows and becomes the dominant peak on increasing $\langle k\rangle^*$. It should disappear for $\langle k\rangle^* \to 1$.

A. Scaling behavior at late times

Eventually, as the networks shrinks, $k_{\max}$ starts to decrease and at the same time the network topology moves toward a starlike structure.

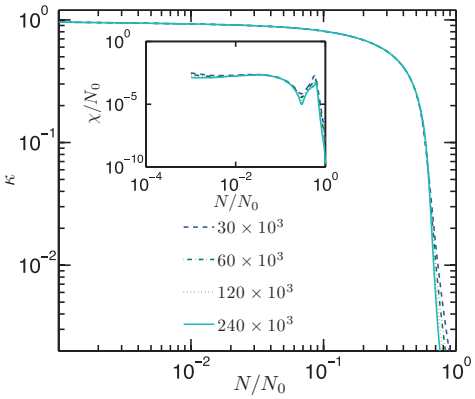

FIG. 16. (Color online) The relative maximum degree, $\kappa = k_{\max}/(N-1)$, vs N/N_0 for different system sizes. The plot shows that the network is starlike at late times since κ approaches 1. (Inset) Variance of κ vs N/N_0. Although the qualitative behavior of graphs under RSR at late times is the same as for the (quasi-)parallel renormalization method [18], the quoted exponents are different.

The relative size of the largest hub $\kappa = k_{\max}/(N-1)$ is a good measure for the similarity of a graph to a star which is a graph whose nodes are at most a distance two apart. Figure 16 shows κ and its variance χ as a function of the relative system size. As one can see, at late stages of RSR κ is close to one, and thus the network has a starlike structure.

The starlike regime was also observed in previous (quasi-) parallel methods used for renormalizing networks [18,19]. Comparing our analysis with those studies, RSR shows scaling and criticality in the flow at early times that was not picked up previously, because the renormalization steps in the quasiparallel method were too large and jumped over the AP transition. Thus, only the scaling at late times was observed in [18,19]. Although the graphs under RSR look qualitatively similar to those obtained with the quasiparallel method at late times, the quoted exponents are different (our Fig. 16 should be compared with Fig. 1 in Ref. [18]).

B. The star regime

We define N_ℓ to be the last size of the network one step before it collapses into a single node. By definition the network has to be a pure star at this point. Figure 17 shows a data collapse for the distribution of N_ℓ for ER graphs of different sizes. It is a broad distribution following the scaling ansatz

$$p(N_\ell) \sim \frac{1}{N_\ell^{\tau_s}} f\left(\frac{N}{N_0^{D_s}}\right), \tag{47}$$

with $\tau_s = 1.40 \pm 0.15$ and $D_s = 0.25 \pm 0.05$.

The exponents τ_s and D_s are similar to the ones obtained for critical trees [21]. This suggests universality in the final structure of the graphs, regardless of the starting structure, as the graph collapses into a single node and all original structure is lost.

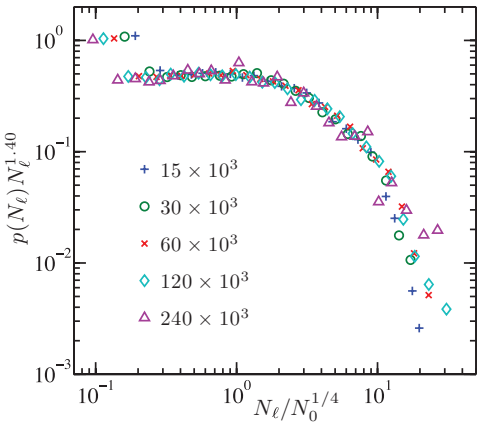

FIG. 17. (Color online) Data collapse for the distribution of the last sizes. The distribution follows the FSS ansatz in Eq. (47) with $\tau_s = 1.40 \pm 0.15$ and $D_s = 0.25 \pm 0.05$, except for the leftmost points. The reason for their special behavior is given in [21].

VI. STARTING WITH OTHER AVERAGE DEGREES

Up to now we studied the behavior of ER graphs with $\langle k \rangle^* = 2$. Here we discuss the effect of the initial average degree on RSR flow, still considering ER graphs.

Figure 18 represents $k_{\max}$ for ER graphs with different values of $\langle k \rangle^*$. The figure demonstrates similar critical behavior for these networks. For higher initial average degree the transition gets sharper and moves to the right, that is, toward earlier times. This is also predicted from Eq. (37). For larger $\langle k \rangle^*$, x_c approaches 1. Note that both $\langle k \rangle_0$ and $\langle k^2 \rangle_0$ affect the position of x_c.

Figure 19 shows an FSS analysis of $M_{\max}$ for ER graphs with $\langle k \rangle^* = 4$. The critical point $x_c = 0.865 \pm 0.010$ and the exponents $1/\nu = 0.215 \pm 0.030$ and $1 - \beta/\nu = 0.62 \pm 0.05$ are obtained by finding the best data collapse. The value of x_c is in agreement with Eq. (37) and the exponent ν and β agree with those for $\langle k \rangle^* = 2$, within our error estimates. For even higher average degrees (not shown) the exponents still agree

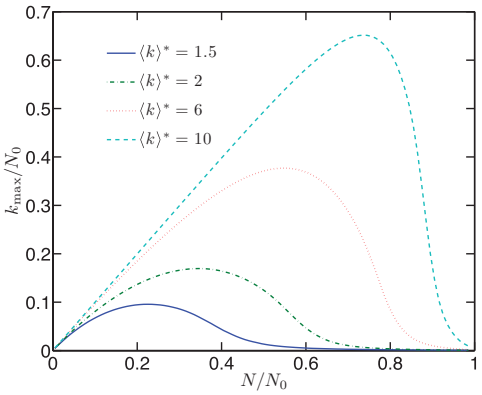

FIG. 18. (Color online) Rescaled maximum degree, $k_{\max}/N_0$ vs system size for ER graphs with $N^* = 30\,000$. The transition shifts to the right with increase of $\langle k \rangle^*$.

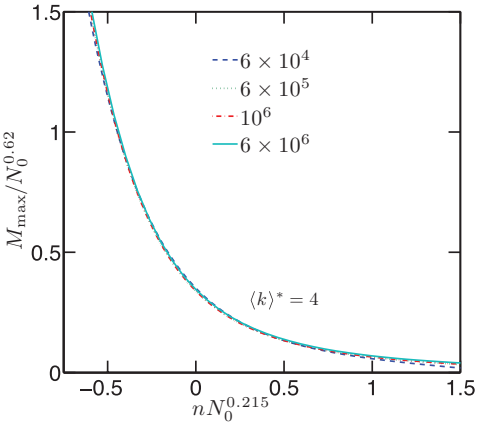

FIG. 19. (Color online) Scaling of $M_{\max}$ for ER graphs with $\langle k \rangle^* = 4$. The values $x_c = 0.865 \pm 0.010$, $1/\nu = 0.215 \pm 0.030$, and $1 - \beta/\nu = 0.62 \pm 0.05$, obtained by finding the best data collapse, agree with Eq. (37) and the exponents for ER graphs with $\langle k \rangle^* = 2$ within error bars.

with the ones obtained for $\langle k \rangle^* = 2$, although the error bars are rather large.

VII. RSR WITH LARGER BOX SIZES

In this section we study RSR with box radius $b > 1$ on ER graphs with $\langle k \rangle^* = 2$. We see evidence for a transition at early times. Figure 20 shows the order parameter as a function of N/N_0 for networks of different system sizes under RSR with $b = 2$. Although one can clearly see evidence for a phase transition at early times, extrapolating the critical point for the infinite system with precision is not possible.

One of the main differences between the $b = 1$ case and $b > 1$ is that for larger box radii there is no star regime. Once the network has diameter two, it will die in the next step with probability one.

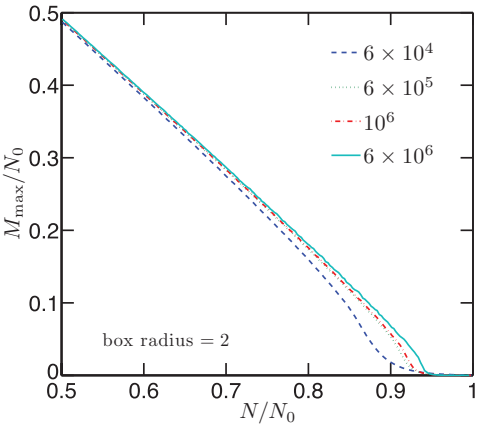

FIG. 20. (Color online) Flow of the order parameter under RSR with box radius $b = 2$ for ER graphs of $\langle k \rangle^* = 2$ and several sizes. The data show a sharp transition at early times, but a clean FSS analysis including precisely locating the critical point is not numerically tractable.

Another point to mention is that with any box size larger than one, the possibility to incorporate the hub at any step is large. The reason is that RSR with $b > 1$ is performed by targeting the same node b successive times. Although the target itself is not likely to be the hub, it is likely that it is the neighbor of the hub and thus merges with it. Hitting the same node again means then hitting the hub with high probability. With this argument any box size higher than one is similar to a *weighted* RSR, where nodes are being targeted with probability proportional to their mass or degree.

VIII. SCALE-FREE NETWORKS

Models with broad or "scale-free" degree distributions are often more interesting in view of their application to real-world networks. We have studied RSR on the Barabasi-Albert model [4]. Figure 21 shows the behavior of the maximum degree under RSR. Since these networks are scale free at the beginning, the transition is pushed all the way to $N/N_0 = 1$. There is perfect data collapse after the hubs are well established.

The critical point can also be obtained from Eq. (37). The value of $\langle k^2\rangle_0$—and thus also the value of $u_0 = \langle k^2_-\rangle_0/\langle k\rangle_0$—diverge for scale-free networks, giving $x_c \approx 1 - 1/u_0^2 \approx 1$.

When analyzing mass distributions for renormalized scale-free networks, it can be argued that one should not give masses $m = 1$ to all nodes of the initial graph. Instead, one might assign to every node a mass equal to its degree, as this allows one to consider mass as a proxy for the degree of nodes in the simulation of the RG flow.

This convention is used in Fig. 22, which illustrates an FSS analysis for the maximum cluster mass, $M_{\max}$, and the second moment of the mass distribution excluding the largest cluster, $\langle m^2\rangle_{ex}$, in BA networks of several sizes. Setting the critical point at $x_c = 1$, we obtained $1/\nu = 0.18 \pm 0.02$, $D = 0.5 \pm 0.1$, and $\gamma/\nu = 0.25 \pm 0.03$.

IX. CONCLUSION

In this paper we have extended random sequential renormalization (RSR) to several networks, namely Erdös-Rényi

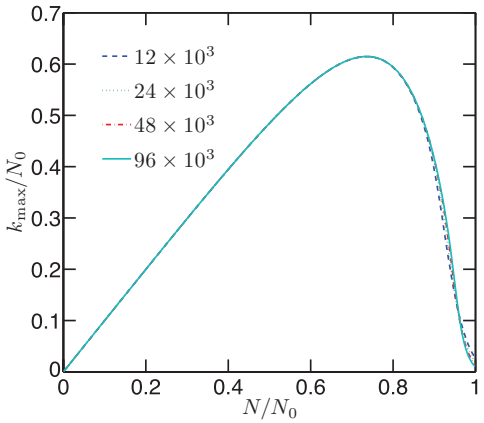

FIG. 21. (Color online) FSS analysis of $k_{\max}/N_0$ for the BA model. The critical point is pushed toward one, and there is a perfect data collapse after the hubs are well established.

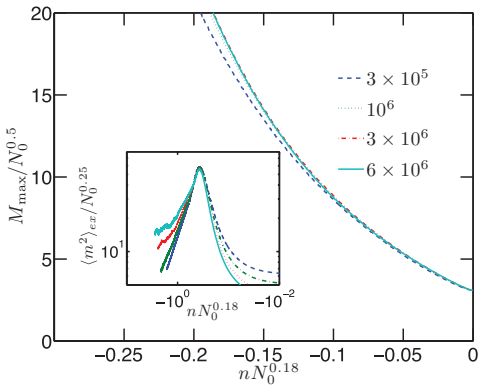

FIG. 22. (Color online) FSS analysis of $M_{\max}$ and $\langle m^2\rangle_{ex}$ for the BA model. The critical point is set at $x_c = 1$. The exponents $1/\nu = 0.18 \pm 0.02$, $D = 0.5 \pm 0.1$, and $\gamma/\nu = 0.25 \pm 0.03$ are obtained from the data collapse.

(ER) graphs and scale-free networks. In each step of RSR only a local part of the network within a fixed distance from a randomly chosen node is coarse-grained into one node. This is in contrast to (quasi-)parallel RG schemes that tile and coarse grain the whole network in one step, which, however, has to be broken up into sequential local substeps for technical reasons. Apart from simplicity of the algorithm, RSR generates considerably larger amount of statistics and allows for a more detailed analysis of the renormalization flow. RSR can be interpreted as a cluster growth process where at each step a randomly chosen cluster grows at its boundary by agglomerating to all its neighboring clusters. Hence, the fast Monte Carlo algorithm of Newman and Ziff [22,23] for percolation can be used to simulate RSR on networks of up to millions—or even billions—of nodes.

For all the graphs we studied, RSR leads to a continuous agglomerative percolation transition (AP) where the largest cluster (node) outgrows all others both in terms of its mass and degree. We found three universality classes (critical trees, sparse ER graphs, and mean-field AP) for evolution of networks under RSR. For sparse ER graphs we derived the corresponding critical exponents numerically and found that the exponents obtained by analysis of the masses of the clusters are not different from the ones obtained by analyzing the degrees of the nodes. Since mass analysis can be performed much faster with the help of the NZ algorithm, we suggest that mass analysis may be better suited to extracting scaling properties of large networks. Regardless of the initial average degree of the ER graph, we found the same critical exponents for the percolation transition, within error. At late stages of RSR, graphs experience a regime in which they switch to a star structure for $b = 1$. For both ER graphs and critical trees this regime extends in the range $1 < N < N_0^{1/4}$.

For scale-free networks the transition is forced to $x_c = 1$. Hence, our data collapse methods for finding the critical exponents of scale-free networks are not as neat as for ER graphs, and this makes it hard to decide whether BA and ER networks are in the same universality class.

While the scaling behavior of critical trees under RSR is similar to graph behavior under the (quasi-)parallel

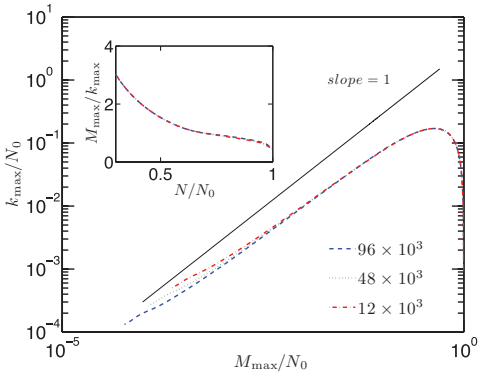

FIG. 23. (Color online) Log-log plot of normalized maximum degree k_{max}/N_0 vs M_{max}/N_0 for ER graphs with $\langle k\rangle^* = 2$ and size $N^* = 1.2 \times 10^5$. These are proportional to each other in a region close to criticality which extends over larger domains with increase of system size. While M_{max} increases with N_0 monotonically, k_{max} is confined to the current system size N and starts to decrease deep in the hub phase. The inset shows the ratio of maximal mass and degree on a linear scale. The curve is linear in the critical region.

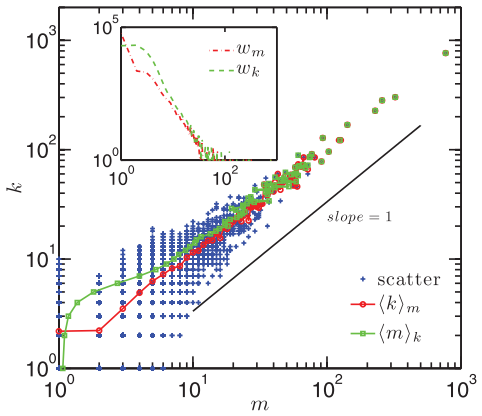

FIG. 24. (Color online) Scatter plot of masses and degrees of all clusters close to criticality. The data are obtained from one RSR trajectory of an ER graph of $N^* = 1.2 \times 10^5$ nodes, with $\langle k\rangle^* = 2$ at $N/N_0 = 0.688$. The red line with circles shows the average degree of clusters of a given mass, and the green line with squares shows the average masses of nodes with a given degree. The inset shows the number of clusters of a given mass (w_m) and the number of nodes of a given degree (w_k).

renormalization scheme studied by Radicchi *et al.* [18,19], the percolation transition revealed by our method in the early stages of the RG flow is not *seen* in their analysis. We conjecture that it exists also there in principle, but it would be very hard to study due to the coarseness of their RG flow observation. At final stages RSR and parallel schemes lead to the same qualitative picture, namely, a starlike structure for $b = 1$, but the scaling behavior and the corresponding exponents are different.

The simplicity of RSR as well as the fact that it is a percolation process both for networks and lattices makes it a useful tool for studying complex networks. For real-world networks finite-size scaling analysis is not generally possible since every network has a fixed (finite) size. However, even in that case high statistics of RSR flow and the efficiency of the algorithm make it possible to study the scaling properties of individual large networks.

ACKNOWLEDGMENTS

We thank Claire Christensen and Seung-Woo Son for numerous discussions and helpful comments.

APPENDIX: RELATIONSHIP BETWEEN MASS AND DEGREE OF NODES

Figure 23 depicts the linear relation between k_{max} and M_{max} in the critical region for ER graphs with $\langle k\rangle^* = 2$ and several system sizes. This shows that either of them can be used to extract renormalization flow properties near the transition. Since RSR can be simulated much faster if we only measure the mass-related quantities (instead of degree), we suggest that the RG analysis in the critical region can be confined to mass-related quantities. In the final stages of the flow ($N/N_0 \lesssim 0.3$), k_{max} decreases as it cannot exceed the number of nodes present in the system. M_{max}, on the other hand, increases monotonically till the end of the process where $M_{max} = N_0$.

The correlation between mass and degree of clusters close to criticality is shown in Fig. 24 for ER graphs of $N^* = 1.2 \times 10^5$ at $N/N_0 = 0.688$. Each point in the scatter plot shows one (m,k) pair in the whole network. Also shown are the average degree $\langle k\rangle_m$ of nodes of a given mass and the average mass $\langle m\rangle_k$ of clusters with a given degree. In the inset we show the number of clusters with a given mass, w_m, and the number of nodes with a given degree, w_k.

The average mass of nodes with degree one is close to 1, which means that most of them have not been hit by RSR, and the average degree of clusters with mass one is more than two, which means that the nodes that have not been hit by RSR keep their starting average degree. Since the two averages differ only for masses (degrees) less than 10, we suggest that one can use either of them to extract the properties of the percolation transition.

[1] R. Pastor-Satorras and A. Vespignani, Phys. Rev. E **63**, 066117 (2001).
[2] M. J. E. Newman, SIAM Rev. **45**, 167 (2003).
[3] S. Boccaletti, V. Latora, Y. Moreno, M. Chavez, and D. U. Hwang, Phys. Rep. **424**, 175 (2006).
[4] A.-L. Barabasi and R. Albert, Science **286**, 509 (1999).
[5] H. E. Stanley, *Introduction to Phase Transitions and Critical Phenomena* (Oxford University Press, Oxford, 1971).
[6] D. Stauffer and A. Aharony, *Introduction to Percolation Theory*, 2nd ed. (Taylor & Francis, London, 1994).

[7] S. Milgram, Psychol. Today **1**, 61 (1967).
[8] D. J. Watts and S. H. Strogatz, Nature (London) **393**, 440 (1998).
[9] C. Song, S. Havlin, and H. A. Makse, Nature (London) **433**, 392 (2005).
[10] C. Song, L. K. Gallos, S. Havlin, and H. A. Makse, J. Stat. Mech.: Theory Exp. (2007) P03006.
[11] C. Song, S. Havlin, and H. A. Makse, Nat. Phys. **2**, 275 (2006).
[12] S.-H. Yook, F. Radicchi, and H. Meyer-Ortmanns, Phys. Rev. E **72**, 045105(R) (2005).
[13] J. S. Kim, K. I. Goh, G. Salvi, E. Oh, B. Kahng, and D. Kim, Phys. Rev. E **75**, 016110 (2007).
[14] J. S. Kim, K. I. Goh, B. Kahng, and D. Kim, New J. Phys. **9**, 177 (2007).
[15] J. S. Kim, K. I. Goh, B. Kahng, and D. Kim, Chaos **17**, 026116 (2007).
[16] K.-I. Goh, G. Salvi, B. Kahng, and D. Kim, Phys. Rev. Lett. **96**, 018701 (2006).
[17] H. D. Rozenfeld, C. Song, and H. A. Makse, Phys. Rev. Lett. **104**, 025701 (2010).
[18] F. Radicchi, J. J. Ramasco, A. Barrat, and S. Fortunato, Phys. Rev. Lett. **101**, 148701 (2008).
[19] F. Radicchi, A. Barrat, S. Fortunato, and J. J. Ramasco, Phys. Rev. E **79**, 026104 (2009).
[20] K. J. Falconer, *The Geometry of Fractal Sets* (Cambridge University Press, Cambridge, 1985).
[21] G. Bizhani, V. Sood, M. Paczuski, and P. Grassberger, Phys. Rev. E **83**, 036110 (2011).
[22] M. E. J. Newman and R. M. Ziff, Phys. Rev. Lett. **85**, 4104 (2000).
[23] M. E. J. Newman and R. M. Ziff, Phys. Rev. E **64**, 016706 (2001).
[24] C. Christensen, G. Bizhani, S.-W. Son, M. Paczuski, and P. Grassberger, to appear in EPL December 2011.
[25] S.-W. Son, G. Bizhani, C. Christensen, P. Grassberger, and M. Paczuski, Europhys. Lett. **95**, 58007 (2011).
[26] S.-W. Son, C. Christensen, G. Bizhani, P. Grassberger, and M. Paczuski, Phys. Rev. E **84**, 040102(R) (2011).
[27] H. W. Lau, *et al.* (unpublished).
[28] M. Z. Bazant, Phys. Rev. E **62**, 1660 (2000).
[29] M. E. J. Newman, S. H. Strogatz, and D. J. Watts, Phys. Rev. E **64**, 026118 (2001).

A Letters Journal Exploring the Frontiers of Physics

September 2011

EPL, **95** (2011) 58007
doi: 10.1209/0295-5075/95/58007

www.epljournal.org

Irreversible aggregation and network renormalization

Seung-Woo Son[1(a)], Golnoosh Bizhani[1], Claire Christensen[1], Peter Grassberger[1,2] and Maya Paczuski[1]

[1] *Complexity Science Group, University of Calgary - Calgary T2N 1N4, Canada*
[2] *FZ Jülich - D-52425 Jülich, Germany, EU*

received 28 April 2011; accepted in final form 22 July 2011
published online 25 August 2011

PACS 89.75.Hc – Networks and genealogical trees
PACS 02.10.Ox – Combinatorics; graph theory
PACS 05.70.Ln – Nonequilibrium and irreversible thermodynamics

Abstract – Irreversible aggregation is revisited in view of recent work on renormalization of complex networks. Its scaling laws and phase transitions are related to percolation transitions seen in the latter. We illustrate our points by giving the complete solution for the probability to find any given state in an aggregation process $(k+1)X \to X$, given a fixed number of unit mass particles in the initial state. Exactly the same probability distributions and scaling are found in one-dimensional systems (a trivial network) and well-mixed solutions. This reveals that scaling laws found in renormalization of complex networks do not prove that they are self-similar.

Droplets beget rain, goblets coagulate to make butter or cream, and dust particles stick together to form aggregates that can eventually coalesce into planets. At the microscopic level, irreversible aggregation of atoms and molecules creates many familiar forms of matter such as aerosols, colloids, gels, suspensions, clusters and solids [1]. Almost a century ago, Smoluchowski proposed a theory based on rate equations to describe processes governed by diffusion, collision and irreversible merging of aggregates [2]. The theory predicts how many small and large clusters exist at any given time and yields a mass distribution that depends on certain details such as the initial conditions, reactions present, relative rates, the presence or absence of spatial structure, etc. A key interest to physicists has been to derive scaling laws that characterize different universality classes ([3], and references therein).

By contrast, wide interest in complex networks [4–7] has emerged recently. Vast applications to physics, computer science, biology, and sociology ([8–10], and references therein) continue to be vigorously investigated. An important question is whether or not complex networks exhibit self-similarity at different length scales and if they can be grouped into universality classes on that basis. Renormalization schemes for networks were proposed [11–14] to address this question. Scaling of the mass or degree distribution of the renormalized nodes was used to argue that many complex networks are self-similar. The semi-sequential renormalization group (RG) flow underlying the box covering of [11–14] was studied carefully in [15,16], where it was found that scaling laws may be related to an "RG fixed point" which was observed for a wide variety of networks. A convenient, fully sequential scheme called random sequential renormalization (RSR) was introduced [17]. At each RSR step, one node is selected at random, and all nodes within a fixed distance ℓ of it are replaced by a single super-node.

We point out a simple mapping between RSR and irreversible aggregation on any graph. Hence any conclusion drawn for one process holds also for the other. Indeed, a local coarse-graining step to produce a new super-node represents one aggregation event, where a "molecule" aggregates with all its neighbors within distance ℓ to produce a new cluster. Exact combinatorial analysis in one dimension without diffusion reveals that even this trivial network exhibits scaling laws for the cluster mass distribution under RSR —with exponents that depend on ℓ. Consequently, and somewhat counterintuitively, self-similarity observed in RSR and similar network renormalization schemes cannot be used to prove that complex networks are themselves self-similar. Instead scaling laws arise due to a percolation transition in irreversible aggregation.

The correspondence between aggregation and renormalization is relevant for any model with stochastic coarse-graining of a network. For instance, the theory of space and time "Graphity" [18,19], based on loop quantum

(a) E-mail: swson@ucalgary.ca

gravity, involves a stochastic coarsening similar (albeit more structured) to RSR. Hence the critical point of aggregation may also be relevant in that and related cases. The breakdown of conventional universality, where critical exponents depend on the microscopic scale of coarse-graining, ℓ, seems to present a dilemma for theories based on stochastic coarse-graining of a network to arrive at, *e.g.*, a universal large-scale theory of gravity.

In order to demonstrate these points, here we consider irreversible aggregation $(k+1)X \to X$, where a randomly picked cluster coalesces with k neighbors. For even $k = 2\ell$ this corresponds precisely to RSR on a 1-d chain with coarsening range ℓ. The mass of the newly formed cluster is the sum of the $(k+1)$ masses. We assume that the "target" cluster is picked with uniform probability from all clusters. Other choices will be discussed elsewhere [20].

Let us start with the model defined on a ring, *i.e.*, with periodic boundary conditions. Initially, N_0 sites labelled by $i \in [1, \ldots, N_0]$ are each occupied by a particle of mass $m = 1$. Time can be either discrete or continuous, but we demand that two events never happen simultaneously. Hence events, ranked by increasing time, are denoted by positive integer values t. For each event, particles coagulate to form clusters of mass $m > 1$. More precisely, an event consists of picking a random cluster with uniform probability and joining it with k clusters to its immediate right, using periodic boundary conditions. We note that no diffusion procedure is involved here. For k even, the same results are found if we aggregate clusters symmetrically. After t events, $N_t = N_0 - kt$ clusters exist. Our main result is the probability to find any sequence of adjacent cluster masses $p_{N_t}^{N_0}(m_1, m_2 \ldots m_{N_t})$ —where a cluster of mass m_1 is followed by a cluster of mass m_2, etc., moving clockwise (see fig. 1). We start with the single-cluster mass probability.

Cluster masses are restricted to any $m \equiv 1 \pmod{k}$. Defining $m - 1 = ks$, the integer s is the number of events needed to make the cluster of mass m. As depicted in fig. 1, we can represent any realization of the process by a forest of N_t rooted trees with N_0 leaves and t internal nodes. Each tree α has s_α internal nodes, with $\sum_\alpha s_\alpha = t$. We simplify the notation by N for N_t.

Let $\pi_N^{N_0}(m)$ denote, for fixed k (the dependence on k is not written explicitly in the following), the probability that a cluster of mass m has its leftmost member at site $i \in [1, \ldots, N_0]$ after t events. The probability that any of the N clusters picked at random has mass m is then

$$p_N^{N_0}(m) = \frac{N_0}{N}\, \pi_N^{N_0}(m), \tag{1}$$

because there are N_0 choices for i and the chance to pick that particular cluster, given that it exists, is $1/N$. Since events occur completely at random, each *history* occurs with equal probability. The term "history" refers to a fixed forest, which includes a fixed temporal order of events. Thus $\pi_N^{N_0}(m)$ is equal to the number of histories leading to a final configuration with a cluster of mass m starting at position i, divided by all possible histories leading to N clusters. The latter is equal to

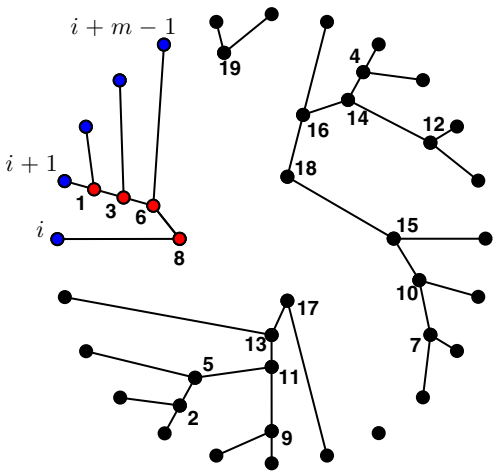

Fig. 1: (Color online) Illustration of aggregation on a ring with $k = 1$, $N_0 = 24$, and $N = 5$. The tree in color corresponds to a cluster of mass $m = 5$. It has five leaves (blue) and four internal nodes (red). Its leaves start at site i and end at site $i + m - 1$. The numbers beside internal nodes correspond to the time order when coalescence occurs.

$$n_{\text{hist,tot}} = \overbrace{N_0 \times (N_0 - k) \times \ldots (N + k)}^{t}, \tag{2}$$

where each of the t factors equals the number of choices for the next event. Using Pochhammer k-symbols or, equivalently, generalized rising factorials [21–24], this can be written as $n_{\text{hist,tot}} = (N + k)_{t,k}$. Similarly, the number of histories leading to a cluster of size m starting at a fixed position i is

$$n_{\text{hist,cluster}} = \overbrace{(m - k)(m - 2k) \times \ldots 1}^{s} = (1)_{s,k} \tag{3}$$

and the number of histories for the remaining $N - 1$ clusters is

$$\begin{aligned} n_{\text{hist,rest}} &= (N_0 - m - k)(N_0 - m - 2k) \times \ldots (N - 1) \\ &= (N - 1)_{t-s,k}. \end{aligned} \tag{4}$$

So far we have not included the number of choices associated with different time orderings for the s events in the cluster and $(t - s)$ events in the rest of the forest. The number of different time orderings is given by

$$n_{\text{orderings}} = \binom{t}{s}. \tag{5}$$

Combining eqs. (1)–(5), we obtain

$$\begin{aligned} p_N^{N_0}(m) &= \frac{N_0}{N} \binom{t}{s} \frac{(N-1)_{t-s,k}(1)_{s,k}}{(N+k)_{t,k}} \\ &= \binom{t}{s} \frac{(N-1)_{t-s,k}(1)_{s,k}}{(N)_{t,k}}. \end{aligned} \tag{6}$$

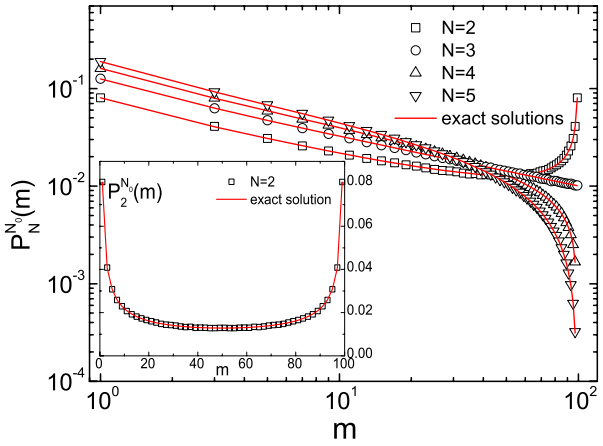

Fig. 2: (Color online) Cluster size distributions after $t=50$ events for $k=2$, for different values of N averaged over 10^6 realizations compared to exact results. The large-size behavior changes from increasing to decreasing power law at $N=k+1$. Inset: the discrete arcsine law found for $N=2$.

This result can be further simplified into beta functions or, more conveniently, k-beta functions (see, *e.g.*, [22]),

$$B_k(x,y)=\frac{1}{k}B\left(\frac{x}{k},\frac{y}{k}\right),$$

giving a remarkably simple final result

$$p_N^{N_0}(m)=\binom{t}{s}\frac{B_k(N_0-m,m)}{B_k(N-1,1)}. \tag{7}$$

We make a number of observations: i) For $k=1$ the process simply maps to *bond percolation* on a 1-d ring. For $N=2$, the mass distribution is uniform over the entire range $m\in[1,N_0-1]$. For $N>2$, the distribution is proportional to the $(N-2)^{nd}$ factorial power $((N_0-m-1)(N_0-m-2)\cdots(N_0-m-N+2))$. ii) For $N=2$ and any $k\geqslant 1$, $p_N^{N_0}(m)$ is symmetric under the exchange $m\leftrightarrow N_0-m$. iii) For $N=2$ and $k=2$ we obtain an equation formally identical to Spitzer's *discrete arcsine law* for fluctuations of random walks [25]. iv) Asymptotic power laws for $N_0\to\infty$ can be determined using Stirling's formula. If N is fixed and both m and $(N_0-m)\to\infty$,

$$p_N^{N_0}(m)\sim\frac{(t-s)^{\frac{N-1}{k}-1}}{s^{1-\frac{1}{k}}}. \tag{8}$$

For small masses, this gives a decreasing power law with exponent $-1+1/k$. For $N=k+1$, the power law $p_N^{N_0}(m)\sim s^{-1+1/k}$ holds up to the largest possible value, $m=N_0-N+1$, and the cutoff is a step function. For $m/N_0\to 1$ different power laws appear if $N\neq k+1$, and the sign of the exponent changes at $N=k+1$. For $N<k+1$, the distribution has a peak at $m/N_0\to 1$, while it goes to zero for $N>k+1$. These scaling laws are illustrated for $k=2$ in fig. 2. v) The scaling laws found for $m\ll N_0$ are identical to those obtained by Krapivsky [26] for the well-mixed case, even no diffusion is considered. However, the behavior for $m/N_0\to 1$ given in [26] does not agree with our result. vi) The probability $p_N^{N_0}(m)$ satisfies a number of recursion relations:

$$p_N^{N_0}(m+k) = \frac{m(N_0-m-N+1)}{(m+k-1)(N_0-m-k)}\,p_N^{N_0}(m),$$

$$p_{N+k}^{N_0}(m) = \frac{N(N_0-m-N+1)}{(N-1)(N_0-N)}\,p_N^{N_0}(m).$$

A third *nonlinear* recursion relation is given later.

Joint distributions for masses of adjacent clusters can also be found. We denote by $p_N^{N_0}(m_1,m_2)$ the probability to find a cluster of mass m_1 followed immediately to the right by a cluster of mass m_2. This is nonzero only if $m_1=1+s_1k$ and $m_2=1+s_2k$, where s_α is the number of events needed to form a cluster of mass m_α. By the same arguments that led to eq. (6) we get

$$p_N^{N_0}(m_1,m_2)=\binom{t}{s_0,s_1,s_2}\frac{(N-2)_{s_0,k}(1)_{s_1,k}(1)_{s_2,k}}{(N)_{t,k}},$$

where $s_0=t-\sum_{\beta=1}^{\alpha}s_\beta$ and the first factor is the multinomial coefficient instead of the binomial coefficient. When $\alpha=2$, it is a trinomial coefficient that counts the number of ways in which the three sequences of events —for the two clusters considered, and for all $(N-2)$ other clusters— can be interleaved in a single history.

For any $1\leqslant\alpha\leqslant N-1$ the joint probability distribution for α consecutive, adjacent clusters is a product of a multinomial coefficient and $(\alpha+1)$ Pochhammer k-symbols, divided by the Pochhammer k-symbol related to the total number of possible histories given N_0 initial particles. Defining again s_0 as the number of events in all clusters except the first α ones, we can write the result compactly as

$$p_N^{N_0}(m_1,\ldots,m_\alpha)=\binom{t}{s_0,\ldots,s_\alpha}\frac{(N-\alpha)_{s_0,k}\prod_{\beta=1}^{\alpha}(1)_{s_\beta,k}}{(N)_{t,k}}. \tag{9}$$

In particular, this can also be done for the joint distribution for all N masses by setting $\alpha=N-1$. The resulting expression is then manifestly invariant under any permutations of N numbers $(m_1,\ldots,m_N)$. Hence the N-cluster probability is independent of the spatial ordering of the clusters. While there are obvious correlations between the mass values (the sum of all cluster masses must be N_0), there are *no spatial correlations*.

We now consider a line of N_0 particles with open boundaries. Again, aggregation events consist of a random choice of a cluster, followed by its amalgamation with its k nearest neighbors to the right. The target cluster must be at least k steps away from the rightmost boundary. Following the same arguments leads immediately to eq. (9) for $\alpha=N-1$, showing that the two models lead to precisely the same statistics.

The absence of spatial correlations indicates that the same dynamics might result for the well-mixed case. Now we start with a bucket containing N_0 balls, each of unit mass. An event consists of taking $k+1$ balls out of the bucket, merging them together, and returning the new ball to the bucket. The $k+1$ balls are chosen completely at random, independently of their masses.

The single-cluster mass distribution for the well-mixed model can be obtained using the same strategy as before, but the details are quite different. Consider the total number of histories. Since events now correspond to choosing any $k+1$ balls out of $N_0 - kt$ balls, we have, instead of the Pochhammer k-symbol, a product of binomial coefficients,

$$n_{\mathrm{hist,tot}} = \overbrace{\binom{N_0}{k+1}\binom{N_0-k}{k+1}\cdots\binom{N+k}{k+1}}^{t}. \qquad (10)$$

The expressions for $n_{\mathrm{hist,cluster}}$ and $n_{\mathrm{hist,rest}}$ are analogous, with the factors $(m-jk)$ (respectively, (N_0-m-jk)) in eq. (3) (respectively, (4)) replaced by binomial coefficients. The number of time orderings $n_{\mathrm{orderings}}$ is exactly the same as before, but the first factor N_0/N in eq. (6) has to be replaced by $\frac{1}{N}\binom{N_0}{m}$. Putting all these things together, many cancellations take place, leading exactly to eq. (7). This argument can be similarly extended to get the full N-particle distribution function, obtaining exactly the same result as before, for any k.

The time-reversed process of aggregation is fragmentation. When considering the fragmentation process associated with any of these models, we have to carefully evaluate fragmentation rates. Assuming uniform rates would not lead to all time-reversed histories having the same probability. Indeed the fraction of all mergers associated with making a cluster of mass m' is $(s'/t) = (m'-1)/(N_0-N)$, which must equal the probability that an existing cluster of mass m' will fragment at the next step in the time-reversed process. If it does, then for consistency its fragmentation products must have a mass distribution given by $p_{k+1}^{m'}(m)$. A quadratic recursion relation for $p_{N+k}^{N_0}(m)$ can then be obtained by considering the likelihood of all fragmentation events in a configuration of N clusters, with m being the mass of one of the resulting $k+1$ fragmentation products. The relation is

$$p_{N+k}^{N_0}(m) = {\sum_{m'=m+k}^{N_0-N+1}}' \frac{N(m'-1)p_N^{N_0}(m')p_{k+1}^{m'}(m)}{N_0-N},$$

where the prime on the summation symbol indicates that m' must increase in steps of k.

In summary, we derived complete solutions for the probability to find any given state in three models —well-mixed solutions, particles on a ring reacting with their k nearest neighbors, and the same reaction for particles on a line with open boundaries— and show that these solutions are precisely the same. The fact that we could solve exactly a one-dimensional model without detailed balance might seem surprising since such models are in general not solvable. It stems from the fact that spatial correlations, although *a priori* not excluded, are in fact absent. Related to this is our finding that the well-mixed models have exactly the same solutions. Our method can be used to solve the model where the target cluster is picked with a probability proportional to its mass [20]. Perhaps generalizations of these observations hold true for more complicated models, in which case weighted path integrals would replace sums over histories.

We have pointed out a direct mapping between irreversible aggregation and RSR. The latter was motivated by claims that one can define finite fractal dimensions for real networks [11], using similar but more complicated and ambiguous schemes. Results for RSR with $\ell = 1$ on various graphs (critical trees [17], Erdös-Rényi and Barabási-Albert networks [27], and regular lattices [28]) concur with our present conclusions for $k = 2$. Apart from studying a system that is sufficiently simple to be exactly solvable and that is obviously not fractal, here we presented results for $\ell > 1$, showing that scaling laws depend in a nontrivial way on ℓ (k). Results for the elementary network (a one-dimensional line) examined analytically here proves that scaling under stochastic network renormalization arises from an underlying percolation transition in aggregation and does not prove fractality or self-similarity of the underlying graph.

Our mapping suggests that the critical behavior of aggregation may also turn up in "Graphity" [18,19] or related models, where geometry, gravity, and matter emerge through an aggregation process of an underlying graph. "Geometrogenesis" is the complementary process of infinite cluster formation in irreversible aggregation. In that case, we expect that a valid microscopic model (unlike the one-dimensional lattice studied here) exhibits large-scale scaling properties that are invariant with respect to the coarse-graining scale of renormalization. This would provide a test to select physically reasonable theories [29].

REFERENCES

[1] Zangwill A., *Nature*, **411** (2001) 651.
[2] von Smoluchowski M., *Z. Phys. Chem.*, **92** (1917) 129.
[3] Leyvraz F., *Phys. Rep.*, **383** (2003) 95.
[4] Strogatz S. H., *Nature*, **410** (2001) 268.
[5] Albert R. and Barabási A.-L., *Rev. Mod. Phys.*, **74** (2002) 47.
[6] Dorogovtsev S. N. and Mendes J. F. F., *Adv. Phys.*, **51** (2002) 1079.
[7] Newman M. E. J., *SIAM Rev.*, **45** (2003) 167.
[8] Dorogovtsev S. N., Goltsev A. V. and Mendes J. F. F., *Rev. Mod. Phys.*, **80** (2008) 1275.
[9] Barabási A.-L., *Science*, **24** (2009) 412.

[10] Barabási A.-L., Gulbahce N. and Loscalzo J., *Nat. Rev. Genet.*, **12** (2011) 56.
[11] Song C., Havlin S. and Makse H., *Nature*, **433** (2005) 392.
[12] Goh K.-I., Salvi G., Kahng B. and Kim D., *Phys. Rev. Lett.*, **96** (2006) 018701.
[13] Kim J. S. *et al.*, *Phys. Rev. E*, **75** (2007) 16110.
[14] Rozenfeld H., Song C. and Makse H., *Phys. Rev. Lett.*, **104** (2010) 25701.
[15] Radicchi F., Ramasco J. J., Barrat A. and Fortunato S., *Phys. Rev. Lett.*, **101** (2008) 148701.
[16] Radicchi F., Barrat A., Fortunato S. and Ramasco J. J., *Phys. Rev. E*, **79** (2009) 26104.
[17] Bizhani G., Sood V., Paczuski M. and Grassberger P., *Phys. Rev. E*, **83** (2011) 036110.
[18] Konopka T., Markopoulou F. and Smolin L., e-print arXiv:hep-th/0611197v1 (2006).
[19] Hamma A. *et al.*, *Phys. Rev. D*, **81** (2010) 104032.
[20] Son S.-W. *et al.*, in preparation (2011).
[21] Normand J., *J. Phys. A*, **37** (2004) 5737.
[22] Díaz R. and Pariguan E., *Divulg. Mat.*, **15** (2007) 179.
[23] Pitman J. and Picard J., *Combinatorial Stochastic Processes* (Springer) 2006.
[24] Kingman J., *J. Appl. Probab.*, **19** (1982) 27.
[25] Spitzer F., *Principles of Random Walk* (Springer Verlag) 2001.
[26] Krapivsky P., *J. Phys. A*, **24** (1991) 4697.
[27] Bizhani G. *et al.*, in preparation (2011).
[28] Christensen C. *et al.*, e-print arXiv:1012.1070 (2010).
[29] Paczuski M. *et al.*, in preparation (2011).

RAPID COMMUNICATIONS

PHYSICAL REVIEW E **84**, 040102(R) (2011)

Exact solutions for mass-dependent irreversible aggregations

Seung-Woo Son,[1] Claire Christensen,[1] Golnoosh Bizhani,[1] Peter Grassberger,[1,2] and Maya Paczuski[1]

[1]*Complexity Science Group, University of Calgary, Calgary T2N 1N4, Canada*

[2]*Forschungszentrum Jülich, D-52425 Jülich, Germany*

(Received 31 August 2011; published 31 October 2011)

We consider the mass-dependent aggregation process $(k+1)X \to X$, given a fixed number of unit mass particles in the initial state. One cluster is chosen proportional to its mass and is merged into one, either with k neighbors in one dimension, or—in the well-mixed case—with k other clusters picked randomly. We find the same combinatorial exact solutions for the probability to find any given configuration of particles on a ring or line, and in the well-mixed case. The mass distribution of a single cluster exhibits scaling laws and the finite-size scaling form is given. The relation to the classical sum kernel of irreversible aggregation is discussed.

DOI: 10.1103/PhysRevE.84.040102 PACS number(s): 05.70.Ln, 89.75.Da, 89.75.Hc

Recently the theory of irreversible aggregation was revisited in view of renormalization of complex networks [1]. In Ref. [1], a simple mapping between random sequential renormalization (RSR) [2,3] and irreversible aggregation [4] was pointed out, where a local random renormalization step to produce a new "supernode" in complex networks corresponds to one aggregation event of "molecules." Exact combinatorial analyses, both in one dimension (without diffusion) and in the well-mixed case, gave the same scaling law of cluster mass distribution. The corresponding exponent only depends on k, the number of interacting neighbors [1]. This RSR procedure corresponds to the "constant" kernel of irreversible aggregation (one of three well-known "classical" kernels—constant, sum, and product kernels [4]). In this Rapid Communication, we show the relation between mass-dependent RSR and irreversible aggregation with the sum kernel. Applying the same combinatorial technique of Ref. [1], we find the exact solutions for mass-dependent irreversible aggregation as well.

Here we consider models governed by the reaction $(k+1)X \to X$, where a cluster is picked randomly, in proportion to its mass, after which it coalesces with k other clusters. In the case of one-dimensional models these are k neighbors, while they are k other clusters chosen randomly in the case of well-mixed systems. In both cases, the other clusters are chosen independent of their masses. The mass of the newly formed cluster is the sum of the $(k+1)$ masses. For one-dimensional models, both a ring with periodic boundary condition and a line with open boundary condition are considered. Reactions are allowed only if there is a sufficient number k of available clusters.

First, let us consider the model defined on a "ring." Initially, N_0 particles of unit mass ($m=1$) are placed on ringlike beads (see Fig. 1). Each particle is labeled by $i \in [1,\ldots,N_0]$. At each time, one cluster is picked in proportion to its mass, and is subsequently merged with its k right neighbors into one big cluster having a mass equal to the sum of the $(k+1)$ masses. Cluster masses are therefore restricted to $m \equiv 1 (\mathrm{mod}\, k)$. This can be written as $m-1=ks$, where s is the number of aggregation events needed to make a cluster of mass m. Similarly the number of clusters at any time t is given by $N=N_0-kt$, where time t is denoted by positive integers representing the total number of aggregation events. We do not allow two events to happen simultaneously in this study. Otherwise they can happen either at regular intervals, intermittently, or according to a Poisson process.

To find the probability that any of the N clusters picked at random has mass m resulting from s aggregation events, we follow an approach similar to the one introduced in Ref. [1]. The crucial observation that makes the analysis simple is that picking clusters according to their mass is equivalent to picking *sites* with uniform probability, since a cluster of mass m occupies m sites. Let i be any site (e.g., $i=1$), and let $\pi_N^{N_0}(m)$ be the probability that a cluster of mass m starts at this site and occupies the sites $(i,i+1,\ldots,i+m-1)$. The probability that any of the N clusters picked at random has mass m after t events is then

$$p_N^{N_0}(m) = \frac{N_0}{N}\pi_N^{N_0}(m), \tag{1}$$

and

$$\pi_N^{N_0}(m) = \binom{t}{s}\frac{n_{\mathrm{cluster}} n_{\mathrm{rest}}}{n_{\mathrm{total}}}, \tag{2}$$

where n_{cluster} is the number of possible histories of aggregation events $(i_1,i_2,\ldots,i_s)$ leading to a cluster of mass m, n_{rest} is the number of possible ways to form the other $(N-1)$ clusters, and n_{total} is the total number of histories for t merging events. The binomial coefficient $\binom{t}{s}$ corresponds to the number of choices associated with different time orderings for the s events in the cluster of mass m and the $(t-s)$ events in the rest of the clusters.

The total number of all histories involving t events is simply

$$n_{\mathrm{total}} = N_0^t. \tag{3}$$

This is to be contrasted to the number of histories $n_N^{[1,N_0]}$ that lead to the first cluster starting at $i=1$ and the Nth ending at N_0. A somewhat more involved argument gives

$$n_N^{[1,N_0]} = N N_0^{t-1}. \tag{4}$$

The number of histories leading to a single cluster of mass m covering the sites of interval $[1,m]$ is thus

$$n_{\mathrm{cluster}} = n_1^{[1,m]} = m^{s-1}, \tag{5}$$

while

$$n_{\mathrm{rest}} = n_{N-1}^{[1,N_0-m]} = (N-1)(N_0-m)^{t-s-1}. \tag{6}$$

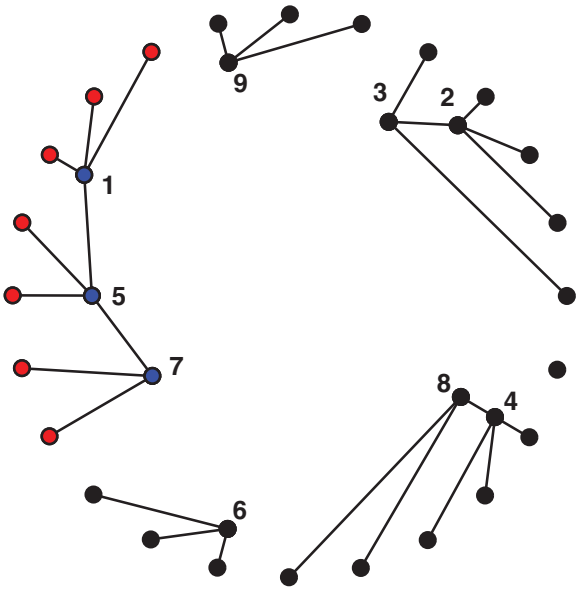

FIG. 1. (Color online) Illustration of aggregation on a ring with $k = 2$, $N_0 = 24$, and $N = 6$. The tree in color corresponds to a cluster of mass $m = 7$. It has seven leaves (red/light gray) and three internal nodes (blue/dark gray). The numbers beside internal nodes correspond to the time when coalescence occurs.

Combining Eqs. (1)–(6), we finally obtain

$$p_N^{N_0}(m) = \frac{N-1}{N}\binom{t}{s}\frac{m^{s-1}(N_0-m)^{t-s-1}}{N_0^{t-1}}. \tag{7}$$

For this mass-dependent aggregation process, we can also work out the joint probability distributions for masses of adjacent clusters. We denote by $p_N^{N_0}(m_1,m_2)$ the probability to find a cluster of mass m_1 followed immediately to the right by a cluster of mass m_2. This is nonzero only if $m_1 = ks_1 + 1$ and $m_2 = ks_2 + 1$, where s_α is the number of aggregation events needed to form a cluster of mass m_α. By the previous arguments, we get

$$p_N^{N_0}(m_1,m_2) = \frac{N-2}{N}\binom{t}{s_0,s_1,s_2}\frac{m_1^{s_1-1}m_2^{s_2-1}m_0^{s_0-1}}{N_0^{t-1}},$$

where $s_0 = t - \sum_{\beta=1}^{\alpha} s_\beta$ and $m_0 = N_0 - \sum_{\beta=1}^{\alpha} m_\beta$. It is interesting to note that this joint probability properly holds the following relation:

$$p_N^{N_0}(m_1,m_2) = p_N^{N_0}(m_1)p_{N-1}^{N_0-m_1}(m_2).$$

For any $1 \leqslant \alpha \leqslant N-1$, the joint probability distribution for α consecutive adjacent clusters is given by

$$p_N^{N_0}(m_1,\ldots,m_\alpha) = \frac{N-\alpha}{N}\frac{\mathcal{T}[t,\{s\},\alpha+1]\prod_{\beta=0}^{\alpha} m_\beta^{s_\beta-1}}{N_0^{t-1}}, \tag{8}$$

where we used the multinomial coefficient

$$\mathcal{T}[t,\{s\},\alpha+1] = \binom{t}{s_0,\ldots,s_\alpha}.$$

In particular, this can be done for the joint distribution for all N masses by setting $\alpha = N-1$. The resulting expression is always invariant under any *permutations* of N numbers $(m_1,\ldots,m_N)$, as was the case with mass-independent aggregation [1]. Hence the N-cluster probability is independent of the spatial ordering of the clusters. Therefore, there are *no spatial correlations*, even though there are obvious correlations between the masses at any given time. For this reason [and as verified in detail using Eq. (4) instead of Eq. (3)], the joint probability for N masses on a line, i.e., a one-dimensional system with open boundaries, is also given as Eq. (8), showing that the two models lead to the same statistics for any α.

The absence of spatial correlations indicates that the same dynamics might also result from the well-mixed case. To check this, we now start with a bucket containing N_0 balls, each of unit mass. An event consists of first picking one ball with probability proportional to its mass and then choosing k balls out of the bucket, independent of their masses. The balls are merged and a new ball, having a mass equal the sum of the masses of its $(k+1)$ constituents, is returned to the bucket. This process repeats until N clusters remain.

The single-cluster mass distribution for the well-mixed model can be obtained using the same strategy as before. Since events now correspond to choosing one ball with a mass-weighted probability, and k balls out of $(N_0 - kt - 1)$ balls randomly, we have a t power of N_0 and a product of binomial coefficients

$$\begin{aligned} n_{\text{total}} &= N_0\binom{N_0-1}{k}\cdots N_0\binom{N+k-1}{k} \\ &= \frac{N_0^t}{(k!)^t}\frac{(N_0-1)!}{(N-1)!} = \frac{N_0^{t-1}}{(k!)^t}\frac{N_0!}{(N-1)!}. \end{aligned} \tag{9}$$

The expressions for n_{cluster} and n_{rest} are analogously

$$n_{\text{cluster}} = \frac{m^{s-1}}{(k!)^s}m!, \tag{10}$$

$$n_{\text{rest}} = \frac{(N_0-m)^{t-s-1}}{(k!)^{t-s}}\frac{(N_0-m)!}{(N-2)!}. \tag{11}$$

The number of time orderings is exactly the same as before, but the first factor N_0/N in Eq. (1) has to be replaced by $\frac{1}{N}\binom{N_0}{m}$. Putting all these considerations together, many cancellations take place, leading exactly to Eq. (7) again. This argument can be similarly extended to get the full N-particle distribution function, obtaining exactly the same result as Eq. (8) for any k and α.

Let us look at the characteristics of the solutions. Even though the composition principle is the same as that of mass-independent aggregation in Ref. [1], the final solution and the characteristics are quite different. First, cluster size distributions at several different times are shown in Fig. 2 for $N_0 = 100$ and $k = 2$. The symbols indicate the numerical simulation results over 10^6 realizations and the solid lines are the exact solutions of Eq. (7). The tail region corresponding to large cluster sizes changes from a fast exponential decay to an increasing power law as the merging process approaches termination. The turning point is at $N \sim \sqrt{N_0}$. When $N = 2$, since the sum of the two cluster sizes is always N_0, the distribution $p_N^{N_0}(m)$ is symmetric under the exchange

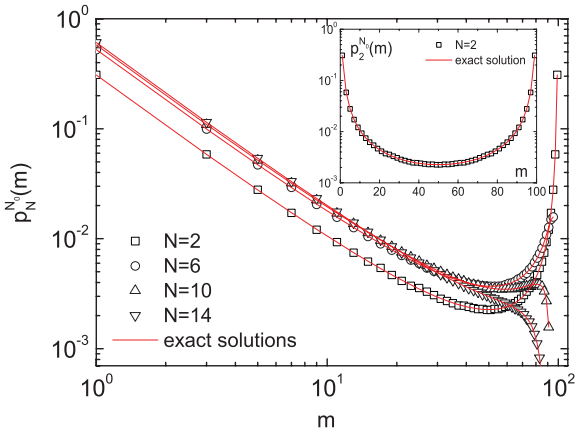

FIG. 2. (Color online) Cluster size distributions after $t = 49$ ($N = 2$) events for $k = 2$, for different values of N averaged over 10^6 realizations compared to exact results. The power-law slope of small m is $-3/2$ independent of k. The large size behavior changes from an increasing power law to a decreasing one at $N \sim \sqrt{N_0}$. The inset shows the symmetric distribution for $N = 2$.

$m \leftrightarrow N_0 - m$ for any k. The symmetric distribution for $N = 2$ is shown in the inset of the Fig. 2.

When $N_0 \to \infty$, asymptotic power laws can be determined using Stirling's formula. If N is fixed and both m and $(N_0 - m) \to \infty$, one obtains the scaling form

$$p_N^{N_0}(m) \sim N_0^{-\frac{3}{2}} \left[\frac{m}{N_0}\left(1-\frac{m}{N_0}\right)\right]^{-\frac{3}{2}} e^{-\frac{N^2}{kN_0}\frac{m}{N_0}(1-\frac{m}{N_0})^{-1}}$$
$$\sim N_0^{-\frac{3}{2}} f\left(\frac{m}{N_0}, \frac{N}{\sqrt{N_0}}\right). \quad (12)$$

For small masses, this gives a decreasing power law, with exponent $-3/2$, independent of k. Interestingly, this is very different from mass-independent aggregation, for which the analogous exponent depends on k and is equal to $-1 + 1/k$ [1]. The exponent $-3/2$ is the same as that for the aggregation with the sum kernel of the irreversible aggregation obtained in Ref. [5]. Indeed, the rate equation for the current aggregation model in mean-field theory is the same as for the sum kernel [4,5]. For the $k = 1$ case, the rate equation is simply

$$\Delta p_m = \sum_{m'=1}^{m} m' p_{m'} p_{m-m'} - p_m \sum_{m'=1}^{\infty} (m + m') p_{m'}$$
$$= \frac{m}{2} \sum_{m'=1}^{m} p_{m'} p_{m-m'} - (m + \bar{m}) p_m, \quad (13)$$

where p_m denotes $p_N^{N_0}(m)$ to make the equation more concise, and where $\bar{m}$ means the mean cluster size. Equation (13) is the same as the rate equation for the sum kernel in Refs. [4] and [5]. The behavior for large m is different, however, and is not described by mean-field theory.

According to Eq. (12), $N_0^{\frac{3}{2}} p_N^{N_0}(m)$ should be a function of m/N_0 only for fixed

$$y = \frac{N^2}{kN_0} \quad (14)$$

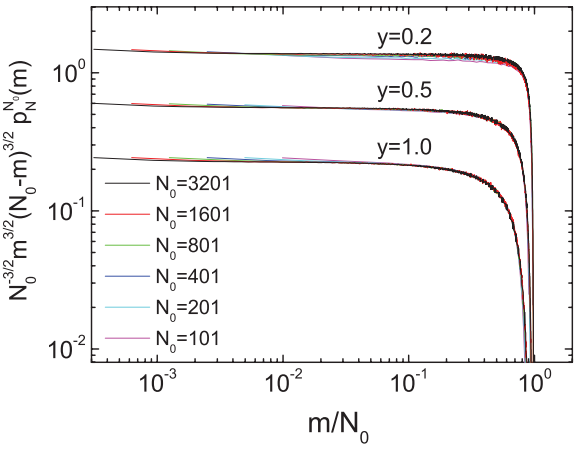

FIG. 3. (Color online) Finite-size scaling collapses for different y and fixed $k = 2$. Collapse lines for $y = 0.2$ and $y = 1.0$ are shifted up and down to make them distinguishable from other collapse lines.

and for $N \ll N_0, N_0 - m$. The resulting data collapse is shown in Fig. 3, where we also factored out a power of m/N_0 to make the curves less steep. Notice that N and N_0 are related by $N \equiv N_0 (\mathrm{mod}\, k)$, which implies that the values of y used in this plot are not strictly constant but deviate slightly from their nominal values for small N_0, which causes the deviation from a perfect collapse for $y = 0.2$. Even for different values of k, this scaling function works, as can be seen in Fig. 4, where the scaling collapses for three cases $k = 1$, 2, and 4, are shown. Surprisingly, this means that the process of choosing a cluster proportional to its mass in conjunction with choosing two clusters at random for $k = 2$ is asymptotically the same as repeating the merging process for $k = 1$ twice in the sense of the scaled mass.

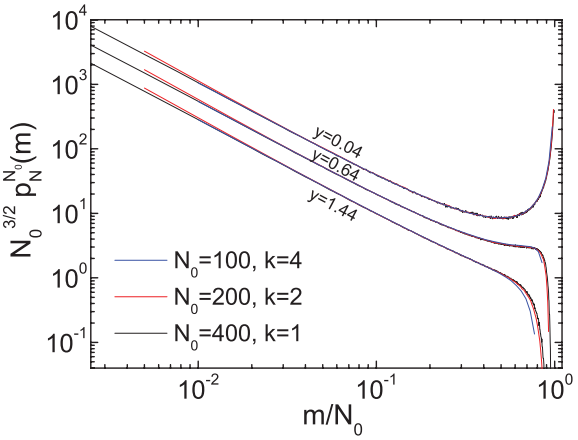

FIG. 4. (Color online) Finite-size scaling collapses for different k. In order to check the scaling collapses for different k, kN_0 is fixed at 400 and $N = 4$, 16, and 24, which correspond to $y = 0.04$, 0.64, and 1.44. Collapse lines for $y = 0.04$ and $y = 1.44$ are shifted up and down to make them distinguishable from each other.

The probability $p_N^{N_0}(m)$ satisfies the following recursion relation:

$$p_{N+k}^{N_0}(m) = A \sum_{m'=m+k}^{N_0-N+1}{}' \frac{m'-1}{m'} p_N^{N_0}(m') p_{k+1}^{m'}(m), \quad (15)$$

with

$$A = \frac{N_0 N(k+1)}{(N_0-N)(N+k)}, \quad (16)$$

where the prime on the summation symbol indicates that m' must increase in steps of k. Interestingly this quadratic recursion relation corresponds to the time-reversed process of aggregation, i.e., *fragmentation*. As with the quadratic recursion relation of mass-independent aggregation [1], the mass distribution at $N+k$ is given by the product of the mass distribution at N describing the relative probabilities with which the cluster fragments, given by $p_{k+1}^{m'}(m)$, and the total fragmentation probability. The latter was just $\propto(m'-1)$ in the mass-independent case [1], while now it is proportional to $\frac{m'-1}{m'}$. Equation (15) follows then by considering how fragmentation leading to a cluster with mass m goes through an intermediary with mass m'.

We also examined numerically the aggregation processes where the clusters were chosen with probabilities proportional to higher powers of their mass, in particular, $\propto m^2$ and $\propto m^3$, i.e., the square of a cluster's mass and the cubic of a cluster's mass. The asymptotic power law exponents are roughly $-5/2$ and $-7/2$ for the m^2 dependence and m^3 dependence, respectively. However, to the best of our knowledge, exact solutions for these cases have not yet been found.

In summary, we derived the exact solutions for the probabilities to find any configuration after a fixed number of aggregation events in the models where a cluster picked with probability proportional to its mass aggregates with k other particles. More specifically, we studied three versions of this process (particles on a ring joining with nearest neighbors, particles on an open-ended line, and the well-mixed case), and found exactly the same solutions using combinatorial counting. We attribute this to the absence of spatial correlations, although they are *a priori* not excluded. Differently from the mass-independent random sequential renormalization (RSR), which shows k-dependent exponents in scaling laws for small masses, the cluster size distribution follows a power law with exponent $-3/2$ independent of k, which is the same with that of the *sum kernel* for irreversible aggregation. Finally, the aggregation process is also related to a time-reversed fragmentation process, the characteristics of which are briefly discussed.

Mass-dependent RSR and the related aggregation process was also considered in two dimensions [3], where a runaway giant cluster exists after a few steps and takes all merging action. The behavior is very similar to the *gelation* in the aggregation process with the product kernel, but aggregation events in two-dimensional RSR involve fluctuating numbers of neighbors, differently from the aggregation process considered in the present Rapid Communication.

[1] S.-W. Son, G. Bizhani, C. Christensen, P. Grassberger, and M. Paczuski, Europhys. Lett. **95**, 58007 (2011).

[2] G. Bizhani, V. Sood, M. Paczuski, and P. Grassberger, Phys. Rev. E **83**, 036110 (2011).

[3] C. Christensen, G. Bizhani, S.-W. Son, M. Paczuski, and P. Grassberger, e-print arXiv:1012.1070.

[4] F. Leyvraz, Phys. Rep. **383**, 95 (2003), and references therein.

[5] P. Krapivsky, J. Phys. A **24**, 4697 (1991).

A Letters Journal Exploring the Frontiers of Physics

January 2012

EPL, **97** (2012) 16004
doi: 10.1209/0295-5075/97/16004

www.epljournal.org

Agglomerative percolation in two dimensions

C. Christensen[1(a)], G. Bizhani[1], S.-W. Son[1], M. Paczuski[1] and P. Grassberger[1,2]

[1] *Complexity Science Group, University of Calgary - Calgary T2N 1N4, Canada*
[2] *FZ Jülich - D-52425 Jülich, Germany, EU*

received 30 September 2011; accepted in final form 18 November 2011
published online 4 January 2012

PACS 64.60.ah – Percolation
PACS 68.43.Jk – Diffusion of adsorbates, kinetics of coarsening and aggregation
PACS 89.75.Da – Systems obeying scaling laws

Abstract – We study a process termed *agglomerative percolation* (AP) in two dimensions. Instead of adding sites or bonds at random, in AP randomly chosen clusters are linked to all their neighbors. As a result the growth process involves a diverging length scale near a critical point. Picking target clusters with probability proportional to their mass leads to a runaway compact cluster. Choosing all clusters equally leads to a continuous transition in a new universality class for the square lattice, while the transition on the triangular lattice has the same critical exponents as ordinary percolation —violating blatantly the basic notion of universality.

Percolation is a pervasive concept in statistical physics and an important branch of mathematics [1]. It typifies the emergence of long-range connectivity in many systems such as the flow of liquids through porous media [2], transport in disordered media [3], spread of disease in populations [4], resilience of networks to attack [5], formation of gels [6] and even of social groups [7]. It also underlies a number of other critical phenomena —like the Ising order/disorder transition, which is a percolation transition on the set of spins with given sign [8].

The phase transition in ordinary percolation (OP), where bonds or sites are added at random, represents a broad universality class. Recently Achlioptas *et al.* [9] made a simple modification by, at each step, selecting between two possibilities the link that leads to the slowest growth of large clusters. This global choice introduces a large length scale —the system size L— which can alter universality. Indeed, they concluded that an unusual, discontinuous transition (called "explosive percolation") emerges where a macroscopic cluster appears suddenly while at the same time scaling in other quantities is observed [10–12]. Various modifications of the rule have been made [13,14] —all finding evidence of a discontinuous transition. Although the claim for discontinuity in [9] was refuted later in [15,16], explosive percolation in that case does represent a new universality class.

Here we discuss a percolation process that also contains a potentially large length scale in its definition, in this case the correlation length ξ. Our process has direct application to the study of complex networks. Instead of adding bonds randomly, we pick a random cluster and add bonds to its entire surface in order to link it to all adjacent clusters. Starting with the state where all clusters have size one, at each update $t \to t+1$ the process repeats until the entire lattice (or graph) is reduced to a single cluster. We call this "agglomerative percolation" (AP), in analogy with cluster growth by aggregation [17]. Thus, if by chance a cluster of length scale ℓ is picked, links are added simultaneously at distances $\mathcal{O}(\ell)$ apart.

AP can be analyzed on any graph. It corresponds to random sequential renormalization [18] of a network, where a single cluster is identified as a "super"-node that is a local coarse-graining of the graph. In this perspective, scaling laws seen in renormalization studies of small-world networks [19–23] are a consequence of an AP phase transition and *do not indicate fractality of the underlying graph* [18,24]. Previously AP was studied on critical trees [18] and in one dimension [24]. Scaling laws were found both analytically and numerically —but no phase transition occurs since both graphs have a topological dimension of one.

In order to establish the phase transition in AP, and its relationship to OP, we analyze it in two dimensions (which is clearly not a fractal graph), where many exact results for OP are known. We consider both square and triangular lattices. Clusters can be chosen with equal probability, or we can make biased choices according to the mass, radius, etc. of the clusters. Here both (a) uniform probabilities

(a) E-mail: christensen44@gmail.com

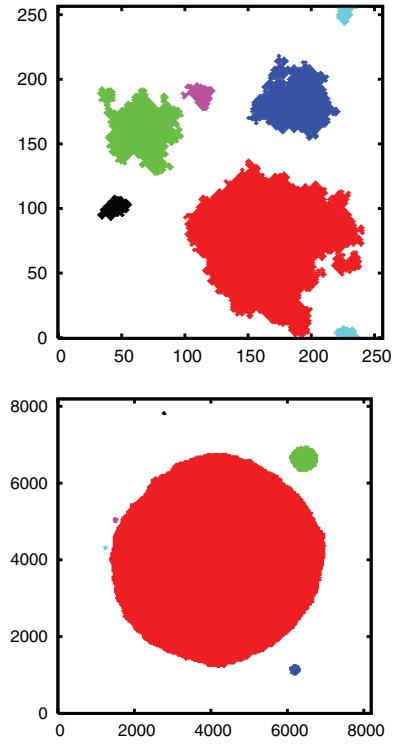

Fig. 1: (Color online) The six largest clusters in mass-weighted AP (model (b)) on a square lattice with $L = 256$ (top), and $L = 8192$ (bottom). The average cluster mass is two, or $n = N/L^2 = 0.5$. The red cluster is close to wrapping. All large clusters are compact.

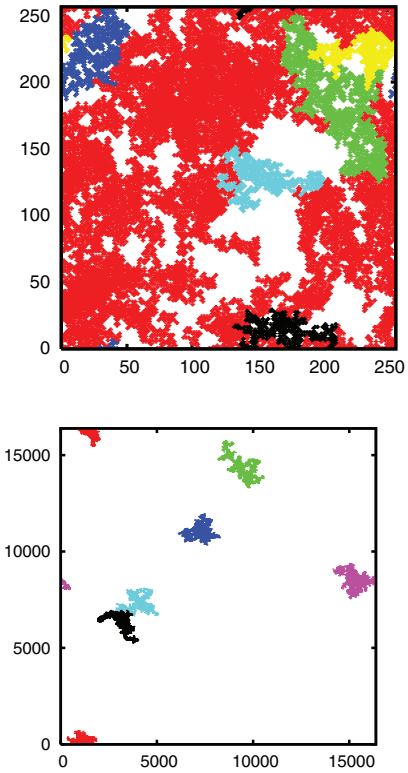

Fig. 2: (Color online) The six largest clusters in typical runs of AP model (a) on square lattices for $n = N/L^2 = 0.1 = 1/\langle m \rangle$. Top panel: for $L = 256$, the red cluster has already wrapped. Bottom panel: for $L = 16384$, all clusters are far from wrapping. In both cases, clusters appear fractal.

and (b) probabilities proportional to the cluster mass are studied. Model (b) coincides with choosing *sites* uniformly, and growing the whole cluster in which they lie [25]. It shows runaway behavior resembling a first-order transition with compact clusters —as in ref. [26] (see fig. 1). Model (a) is more subtle. Although clusters appear fractal (see fig. 2) and the overall character resembles OP, fundamental differences arise. Most conspicuous is an unexpected difference between the two lattice types: While model (a) on the square lattice is definitely not in the OP universality class (*e.g.* the average cluster size diverges at the transition), the triangular lattice shares the same critical exponents as OP. We believe this violation of universality must be related to the long-range nature of the growth process for large clusters.

We use $L \times L$ lattices, with $2^5 \leqslant L \leqslant 2^{14}$. Boundary conditions are helical: periodic in the y-direction while the right neighbor of site $(x = L, y)$ is $(x' = 1, y' \equiv y (\mathrm{mod}\, L) + 1)$. Diagonal bonds are added to obtain triangular lattices. We use an algorithm based on that in [27], augmented by a depth first search on the target cluster, in order to find all its neighboring clusters. The natural control parameter in OP is p, the fraction of existing bonds or sites. In AP, however, the number of links is not uniquely defined, although it is a version of (correlated) bond percolation. One might join two clusters via a single link, but one might also put multiple links between them. Therefore, in AP it is more natural to use the average cluster number per site,

$$n = N/L^2 = \langle m \rangle^{-1}, \tag{1}$$

where $\langle m \rangle$ is the average cluster mass. For OP, $n(p)$ is not analytic at $p = p_c$, but is monotonic with two continuous derivatives. Thus, one can use n as the control parameter in OP and reproduce all known scaling laws. (We checked this explicitly; see also [10].) Instead of n, one might also use the number of agglomeration events, t, as the control parameter. In agreement with [18,28], we found that t is more "noisy" than n and leads to slightly less clear results. We analyze the distribution $P_n(m)$ of cluster masses m in configurations with cluster density n, and the probability $p_{\mathrm{wrap}}(n)$, that a cluster wraps the torus in the y-direction, for each L.

In model (b), the growth rate for a cluster of mass m accelerates steeply with m, leading to a runaway effect. A cluster's chance to be selected is m/L^2. Once chosen it

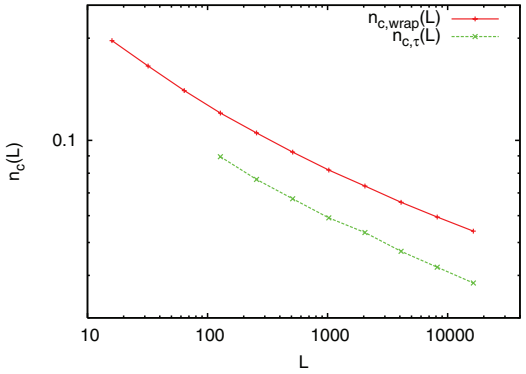

Fig. 3: (Color online) Critical densities $n_c(L)$ *vs.* L for AP model (a) on square lattices. The upper curve is the average wrapping threshold. The lower one is the density at which the power law range in the cluster mass distribution extends furthest. Error bars are smaller than the symbol size.

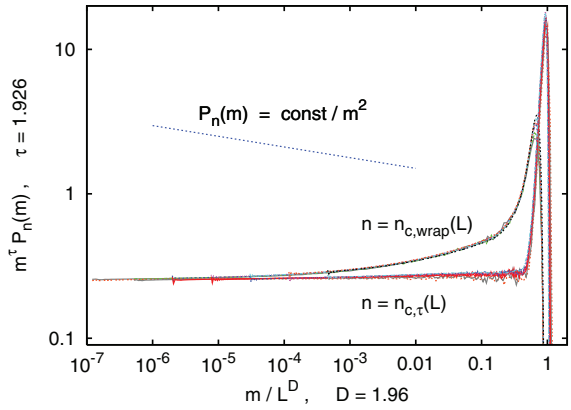

Fig. 4: (Color online) Data collapse for AP model (a) on square lattices: $m^\tau P_n(m)$ *vs.* m/L^D with $\tau = 1.926$ and $D = 1.96$. The curves with the smaller peaks are for $n = n_{c,\mathrm{wrap}}(L)$, while the others are for $n = n_{c,\tau}(L)$. The first are at the wrapping threshold, while the second are when $P_n(m)$ has the broadest power law range. The straight tilted line corresponds to $P_n(m) \propto m^{-2}$. System sizes are $L = 256, 512, \ldots, 16384$.

grows all along its perimeter. Since most of its neighbors are small, it grows into a compact shape. For any $0 < \alpha < 2$ and for $L \to \infty$, we conjecture that the largest cluster reaches mass $m \sim L^\alpha$ at a time when $\langle m \rangle \to 1$. This "incipient" cluster continues to separate in mass from the others. It wraps the torus when $m/L^2 = \mathcal{O}(1)$. Thus an infinite incipient cluster appears at density $n_c \to 1$ in the limit $L \to \infty$, while wrapping occurs much later, at $0 < n_c < 1$. Figure 1 shows the six largest clusters in a typical run on a square lattice for both small and large L at $n = 0.5$. These snapshots were taken at a time long past the appearance of the incipient cluster and long before it wraps. One sees that the giant cluster becomes more dominant over all other clusters as L increases. Although convergence of $n_c \to 1$ as $L \to \infty$ is slow, it is in perfect agreement with numerical simulation results (data not shown). The same scenario holds for the triangular lattice.

In OP, cluster perimeters are for large clusters proportional to their mass. Thus, if a new bond is added at each time step, the average growth rate of a cluster is roughly $\mathrm{d}m/\mathrm{d}t \propto m$. In AP model (a) —where clusters are picked with uniform probability— those chosen grow by an amount proportional to their perimeter, so again (roughly) $\mathrm{d}m/\mathrm{d}t \propto m$. This leads neither to a runaway of large clusters as in model (b) nor to the retardation of their growth as in the Achlioptas process. Therefore, model (a) and OP cannot be distinguished by such a crude argument and their relationship could conceivably depend on microscopic details such as the type of lattice.

For model (a), we first consider square lattices. By eye individual configurations look like OP. However, wrapping thresholds depend strongly on L. Figure 2 displays the six largest clusters in a typical run when $n = 0.1$ for both $L = 256$ (top) and for $L = 16384$ (bottom). While the largest cluster clearly wraps the small lattice, it is far from this point on the large one. Figure 3 shows the density $n_{c,\mathrm{wrap}}(L)$ at which half the runs contain a wrapping cluster. The data fall roughly on a straight line on a log-log plot. If deviations from a straight line were typical finite-size corrections, this would mean that the average cluster size at the wrapping threshold diverges as a power of L when $L \to \infty$. However, for reasons explained below, we believe that $n_{c,\mathrm{wrap}}(L) \to 0$ logarithmically as $L \to \infty$ (for explicit fits, see the supplementary material [29]). This implies that the correlation length exhibits an essential singularity as $n \to n_c = 0$.

Mass distributions $P_n(m)$ for $n = n_{c,\mathrm{wrap}}(L)$ are displayed in fig. 4 using a data collapse method which compares $m^\tau P_n(m)$ to m/L^D, with $\tau = 1.926$ and $D = 1.96$. A perfect collapse corresponds to a finite-size scaling (FSS) *ansatz*

$$P_n(m) = m^{-\tau} f(\psi(n, L), m/L^D), \tag{2}$$

which generalizes the standard FSS *ansatz* [2] where $\psi(n, L) = (n - n_c)L^{1/\nu}$. Except for peak heights the data collapse is excellent. The apparent values for τ and D deviate significantly from their values in OP ($\tau = 2.055$ and $D = 1.89$ in two dimensions). At $n = n_{c,\mathrm{wrap}}(L)$, $m^\tau P_n(m)$ is not horizontal over a wide range of masses. Hence $n = n_{c,\mathrm{wrap}}(L)$ is not equal to $n_{c,\tau}(L)$. The latter is the density at which a power law in $P_n(m)$ extends over the broadest range. Curves for $m^\tau P_{n=n_{c,\tau}(L)}(m)$ are also shown in fig. 4 and exhibit data collapse with a remarkably wide power law range. The power law regime describes the relatively few remaining clusters in configurations dominated by one wrapping cluster. The values $n_{c,\tau}(L)$ are also shown in fig. 3 and decrease similarly to $n_{c,\mathrm{wrap}}(L)$ as L increases.

If $\tau \leqslant 2$ as suggested by fig. 4, then the average cluster size at criticality diverges as $L \to \infty$, in agreement with

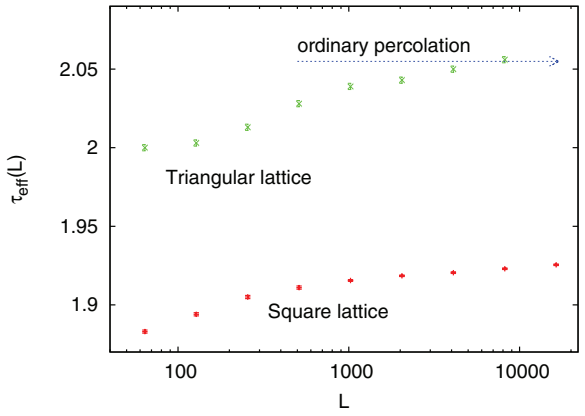

Fig. 5: (Color online) Plots of $\tau_{\rm eff}(L)$, the effective Fisher exponents estimated from the longest stretches in $P_n(m)$ that are compatible with pure power laws. As these estimates are somewhat subjective, the error bars are subjective as well. But their order of magnitude is consistent with the smoothness of the data with varying L. Clearly there is non-trivial L-dependence both for the triangular and for the square lattice, with $\tau_{\rm eff}(L)$ increasing with L in both cases. While $\tau_{\rm eff}$ is compatible with the value $\tau = 187/91 = 2.0549\ldots$ in the case of the triangular lattice, it is much smaller for the square lattice.

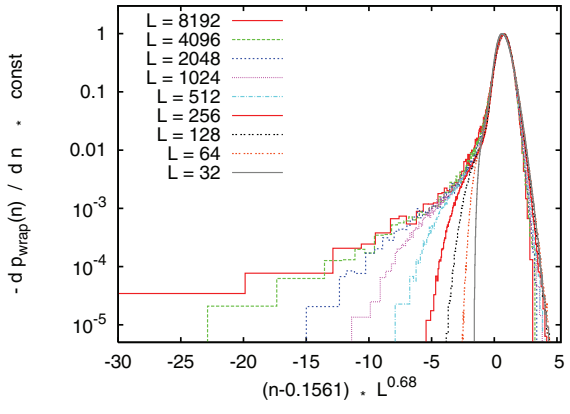

Fig. 6: (Color online) Data collapse plot for the probability density $\mathrm{d}p_{\rm wrap}(n)/\mathrm{d}n$ against $(n-n_c)L^{1/\nu}$ with $n_c = 0.1561$ and $\nu = 1.47$ for model (a) on triangular lattices. The scale on the y-axis is adjusted such that all curves peak at $y = 1$.

fig. 3 but in stark contrast to OP. Accepting this, the two possible (scaling) scenarios are $\tau = 2$ or $\tau < 2$. If $\tau < 2$, $n_c(L)$ vanishes as $\sim L^{-\delta}$ with some $\delta > 0$, and apparent values for τ and D should not vary much with L. Neither of these statements is correct. Figure 3 shows definite curvature, and the best fit values for τ and D both increase slightly but significantly with L, see fig. 5 and [29]). While these small shifts are not visible on the scales shown in fig. 4, they do not diminish as L increases. One would not expect to see large corrections to scaling that could explain fig. 5 if $\tau > 2$ since in that case the average cluster size is finite.

Since the numerical value of D is determined from the positions of the peaks in fig. 4, D is actually the fractal dimension of the largest cluster. The contribution to $\langle m \rangle$ from this cluster is $s_{\max}/N = s_{\max}\langle m \rangle / L^2$. If one assumes eq. (2) and $\tau < 2$, then one can show that the largest cluster makes a non-vanishing contribution to $\langle m \rangle$ as $L \to \infty$. This can only happen if $s_{\max} \sim L^2$, showing that the largest cluster has $D = 2$ if $\tau < 2$. Furthermore, one would expect convergence of the apparent D to follow a power law in that case. But the slow convergence of D from below indicates again that the behavior is dominated by logarithms.

We conclude thus that the true asymptotic values are $\tau = D = 2$ and $\nu = \infty$. In addition, we measured the exponent σ [2]. In agreement with the scaling relation $\sigma = D/\nu$, we found $\sigma \approx 0$ with rather slow convergence. Thus, all scaling relations are (trivially) satisfied (notice that the other exponents give no constraint, in the present case, on the order parameter exponent β).

For the triangular lattice, clusters look like those in OP. Both $n_{c,\tau}(L)$ and $n_{c,\rm wrap}(L)$ converge rapidly to the same (finite) critical value $n_c = 0.1561 \pm 0.0002$. Indeed, the best estimates of $\tau(L)$, obtained by fitting power laws to $P_{n=n_{c,\tau}(L)}(m)$, also converge rapidly to $\tau = 2.057 \pm 0.002$, in perfect agreement with OP (see fig. 5). Also D, obtained from a data collapse as in fig. 4, and the exponent σ are both within error equal to their values in OP, although these error bars are larger than for τ, see [29].

Small apparent inconsistencies with OP arise when we try to estimate ν using the scaling hypotheses $n_{c,\tau}(L) - n_c \sim L^{-1/\nu}$ or $p_{\rm wrap}(n) = \phi[(n-n_c)L^{1/\nu}]$. The first relation gives $\nu = 1.10 \pm 0.07$, significantly smaller than the value $\nu = 4/3$ for OP. The second one gives $\nu = 1.47 \pm 0.05$ for $n \gtrsim n_c$. Taken at face value, these estimates would exclude universality with OP. But we believe that they are artifacts of large finite-size corrections. Figure 6 shows an attempted data collapse for $\mathrm{d}p_{\rm wrap}(n)/\mathrm{d}n$. While the collapse is acceptable for $n > n_c$, huge tails develop for $n \ll n_c$ as L increases. For small n these tails decay roughly as $[(n_c - n)L^{0.6}]^{-\mu}$ with $\mu \approx 1.5$. We checked explicitly that the tails result from events where wrapping happened when a large target cluster was hit. In such cases, N can make huge jumps, so that the largest n at which the cluster wraps is far below the actual threshold. Thus we conclude that AP on the triangular lattice is in the OP universality class, with the caveat that the definition of n is affected by occasional large jumps which do not modify the main critical exponents but which do modify the tails of scaling functions as in fig. 6.

For an appreciation of how different the behaviors are on the square and triangular lattices, we show in fig. 7 effective critical cluster densities. We plot them against $L^{-3/4}$, since this should give for OP straight lines, according to the FSS *ansatz*. While the data for the triangular lattice indeed follow roughly straight lines and give a finite non-zero value of n_c, the same is definitely

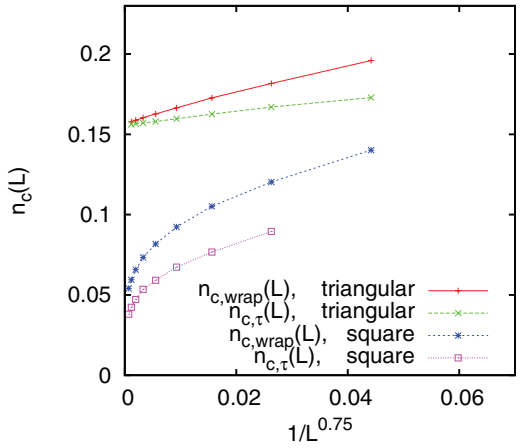

Fig. 7: (Color online) Effective critical cluster densities for model (a) *vs.* $L^{-3/4}$, where L is the lattice size. For ordinary percolation, where $n_c(L) - n_c \sim L^{-1/\nu}$ with $\nu = 4/3$, this should give straight lines. For each lattice type (triangular: upper pair of curves; square: lower pair of curves) we show results obtained with two different operational definitions for the critical point: i) maximal range of the power law $P_n(m) \sim m^{-\tau}$, and ii) the probability to have a cluster that wraps around a lattice with helical boundary conditions is equal to 1/2. The corresponding values of $n_c(L)$ are called $n_{c,\tau}(L)$ and $n_{c,\mathrm{wrap}}(L)$. Error bars are typically of the size of the symbols.

not true for the square lattice: those curves strongly bend down for $L \to \infty$, suggesting that $n_c = 1/\nu = 0$. Whether the latter is correct or not, this figure should leave no doubt that the square lattice model is not in the ordinary percolation universality class.

In summary, we have studied agglomerative percolation (AP) in two dimensions. This class of models is equivalent to random sequential renormalization schemes [18] first introduced to scrutinize the supposed fractality [19–23] of real-world —in particular, small-world— networks. Regular lattices were chosen for two reasons: 1) they are not fractal; 2) detailed comparison can be made with exact results for ordinary percolation (OP). Our results display some of the rich behavior possible in this general class of models and indicate that at least some of the scaling behavior found in [19–23] is due to AP rather than any supposed fractality of the underlying graph. If clusters are chosen with a bias for larger mass (model (b)), a runaway effect separates the largest cluster from the others and the behavior is completely different from OP. If clusters are chosen with equal probability (model (a)), then only a detailed numerical scaling analysis shows that AP is not in the OP universality class on the square lattice. On the other hand, AP on the triangular lattice shares critical exponents with OP.

AP may have applications beyond network renormalization. Growing clusters appear in many different physical situations. It could happen that further growth is triggered by some excitation where the entire cluster suddenly invades neighboring clusters at its boundary. Agglomerative percolation could also describe the growth of countries or urban areas. Countries often grow by overrunning and incorporating neighbors during aggressive periods, when they attack and incorporate simultaneously several of their neighbors.

* * *

We thank B. Ziff for correspondence that helped us sharpen some of our arguments.

REFERENCES

[1] Kesten H., *Percolation Theory for Mathematicians* (Birkhauser, Boston) 1982.
[2] Stauffer D. and Aharony A., *Introduction to Percolation Theory* (Taylor & Francis, London) 1994.
[3] Kirkpatrick S., *Rev. Mod. Phys.*, **45** (1973) 574.
[4] Moore C. and Newman M. E. J., *Phys. Rev. E*, **61** (2000) .
[5] Callaway D. S. *et al.*, *Phys. Rev. Lett.*, **85** (2000) 5468.
[6] Adam M., Delsanti M., Durand D., Hild G. and Munch J. P., *Pure Appl. Chem.*, **53** (1981) 1489.
[7] Michels R., *Political Parties* (Free Press) 1996.
[8] Fortuin C. M. and Kasteleyn P. W., *Physica*, **57** (1972) 536.
[9] Achlioptas D. *et al.*, *Science*, **323** (2009) 1453.
[10] Ziff R. M., *Phys. Rev. Lett.*, **103** (2009) 045701.
[11] Ziff R. M., *Phys. Rev. E*, **82** (2010) 051105.
[12] Radicchi F. and Fortunato S., *Phys. Rev. E*, **81** (2010) 036110.
[13] D'Souza R. M. and Mitzenmacher M., *Phys. Rev. Lett.*, **104** (2010) 195702.
[14] Araujo N. A. M. and Herrmann H. J., *Phys. Rev. Lett.*, **105** (2010) 35701.
[15] da Costa *et al.*, *Phys. Rev. Lett.*, **105** (2010) 255701.
[16] Grassberger P. *et al.*, *Phys. Rev. Lett.*, **106** (2011) 225701.
[17] Leyvraz F., *Phys. Rep.*, **383** (2003) 95.
[18] Bizhani G. *et al.*, *Phys. Rev. E*, **85** (2010) 036110.
[19] Song C., Havlin S. and Makse H. A., *Nature*, **433** (2004) 392.
[20] Goh K. I. *et al.*, *Phys. Rev. Lett.*, **96** (2006) 018701.
[21] Radicchi F., Ramasco J. J., Barrat A. and Fortunato S., *Phys. Rev. Lett.*, **101** (2008) 148701.
[22] Serrano M. A., Krioukov D. and Boguñá M., *Phys. Rev. Lett.*, **100** (2008) 248701.
[23] Rozenfeld H. D., Song C. and Makse H., *Rev. Mod. Phys.*, **104** (2010) 025701.
[24] Son S.-W. *et al.*, *EPL*, **95** (2010) 58007.
[25] Son S.-W., *Phys. Rev. E*, **84** (2011) 040102(R).
[26] Janssen H.-K., Müller M. and Stenull O., *Phys. Rev. B*, **70** (2004) 026114.
[27] Newman M. E. J. and Ziff R. M., *Phys. Rev. E*, **64** (2001) 016706.
[28] Bizhani G. *et al.*, eprint arXiv:1109.4631 (2011).
[29] Supplementary material at the end of the article: Christensen C., Bizhani G., Son S.-W., Paczuski M. and Grassberger P., `http://arxiv.org/abs/1012.1070`.

Supplementary Material for "Agglomerative Percolation in Two Dimensions"

Claire Christensen,[1] Golnoosh Bizhani,[1] Seung-Woo Son,[1] Maya Paczuski,[1] and Peter Grassberger[1,2]

[1] *Complexity Science Group, University of Calgary, Calgary T2N 1N4, Canada*
[2] *IAS, JSC, FZ Jülich, D-52425 Jülich, Germany*

(Dated: November 10, 2011)

In this supplementary material, we present several plots. They illustrate claims for which in the main paper either the actual data were not shown or they were plotted in different ways. The present plots are to convince the reader that:

- Model (b) (where clusters are selected for agglomeration according to their mass) develops runaway clusters very early in the process, leading to a "phase transition" at $\langle m \rangle = 1$ in the infinite system limit $N \to \infty$ (here, $\langle m \rangle$ is the average mass per cluster) (Fig. S1);
- The same is not true for model (a), but model (a) shows qualitatively different behaviors on the square and triangular lattices (Figs. S2 to S5);
- In particular, while model (a) on the triangular lattice is in the ordinary percolation universality class, it is definitely not in that universality class on the square lattice;
- For the square lattice, *superficial analyses* would give a Fisher exponent τ and a fractal dimension D that are both smaller than 2, but a more careful analysis, combined with analytic arguments, leads to the conclusion that $\tau = D = 2$ exactly.

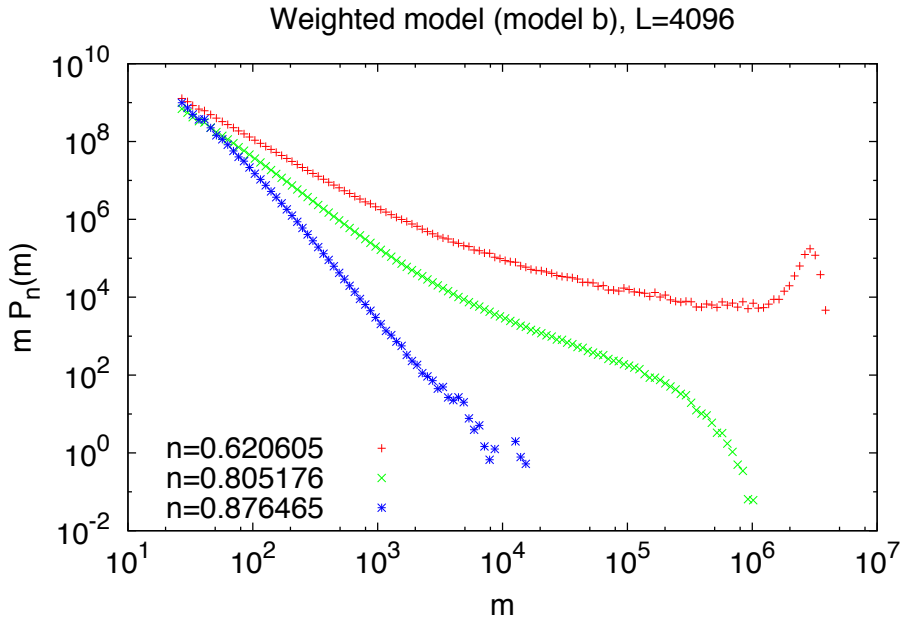

FIG. 1. (Color online) Mass distributions for model (b) with $L = 4096$. Each curve corresponds to a fixed value of n (number of clusters per site), corresponding to an average cluster mass $\langle m \rangle = 1/n$. The uppermost (red) curve shows a clear narrow peak, corresponding to a single cluster that involves a substantial (and thus not strongly fluctuating) fraction of all sites. The middle (green) curve shows a broad bump at its upper end, corresponding still to a runaway cluster in most realizations, albeit with a much wider mass range centered typically at a few percent of the total mass. The lowest (blue) curve corresponds to $\langle m \rangle \approx 1.14$, i.e. by far most clusters consist of a single site. In spite of this, it shows a long tail implying that *some* clusters have reached size 10^4 and beyond. In addition to Fig.1 in the main paper, this shows most directly the existence of runaway clusters at values of $\langle m \rangle$ that converge to 1 as $N \to \infty$.

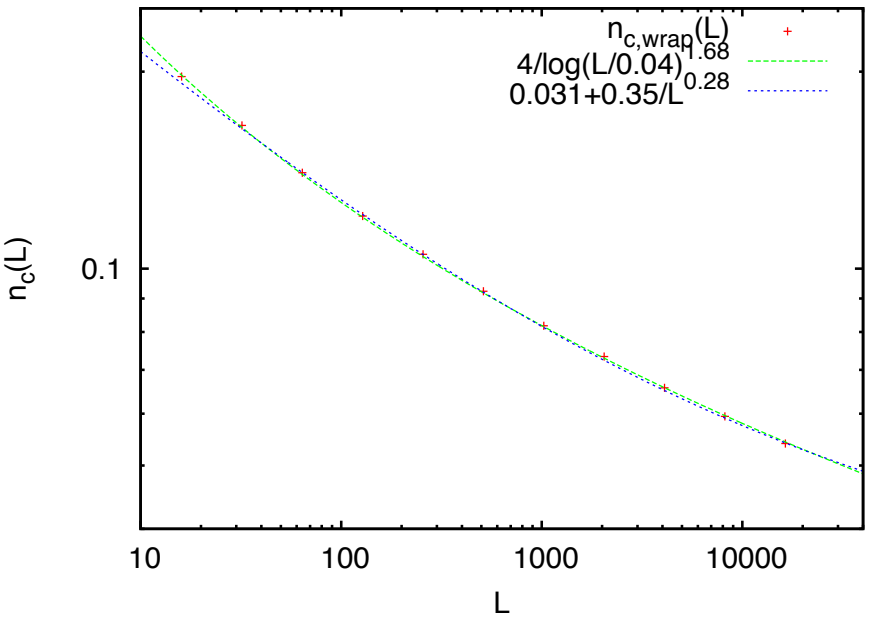

FIG. 2. (Color online) Plot of $n_{c,\mathrm{wrap}}(L)$ versus $\log L$ for model (a) on the square lattice, together with two typical fits. One fit (green curve) is logarithmic, $n_{c,\mathrm{wrap}}(L) = 4/\ln(25L)^{1.68}$. It assumes that $n_{c,\mathrm{wrap}} \equiv n_{c,\mathrm{wrap}}(L=\infty) = 0$. The other fit (blue) assumes that $n_{c,\mathrm{wrap}}$ is non-zero, and that $n_{c,\mathrm{wrap}}(L)$ has power law finite size corrections: $n_{c,\mathrm{wrap}}(L) = 0.031 + 0.35/L^{0.28}$. Notice that both fits involve three free parameters. The logarithmic fit is slightly better, but it is not clear how significant this is, since one should expect an infinite series of further correction terms in any such fit. Notice also that $n_{c,\mathrm{wrap}}$ is very small (i.e., the average cluster mass at criticality is huge) in the second fit, in striking contrast to other (bond, site) percolation models on any 2-d lattice. In our opinion, this is a stronger argument against the second fit than the quality of the fit itself. Finally, no decent fit is possible with a pure power law $n_{c,\mathrm{wrap}}(L) = a/L^{\alpha}$, expected if $\tau < 2$ – although fits with two or more powers with different exponents would be possible.

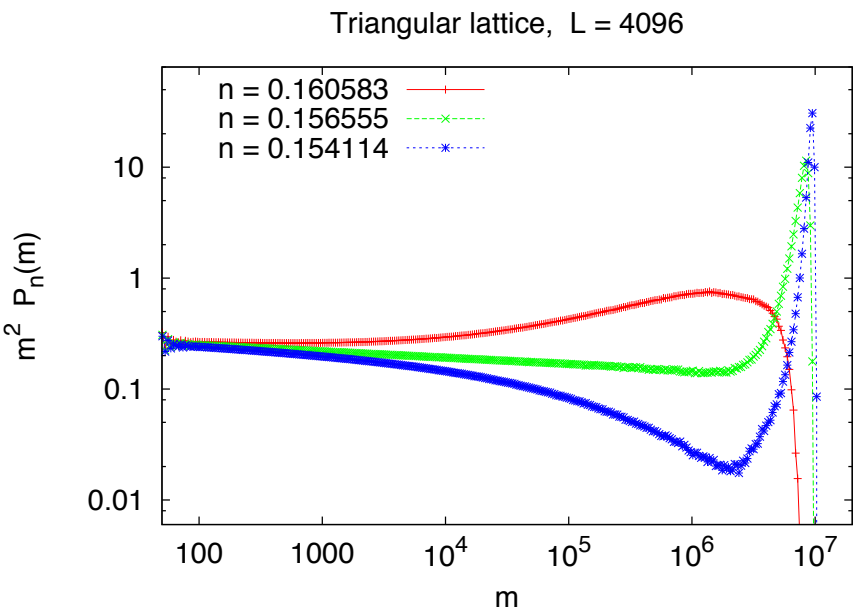

FIG. 3. (Color online) Mass distributions (log-log) for model (a) on the triangular lattice with $L = 4096$, for three different values of n. The middle (green) curve has the longest straight piece and is thus used to define $n_{c,\tau}$. The other two curves show the sub- (super-)critical behavior. For increased significance, we actually do not show $P_n(m)$ but rather $m^2 P_n(m)$. The fact that the central (green) curve has a negative slope clearly indicates $\tau > 2$. Notice that this conclusion is rather robust and would not require a very precise estimate of $n_{c,\tau}$.

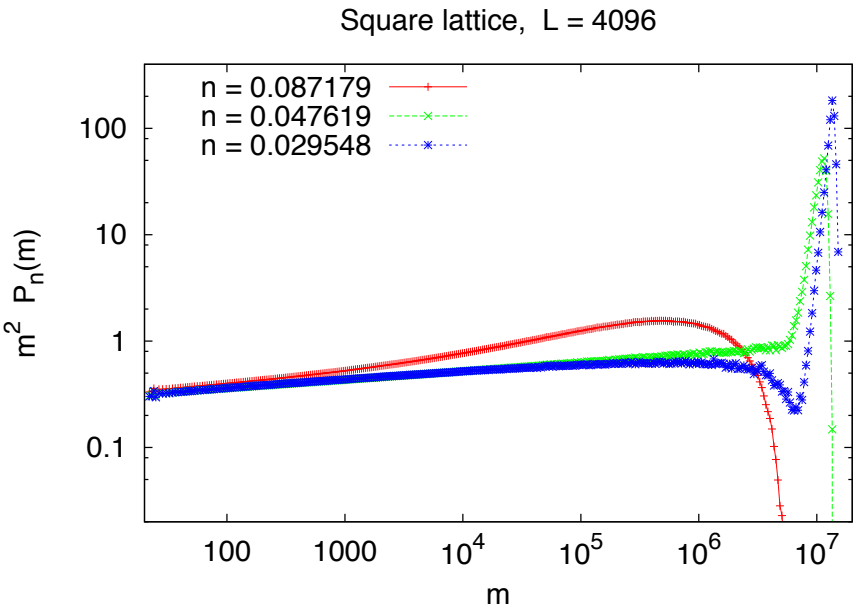

FIG. 4. (Color online) Same as Fig. S3, but for the square lattice. Superficially, the graph looks similar to Fig. S3, but the slope of the critical (green) curve now is positive, clearly suggesting that $\tau < 2$ unless there are very strong corrections to scaling.

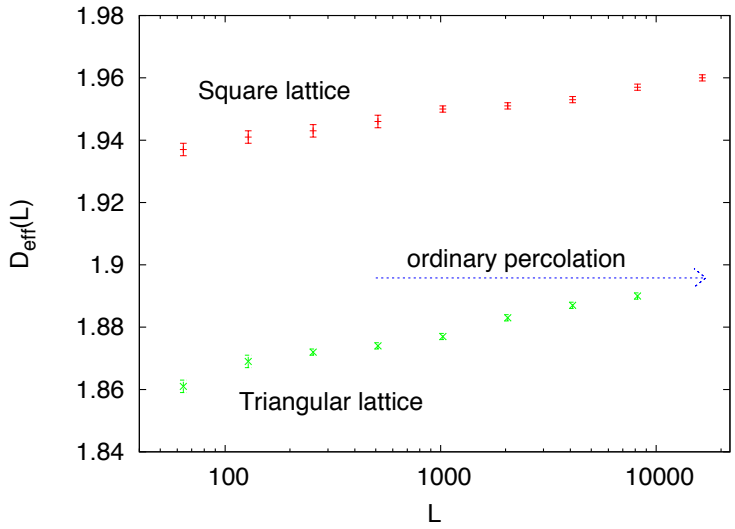

FIG. 5. (Color online) Similar to Fig. 5 of the main paper, but for the fractal dimension of the largest (percolating) cluster. It is obtained from the positions of the peaks of the central (critical) curves in mass distribution plots such as those in Figs. S4 and S5. Again we see that both curves increase with L. Again the triangular lattice data are compatible with ordinary percolation, $D = 91/48 = 1.8958\ldots$, but the square lattice data are not. There, the percolating cluster has a distinctly larger dimension which is moving *away* from the ordinary percolation value. The analytical arguments given in the main paper allow only three possible scenarios: (i) $D < 2, \tau > 2, \nu < \infty$, and power law corrections to scaling; (ii) $D = \tau = 2, \nu = \infty$, and logarithmic corrections; and (iii) $D = 2, \tau < 2, \nu < \infty$, and power law corrections to scaling. Scenario (i) (i.e., $\tau > 2$) seems definitely ruled out for the square lattice by the data. Scenarios (ii) and (iii) are both possible, but would require very large and slowly vanishing finite size corrections for $D_{\rm eff}(L)$. At face value, the data for $n_c(L)$ shown in Fig. S2 and in Fig. 3 of the main paper would favor scenario (ii), while $\tau_{\rm eff}(L)$ (Fig. 5) would favor scenario (iii). Our final preference of scenario (ii) is based on the fact that it is the only one which can naturally accommodate logarithmic (and thus very slowly vanishing) finite size corrections.

Chapter 4

Other Complex Percolation Models

As mentioned in section 1.4, in addition to the extensive studies on the standard percolation problem, new forms of percolation have been discussed in the past decade. Percolation in its classical form is a type of continuous (second order) phase transition. In critical phenomena, and in the vicinity of a continuous phase transition, many system properties obey power-laws with universal exponents and scaling relations. Recent surprising findings show that a multitude of seemingly minor variations in the percolation process can change the nature of the transition from continuous, to abrupt and discontinuous without scaling. Discontinuous (first order) transitions are history dependent and are more difficult to predict and control, yet they appear frequently in many settings.

Since in many cases the function of a network is highly influenced by its connectivity properties, it is important to develop and explore other percolation models where the giant cluster emerges discontinuously, and then find the factors that can affect the continuity, sharpness, predictability and history dependence of percolation.

Here we show that one of these factors — which is actually present in many complex systems — is cooperativity and suggest methods of implementing them in the study of percolation. We start with the analysis of explosive percolation [Achlioptas 09], a new class of models that were claimed to have discontinuous transitions, and show that percolation in these models is in fact continuous [Grassberger 11]. Next, we study percolation transitions in interdependent networks, where we show interdependency and cooperation of networks might lead to discontinuous transitions [Son 12]. We then introduce generalized epidemic processes as a mathematical framework for incorporating cooperativity in the study of epidemics and percolation, and show that cooperative effects — if large enough — can change

the percolation transition from continuous to discontinuous. Finally we show that in equilibrium dynamics as well, cooperativity can affect the order of percolation [Bizhani 12].

4.1 Explosive Percolation

A new class of percolation models called "explosive percolation" (EP) was suggested by Achlioptas et al., where instead of laying down an edge between two random nodes (as in the ER model), two candidate edges are selected at random, and one of them is finally laid down according to some selection criteria [Achlioptas 09]. These models were suggested to delay the emergence of the percolating cluster, and were inspired by the balanced allocations of balls into boxes. In random allocation of n balls into n boxes each ball is put into a randomly chosen box, while in balanced allocation two boxes are chosen at random and the ball goes to the one with less balls. This way the fullest box will end up having substantially fewer balls than random allocations [Azar 99].

In the original form of EP [Achlioptas 09], two edges are proposed randomly. The two products of the sizes of the clusters whom the proposed edges are about to join, are then compared, and the one leading to the smaller product is selected (the 'product rule'). This attempt to slow down the percolation transition by merging smaller clusters, was shown to result in sharpening the transition. Other variations including the sum rule (where the sum of the sizes of the merging clusters should be smaller), da Costa model [da Costa 10] (where two pairs of random nodes are chosen, and from each pair the one belonging to the smaller cluster is selected and joined by a link), and the adjacent edge model [D'Souza 10a] (where one randomly chosen node is connected to one of the two candidate nodes that is connected to a smaller cluster), were also shown to exhibit similar behavior.

The phase transitions in EP was claimed to be discontinuous. In such transitions the order parameter jumps discontinuously to a nonzero value at the critical point as opposed to classical percolation where it increases continuously.

Here we study four EP models: the original process of Achlioptas [Achlioptas 09], the product rule on two dimensional lattices, the adjacent edge model [D'Souza 10a], and da Costa's model [da Costa 10]. In computer simulations of these models the conventional order parameter shows a very sharp rise, but they lack other attributes of discontinuous transitions like phase coexistence, nucleation and cooperativity. We show that the transitions in these models are actually continuous, although their finite size scaling is unusual. The details of this study was published in [Grassberger 11], and reprinted in section 4.5 of this chapter.

It was also shown analytically in [da Costa 10] that EP is continuous, but is in a different universality class than ordinary percolation. For EP, the order parameter exponent $\beta = 0.0555$, whereas for ordinary percolation $\beta = 1$. This means that the transition is so sharp that it appears discontinuous even in very large systems.

4.2 Percolation on Interdependent Networks

As mentioned in section 1.3, most real-world networks are not isolated and interact at many levels. A consequence of this interdependency is that failure of a node in one network can lead to the failure of the nodes that depend on it in other networks, and as a result a small perturbation in one network can start a series of failures that escalate as they move from one network to another. Such a catastrophic failure happened in 2003 in Italy, when the shutdown of a power station started a cascade of events that finally led to a complete black out in half of the county [Buldyrev 10a]. It is claimed in [Buldyrev 10b] that this was due to an interdependence between the power grid and an information networks necessary to control the power stations, but similar cascades happen also in single networks [Motter 02].

The increasing amount of interdependency in the networks of critical infrastructure such as water supply, electricity, transportation and fuel distribution, urges the need for understanding the fragility induced by these couplings, finding ways to increase the resilience, and designing alternative structures that are more robust to random perturba-

tions [Vespignani 10, Schneider 11, Brummitta 12].

Percolation theory is used to analyze and predict the robustness of networks. However, most of network studies including network percolation are dedicated to single isolated networks, and were not generalized to the case of interdependent networks until recently [Leicht 09].

Cascade of failures in interdependent networks was studied in the view of percolation in [Buldyrev 10a], and it was shown that by increasing the amount of interdependency between networks, the percolation transition becomes discontinuous in random networks [Buldyrev 10a, Parshani 10, Parshani 11]. Other works showed that this is not the case for coupled lattices of two and three dimensions, where the order parameter exponent β is less than the exponent for isolated lattices, meaning that the transition is even less sharp [Son 11c]. Considering the behavior of lattices in this work is particularly important since most infrastructure networks are embedded in Euclidean space.

In our paper which is published as [Son 12], and is reprinted in section 4.5 of this chapter, we developed a general percolation theory for locally treelike and interdependent networks based on epidemic spreading, where we modeled the cascade of failure as an epidemic process. We adapted the usual consistency condition for the existence of a percolating cluster in isolated networks to accommodate the case where several networks interdepend on each other. Our theory also incorporates the case where only a fraction of nodes are interdependent. Our formulation is based on generating functions [Newman 01a], and in some cases is fully solvable.

We solved our model analytically for two interdependent ER networks, for the following cases:

Two fully interdependent ER networks: In this case the percolation transition is always discontinuous. For networks of the same average degree, there is no percolating cluster if the average degree, z is less than $z_c = 0.24554$, and At $z = z_c$ a percolating cluster with relative

size $S_c = 0.511699\ldots$ emerges. In the general case of $z_{\mathcal{A}} \neq z_{\mathcal{B}}$, where $z_{\mathcal{A}}$ and $z_{\mathcal{B}}$ are the average degrees of the two networks, we obtained a line of first order transitions in the phase space of $\{z_{\mathcal{A}},\ z_{\mathcal{B}}\}$.

Two partially interdependent ER networks: Here only a fraction q of the nodes in each network are interdependent. Depending on q the transition can be continuous or discontinuous. For $z_{\mathcal{A}} = z_{\mathcal{B}} = z$, we found a tricritical point separating the two regimes at $(q_c, z_c) = (1/3, 3/2)$, below which the percolation transition is continuous. In the case $z_{\mathcal{A}} \neq z_{\mathcal{B}}$, again we found the first and second order transition lines in the phase diagram of $\{z_{\mathcal{A}},\ z_{\mathcal{B}}\}$. The first order line shrinks as the interdependency q decreases, and vanishes for $q < 1/3$.

This formulation can be easily used for more complicated network structures as long as they are locally tree like.

Interdependency of networks can be viewed as a cooperative phenomenon, where a node can only operate if its adjacent node(s) in the other network(s) cooperate with it. We suggest that adding such cooperative effects in percolation can change the transition from continuous to discontinuous. We formulate this more precisely with the help of generalized epidemic processes in the next section.

4.3 Generalized Epidemic Processes and Cooperative Percolation

In epidemic processes, usually an infected node attacks all of its neighbors and can infect each of them with probability p. In *generalized epidemic processes* (GEP), the probability of the infections to succeed depends on the number of previous attacks it has fended off: each attack makes the target weaker and the infection probability, p_n, increases with the number of previous attacks, n. In other words, nodes should cooperate in order to infect their common neighbor.

On random graphs, this model is similar to the contagion model, proposed by Dodds

and Watts [Dodds 04, Dodds 05], where they assumed agents keep a memory of the previous exposures in an SIR (susceptible-infected-removed) model. Each agent receives a random dose after each exposure. These doses accumulate until a threshold (again random) is reached and the agent becomes infected. We showed that our formulation of the generalized epidemic processes, leads exactly to the same results as the Dodds and Watts model, but with much simpler mathematics.

On lattices, GEP maps to the problem of surface depinning in random media at zero temperature. We obtained the phase diagram of this model numerically and showed that here again depending on the amount of cooperativity, the percolation transition can be continuous or discontinuous. The two regimes here are separated by a tricritical point for $(d > 2)$. We suggest that simulation inspired by GEP could lead to better understanding of the depinning transition of rough surfaces.

The details of this work was published as a part of [Bizhani 12], which is reprinted at the end of this chapter.

4.4 Percolation in Equilibrium Dynamics: Hamiltonian Graphs

The Erdös Rényi model of networks can also be redefined as an equilibrium process, and studied via the methods of statistical mechanics. The ER model is then a canonical ensemble of graphs with a given average number of links. Generally one can impose other constraints on the ensemble based on the specific model under study.

In this statistical view, an ensemble of all simple graphs (graphs with no multiple and self-links), $\mathcal{G}$, is considered. Each graph $G \in \mathcal{G}$ can exist in this ensemble with probability $P(G)$. We would like to choose P such that the expectation value of a set of observables $\{x_i\}$, be equal to the ones observed in the system under study, $\sum_G P(G)x_i(G) = \langle x_i \rangle$. We know from statistical physics that the best choice of P is the one that maximizes the Gibbs

entropy

$$S = -\sum_{g\in\mathcal{G}} P(G)\ln[P(G)] \quad . \tag{4.1}$$

Using the method of Lagrange multipliers one obtains

$$P(G) = \frac{e^{-H(g)}}{Z} \quad , \tag{4.2}$$

where the graph Hamiltonian, H, is a sum of bilinear terms

$$H = \sum_i \theta_i x_i(g) \quad , \tag{4.3}$$

and Z is the partition sum $\sum_G e^{-H(G)}$. The Lagrange multipliers $\{\theta_i\}$ are the chemical potentials for the observables $\{x_i\}$, and are to be determined from the constraints.

In the case of ER graphs of size n, the Hamiltonian is simply $H_{\rm ER} = \theta m$, where m is the number of links in the graph. Straight forward calculations lead to

$$\langle m\rangle = \binom{n}{2}\frac{1}{e^\theta + 1} \quad . \tag{4.4}$$

This maps to mean-field percolation if we define $p = \frac{1}{e^\theta+1}$, so that $\langle m\rangle = \binom{n}{2}p$, and the model undergoes a continuous percolation transition at $p = 1/n$, or $\theta \sim \ln(n)$.

The above formalism can be generalized to accommodate more features of complex networks. These models are widely used in the context of social sciences and are known as "exponential graph models" [Robins 07]. Here we show that in some Hamiltonian graph models, where cooperative effects are taken into account, the percolation transition can switch to discontinuous with mixed hysteresis loops.

The two-star and the Strauss models

The Hamiltonian for the two-star model [Robins 07] is

$$H_2 = \theta L - \frac{J}{n}n_2 \quad , \tag{4.5}$$

with n_2 being the number of two-stars (pairs of links attached to the same node), and the Hamiltonian for the Strauss model [Strauss 86] is

$$H_2 = \theta L - \frac{B}{n}n_\Delta \quad , \tag{4.6}$$

with n_Δ being the number of triangles in the networks. The second term in both Hamiltonians is a cooperative term where two (or three) links have to cooperate to make a contribution to the Hamiltonian. In both models the link density and consequently the number of two-stars (triangles) show a discontinuous transition from a sparse phase where the graphs are essentially ER-like and lack any nontrivial features (large number of hubs or high clustering), to a condensed phase where the graphs are almost complete and again lack nontrivial structure.

Percolation properties of Hamiltonian graph models

We study the percolation properties of these models by Monte Carlo simulations, where we keep one of the chemical potentials fixed, sweep the other one, and examine the hysteresis loops of the link density and the size of the largest component. Our detailed results are published as a part of [Bizhani 12] which is reprinted in section 4.5 of this chapter.

When the chemical potentials are $\mathcal{O}(1)$, a percolating cluster exists both below and above the link density transition, and percolation is not affected by the cooperative term.

With a particular choice of the chemical potentials namely when $\theta = J = \ln n$ (and equivalently $B = 3\theta \sim \ln n$, for the Strauss model), the percolation transition and the link density transition overlap and the size of the largest cluster shows a mixed hysteresis loop which is continuous on one side and jumps discontinuously on the other.

This study shows that in equilibrium dynamics as well, cooperative effects can change the nature of percolation transition from continuous to discontinuous.

4.5 Publications

This section includes reprints of the publication mentioned in this chapter. These publications include:

1 – [Grassberger 11]

Explosive percolation is actually continuous, but with unusual finite size behavior

P. Grassberger, C. Christensen, G. Bizhani, S-W. Son, and M. Paczuski, *Phys. Rev. Lett.*, **106**, 225701 (2011).

2 – [Son 12]

Percolation Theory on interdependent networks based on epidemic spreading

S.-W. Son, G. Bizhani, C. Christensen, P. Grassberger, and M. Paczuski, *Europhys. Lett.*, **97**, 16006 (2012).

3 – [Bizhani 12]

Discontinuous percolation transitions in epidemic processes, surface depinning in random media, and Hamiltonian random graphs

G. Bizhani, M. Paczuski, and P. Grassberger, *Phys. Rev. E*, **86**, 011128 (2012).

Explosive Percolation is Continuous, but with Unusual Finite Size Behavior

Peter Grassberger,[1,2] Claire Christensen,[2] Golnoosh Bizhani,[2] Seung-Woo Son,[2] and Maya Paczuski[2]

[1]*FZ Jülich, D-52425 Jülich, Germany*

[2]*Complexity Science Group, University of Calgary, Calgary T2N 1N4, Canada*

(Received 23 March 2011; published 31 May 2011)

We study four Achlioptas-type processes with "explosive" percolation transitions. All transitions are clearly continuous, but their finite size scaling functions are not entirely holomorphic. The distributions of the order parameter, i.e., the relative size $s_{\max}/N$ of the largest cluster, are double humped. But—in contrast to first-order phase transitions—the distance between the two peaks decreases with system size N as $N^{-\eta}$ with $\eta > 0$. We find different positive values of β (defined via $\langle s_{\max}/N\rangle \sim (p - p_c)^{\beta}$ for infinite systems) for each model, showing that they are all in different universality classes. In contrast, the exponent Θ (defined such that observables are homogeneous functions of $(p - p_c)N^{\Theta}$) is close to—or even equal to—$1/2$ for all models.

DOI: 10.1103/PhysRevLett.106.225701 PACS numbers: 64.60.ah, 05.40.−a, 05.70.Jk, 89.75.Da

Percolation is a pervasive concept in statistical physics and probability theory and has been studied *in extenso* in the past. It came thus as a surprise to many when Achlioptas *et al.* [1] claimed that a seemingly mild modification of standard percolation models leads to a discontinuous phase transition—named "explosive percolation" (EP) by them—in contrast to the continuous phase transition seen in ordinary percolation. Following [1] there appeared a flood of papers [2–20] studying various aspects and generalizations of EP. In all cases, with one exception [20], the authors agreed that the transition is discontinuous: the "order parameter", defined as the fraction of vertices or sites in the largest cluster, makes a discrete jump at the percolation transition. Here we join the dissenting minority and add further strong evidence that the EP transition is *continuous* in all models, but with unusual finite size behavior (recently, continuity of EP was also shown in [21]).

From the physical point of view, the model seems somewhat unnatural. To establish a new link, a set of "candidate" links is chosen at random, only one of which is really established. This is done such that the formation of large clusters is delayed, as compared to random (bond) percolation. Since the nonchosen candidate links will in general connect distant nodes in the final network, this implies *nonlocal* control [22]. Also, notwithstanding [8], no realistic applications have been proposed. It is well known that including long-range interactions can alter the universality class, or drive a transition first order. Thus it is not so surprising that a percolation model with global control can show different behavior [23].

Usually, e.g., in thermal equilibrium systems, discontinuous phase transitions are identified with "first-order" transitions, while continuous transitions are called "second order." This notation is also often applied to percolative transitions. But EP lacks most attributes—except possibly for the discontinuous order parameter jump—considered essential for first-order transitions. None of these other attributes (cooperativity, phase coexistence, and nucleation) is observed in Achlioptas type processes, although they are observed in other percolation-type transitions [24]. Thus EP should never have been viewed as a first-order transition, and it is gratifying that it is also not discontinuous.

Apart from the behavior of the average value $\langle m\rangle$ of the order parameter m, phase transitions can also be characterized by the distribution $P_{p,N}(m)$ of m in finite systems, where p is the control parameter and N measures the system size. For infinite N, $\langle m\rangle$ jumps at $p = p_c$ if the transition is discontinuous, while it varies continuously with a power law singularity $\langle m\rangle \sim (p - p_c)^{\beta}$ for a continuous transition. The distribution $P_{p=p_c,N}(m)$ at criticality scales, for continuous transitions, as [25]

$$P_{p=p_c,N}(m) \sim N^{\eta} f(mN^{\eta}), \tag{1}$$

where $\eta = \beta/(d\nu)$ for standard thermal second order phase transitions. The universal function $f(z)$ might be double humped, as in the Ising model [25]. But then, as $N \to \infty$, the dip between the humps usually does not deepen and the horizontal distance between them shrinks to zero so that $P_{p=p_c,N}(m)$ becomes single humped.

Equation (1) is directly related to the finite size scaling (FSS) of $\langle m\rangle$ [26],

$$\langle m\rangle \sim (p - p_c)^{\beta} g[(p - p_c)N^{\Theta}], \tag{2}$$

where the universal scaling function $g(z)$ is analytic at all finite z, reflecting the fact that the critical point was the only singularity of the partition function, before it was regularized by Eq. (2). Notice that the usual FSS ansatz [26] involves the linear system size L instead of N with $\Theta = 1/(d\nu)$, where d is the dimension and ν is the correlation length exponent.

In typical first-order transitions, in contrast, $P_{p=p_c,N}(m)$ is double humped with a deepening valley between the two

peaks. The distance between the peaks tends to a positive constant which is equal to the jump in $\langle m \rangle$. The depth of the valley between the peaks reflects the fact that values of m between the peaks correspond to systems with two coexisting phases and an interface between them that costs energy and is disfavored. As a consequence, systems with first-order transitions typically do not show FSS (unless the interface energy does not increase with system size [27]).

In percolation, usually the relative size of the largest cluster, $m \equiv s_{\max}/N$, is taken as an order parameter. Here, N is the number of nodes, and $s_{\max}/N \to 0$ for $p < p_c$ and $N \to \infty$. In [6,16] it was observed that $P_{p=p_c,N}(m)$ is strongly double peaked in EP transitions. In [16] this was also backed by careful measurements of the depth of the valley between the peaks, which indeed lowered with increasing N. This was taken as a clear indication for the transition being first order and for phase coexistence. Notice that the latter is not justified since $s_{\max}/N$ is, in contrast to the local order parameters in thermal systems, a global quantity and cannot be used to characterize any part of a large system. Rather, the structure of $P_{p=p_c,N}(m)$ in EP reflects the suddenness of the transition, combined with a scatter of the precise p values where individual systems acquire giant clusters. At p values where both peaks have the same height, it is much more likely to find either no giant cluster or a fully developed one, than to find a half-grown giant cluster. Hence, the two peaks are more reminiscent of systems without self-averaging [28] than of phase coexistence.

While the two peaks prove the suddenness of the transition that was claimed as a hallmark of EP, they do not yet prove that EP is discontinuous. For that, one must also show that the distance between the peaks does not vanish for $N \to \infty$. In order to check this, we have made extensive simulations of four models: The original product rule of [1], denoted in the following as "PR"; The product rule on 2D square lattices [3,4] with helical boundary conditions ("2D"); The "adjacent edge" rule [7] ("AE"); And the rule of [20] ("CDGM"). For details on the simulations, see the supplemental material (SM) [29].

Distributions $P_{p,N}(m)$ for these models are shown in Fig. 1. In all cases p was chosen such that both peaks have equal height (set arbitrarily to 1). The extrapolations of these values for $N \to \infty$ are given in Table I. They agree within errors with the critical p_c values quoted in the literature. We see that in each case the valley between the peaks deepens with increasing N [16], but at the same time both peaks shift to the left. Among the three off-lattice models, the AE model (the least nonlocal) shows the fastest peak shifting and slowest valley deepening, while the opposite is true for the CDGM model. In all cases this shift is compatible with power laws

$$m_{\pm} \sim N^{-\eta_{\pm}}, \tag{3}$$

where $m_+(m_-)$ is the position of the right (left) peak at the critical point. In all cases $0 < \eta_+ < \eta_-$ (see Table I), i.e.,

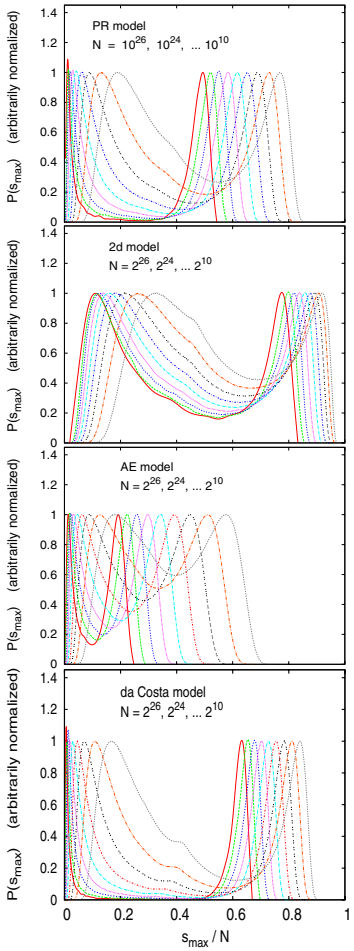

FIG. 1 (color online). Distributions of the order parameter $s_{\max}/N$ for four EP models. They are shown at the effective critical point, defined such that both peaks have the same height. Normalization is such that their height is 1. For the largest systems, curves were approximated by cubic splines to make them smooth.

the right peak moves slower than the left one. Therefore the distance between the peaks increases for small N, but finally decreases $\sim N^{-\eta_+}$. When p is chosen such that the two peaks have equal *area*, the distance between them is asymptotically proportional to the maximum of the variance of m. Since the peak positions change very little when passing from equal heights to equal masses [16], the variances first increase with N (in agreement with [4]), but ultimately decreases.

Indeed, basing Eq. (3) on peak positions when both peaks have equal areas would seem more natural than basing it on equal peak heights. It was not done in Figs. 1 and 2 for purely technical reasons—peak areas are difficult to define for shallow minima, and the shifts in position would be visually less evident in view of the

TABLE I. Critical points and critical exponents for the four models. The Θ_i are different estimates of the exponent Θ: Θ_1 is obtained from the scaling relation $\Theta = \eta_+/\beta$, Θ_2 is obtained from a data collapse in the slightly supercritical region where $\langle m\rangle \approx m_+$, and Θ_{conj} is the conjectured exact value. For the CDGM model, p_c is taken from [20]. For the other models it is obtained from plots analogous to the inset in Fig. 4.

	PR	2d	AE	CDGM
p_c	0.888449(2)	0.526562(3)	0.797013(3)	0.923207508
η_+	0.0402(15)	0.018(2)	0.103(2)	0.0255(8)
η_-	0.270(7)	0.078(7)	0.228(5)	0.300(5)
β	0.0861(5)	0.040(2)	0.214(2)	0.0557(5)
Θ_1	0.47(2)	0.45(6)	0.48(1)	0.46(2)
Θ_2	0.52(1)	0.47(3)	0.51(1)	0.53(1)
Θ_{conj}	1/2	-	1/2	1/2
η_0	0.0567(9)	0.0612(8)	0.1113(8)	0.0356(8)

vastly different heights. The resulting values of $\eta_\pm$ would be slightly larger (by 5% to 10%) than those given in Table I. This would eliminate the small differences between Θ_1 and Θ_2 discussed below, but it would not otherwise affect our conclusions.

As shown in Fig. 2 for the CDGM model, not only the positions of the peaks scale, but also their widths. This indicates that the asymptotic scenario is two well separated peaks with N-independent shapes whose widths are proportional to their positions. If we switch from defining p_c by equal peak heights to equal peak areas and allow weak convergence for $N \to \infty$ (in contrast to the usual assumption of pointwise convergence; see the SM [29]) the full distributions at $p_c(N)$ then show asymptotic scaling

$$P_{p_c(N),N}(m) \sim N^{\eta_+} f(mN^{\eta_+}) \tag{4}$$

with the scaling function $f(x)$ consisting of a finite width right hand peak and a δ peak at $x = 0$.

For p strictly larger than $p_c(N)$, only the right hand peak dominates the average $\langle m\rangle$. We then expect only small finite size scaling corrections to its asymptotic values, i.e., we expect the curves $\langle m\rangle_{p,N}$ for different N to coincide for $p > p_c(N)$ on a common curve $\langle m\rangle_p$. Since the scenario in this regime is not much different from other critical phenomena this should be a power law $\langle m\rangle \sim (p - p_c)^\beta$ that holds in the range $m_+ < \langle m\rangle \ll 1$. Measured values of β are given in Table I. For the CDGM model the agreement with [20] is perfect. Assuming Eq. (2), it follows that $\Theta = \eta_+/\beta$. Values of Θ obtained from this, denoted as Θ_1, are slightly smaller than 1/2 for all models (see Table I).

Deviations from this common power law are expected to set in when $\langle m\rangle$ decreases below m_+. The data for the CDGM model are shown in Figs. 3. For all $p > p_c$ (except for very small values of $z = (p - p_c)N^\Theta$), these deviations are fully described by the FSS ansatz in Eq. (2). In Figs. 3 we chose Θ so that the collapse is best at $\langle m\rangle \approx m_+$, resulting in the value Θ_2 quoted in Table I. For the other models the data collapse is similarly good, except for the 2D model where it is worse (see SM). For all models, Θ_2 is slightly larger than Θ_1.

The fact that $f(z)$ in Eq. (4) contains a δ peak at its leftmost extremity $z = 0$ implies that $g(z)$ in Eq. (2) must vanish for all z below some value $z_0 \le 0$, which in turn means that $g(z)$ must have a singularity at z_0. Indeed, Fig. 4 shows that the values of $g(z)$ for $z < -1$ approach 0 very fast with increasing N, implying $-1 < z_0 \le 0$ (the latter is also true for the other models). We cannot exclude the possibility the curves in Fig. 4 approach a pure power law az^β (dashed red line) in the limit $N \to \infty$.

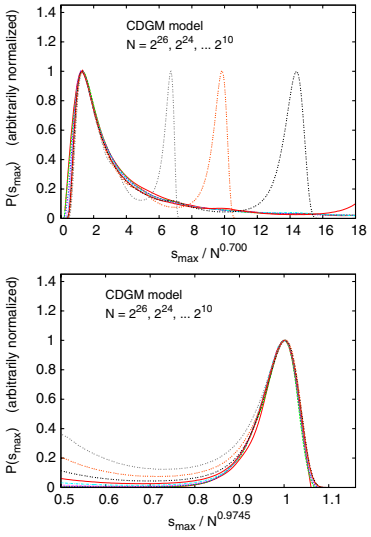

FIG. 2 (color online). Data collapses for the two peaks in the order parameter distribution for the CDGM model. Colors and line styles are the same as in Fig. 1.

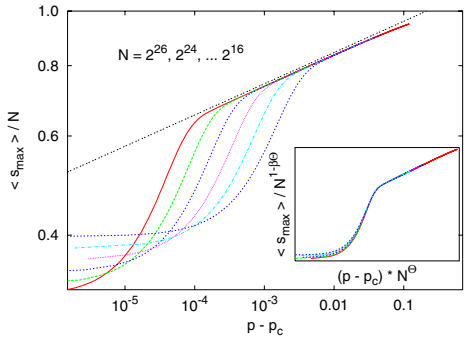

FIG. 3 (color online). Log-log plot of the average order parameter for the CGDM model *versus* $p - p_c$, for six different values of N. One sees clearly a common part with slope β (indicated also by the straight line), from which curves for different N deviate later and later, as N increases. The inset shows the collapse of these data as predicted by Eq. (2). While Θ is fitted, both β and p_c are taken from [20].

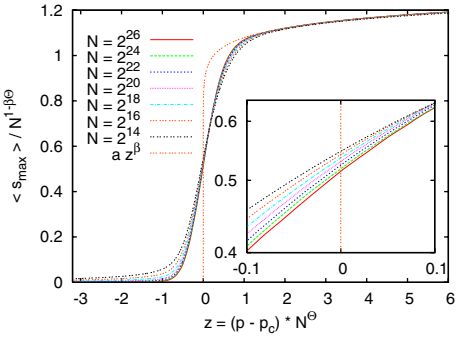

FIG. 4 (color online). Doubly linear plot of the same data shown in Fig. 3, but extended to values $p < p_c$. Here we used $\Theta = 1/2$, which gives worse data collapse for $p > p_c$, but vastly more systematic behavior for $p < p_c$. The inset shows a blowup of the region around $p = p_c$, with logarithmic y axis. The decrease of the curves at $z = 0$ with N suggests that $z_0 = 0$, and that a new power law holds for $p = p_c$.

The blowup of the region around $z = 0$ shown in the inset in Fig. 4 hints at a power law $\langle m \rangle|_{p=p_c} \sim N^{-\eta_0}$ with $\eta_0 = 0.0356(8) > \eta_+$ (see also SM). The same is qualitatively true for the other models, where always $\eta_0 > \eta_+$ (see Table I). We find therefore that $z = 0$ is no longer in the realm of uniform pointwise convergence to the FSS ansatz, and hence that $z_0 = 0$. We finally mention that we used $\Theta = 0.5$ in Fig. 4, a value in between Θ_1 and Θ_2, as it gives the simplest behavior for $z < 0$. The same is true for the other off-lattice models (but not for the 2D model, see [29]), when we conjecture that $\Theta = 0.5$ for them.

The singularity of $g(z)$ at $z = 0$ implies also that one cannot expect the effective critical points to scale as $p_c(N) - p \sim N^{-\Theta}$. Results obtained for the CDGM model, with $p_c(N)$ defined via equal peak masses, are shown in the SM [29]. They indicate that $p_c(N) - p \sim N^{-\delta}$ with $\delta = 0.9(1) > \Theta$. The agreement with the prediction $\delta = 0.818(1)$ of [20]—based on "standard scaling relations"—seems fortitious.

In this Letter we do not present a detailed theory for the convergence to $g(z)$ for $z \leq 0$, in particular, we do not explain how η_0 and δ are related to η_-. Such a theory is presumably formulated more easily by using either $\langle \log s_{\max} \rangle$ or $\langle 1/s_{\max} \rangle$ as an order parameter. But this would be beyond the scope of the present Letter.

In summary, we have shown that four models of explosive percolation, including the original product rule of Achlioptas *et al.* [1], have continuous transitions. Each is in a different universality class, but all of them show unusual finite size behavior with a nonanalytic scaling function. They all show double-peaked order parameter distributions with the sharpness of the peaks increasing with system size, and different scaling laws for the width of the scaling region ($\sim N^{-\Theta}$) and for the shift of the effective $p_c(N)$. This scenario is *not* found for other recent models [9,17,30] that do indeed show discontinuous transitions. It could be that the features found in the present Letter arise from the specific nonlocality of the Achlioptas process, and that this is why it was not seen previously in other critical phenomena.

We are indebted to Bob Ziff and Liang Tian for most useful correspondence.

[1] D. Achlioptas, R. M. D'Souza, and J. Spencer, Science **323**, 1453 (2009).
[2] E. J. Friedman and A. S. Landsberg, Phys. Rev. Lett. **103**, 255701 (2009).
[3] R. M. Ziff, Phys. Rev. Lett. **103**, 045701 (2009).
[4] R. M. Ziff, Phys. Rev. E **82**, 051105 (2010).
[5] F. Radicchi and S. Fortunato, Phys. Rev. Lett. **103**, 168701 (2009).
[6] F. Radicchi and S. Fortunato, Phys. Rev. E **81**, 036110 (2010).
[7] R. M. D'Souza and M. Mitzenmacher, Phys. Rev. Lett. **104**, 195702 (2010).
[8] H. D. Rozenfeld, L. K. Gallos, and H. A. Makse, Eur. Phys. J. B **75**, 305 (2010).
[9] S. S. Manna and A. Chatterjee, Physica (Amsterdam) **390A**, 177 (2011).
[10] A. A. Moreira *et al.*, Phys. Rev. E **81**, 040101 (2010).
[11] Y. S. Cho, B. Kahng, and D. Kim, Phys. Rev. E **81**, 030103 (2010).
[12] Y. S. Cho *et al.*, Phys. Rev. Lett. **103**, 135702 (2009).
[13] Y. S. Cho *et al.*, Phys. Rev. E **82**, 042102 (2010).
[14] N. A. M. Araújo and H. J. Herrmann, Phys. Rev. Lett. **105**, 035701 (2010).
[15] U. Basu *et al.*, arXiv:1008.4293.
[16] L. Tian and D.-N. Shi, arXiv:1010.5990.
[17] W. Chen and R. M. D'Souza, Phys. Rev. Lett. **106**, 115701 (2011).
[18] J. Nagler, A. Levina, and M. Timme, Nature Phys. **7**, 265 (2011).
[19] H. Hooyberghs and B. Van Schaeybroeck, Phys. Rev. E **83**, 032101 (2011).
[20] R. A. da Costa *et al.*, Phys. Rev. Lett. **105**, 255701 (2010).
[21] O. Riordan and L. Warnke, arXiv:1102.5306.
[22] In contrast to claims made by the authors, the model in [7] is also nonlocal by any standard physics definition.
[23] C. Christensen *et al.*, arXiv:1012.1070.
[24] H.-K. Janssen, M. Müller, and O. Stenull, Phys. Rev. E **70**, 026114 (2004).
[25] A. D. Bruce and N. B. Wilding, Phys. Rev. Lett. **68**, 193 (1992).
[26] K. Binder and D. W. Heermann, *Monte Carlo Simulations in Statistical Physics* (Springer, Heidelberg, 2010), 5th ed.
[27] M. S. Causo, B. Coluzzi, and P. Grassberger, Phys. Rev. E **62**, 3958 (2000).
[28] S. Wiseman and E. Domany, Phys. Rev. Lett. **81**, 22 (1998).
[29] See supplemental material at http://link.aps.org/supplemental/10.1103/PhysRevLett.106.225701.
[30] S. V. Buldyrev *et al.*, Nature (London) **464**, 1025 (2010).

Supplementary Material for "Explosive Percolation is Continuous, but with Unusual Finite Size Behavior"

Peter Grassberger,[1,2] Claire Christensen,[2] Golnoosh Bizhani,[2] Seung-Woo Son,[2] and Maya Paczuski[2]

[1] *FZ Jülich, D-52425 Jülich, Germany*

[2] *Complexity Science Group, University of Calgary, Calgary T2N 1N4, Canada*

(Dated: August 19, 2012)

SIMULATION DETAILS

All simulations reported in the paper were made using modified versions of the fast Newman-Ziff algorithm [1], on a Linux workstation cluster. System sizes varied between $N = 2^{10}$ and $N = 2^{26} (\approx 6.7 \times 10^7)$ (N is the number of nodes). For the smaller systems $\approx 10^8$ realizations were made for each model, and for the largest systems this number was still $> 10^4$. The control parameter p is defined as in the references where the 4 models were introduced, as $p = L/N$ where L is the number of links.

Data were actually collected for fixed n, where n is the number of clusters – more precisely, in order to reduce the data files, n was binned (typically with $\Delta n = 1$ for smallest N and $\Delta n = 2^8$ for largest N). The values of p quoted in the paper are average values over these bins. Since most clusters in all four models are trees, except when p is very large, there are very small fluctuations of p for fixed n, and $\langle p \rangle$ depends smoothly on n. Moreover, test runs showed that the dependence of $s_{\max}$ on n is at least as crisp as the dependence on p, i.e. n is actually the more relevant control parameter.

Mass distributions (Figs. 1 and 2 in the main paper) are obtained by binning, with typically 200 to 500 bins, and with bin sizes slowly increasing with $s_{\max}$ in order to take into account that the left hand peaks in Fig. 1 are sharper than the right hand peaks. For small N the distributions shown in Figs. 1 and 2 are the raw data, modified just by interpolating between neighboring n bins to obtain exactly equally high peaks (usually, no bin will have two peaks which have exactly equal height; by "interpolating" we mean taking weighted linear averages of the two histograms) and by normalizing them. For the largest N this would have given too noisy plots, and cubic splines were used to make the plots more smooth.

Unless otherwise noted, p_c values are those in Table 1. They were determined by having best power laws $\sim N^{-\eta_0}$ for $\langle m \rangle$ at $p = p_c$.

MODIFIED FINITE SIZE SCALING

The finite size scaling ansaetze Eqs. (1) and (2) are of course never exact, and are usually understood as

$$\lim_{N\to\infty} N^{-\eta} P_{p=p_c,N}(m = z/N^{\eta}) = f(z) \tag{1}$$

and

$$\lim_{N\to\infty} (p - p_c = z/N^{\Theta})^{-\beta} \langle m \rangle = g(z) \tag{2}$$

for any fixed finite value of z. The limits here are pointwise limits, i.e. the norms of the differences between left and right hands converge uniformly to zero in any finite interval of z. Furthermore, $f(z)$ and $g(z)$ are usually analytic (holomorphic) for all finite z.

In a typical first order (discontinuous) transition, an attempt to construct $f(z)$ would give a function with two δ-peaks. In that case the convergence could at best be *weak*, i.e. in distribution sense. Usually one prefers to call this not finite size scaling at all, although this is strictly spoken a matter of taste and convention.

In explosive percolation one has a "mixed" situation: For the right hand peaks in Figs. 1 and 2 of the main paper one has pointwise convergence, if one chooses $\eta = \eta_+$. But then the left hand peak converges to a δ-peak, i.e. the entire function $f(z)$ is approached only in the weak sense. Similarly, for $g(z)$ the convergence is strong (and $g(z)$ is analytic) for $z > 0$ (strict inequality!), where only the right hand peak of $f(z)$ contributes. The function $g(z)$ must vanish identically when only the left (δ-) peak contributes, which means that it must have a singularity at $z_0 \leq 0$, and convergence can only be weak in any interval containing z_0. As for first order transitions, it is a matter of convention whether one calls this finite size scaling at all (as we did in this paper).

ANALOGA TO FIG. 3 (MAIN PAPER) FOR THE OTHER THREE MODELS

In the main paper, we showed in Fig. 3 for the da Costa model how $\langle m \rangle$ scales for $p > p_c$, and we said that a data collapse similar to that shown in the inset holds also for the other two off-lattice models, while the collapse is much worse for the 2d model. We now show these data in Figs. S1 to S3.

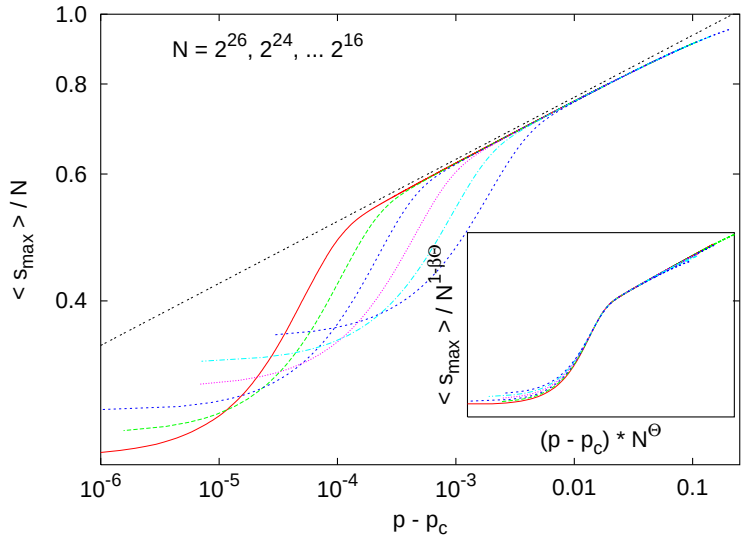

FIG. 1. (Color online) Log-log plot of the average order parameter for the PR model *versus* $p - p_c$, for six different values of N, similar to Fig. 3 of the main paper. The value of p_c is chosen such that decrease of $\langle m \rangle$ with N, for $p \to p_c$, is a pure power law.

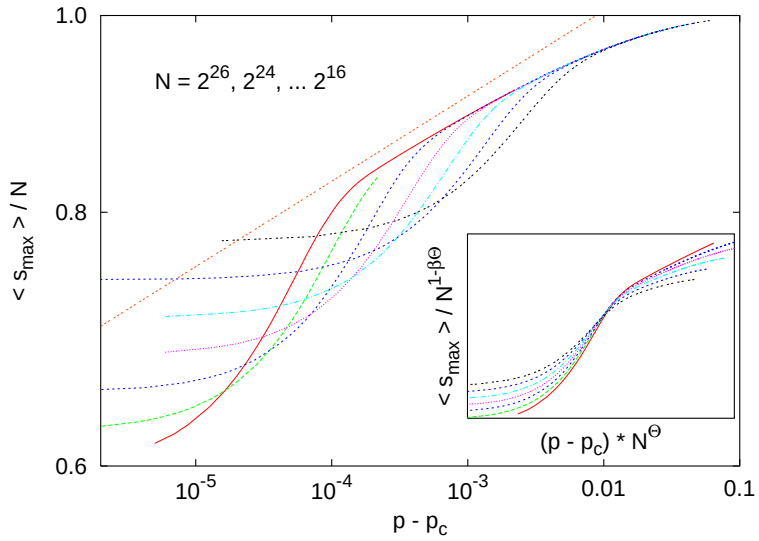

FIG. 2. (Color online) Same as Fig. S1, but for the 2d model. This time the data collapse is much worse (see the inset). For large $z \equiv (p - p_c)N^{\Theta}$ this is due to the much slower drift of the right hand peak in Fig. 1. For $z \to 0$ it reflects the large difference between η_0 and η_+.

VARIOUS OTHER PLOTS FOR THE DA COSTA MODEL

Although the scaling behavior of the order parameter with N at $p = p_c$ can, in principle, be inferred from Fig. 4 (main paper), we show the data also explicitly in Fig. S4. In this figure we use three possible values of p_c (one of them being the value obtained in [2], in order to show how strongly the exponent η_0 depends on p_c.

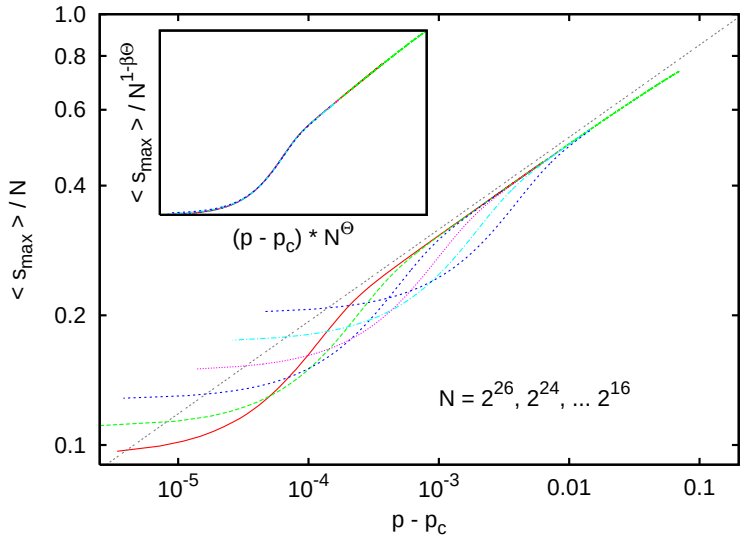

FIG. 3. (Color online) Same as Fig. S1, but for the AE model. This time the data collapse is better than in the other models (see the inset), reflecting the fact that the AE model is closest to an ordinary second order transition, among the four models studied here.

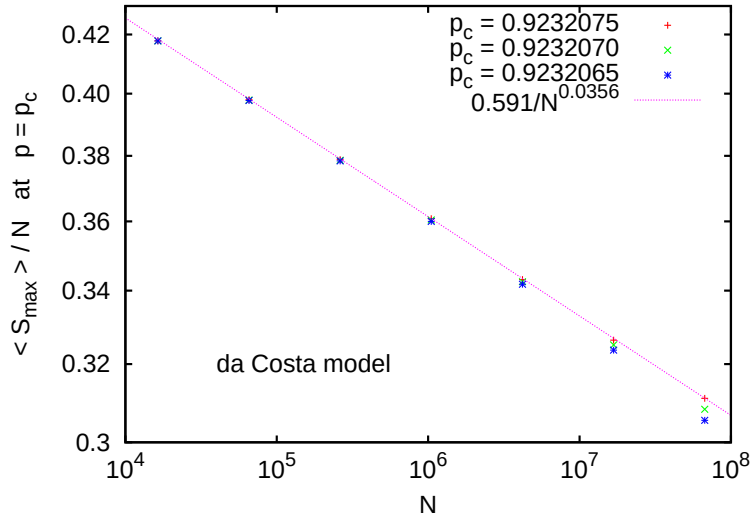

FIG. 4. (Color online) Log-log plot of $\langle m \rangle$ at $p = p_c$ plotted *versus* N. In order to show the sensitivity of the exponent η_0 to the precise value of p_c, curves for three values of the latter are shown.

Results for $p_c(N)$, the effective critical points on finite systems, are given in Fig. S5. Notice that values of $p_c(N)$ depend crucially on the operational procedure used to define effective critical points. One possibility would be e.g. the point where the two peaks in $P(s_{\max})$ have equal height (Fig. 1). For the da Costa model, this would give non-monotonic dependence on N. More natural seems the definition via equal areas under the two peaks. Notice that this would give ambiguous results for the 2d and AE models, as there the dips between the peaks are not very deep. But for the da Costa model this is unproblematic. Figure 5 shows that our best estimate of p_c is slightly below the

value of [2], giving thereby the largest contribution to the uncertainty of the exponent δ (this slight inconsistency is also the reason why we used also these smaller p_c values in Fig. S4).

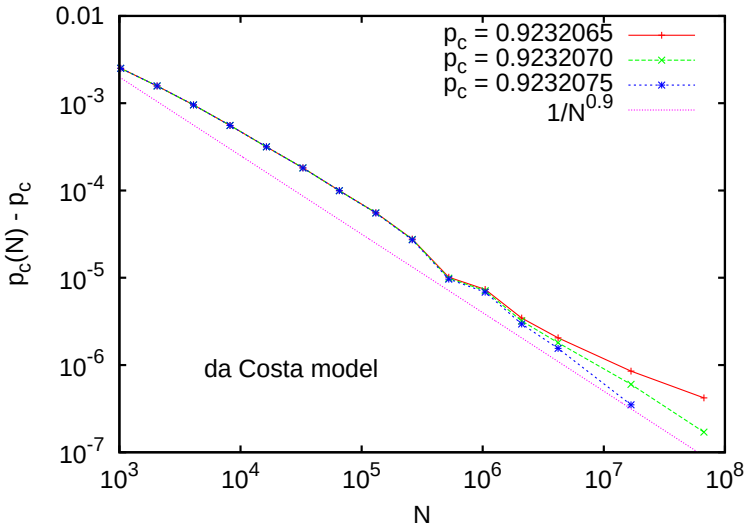

FIG. 5. (Color online) Log-log plot of $p_c(N)$, defined as the value where the areas under both peaks in $P(s_{\max})$ have equal height, *versus* N. Notice that there are only two points for $N = 2^{26}$, since our $p_c(N = 2^{26})$ is smaller than the p_c value of [2].

Alternatively, we could define $p_c(N)$ as the point where $P(s_{\max})$ has maximal variance. Variances of $P(s_{\max})/N^{1-\eta_+}$ are plotted in Fig. S6 against $(p - p_c)N^{1/2}$. We see distributions which are for small N markedly skewed and shifted away from the origin, but which become increasingly symmetric and centered at the origin as N increases. Although this gives a much less precise estimate of δ than Fig. S5, it demonstrates also that $\delta > \Theta$.

Plots similar to Figs. S5 and S6 were not made for the other models, the main reason being the larger uncertainties of p_c.

FOR THE 2D MODEL, Θ IS STRICTLY SMALLER THAN 1/2

As we said in the paper, one observation that corroborates $\Theta = 1/2$ for the off-lattice models is that it gives very "regular" behavior of $\langle m \rangle$ in the near subcritical region. Instead of showing here the evidence for this, we show for the 2d model what can go wrong, if Θ is chosen badly. More precisely, we show in the top panel of Fig. S7 results for $\Theta = 0.47$, and results for $\Theta = 0.5$ in the lower panel. It seems clear that panel (b) is not very plausible, in particular since the scaling $m_- \sim N^{-\eta_-}$ with $\eta_- > \eta_+$ of the left hand peaks in Fig. 1 requires that the curves decrease with N for $z < 0$. For the other models similar curve crossings appeared when $\Theta = \Theta_2$ was used instead of $\Theta = 1/2$.

FURTHER COMPARISONS WITH PREVIOUS PAPERS

a) To our knowledge, the only previous work where $\Theta \neq \delta$ was seen in a continuous phase transition is [3]. This dealt with interacting self avoiding walks in 4 dimensions. The authors also found double-peaked distributions of the order parameter, but they did not report different scaling laws for both peaks. Thus the reason for $\Theta \neq \delta$ was not explained, as in our case, via a singularity of the scaling function $g(z)$. Also, in [3] the authors found $\Theta \gg \delta$, while we found in our models $\Theta < \delta$.

b) A different scaling theory for the PR model was presented in [4]. The authors there started from the assumption that $\langle m \rangle$ is independent of N at $p = p_c$, which is definitely not true for any of the four models according to our simulations. Although this prevents our theories from being equivalent, there are some similarities. In particular,

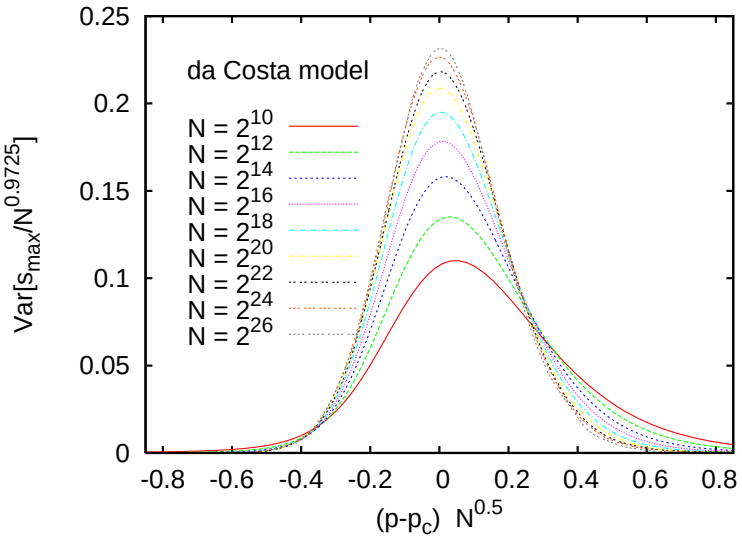

FIG. 6. (Color online) Variances of $s_{\max}$ for fixed N, plotted *versus* $z = (p - p_c)N^{1/2}$, using the p_c value of [2]. The width rescaling and the normalization are such that the curves should collapse for $N \to \infty$. For the N values shown in the figure, the collapse is far from perfect, but this is to be expected. Notice that the horizontal peak positions hardly change for $N > 2^{20}$, showing that $\delta > \Theta$.

the authors of [4] show that the width of the FSS region scales as $N^{-\theta}$ with $\theta = 0.48$, which is very close to our conjectured value $\Theta = 1/2$.

c) A detailed study of the 2d model was made in [5]. The most remarkable agreement is that η_0 was measured there as 0.0589(10), while we found 0.0612(8). The slight discrepancy is partially due to a slightly different estimate of p_c (0.526565(5) in [5] against 0.526562(3) in the present work). Also the estimate of the Fisher exponent τ in [5] is fully compatible with our value of β, if we accept the relationship between the two exponents given in [2].

[1] M. E. J. Newman and R. M. Ziff, Phys. Rev. E **64**, 016706 (2001)
[2] R. A. da Costa *et al.*, Phys. Rev. Lett. **105**, 255701 (2010)
[3] T. Prellberg and A. L. Owczarek, Phys. Rev. E **62**, 3780 (2000)
[4] Y. S. Cho *et al.*, Phys. Rev. E **82**, 042102 (2010)
[5] R. M. Ziff, Phys. Rev. E **82**, 051105 (2010)

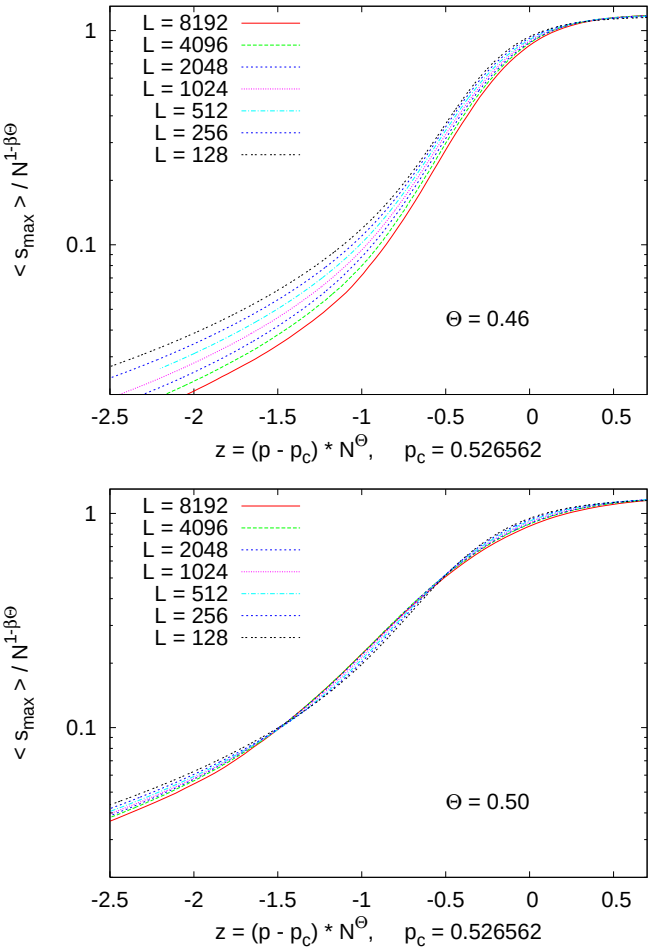

FIG. 7. (Color online) Linear-log plots of $\langle s_{\max}\rangle/N^{1-\beta\Theta}$ against $(p-p_c)N^{\Theta}$ for the 2d model. In both plots we used the values for β and p_c given in Table 1. In the upper panel we used $\Theta = 0.46$ (the average between Θ_1 and Θ_2), while we used $\Theta = 0.5$ in the lower panel.

A Letters Journal Exploring the Frontiers of Physics

January 2012

EPL, **97** (2012) 16006
doi: 10.1209/0295-5075/97/16006

www.epljournal.org

Percolation theory on interdependent networks based on epidemic spreading

Seung-Woo Son[1(a)], Golnoosh Bizhani[1], Claire Christensen[1], Peter Grassberger[1,2] and Maya Paczuski[1]

[1] *Complexity Science Group, University of Calgary - Calgary T2N 1N4, Canada*
[2] *FZ Jülich - D-52425 Jülich, Germany, EU*

received 21 September 2011; accepted 28 November 2011
published online 3 January 2012

PACS 64.60.ah – Percolation
PACS 05.70.Jk – Critical point phenomena
PACS 05.40.-a – Fluctuation phenomena, random processes, noise, and Brownian motion

Abstract – We consider percolation on interdependent locally treelike networks, recently introduced by Buldyrev S. V. *et al.*, *Nature*, **464** (2010) 1025, and demonstrate that the problem can be simplified conceptually by deleting all references to cascades of failures. Such cascades do exist, but their explicit treatment just complicates the theory —which is a straightforward extension of the usual epidemic spreading theory on a single network. Our method has the added benefits that it is directly formulated in terms of an order parameter and its modular structure can be easily extended to other problems, *e.g.* to any number of interdependent networks, or to networks with dependency links.

On September 28, 2003, Italy experienced its most severe blackout in over 20 years [1]. The blackout's severity was later attributed to the fact that an initial failure on the physical power grid disrupted not only the grid, itself, but also a computer network that depended on this grid for electricity [1,2]. Since the grid's substations were, in turn, dependent on this computer network for their regulation, further failures in the grid ensued as communication among the stations was lost. Ultimately, recursive cascading failures throughout *both* networks occurred, and both networks changed from percolating to non-percolating [1–4]. While this is a spectacular example of percolation on interdependent networks, it is, by no means the only one: in fact, *most* real-world networks can be seen as having some interdependency [5–7]. A clear description of how perturbations propagate through such networks —*i.e.* of how perturbations can effect percolation (fragmentation)— is essential to understanding systems involving interdependence, including economic markets, interrelated technological and infrastructural systems, social networks, disease dynamics, or human physiology.

Recent models of percolation on interdependent networks have been described in terms of failures cascading back and forth between the networks [2–4]. While there is no doubt that percolation on interdependent networks *can* be seen as a cascading phenomenon, the mathematics behind such a description is cumbersome and far from transparent. Here we simplify matters by omitting all aspects of cascading and treat percolation on interdependent networks as an epidemic spreading process in complete analogy to ordinary percolation. If one wants to consider cascades explicitly, this can be done in a second step, after the phase transition itself is well understood. We also show that percolation on dependency networks [4,8], which are single networks composed of both connectivity links and dependency links, can be described within the same paradigm.

Both the theory of [2–4] and the present paper deal only with *locally treelike* random networks, for which mean-field theory based on generating functions becomes exact in the large system limit. The cascade-based studies in [2–4] considered site percolation networks from which a certain fraction $1-p$ of nodes had been removed. On general networks (including lattices), this site dilution can lead to a topological modification of the networks [9], but in the present cases it just leads to a trivial rescaling of the number of nodes and links. Thus we can restrict ourselves, without loss of generality, to the case $p=1$ and only consider bond percolation, which further simplifies the discussion.

(a) E-mail: sonswoo@gmail.com

In the following, we first recall the theory of epidemic spreading (ordinary percolation theory) on single networks [10,11], and then demonstrate how this can be easily adjusted to accommodate percolation on interdependent networks or on dependency networks. We only consider the limit of large networks, where the number of nodes $N \to \infty$.

i) *Single network*: First consider a single (isolated) random network with mean degree z, with an epidemic spreading from some starting node. Let S_i be the probability that node i is infected during this epidemic (*i.e.* that it is part of the infinite percolating cluster). Its average over all nodes, denoted as S, is taken as the order parameter of the model. The probability that node i is not infected is equal to the chance that none of its neighbors are infected through their remaining links:

$$1 - S_i = \prod_{\langle ij \rangle} (1 - S'_j), \tag{1}$$

where the product runs over all neighbors of i and S'_j is the probability that node j is infected through a randomly chosen edge *not* attached to i. When the graph is locally treelike, all S'_j are independent. Averaging eq. (1) over all nodes gives then

$$S = 1 - \sum_k p(k)(1 - S')^k \equiv 1 - G_0(1 - S'), \tag{2}$$

where $p(k)$ is the probability that a node has k links and $G_0(x)$ is the corresponding generating function $G_0(x) \equiv \sum_k p(k) x^k$. Similarly, one can write down the equation for S'

$$S' = 1 - \sum_k \frac{k p(k)}{z} (1 - S')^{k-1} \equiv 1 - G_1(1 - S'), \tag{3}$$

where $z = G'_0(1)$ and $G_1(x) \equiv G'_0(x)/z$. For any given degree distribution we can first solve eq. (3) to obtain S', and then insert it into eq. (2) to obtain S. The percolation transition threshold z_c is given by $S = 0$ for $z < z_c$ and $S > 0$ for $z > z_c$ [10,11].

For instance, the degree distribution of Erdös-Rényi (ER) graphs [11,12] is Poissonian. Therefore,

$$\begin{aligned} G_0(1 - S') &= \sum_k \frac{e^{-z} z^k}{k!} (1 - S')^k = e^{-zS'} \\ &= G_1(1 - S'). \end{aligned} \tag{4}$$

Thus, $S = S'$ and eqs. (2) and (3) give simply $S = 1 - e^{-zS}$. Defining $f(S) = S - 1 + e^{-zS}$, one can find the solution $S(z)$ by solving $f(S) = 0$ graphically, as shown in fig. 1. A continuous ("second-order") phase transition is clearly evident in the inset of fig. 1.

Equations (2) and (3), are the order parameters for a single network, where S represents the probability that a randomly chosen node places in the infinite percolating cluster and S' is the same probability, but defined when we pick an edge randomly and look at the end node. These equations act as fundamental "building blocks" or "modules" for treating analogously the probability, on fully or partially interdependent networks, to be connected to the infinite percolating clusters.

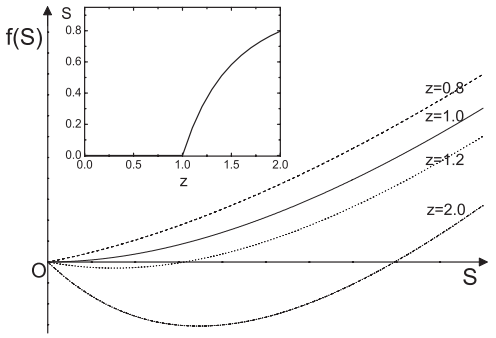

Fig. 1: Graphical solutions for ordinary percolation on a single ER network. The inset shows the *continuous* change of order parameter S as z increases.

ii) *Two fully interdependent networks*: Consider now two networks $\mathcal{A}$ and $\mathcal{B}$, where each node in $\mathcal{A}$ depends only on one node in $\mathcal{B}$ and vice versa. In order for a node in network $\mathcal{A}$ to be part of the percolating cluster, its partner in $\mathcal{B}$ must also be part of that cluster. Since this mapping is one-to-one we can merge each node in $\mathcal{A}$ with its partner in $\mathcal{B}$ to have one set of nodes, each with two sets of links. We define $\mathcal{AB}$-clusters as subsets of nodes connected both in $\mathcal{A}$ and in $\mathcal{B}$. More precisely a set of nodes $C = \{i_1, i_2, \dots i_m\}$ is an $\mathcal{AB}$-cluster if any two points $i, j \in C$ are connected by two paths: one path using only links $\in \mathcal{A}$ and nodes only $\in C$, and the other using only links $\in \mathcal{B}$ and also using nodes only $\in C$. We do not allow paths that involve nodes outside C, so $\mathcal{AB}$-clusters are *self-sustaining* [9].

The probability that any node belongs to the infinite $\mathcal{AB}$-cluster is equal to the probability to be linked to it both via $\mathcal{A}$- and via $\mathcal{B}$-links. That is, a node looks out at its $\mathcal{A}$-links to see if it has a neighbor on the percolating $\mathcal{AB}$-cluster. It also looks out via its $\mathcal{B}$ links. Only if it has a neighbor via both sets of links is it a member of this cluster. Therefore S is simply a product of the right-hand side of eq. (2) for networks $\mathcal{A}$ and $\mathcal{B}$,

$$S = (1 - G_0^{\mathcal{A}}(1 - S'_{\mathcal{A}}))(1 - G_0^{\mathcal{B}}(1 - S'_{\mathcal{B}})), \tag{5}$$

where the superscripts (subscripts) $\mathcal{A}$ and $\mathcal{B}$ refer to networks $\mathcal{A}$ and $\mathcal{B}$, respectively and $S_{\mathcal{A}} = S_{\mathcal{B}} = S$. Here, $S'_{\mathcal{A}}$ (and analogously $S'_{\mathcal{B}}$) is defined as the probability that a node reached by following a random $\mathcal{A}$-link is in the $\mathcal{AB}$-cluster. For this to happen, its partner node —which is a random node from the point of view of network $\mathcal{B}$— has also to be connected to the $\mathcal{AB}$-cluster via $\mathcal{B}$-links. $S'_{\mathcal{A}}$ and $S'_{\mathcal{B}}$ are different from each other since they depend on the degree distribution of each network. When choosing edges at random, the end node of a randomly chosen edge in network $\mathcal{A}$ belongs to the $\mathcal{AB}$-cluster only when its partner

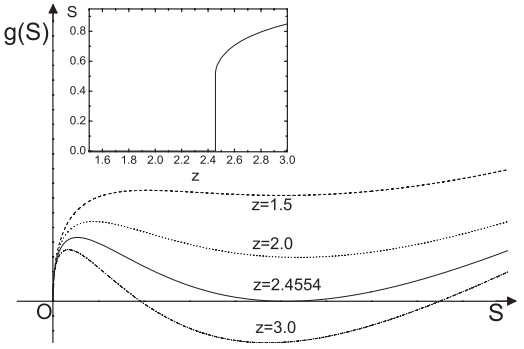

Fig. 2: Graphical solutions for the percolating cluster on two fully coupled ER networks with the same mean degree z. The inset shows a *discontinuous* change of order parameter S as z increases.

node in network $\mathcal{B}$ is concurrently a member of this cluster, and vice versa. The probabilities of these events occurring —$S'_{\mathcal{A}}$ and $S'_{\mathcal{B}}$— are given by

$$\begin{aligned} S'_{\mathcal{A}} &= (1 - G_1^{\mathcal{A}}(1 - S'_{\mathcal{A}}))(1 - G_0^{\mathcal{B}}(1 - S'_{\mathcal{B}})), \\ S'_{\mathcal{B}} &= (1 - G_1^{\mathcal{B}}(1 - S'_{\mathcal{B}}))(1 - G_0^{\mathcal{A}}(1 - S'_{\mathcal{A}})). \end{aligned} \tag{6}$$

Using this and eq. (4) for two interdependent ER networks with mean degrees $z_{\mathcal{A}}$ and $z_{\mathcal{B}}$ gives

$$S = (1 - e^{-z_{\mathcal{A}} S})(1 - e^{-z_{\mathcal{B}} S}). \tag{7}$$

In particular, when $z_{\mathcal{A}} = z_{\mathcal{B}} = z$, the order parameter obeys

$$S = (1 - e^{-zS})^2. \tag{8}$$

Defining $g(S) = S - (1 - e^{-zS})^2$, one can find graphically the value of S as a function of z that solves $g(S) = 0$ (see fig. 2). This solution shows a discontinuous ("first-order") phase transition (inset of fig. 2), contrary to the result for the single network in fig. 1. Demanding $g(S) = g'(S) = 0$ we find a critical point $S_c = 0.511699\cdots$ and $z_c = 2.455407\cdots$. The value of z_c agrees with that given for ER networks in [2,9] and our explicitly determined value of the order parameter just above the critical point, S_c, can also be obtained from appropriate combinations of their results.

For the general case $z_{\mathcal{A}} \neq z_{\mathcal{B}}$, defining

$$h(S) = S - (1 - e^{-z_{\mathcal{A}} S})(1 - e^{-z_{\mathcal{B}} S}), \tag{9}$$

we obtain a line of discontinuous transition points from the conditions $h(S) = 0$ and $h'(S) = 0$. Assuming $h(S) = 0$, the second condition can be written as

$$\begin{aligned} h'(S) &= 1 - z_{\mathcal{A}} e^{-z_{\mathcal{A}} S}(1 - e^{-z_{\mathcal{B}} S}) - z_{\mathcal{B}} e^{-z_{\mathcal{B}} S}(1 - e^{-z_{\mathcal{A}} S}) \\ &= 1 - \frac{z_{\mathcal{A}} S e^{-z_{\mathcal{A}} S}}{1 - e^{-z_{\mathcal{A}} S}} - \frac{z_{\mathcal{B}} S e^{-z_{\mathcal{B}} S}}{1 - e^{-z_{\mathcal{B}} S}} \\ &= 1 - \frac{x}{e^x - 1} - \frac{y}{e^y - 1} = 0, \end{aligned} \tag{10}$$

where $x = z_{\mathcal{A}} S$ and $y = z_{\mathcal{B}} S$. This gives a one-parameter set of solutions $y(x)$, from which S_c can be obtained using

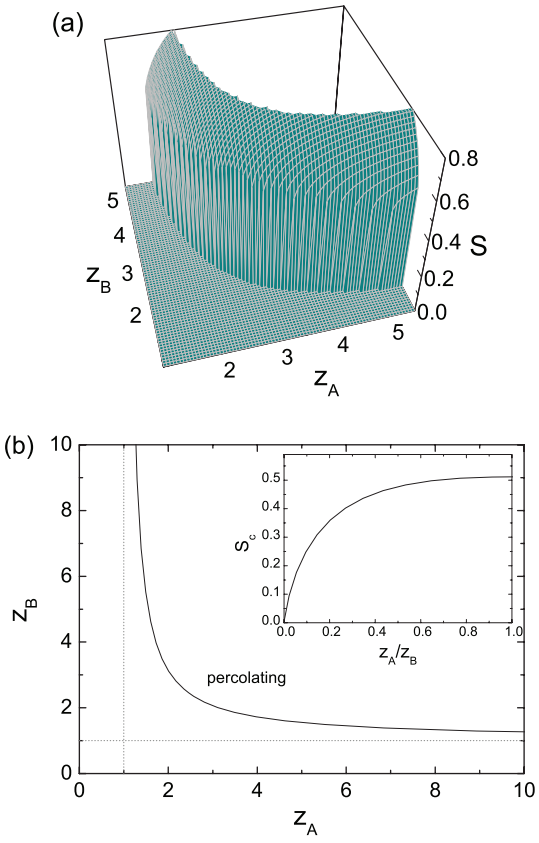

Fig. 3: (Color online) (a) S as a function of $z_{\mathcal{A}}$ and $z_{\mathcal{B}}$ for eq. (7). (b) The discontinuous phase transition line on the plane of $z_{\mathcal{A}}$ and $z_{\mathcal{B}}$. It is symmetric about the line $z_{\mathcal{A}} = z_{\mathcal{B}}$. In the inset, the jump size S_c at the transition line is shown as a function of the ratio $z_{\mathcal{A}}/z_{\mathcal{B}}$.

eq. (7). Finally, $z_{\mathcal{A}}$ and $z_{\mathcal{B}}$ are obtained by $z_{\mathcal{A}} = x/S$ and $z_{\mathcal{B}} = y/S$. The resulting discontinuous phase transition line is shown in fig. 3(b), where $z_{\mathcal{A}} = 1$ and $z_{\mathcal{B}} = 1$ act as asymptotes. In the inset of fig. 3(b), the jump size S_c is shown as a function of the ratio $z_{\mathcal{A}}/z_{\mathcal{B}}$ (only $z_{\mathcal{A}}/z_{\mathcal{B}} < 1$ is shown, since the transition line is symmetric about the line $z_{\mathcal{A}} = z_{\mathcal{B}}$). The full dependence of S on $z_{\mathcal{A}}$ and $z_{\mathcal{B}}$ is shown in fig. 3(a).

iii) *An arbitrary number of interdependent networks*: Our approach is easily extended to treat coupling of more than two networks [13]. For M networks, eqs. (5) and (6) can be simply replaced by

$$\begin{aligned} S &= \prod_{m=1}^{M} (1 - G_0^m(1 - S'_m)), \\ S'_m &= \frac{1 - G_1^m(1 - S'_m)}{1 - G_0^m(1 - S'_m)}\ S. \end{aligned} \tag{11}$$

This is due to the fact that in order to be part of the infinite percolating cluster each node must, by definition, be connected to it via all of the M networks. Order

parameters and transition points can be obtained in an analogous way and the transition is discontinuous for any $M > 1$.

iv) *Partially interdependent networks*: Assume now that two networks are not totally interdependent. In network $\mathcal{A}$ only a fraction $q_{\mathcal{A}}$ of the nodes are dependent on a node in network $\mathcal{B}$. To be on the percolating cluster, a node has to be connected to the cluster via $\mathcal{A}$ links and the node on which it depends has to be connected to the cluster via $\mathcal{B}$ links. Similarly a fraction $q_{\mathcal{B}}$ of nodes in network $\mathcal{B}$ depend on a node in $\mathcal{A}$. Note that here one node from a network depends only on one node from the other network, *i.e.*, each node can have only one dependency link, which can be unidirectional or bidirectional [3]. In that case, in general we must expect that the two order parameters $S_{\mathcal{A}}$ and $S_{\mathcal{B}}$ are different. They indicate the chance that a randomly picked node in $\mathcal{A}$ (respectively, $\mathcal{B}$) is a member of the percolating $\mathcal{AB}$-cluster.

Let us first discuss the symmetric case $q_{\mathcal{A}} = q_{\mathcal{B}} = q$. If a given node in network $\mathcal{A}$ does *not* depend on network $\mathcal{B}$ (which happens with probability $1-q$), it is a member of the percolating $\mathcal{AB}$-cluster *iff* at least one of its neighbors in $\mathcal{A}$ is also a member of that cluster. On the other hand, with probability q, the node does depend on a node in $\mathcal{B}$. In that case, in order for it to be part of the percolating $\mathcal{AB}$-cluster, its dependency partner also must be connected via network $\mathcal{B}$ to at least one node in that cluster. Therefore, the probability $S_{\mathcal{A}}$ can be expressed by summing the conditional probability to be connected multiplied by the corresponding probability to be dependent (q) or not ($1-q$):

$$\begin{aligned} S_{\mathcal{A}} &= q(1-G_0^{\mathcal{A}}(1-S'_{\mathcal{A}}))(1-G_0^{\mathcal{B}}(1-S'_{\mathcal{B}})) \\ &\quad + (1-q)(1-G_0^{\mathcal{A}}(1-S'_{\mathcal{A}})) \\ &= (1-G_0^{\mathcal{A}}(1-S'_{\mathcal{A}}))(1-qG_0^{\mathcal{B}}(1-S'_{\mathcal{B}})). \end{aligned} \tag{12}$$

Similarly,

$$S'_{\mathcal{A}} = (1-G_1^{\mathcal{A}}(1-S'_{\mathcal{A}}))(1-qG_0^{\mathcal{B}}(1-S'_{\mathcal{B}})). \tag{13}$$

By symmetry, another pair of conditions exists for network $\mathcal{B}$:

$$\begin{aligned} S_{\mathcal{B}} &= (1-G_0^{\mathcal{B}}(1-S'_{\mathcal{B}}))(1-qG_0^{\mathcal{A}}(1-S'_{\mathcal{A}})), \\ S'_{\mathcal{B}} &= (1-G_1^{\mathcal{B}}(1-S'_{\mathcal{B}}))(1-qG_0^{\mathcal{A}}(1-S'_{\mathcal{A}})). \end{aligned} \tag{14}$$

More generally, if $q_{\mathcal{A}} \neq q_{\mathcal{B}}$,

$$\begin{aligned} S_{\mathcal{A}} &= (1-G_0^{\mathcal{A}}(1-S'_{\mathcal{A}}))(1-q_{\mathcal{A}}G_0^{\mathcal{B}}(1-S'_{\mathcal{B}})), \\ S'_{\mathcal{A}} &= (1-G_1^{\mathcal{A}}(1-S'_{\mathcal{A}}))(1-q_{\mathcal{A}}G_0^{\mathcal{B}}(1-S'_{\mathcal{B}})), \\ S_{\mathcal{B}} &= (1-G_0^{\mathcal{B}}(1-S'_{\mathcal{B}}))(1-q_{\mathcal{B}}G_0^{\mathcal{A}}(1-S'_{\mathcal{A}})), \\ S'_{\mathcal{B}} &= (1-G_1^{\mathcal{B}}(1-S'_{\mathcal{B}}))(1-q_{\mathcal{B}}G_0^{\mathcal{A}}(1-S'_{\mathcal{A}})). \end{aligned} \tag{15}$$

Again, these four coupled equations involve nothing more complicated than (weighted) products of the network-specific fundamental factors from eqs. (2) and (3). Together, they give the behavior of the order parameters $S_{\mathcal{A}}$ and $S_{\mathcal{B}}$. These expressions are completely equivalent to the more complicated results in [3]. If $q_{\mathcal{A}} = q_{\mathcal{B}} = q = 1$, these equations reduce to eqs. (5) and (6).

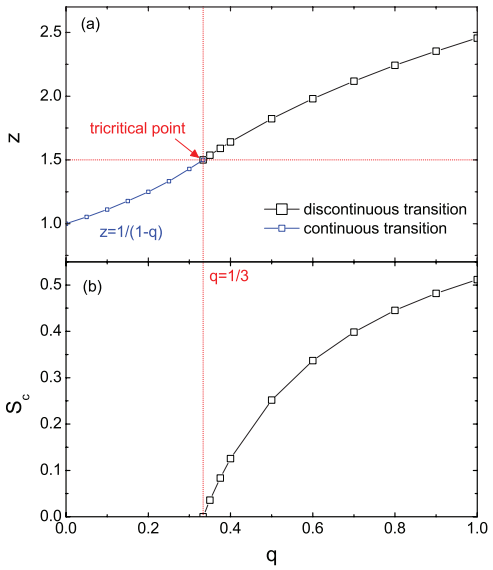

Fig. 4: (Color online) (a) Percolation transition points for two partially coupled ER networks with the same mean degree z at different values of the dependency q. (b) The jump size S_c at the transition point. The first-order phase transition line ($q > 1/3$) meets the second-order phase transition line ($q < 1/3$) at $q = 1/3$. The red dotted line indicates the tricritical point $(q_c, z_c) = (1/3, 3/2)$.

If $q_{\mathcal{A}} = q_{\mathcal{B}} = q \neq 1$ and if the two networks have the same degree distribution, $S_{\mathcal{A}} = S_{\mathcal{B}} = S$. For example, if two ER networks having the same mean degree z are coupled with the dependency probability $q \neq 1$, the solution is simply

$$S = (1-e^{-zS})(1-qe^{-zS}). \tag{16}$$

The solution S can now be expressed as a function of both z and q. When $q = 0$, $S(z)$ shows a continuous transition, since now both networks are fully independent. On the other hand, when $q = 1$, the transition is discontinuous. A crossover from *second-order* behavior to *first-order* behavior at the tricritical point q_c is observed as q is increased from 0 to 1. In analogy to eq. (9), we now define

$$h(S) = S - (1-e^{-zS})(1-qe^{-zS}). \tag{17}$$

The tricritical point is found by demanding $S = h(S) = h'(S) = h''(S) = 0$, which gives $q_c = 1/3$ and $z_c = 3/2$ [3].

For $q > q_c$, we can find the first-order transition point by considering $h(S) = 0$ and $h'(S) = 0$. The subsequent analysis is straightforward and follows closely our previous method. Its results are displayed in fig. 4.

Let us briefly discuss the case $q_{\mathcal{A}} = q_{\mathcal{B}} = q$ and $z_{\mathcal{A}} \neq z_{\mathcal{B}}$ of ER networks, which was not treated before. In this case,

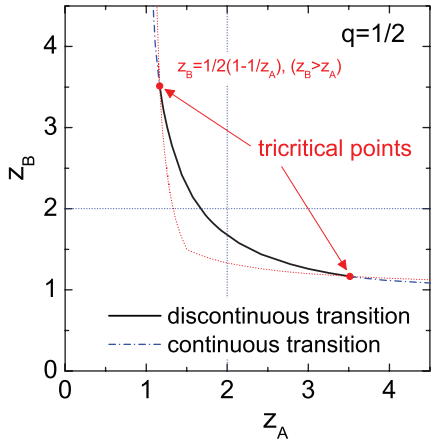

Fig. 5: (Color online) Phase transition line at $q=1/2$ for different $z_{\mathcal{A}}$ and $z_{\mathcal{B}}$. The black solid line indicates the first-order transition line and the blue dash-dotted line represents the second-order transitions. They meet two tricritical points (red bullets). The tricritical points move along the red dotted line as q changes. When $q=1/3$, the tricritical points meet at $z_{\mathcal{A}}=z_{\mathcal{B}}=3/2$.

also $S_{\mathcal{A}} \neq S_{\mathcal{B}}$, and we have to solve the coupled equations

$$\begin{aligned} h_{\mathcal{A}}(S_{\mathcal{A}}) &= S_{\mathcal{A}} - (1-e^{-z_{\mathcal{A}}S_{\mathcal{A}}})(1-qe^{-z_{\mathcal{B}}S_{\mathcal{B}}}) = 0, \\ h_{\mathcal{B}}(S_{\mathcal{B}}) &= S_{\mathcal{B}} - (1-e^{-z_{\mathcal{B}}S_{\mathcal{B}}})(1-qe^{-z_{\mathcal{A}}S_{\mathcal{A}}}) = 0. \end{aligned} \tag{18}$$

The percolation transition is obtained by imposing in addition $h'_{\mathcal{A}}(S_{\mathcal{A}}) = h'_{\mathcal{B}}(S_{\mathcal{B}}) = 0$. Defining again $x = z_{\mathcal{A}}S_{\mathcal{A}}$ and $y = z_{\mathcal{B}}S_{\mathcal{B}}$, we find

$$\left(1-\frac{x}{e^x-1}\right)\left(1-\frac{y}{e^y-1}\right) = \frac{qx}{e^x-q} \times \frac{qy}{e^y-q}. \tag{19}$$

For given q this is solved graphically (fig. 5). The values of $S_{\mathcal{A}}$ and $S_{\mathcal{B}}$ at the transition point are then obtained from eq. (18). If they vanish, the transition is continuous, otherwise it is discontinuous. Results are shown in fig. 5 for $q=1/2$. If q decreases, the two tricritical points move together. They coalesce at $z_{\mathcal{A}}=z_{\mathcal{B}}=3/2$ when $q \to 1/3$.

v) *Dependency networks*: A dependency network [4,8] is a *single* network that contains two types of links, connectivity links and dependency links. In the simplest case each node in the network depends on one other node in that network and all dependencies are mutual. In order for a node to be connected to the infinite self-sustaining cluster both it and its partner must be part of that cluster. For random networks this leads immediately to eqs. (5) and (6) where the subscripts $\mathcal{A}$ and $\mathcal{B}$ are dropped since there is only one network. In the case that only a fraction q of nodes have dependency links we get eqs. (12) and (13), again dropping the subscripts labelling the networks. Again the type of transition depends on the value of q, with a tricritical point separating the two regimes.

In the most general case where a node has m dependency links with probability $p(m)$ the resulting equations are

$$\begin{aligned} S &= \sum_{m=0}^{N-1} p(m)(1-G_0(1-S'))^{m+1}, \\ S' &= (1-G_1(1-S')) \sum_{m=0}^{N-1} p(m)(1-G_0(1-S'))^{m}. \end{aligned}$$

Again the precise behavior reflects the extent to which the network is dependent, with a low dependency regime exhibiting a continuous transition in the universality class of ordinary percolation and a high dependency regime exhibiting a first-order transition, with crossover controlled by a tricritical point. Similar arguments can be used to derive the general case for interdependent networks where a single node has dependencies to m other networks with probability $p(m)$. In that case the equations are more complicated because each network's structure may be different and they will have different order parameters, but the arguments used to derive the equations are precisely the same. The above does not apply to networks with directed (non-mutual) dependencies, for which different arguments apply.

In summary, we consider percolation on various interdependent or dependency networks, pointing out the close analogy to epidemic spreading on single networks without these dependencies. Our arguments are much more straightforward, both conceptually and mathematically, than previous ones built on cascades of failures. We should however stress that they apply, like those of [2–4,8,13] only to random locally treelike graphs. For interdependent networks that are correlated with each other [14] or that are spatially embedded [9,15] the transition is in general not first order, and the interdependency can make the transition even less sharp than in ordinary percolation [9,15]. For these more realistic cases no analytical theory is yet available.

REFERENCES

[1] Rosato V. *et al.*, *Int. J. Crit. Infrastruct.*, **4** (2008) 63.
[2] Buldyrev S. V., Parshani R., Paul G., Stanley H. E. and Havlin S., *Nature*, **464** (2010) 1025.
[3] Parshani R., Buldyrev S. V. and Havlin S., *Phys. Rev. Lett.*, **105** (2010) 048701.
[4] Parshani R., Buldyrev S. V. and Havlin S., *Proc. Natl. Acad. Sci. U.S.A.*, **108** (2011) 1007.
[5] Moreno Y., Pastor-Satorras R., Vázquez A. and Vespignani A., *Europhys. Lett.*, **62** (2003) 292.
[6] Motter A. E., *Phys. Rev. Lett.*, **93** (2004) 098701.
[7] Kurant M. and Thiran P., *Phys. Rev. Lett.*, **96** (2006) 138701.
[8] Bashan A. and Havlin S., arXiv:1106.1631 (2011).
[9] Son S.-W., Grassberger P. and Paczuski M., *Phys. Rev. Lett.*, **107** (2011) 195702.

[10] Newman M. E. J., *Phys. Rev. Lett.*, **95** (2005) 108701.
[11] Newman M. E. J., Strogatz S. H. and Watts D. J., *Phys. Rev. E*, **64** (2001) 026118.
[12] Bollobás B., *Random Graphs* (Academic Press, London) 1985.
[13] Gao J., Buldyrev S. V., Havlin S. and Stanley H. E., *Phys. Rev. Lett.*, **107** (2011) 195701.
[14] Parshani R., Rozenblat C., Ietri D., Ducruet C. and Havlin S., *EPL*, **92** (2010) 68002.
[15] Son S.-W., Grassberger P. and Paczuski M., in preparation.

Discontinuous percolation transitions in epidemic processes, surface depinning in random media, and Hamiltonian random graphs

Golnoosh Bizhani, Maya Paczuski, and Peter Grassberger
Complexity Science Group, University of Calgary, Calgary T2N 1N4, Canada
(Received 6 April 2012; revised manuscript received 6 July 2012; published 25 July 2012)

Discontinuous percolation transitions and the associated tricritical points are manifest in a wide range of both equilibrium and nonequilibrium cooperative phenomena. To demonstrate this, we present and relate the continuous and first-order behaviors in two different classes of models: The first are generalized epidemic processes that describe in their spatially embedded version—either on or off a regular lattice—compact or fractal cluster growth in random media at zero temperature. A random graph version of these processes is mapped onto a model previously proposed for complex social contagion. We compute detailed phase diagrams and compare our numerical results at the tricritical point in $d = 3$ with field theory predictions of Janssen *et al*. [Phys. Rev. E **70**, 026114 (2004)]. The second class consists of exponential ("Hamiltonian," i.e., formally equilibrium) random graph models and includes the Strauss and the two-star model, where "chemical potentials" control the densities of links, triangles, or two-stars. When the chemical potentials in either graph model are $\mathcal{O}(\log N)$, the percolation transition can coincide with a first-order phase transition in the density of links, making the former also discontinuous. Hysteresis loops can then be of mixed order, with second-order behavior for decreasing link fugacity, and a jump (first order) when it increases.

DOI: 10.1103/PhysRevE.86.011128 PACS number(s): 64.60.ah, 68.43.Jk, 89.75.Da

I. INTRODUCTION

Percolation describes the sudden appearance of systemwide connectivity arising from microscopic processes. It is a classic example [1] of a continuous ("second-order") phase transition. Interest in systems where the percolation transition is discontinuous ("first order") was sparked recently by claims for this in *Achlioptas processes* [2]. Although these transitions were later shown to be continuous [3–6]—albeit with unusual finite-size scaling behavior [5]—the fact that percolation transitions could be discontinuous was claimed to be novel [3,4,7–24]. After this, discontinuous percolation transitions were observed in interdependent networks [25–27], in models inspired by [2] but not using the Achlioptas trick [15–18], and in a hierarchical lattice [28].

One purpose of this work is to point out that discontinuous percolation transitions are not surprising and, indeed, are common to a variety of (e.g., social or physical) cooperative phenomena. The existence of such transitions, together with an associated tricritical point, was proposed 25 years ago [29] in the context of directed percolation. This was verified in the seminal field theoretic work of Janssen *et al*. [30] who introduced the *generalized epidemic process* (GEP) [31]. In this scenario, the continuous transition is just ordinary percolation (OP), while the discontinuous one is the depinning transition of driven surfaces in random media at zero temperature [32,33].

Although the latter is continuous from the point of view of surface properties, it is discontinuous so far as the percolation order parameter is concerned [34]. Indeed, the density of "wetted" sites in the presence of a driven interface jumps discontinuously from zero to a finite value at depinning.

A closely related line of papers finding discontinuous percolation transitions started independently in a social science context [35–37] and addresses complex contagion or epidemics in random networks. It turns out that the model of [36] is basically the random graph version of the GEP, as we explain in detail below. Our unified formulation based on GEP, that includes both social contagion and interface depinning, simplifies the description of both and isolates relevant variables that can affect the actual outcome in terms of potentially measurable observables.

We present numerical simulation results for the GEP, including the time dependence of the number of growth sites in three dimensions. At the first-order (=depinning) transition line, activity decays as a stretched exponential in time while it behaves as a power law both at the OP transition and at the tricritical point which separates rough from fractal growth. We give (tri-)critical exponents and compare them to theoretical predictions [30].

The main property that leads to first-order transitions in the models we consider is cooperativity (or "synergy") in establishing links. This cooperativity can be implemented technically in different ways. We do this via stochastic dynamics as in [30,35–37] for the GEP, and also via Gibbs-Boltzmann *equilibrium* distributions in Hamiltonian (or "exponential") ensembles, which have been used extensively to model social networks.

Indeed, we also find discontinuous percolation transitions in two exponential random graph models : the Strauss [38,39] and the two-star model [40]. They are both formulated in terms of a partition function and are generalizations of the standard Erdös-Renyi (ER) random graph [41]. The Hamiltonians are bilinear with a control parameter (θ) conjugate to the number of links and another control parameter conjugate to either the number of triangles or the number of "two stars." When all control parameters are $\mathcal{O}(\log N)$ (where N is the number of nodes in the graph), the percolation transition can be either continuous or discontinuous, with hysteresis loops typical of first-order transitions. But for certain parameter regimes unusual hysteresis loops occur, where the percolation order parameter exhibits second-order (singular but continuous) behavior for decreasing θ, but jumps discontinuously for increasing θ. Similar "mixed-order" hysteresis loops have been found in heterogeneous k-core percolation [42].

It is well known that the observation of continuity of a phase transition depends not only on the choice of the order parameter, but also on the choice of the control parameter. Take, for example, the standard example of a liquid-gas transition. If the temperature of water is increased at constant pressure, then the density and the free energy jump discontinuously at the boiling temperature. If, however, the volume is kept fixed, no such jump is observed. Instead, as temperature is increased, a larger and larger fraction of the sample turns into vapor, but this happens in a completely continuous way. The standard assumption in thermostatics is that the order parameter is a density or inverse density (e.g., specific volume), and the control parameter is its conjugate (e.g., pressure). But in percolation, the standard choice of order parameter is the fraction $S_{\max}/N$ of sites belonging to the giant cluster, while the control parameter is usually also a density—the density of occupied sites (bonds) in site (bond) percolation. Although this choice is legitimate, it can obscure the notion of first- versus second-order transitions, since other choices more in line with thermostatics can lead to different conclusions. This might explain why previous works on first-order percolation transitions were not recognized as such in the recent literature.

II. THE GENERALIZED EPIDEMIC MODEL: COMPLEX CONTAGION TREATED AS A STOCHASTIC PROCESS

Although the epidemic model of Ref. [30] is formulated as a continuum field theory, the situation becomes more clear on a lattice. Consider a process where the probability of a given site becoming infected (or invaded) by one of its neighbors depends on the number of previous attempts by other neighbors. Once a site is infected, it tries once to infect every one of its not yet infected neighbors. Denote by p_k the probability that an infection succeeds, if the attacked site has already fended off k previous attacks. If every attack increases the strength of the defender, p_k decreases with k, otherwise (if it weakens it), p_k increases. Site percolation is described by $p_0 > 0$ and $p_k = 0$ for $k \geqslant 1$: If the first attack does not succeed, all later attempts are futile. Bond percolation is described by $p_k = p$ for all $k \geqslant 0$. Ordinary (second-order) percolation is observed whenever p_k decreases with k (see also [43]), but the transition switches to first order when p_k increases sufficiently fast. In that case, infected clusters fill in most holes and bays, while protrusions are avoided—thereby making the clusters compact with rough but nonfractal surfaces. (The same effect is caused by high surface tension compared to disorder at the cluster-void interface in random media). Detailed predictions for the tricritical behavior in terms of an $\epsilon = 5 - d$ expansion were given in [30].

A. The GEP on random graphs

Although Dodds *et al.* [36,37] assume a somewhat more complex mechanism of infection, their basic model can be mapped onto a sparse random graph model where each node with n neighbors in the giant cluster is itself in the giant cluster with probability q_n. This is precisely the mean-field (random graph) version of the above model, if $q_1 = p_0$ and $q_{n+1} = q_n + (1 - q_n)p_n$ [44]. Due to the absence of short loops in this case, the condition for tricriticality (transition between classes I and II in [36,37]) simplifies to

$$q_2 = 2q_1, \tag{1}$$

with no restriction on any q_n with $n \geqslant 3$. Since the derivation of this in [36,37] is somewhat involved and obscures the relationship to the GEP as defined in [30], a simple proof of Eq. (1) is given Appendix A.

B. The GEP on regular lattices: tricritical behavior and rough pinned surfaces

In the present work we studied in detail the case where $p_k \equiv p$ is the same for all $k > 0$, while p_0 is different. A technical advantage of this choice is that we have to distinguish only between four types of sites (virgin, attacked but still not infected, infected, and removed), which allows one to store the type in two bits and to simulate larger lattices. Phase diagrams for simple (hyper-) cubic lattices and for random regular graphs are shown in Fig. 1. To the left of the curves, no infinite clusters exist, while such clusters do exist to their right. Since percolation thresholds on lattices scale as $p_c \sim 1/(2d - 1)$

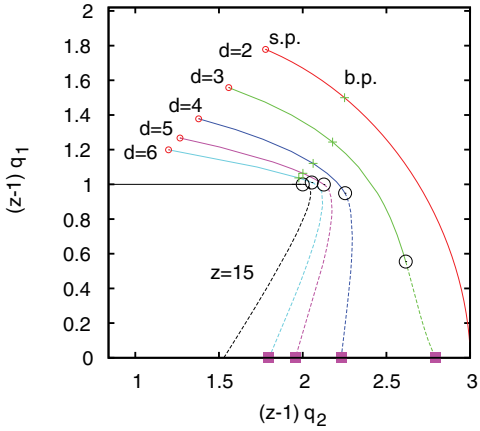

FIG. 1. (Color online) Phase diagrams for the generalized epidemic process where infection of a site succeeds with probability p_0 in the first encounter with an infected neighbor, while it succeeds with chance p in all later encounters. Following [36], we use instead of p_k the probabilities $q_1 = p_0$ and $q_2 = p_0 + (1 - p_0)p$ that an infection has occurred after two encounters. Since percolation thresholds on regular graphs are roughly $\propto 1/(z - 1)$ for large degree z, we use $(z - 1)q_n$ for the two axes. The curves labeled by $d = 2$ to $d = 6$ correspond to d-dimensional hypercubic lattices, where $z = 2d$, while the curve labeled "$z = 15$" is for random (i.e., locally loopless) networks. All curves start at the site percolation point $q_2 = q_1$ (small red circles). The bond percolation points (green crosses) are at $q_2 = (2 - q_1)q_1$. For large d they approach the tricritical points (big black circles) that converge to the point $(2,1)$ for large k. The percolation transitions are first order below the tricritical points, and second order above. For $d = 2$ there is no tricritical point (i.e., clusters and their surfaces are always fractal). In the first-order regime (dashed curves), surfaces develop strong overhangs and seem for $d = 3$ *not* to be described by models where these overhangs are neglected (in particular when $q_1 = 0$ (magenta squares), but they seem to be in the standard universality class of self-affine pinned rough surfaces for $d > 3$.

for large d, we used $(z-1)q_1$ and $(z-1)q_2$ as coordinates in Fig. 1, where z is the coordination number. All curves start at site percolation ($p_1 = 0$, $q_1 = q_2 = p_0$), since we do not consider here antagonistic effects (i.e., two attacks together cannot have less success than a single one). Tricritical points are marked by circles. There is no tricricital transition in $d = 2$ [33] (i.e., isotropic rough 1-d surfaces are always fractal). For large dimensions, the lattice results converge to those for regular random graphs with degree $z = 2d$, as short loops become less and less important with increasing d.

Previously, most studies of pinned rough surfaces were either done for the random field Ising model at zero temperature [32,33,45–47] (which is indeed a special case of GEP [33,48], but not the most convenient one for simulations), or for models where overhangs are neglected. In the latter case the surface can be described by a single-valued self-affine function [49–51]. This makes it much easier to study both numerically and analytically, but the neglect of overhangs is not guaranteed to be justified. The critical exponents obtained in [49–51] seem to agree with simulation results for the random field Ising model [45], but the latter have large uncertainties. Our preliminary results indicate that surface properties in the first-order regimes (i.e., below the tricritical points, but with $q_1 = 0$) are for $d > 3$ indeed in the same universality class of surfaces without overhangs, but not $d = 3$. There the pinned surfaces seem to be rougher than predicted by [49–51], but much more detailed studies are needed and will be reported elsewhere [52].

The case $q_1 = 0$, where at least two infected neighbors are needed for a site to become infected, is similar to bootstrap percolation [53,54]. There, epidemics can neither spread from single sites nor from surfaces with Miller indices $(1,0,0\ldots)$, but they can spread from surfaces with Miller indices $(1,1,1\ldots)$. This means also that no infinite epidemic can spread from an initial distribution of infected sites confined within a finite region. Nevertheless, at least for $d > 3$ there is a critical value of q_2 above which infinite clusters are self-supported, and spreading from an infinite $(1,1,1\ldots)$ surface seems to be in the same universality class of self-affine surfaces as for $q_1 > 0$. Again, the situation is less clear for $d = 3$, where the spreading from a $(1,1,1)$ surface definitely is not in this universality class [52].

For the simple cubic lattice, simulations show that the tricritical point for this model is at $p_0 = 0.111(2)$ and $p_k = 0.464(8)$ for $k > 0$. Results of such simulations for epidemics starting from a single infected site are shown in Fig. 2, where $n(t)$ is the number of sites newly infected at time t. For OP, $n(t)$ increases as a power law t^η with $\eta \approx 0.35$ [1], and it decreases at the tricritical point as $n(t) \sim t^{\eta_s}$ with $\eta_s = -0.70(1)$. This is in stark contrast to the prediction $\eta_s \approx 0.05$ of [30]. The tricritical point and OP are the only cases where $n(t)$ shows a power law. For critical percolation with $p_0 > 0.111$ the behavior crosses over to the OP scaling, while for $p_0 < 0.111$ the data are compatible with a stretched exponential at the transition line (see lowest three curves in Fig. 2). Analogous plots for the probability $P(t)$ that the epidemic survives at least t time steps and for its average squared radius $R^2(t)$ are given in Appendix B. They give $\delta_s = 1.49(2)$ and $z_s = 1.205(4)$, where δ_s and z_s are defined via $P(t) \sim t^{-\delta_s}$ and $R^2(t) \sim t^{z_s}$. The predictions of [30] are $\delta_s \approx 0.87$ and $z_s \approx 1.06$. Again, the agreement is far from perfect, although the changes from the OP critical exponents are in the right directions. More details are given in Appendix B and in [52]. For the completely analogous case of directed percolation (SIS epidemics), see [55–57].

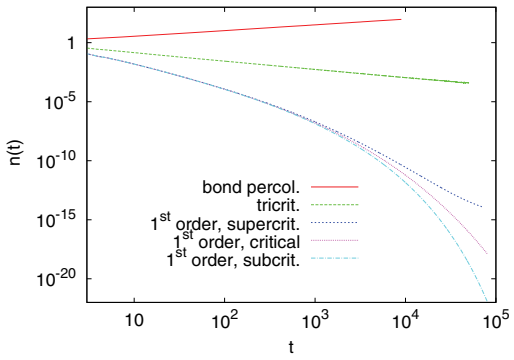

FIG. 2. (Color online) Time dependence of the activity $n(t)$ at five different pairs (p_0, p) where $p_k = p$ for all $k \geqslant 1$, for the generalized epidemic process on the simple 3-d cubic lattice starting from a single infected site. The uppermost (red) curve is for $p_0 = p = 0.2488\ldots$, which is critical bond percolation. The middle (green) curve is for the tricritical point $(p_0, p) = (0.111, 0.464)$ [i.e., $(q_1, q_2) = (0.111, 0.523)$]. Within the resolution of the figure, both these lines are straight. The lowest three curves are near the first-order (depinning) transition line $(p_0, p) = (0.07, 0.792318 + \Delta)$, where $\Delta = 0$ (magenta), $+0.00022$ (dark blue), and -0.00022 (light blue). Statistical error bars are all smaller than the line widths.

III. COOPERATIVE PERCOLATION IN HAMILTONIAN RANDOM GRAPH MODELS

The above discussion suggests that cooperativity in finite temperature equilibrium systems may also lead to discontinuous percolation transitions. Indeed, the mean-field percolation transition corresponds to the emergence of the giant component in ER random graphs, where links appear *independently* with probability p [41]. The ER random graph is the simplest "exponential model" [58–60]. In this approach one considers graphs G with N nodes, where the probability for a given graph is defined by the Boltzmann-Gibbs equilibrium formula,

$$P(G;\theta_1,\theta_2,\ldots) = \frac{1}{Z} e^{-H(G;\theta_1,\theta_2,\ldots)}, \tag{2}$$

with $Z = \sum_G e^{-H(G;\theta_1,\theta_2,\ldots)}$. Here H is the Hamiltonian, $\{\theta_1,\theta_2,\ldots\}$ represents a set of control parameters, and we have set $\beta \equiv 1/kT = 1$. More precisely, we assume that H is a sum of bilinear terms,

$$H(G;\theta_1,\theta_2,\ldots) = \sum_\alpha \theta_\alpha A_\alpha(G), \tag{3}$$

where each A_α is an observable ("statistic") of the graph, and θ_α is the associated chemical potential. Typically, each A_α represents the total number of small subgraphs (links, triangles, p stars, four cliques,...,) in the graph.

Models of this type have been popular in mathematical sociology [38,60], although they tend to be unrealistic. In many cases, such models reduce to equivalent ER graphs without

clustering and are trivial, apart from the usual, nontrivial dependence of the observables A_α on the control parameters θ_α [61].

The Hamiltonian for the ER model is

$$H_{\rm ER}(G;\theta) = \theta L(G), \tag{4}$$

where $L(G)$ is the number of links in G and $\theta = \ln[(1-p)/p]$. It exhibits a percolation transition at $p = 1/N$ (when $N \to \infty$) [41], thus the critical value of θ is

$$\theta_p = \ln N. \tag{5}$$

In the following, we study the two-star model [40] with

$$H_{\text{two-star}}(G;\theta,J) = \theta L(G) - \frac{J}{N} n_2(G). \tag{6}$$

Here $n_2(G)$ is the total number of 'two stars" (i.e., pairs of links attached to the same node). We also consider the Strauss model [38,39] with

$$H_{\rm Strauss}(G;\theta,B) = \theta L(G) - \frac{B}{N} n_\Delta(G), \tag{7}$$

where $n_\Delta(G)$ is the total number of distinct triangles (i.e., of loops of length 3). In terms of the degree sequence $\{k_i, i = 1 \ldots N\}$,

$$L(G) = \frac{1}{2}\sum_{i\in G} k_i, \quad \text{and} \quad n_2(G) = \frac{1}{2}\sum_{i\in G} k_i(k_i-1), \tag{8}$$

while $n_\Delta(G)$ depends also on degree correlations.

For a typical (nonsparse) graph L increases quadratically with N, while both n_2 and $n_\Delta \sim N^3$. This is why J/N and B/N are used as control parameters in Eqs. (6) and (7) instead of J and B. The two-star model has, for any $\theta > 2$, a first-order transition in the density of links at $J^*(\theta)$ and strong hysteresis. The results of [40], together with a standard Maxwell construction, show that

$$J^*(\theta) = \theta. \tag{9}$$

The line of first-order transitions terminates at the critical point $\theta_c^* = J_c^* = 2$. [We neglect here all terms that are $\mathcal{O}(1/N)$ relative to the leading ones]. Similarly, for the Strauss model a first-order transition in the link density $p = \langle L\rangle/N$ occurs for any $\theta \gtrsim 0.81$ [39]. This time it is more complicated to obtain the exact transition line $B^*(\theta)$, but one can show that (see Appendix C)

$$B^*(\theta) \approx 3\theta \quad \text{for } \theta \gg 1, \tag{10}$$

with a critical point at $p_c^* = 2/3, B_c^* = 27/8 = 3.375$, and $\theta_c^* = 3/2 - \ln(2) \approx 0.807$.

For both models, a giant component exists in both the high and low link density phases, whenever $\theta = \mathcal{O}(1)$. Thus the density transition happens when they are already percolating, as long as θ is finite. In order to reach a percolation transition one has to take $\theta \sim \ln N$ to get a sparse graph. In this regime the above estimates for the density transitions are still valid. Moreover, when $B < B^*$ or $J < J^*$, respectively, the second terms in the Hamiltonians [Eqs. (6) and (7)] have no influence on the percolation transition, for $N \to \infty$. This is illustrated for the two-star model in Fig. 3, where we show numerical results averaged over 50 hysteresis loops for a network with $N = 2000$ and $J = 3.0$. The density transition (monitored via the average degree) indeed appears to be first order with strong hysteresis, while the percolation transition (monitored via $\langle S_{\rm max}\rangle/N$) shows no hysteresis and is *exactly* the same as for ordinary ER networks.

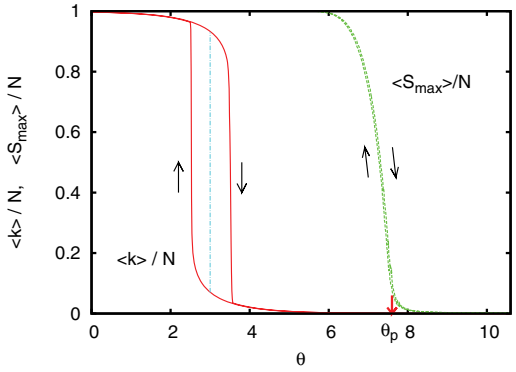

FIG. 3. (Color online) Hysteresis loops for the two-star model for fixing the two-star control parameter at $J = 3$ and sweeping the control parameter θ for links. The loop on the left (red) is for the normalized average degree, while the one on the right (green) is for the percolation order parameter $\langle S_{\rm max}\rangle/N$. The vertical dashed (blue) line is the Maxwell prediction for the true density transition. The curve for $\langle S_{\rm max}\rangle/N$ shows practically no hysteresis and agrees within error with the one for OP. The percolation threshold $\theta_p = \ln N$ is indicated on the x axis. The rounding of the green curve near θ_p is a finite size effect ($N = 2000$).

When $J > \ln N$ (or $B > \ln N$, respectively) this scenario breaks down because the true equilibrium state at the ER percolation threshold, θ_p, is a dense graph that consists of a single giant component. Although the equilibrium network percolates at θ_p, a hysteresis loop starting at $\theta > J$ begins with a sparse nonpercolating graph, and due to metastability the effect of J (or B) is not seen until one passes the ER percolation threshold—provided that it remains in the metastable region. This scenario is illustrated in Fig. 4 for $J = \theta_p = \ln N$. Now the hysteresis loop for $\langle k\rangle/N$ is quite wide. The hysteresis loop

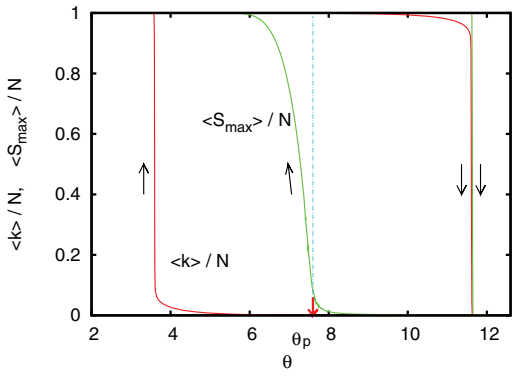

FIG. 4. (Color online) Analogous to Fig. 3, but for $J = \theta_p = \ln N = 7.601$. This time the percolation threshold coincides with the true (Maxwell) density transition. As a consequence, also the curve for $\langle S_{\rm max}\rangle/N$ shows hysteresis, with a continuous lower branch and a discontinuous upper branch ($N = 2000$).

for $\langle S_{\max}\rangle/N$ shows the ordinary ER percolation shape on its lower branch, while it follows the discontinuous behavior of $\langle k\rangle/N$ on the upper (return) branch. To our knowledge, such a mixed-order hysteresis loop has not been observed before, although a similar phenomenon was seen in heterogeneous k-core percolation [42]. But since the latter is not Hamiltonian and does not allow for the notion of thermal equilibrium, the two cannot be strictly compared.

IV. CONCLUSIONS

As we already mentioned and as was pointed out repeatedly before [39,40,61], the two-star and Strauss models are not realistic for real world applications. Accordingly, our demonstration that they exhibit both second- and first-order percolation transitions should be considered only as a proof that this phenomenon exists in equilibrium. More interesting examples can be easily suggested. A class of models that come into mind are random graphs (i.e., mean-field type) where not only the number of nodes but also the number of links is set by hard constraints ("microcanonical models") [62]. A model with two control parameters (B and J) studied in [63] exhibits the zoo of metastable states, but it seems that most of these states are still too extreme to be physical. A further step in this direction could be to fix not only the average degree, but to fix the entire degree distribution, either by soft [64] or by hard [65] constraints.

A more realistic class of Hamiltonian models with first-order phase transitions could be spatially embedded (e.g., finite dimensional lattice) systems. Such models have not been studied much in the social science literature, although it is well known that, for instance, spatial structure is essential to maintain diversity in ecosystems. We believe that such models might provide a suitable mixture of structure and randomness to reveal important features of real, complex networks, including presumably percolation transitions of both continuous and discontinuous type.

In summary, we have shown that various percolation models can be naturally generalized such that they switch from ordinary, continuous behavior at the transition point to discontinuous ("first-order") behavior, as some parameter is varied. This parameter usually is a measure of cooperativity in linking or "infecting" sites (the probability for sites to get linked is increased by other links already present), such that the percolation transition is more abrupt when cooperativity is high. We present a unified treatment including examples that range from social dynamics to condensed matter physics, and we also show that analogous phenomena occur both in stochastic dynamics out of equilibrium as well as in a Gibbs-Boltzmann equilibrium framework. We also simplify the dynamical description of the social contagion process introduced by Dodds and Watts [36], clarifying thereby its relation to percolation and to the generalized epidemic process defined in [30].

In condensed matter physics, the first-order percolation transition is just the depinning transition of driven interfaces in disordered media at zero temperature. Treating it also in our unified framework not only allows us to study in detail the tricritical point (where we found for $d = 3$ striking disagreement with theoretical predictions), but also to numerically investigate more efficiently a model for pinned surfaces in which overhangs are fully included and hence the rotational symmetry of the growth process is not explicitly broken at scales much less than the system size. In this latter context, the most important (but so far only preliminary) result we find is that overhangs are indeed crucial for such surfaces, and that all existing theories for critically pinned rough surfaces (which neglect overhangs and are based on a single-valued "height function") might be obsolete, not being relevant to the most interesting physical case of isotropic media.

APPENDIX A: THE EPIDEMIC THRESHOLD IN THE DODDS-WATTS SOCIAL CONTAGION MODEL

Since the original derivation of the result $q_2 = 2q_1$ by Dodds and Watts [36] is somewhat cumbersome and involves more than a minimal set of assumptions, we give here a simpler derivation following the typical arguments for epidemic thresholds via consistency conditions [27,66,67]. We start by recalling the condition for the threshold of the standard epidemic process that leads to ordinary percolation, and we then modify a suitable reformulation so that it also applies to the more general case with different infection probabilities p_k. We finally obtain the critical line and the tricritical point by straightforward algebra.

Let us call S the probability that a node at one end of a randomly chosen link gets infected during an epidemic process on a sparse random network with degree distribution P_k. If the infection can pass through any link with probability p, then the locally treelike structure of the network results in the consistency condition [66,67],

$$1 - S = z^{-1} \sum_{k=1}^{\infty} k P_k (1 - pS)^{k-1}, \tag{A1}$$

where $z = \langle k\rangle = \sum_k k P_k$. We write this as

$$F_{\rm OP}(S) \equiv \sum_{k=1}^{\infty} k P_k (1 - pS)^{k-1} + z(S - 1) = 0 \tag{A2}$$

(the subscripts stand for "ordinary percolation"). The percolation threshold is then defined by

$$F_{\rm OP}(0) = F'_{\rm OP}(0) = 0, \tag{A3}$$

where $F'_{\rm OP}(S) \equiv d F_{\rm OP}/dS$. Straightforward calculations give [41,66,67]

$$p_c = \frac{\langle k\rangle}{\langle k(k-1)\rangle}. \tag{A4}$$

We also notice that $F''_{\rm OP}(0) > 0$.

In order to modify this to arbitrary infection probabilities p_n for attacks following n previous attacks, we first rewrite Eq. (A2) such that contributions from different numbers of infected neighbors are separated. In order to do this we write $1 - pS = (1 - S) + (1 - p)S$, such that the first term is the probability that the considered node is not infected, while the second terms is the probability that it is infected, but it cannot infect its neighbor since the link cannot be passed. Similarly

we write

$$(1-pS)^k = \sum_{n=0}^{k-1} \binom{k-1}{n} [(1-p)S]^n (1-S)^{k-n-1}, \quad \text{(A5)}$$

such that each term in the sum corresponds to exactly n infected neighbors. The modification to the generalized process is now obvious: We just have to replace the power $(1-p)^n$ by $(1-p_0)(1-p_1)\dots(1-p_{n-1})$. Alternatively, we can replace it by $1-q_n$ where q_n is the probability that n attacks succeed in infecting the site. The formulations using p_n and q_n are fully equivalent.

Making this modification in Eq. (A2) results in

$$F_{\mathrm{GEP}}(S) = \sum_{k=1}^{\infty} k P_k \sum_{n=0}^{k-1} \binom{k-1}{n} \times [1-q_n] S^n (1-S)^{k-n-1} + z(S-1), \quad \text{(A6)}$$

where GEP stands for "generalized epidemic process." As before, the condition for criticality is

$$F_{\mathrm{GEP}}(0) = F'_{\mathrm{GEP}}(0) = 0, \quad F''_{\mathrm{GEP}}(0) > 0, \quad \text{(A7)}$$

while the tricritical point is given by

$$F_{\mathrm{GEP}}(0) = F'_{\mathrm{GEP}}(0) = F''_{\mathrm{GEP}}(0) = 0, \quad \text{(A8)}$$

Evaluating the derivatives is straightforward and gives [36]

$$q_2 = 2q_1, \quad \text{(A9)}$$

and q_1 is given by Eq. (A4). Notice that the location of the tricritical point does not depend on any q_n with $n > 2$, and its existence does not put any constraints on them.

In the first-order regime, the threshold condition for an epidemic is

$$F_{\mathrm{GEP}}(S) = F'_{\mathrm{GEP}}(S) = 0, \quad \text{(A10)}$$

which depends nontrivially both on the degree distribution and on all p_n (or all q_n). For regular graphs with degree z (i.e., $P_k = \delta_{k,z}$) and $p_n = p$ for all $n \geqslant 1$ it approaches in the limit $z \to \infty$ the linear relation $q_2 = 1/z + p_1$. For $z = 15$, numerical solution of Eq. (11) gives the line plotted in Fig. 1.

APPENDIX B: DETAILS ON THE SIMULATION OF TRICRITICAL AND FIRST-ORDER PERCOLATION ON 3-*d* LATTICES

All simulations were done on simple cubic lattices, with synchronous (discrete time) updates. We followed the spreading of epidemics that started either with point seeds or with the seed consisting of an entire infected plane. In the former we used lattices of size up to 2048^3 and checked that clusters never reached the boundary. For small values of p_0, when growth from a point seed has a very high chance to die out, we used PERM [68] to grow clusters even if their probability was as low as 10^{-300}. For simulations initiated from an entire infected plane (results of which are not shown here but are used, in addition, to better estimate (tri-)critical points) we used lattices of sizes up to $4096^2 \times 2048$ with helical lateral boundary conditions. In that case we also implemented multispin coding in order to use only 2 bits to store the status of any site. We also recycled memory in order to grow epidemics that spread

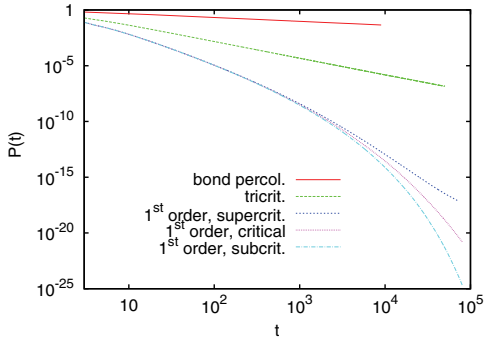

FIG. 5. (Color online) Log-log plot analogous to Fig. 1, but for $P(t)$ instead of $n(t)$. Here $P(t)$ is the probability that an epidemic started with a single infected site is still growing after t time steps. The decay follows a power law both at OP and at the tricritical point [with exponent $-1.49(2)$ for the latter], while it seems to follow a stretched exponential at the first-order (i.e., rough surface depinning) transition point. Again the central one of the three lowest curves (for $p_0 = 0.07$) corresponds to depinning.

far from the initial infected boundary, by overwriting older parts of the cluster that were no longer growing. This enlarges the effective lattice size to $4096^2 \times L_z$ with $L_z \gg 2048$. The precise thickness that we must not overwrite depended of course on the actual roughness of the growing surface. It was always checked that the cluster could grow without improperly interfering with some of its older parts.

Further details will be given elsewhere [52]. They will concern statistics, the precise methods used to estimate exact tricritical properties, critical exponents for rough pinned surfaces, and the behavior in dimensions different from 3. Here we present just two more figures (Figs. 5 and 6), similar to

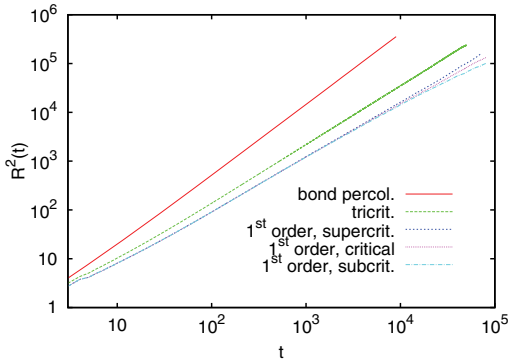

FIG. 6. (Color online) Analogous to Figs. 1 and 5, but for $R^2(t)$ which is the average distance of active (i.e., newly infected) sites from the seed. In the first-order regime the cluster grows very slowly, and $R^2(t)$ should be dominated by the motion of their center of mass. Since clusters can grow only into new (not previously infected) areas, this motion should be essentially a self-avoiding random walk. Our estimate for the critical exponent is consistent with this, although there are large finite time corrections that make $R^2(t)$ grow even less fast than t for very long times, in particular for p below the transition. At the tricritical point, $R^2(t)$ is a power law with exponent 1.205(4).

Fig. 1, that show the survival probability $P(t)$ and the average squared radius $R^2(t)$ of newly infected sites, measured from the starting point of the epidemic. They show power-law behavior at the tricritical point (straight lines on log-log plots), with exponent values given in the main text.

A detailed comparison of our results with the field theoretic predictions of [30] will also be given in [52]. Here we just mention that our results for the critical exponents are qualitatively similar (the changes relative to the exponents for OP go in the right directions), but the agreement is far from perfect. The biggest disagreement is for η_s, defined via $n(t) \sim t^{\eta_s}$. While a positive value,

$$\eta_s = \left(\frac{1}{3} + \frac{4-\sqrt{3}}{\pi}\right)\frac{\epsilon}{45} + O(\epsilon^2), \tag{B1}$$

with $\epsilon = 5 - d = 2$, was predicted in [30], we found $\eta_s = -0.702(10)$.

APPENDIX C: THE STRAUSS MODEL

We start from Eqs. (5) and (6) of Ref. [39], which read in our notation,

$$p = \frac{1}{e^{\theta - Bq(1-2/N)} + 1}, \tag{C1}$$

and

$$q = \frac{1 + (e^{B/N} - 1)p}{(e^{\theta - Bq(1-3/N)} + 1)^2 + (e^{B/N} - 1)p}. \tag{C2}$$

Here p is the link density and q is defined in [39]. In the limit $N \to \infty$ and $B,\theta \ll N$ of interest to us, these simplify to

$$p = \frac{1}{e^{\theta - Bq} + 1}, \tag{C3}$$

and

$$q = \frac{1}{(e^{\theta - Bq} + 1)^2} = p^2. \tag{C4}$$

Combining these gives an equation for p in terms of B and θ which we can write as

$$F(p) \equiv e^{\theta - Bp^2} + 1 - \frac{1}{p} = 0. \tag{C5}$$

This equation can have four outcomes (see Fig. 7):

(a) one simple solution, corresponding to one single phase [i.e., no phase coexistence; Fig. 7(a)];

(b) three different solutions (two stable + one unstable), corresponding to phase coexistence [Fig. 7(b)];

(c) one single plus one doubly degenerate solution, corresponding to the boundaries of the coexistence region [Figs. 7(c1) and 7(c2)]; and

(d) one triply degenerate solution, corresponding to the critical point [Fig. 7(d)].

The critical point is thus obtained from $F(p) = F'(p) = F''(p) = 0$, leading to the values quoted in the main text.

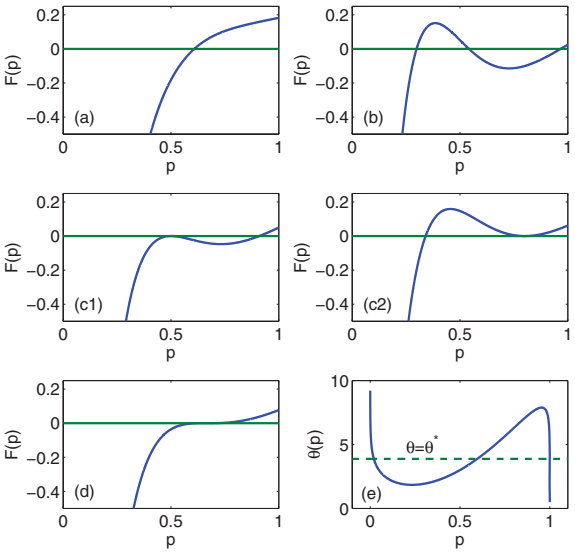

FIG. 7. (Color online) Panels (a)–(d) illustrate the cases (a)–(d) for the possible solutions of $F(p) = 0$. Panel (e) illustrates the Maxwell construction. The function $\theta(p)$ is given by Eq. (C8), and the dashed horizontal line is placed such that the two areas between it and the curve $\theta = \theta(p)$ are equal.

The boundaries of the bistable region are given parametrically by

$$B = \frac{1}{2(1-p)p^2}, \quad \theta = \ln(1/p - 1) + \frac{1}{2(1-p)}, \tag{C6}$$

which give asymptotically for large θ,

$$B_-(\theta) \approx \theta\ , \quad B_+ \approx \exp(2\theta), \tag{C7}$$

for the lower (upper) boundaries in a plot of B versus θ (see Fig. 2 of [39]).

The actual transition curve $B^*(\theta)$, or rather $\theta^*(B)$, is obtained from a Maxwell construction: For some given value of $B > B_c^*$, we first obtain θ as a function of p from Eq. (C5),

$$\theta(p) = Bp^2 + \ln(1/p - 1). \tag{C8}$$

For any θ_0 in the coexistence region, the equation $\theta(p) = \theta_0$ has three roots $p_1 < p_2 < p_3$. The transition point $\theta^*(B)$ is then given by

$$\int_{p_1}^{p_3} dp\ [\theta(p) - \theta^*(B)] = 0. \tag{C9}$$

For large B, the curve of $\theta(p)$ versus p tends (except near the points $p = 0$ and $p = 1$) to a parabola, which gives in this limit $\theta^*(B) \approx B/3$ as stated in the main text.

[1] D. Stauffer and A. Aharony, *Introduction to Percolation Theory* (Taylor & Francis, London, 1994).

[2] D. Achlioptas, R. M. D'Souza, and J. Spencer, Science **323**, 1453 (2009).

[3] R. A. da Costa, S. N. Dorogovtsev, A. V. Goltsev, and J. F. F. Mendes, Phys. Rev. Lett. **105**, 255701 (2010).

[4] O. Riordan and L. Warnke, Science **333**, 322 (2011).

[5] P. Grassberger, C. Christensen, G. Bizhani, S.-W. Son, and M. Paczuski, Phys. Rev. Lett. **106**, 225701 (2011).

[6] H. K. Lee, B. J. Kim, and H. Park, arXiv:1103.4439 (2011).

[7] A. Vespignani, Nature (London) **464**, 15 (2010).

[8] E. J. Friedman and A. S. Landsberg, Phys. Rev. Lett. **103**, 255701 (2009).

[9] R. M. Ziff, Phys. Rev. Lett. **103**, 045701 (2009).

[10] R. M. Ziff, Phys. Rev. E **82**, 051105 (2010).

[11] F. Radicchi and S. Fortunato, Phys. Rev. Lett. **103**, 168701 (2009).

[12] F. Radicchi and S. Fortunato, Phys. Rev. E **81**, 036110 (2010).

[13] R. M. D'Souza and M. Mitzenmacher, Phys. Rev. Lett. **104**, 195702 (2010).

[14] H. D. Rozenfeld, L. K. Gallos, and H. A. Makse, Eur. Phys. J. B **75**, 305 (2010).

[15] S. S. Manna and A. Chatterjee, Physica A **390**, 177 (2009).

[16] A. A. Moreira, E. A. Oliveira, S. D. S. Reis, H. J. Herrmann, and J. S. Andrade Jr., Phys. Rev. E **81**, 040101 (2010).

[17] N. A. M. Araújo and H. J. Herrmann, Phys. Rev. Lett. **105**, 035701 (2010).

[18] W. Chen and R. M. D'Souza, Phys. Rev. Lett. **106**, 115701 (2011).

[19] Y. S. Cho, B. Kahng, and D. Kim, Phys. Rev. E **81**, 030103 (2010).

[20] Y. S. Cho, J. S. Kim, J. Park, B. Kahng, and D. Kim, Phys. Rev. Lett. **103**, 135702 (2009).

[21] Y. S. Cho, S.-W. Kim, J. D. Noh, B. Kahng, and D. Kim, Phys. Rev. E **82**, 042102 (2010).

[22] L. Tian and D.-N. Shi, Phys. Lett. A **376**, 286 (2012).

[23] J. Nagler, A. Levina, and M. Timme, Nature **7**, 265 (2011).

[24] H. Hooyberghs and B. Van Schaeybroeck, Phys. Rev. E **83**, 032101 (2011).

[25] S. V. Buldyrev, R. Parshani, G. Paul, H. E. Stanley, and S. Havlin, Nature (London) **464**, 1025 (2010).

[26] R. Parshani, S. V. Buldyrev, and S. Havlin, Phys. Rev. Lett. **105**, 048701 (2010).

[27] S.-W. Son, G. Bizhani, C. Christensen, P. Grassberger, and M. Paczuski, Europhys. Lett. **97**, 16006 (2012).

[28] S. Boettcher, V. Singh, and R. M. Ziff, Nat. Comm. **3**, 787 (2012).

[29] T. Ohtsuki and T. Keyes, Phys. Rev. A **36**, 4434 (1987).

[30] H.-K. Janssen, M. Müller, and O. Stenull, Phys. Rev. E **70**, 026114 (2004).

[31] Janssen *et al*. called this the generalized general epidemic process (GGEP), in order to distinguish it from the general epidemic process [D. Mollison, J. Royal Statist. Soc. B **39**, 283 (1977)]. The latter is now usually called a susceptible-infected-removed (SIR) epidemic, while a "simple epidemic" in the notation of Mollison is now called SIS. We feel thus free to use the simpler acronym GEP for the generalized process.

[32] M. Cieplak and M. O. Robbins, Phys. Rev. Lett. **60**, 2042 (1988); N. Martys, M. Cieplak, and M. O. Robbins, *ibid*. **66**, 1058 (1991); N. Martys, M. O. Robbins, and M. Cieplak, Phys. Rev. B **44**, 12294 (1991); H. Ji and M. O. Robbins, *ibid*. **46**, 14519 (1992); C. S. Nolle, B. Koiller, N. Martys, and M. O. Robbins, Phys. Rev. Lett. **71**, 2074 (1993).

[33] B. Drossel and K. Dahmen, Euro. Phys. J. B **3**, 485 (1998).

[34] Note that the co-appearance of first-order bulk transitions with continuous surface transitions was discussed already in [69].

[35] D. J. Watts, PNAS **99**, 5766 (2002).

[36] P. S. Dodds and D. J. Watts, Phys. Rev. Lett. **92**, 218701 (2004).

[37] P. S. Dodds and D. J. Watts, J. Theor. Biol. **232**, 587 (2005).

[38] D. Strauss, SIAM Rev. **28**, 513 (1986).

[39] J. Park and M. E. J. Newman, Phys. Rev. E **70**, 026136 (2005).

[40] J. Park and M. E. J. Newman, Phys. Rev. E **70**, 066146 (2004).

[41] B. Bollobás, *Random Graphs* (Cambridge University Press, Cambridge, 1985).

[42] G. J. Baxter, S. N. Dorogovtsev, A. V. Goltsev, and J. F. F. Mendes, Phys. Rev. E **83**, 051134 (2011).

[43] F. J. Pérez-Reche, J. J. Ludlam, S. N. Taraskin, and C. A. Gilligan, Phys. Rev. Lett. **106**, 218701 (2011).

[44] Strictly spoken this is only true for static (i.e., percolation in the narrow sense) aspects at threshold. Dynamics and the behavior above the threshold are different in both models, since the memory about previous contacts with infected neighbors is short lived in [36,37], while it is long lived (previous attacks are never forgotten) in the model of [30] and in the simulations reported in the next subsection.

[45] L. Roters, A. Hucht, S. Lübeck, U. Nowak, and K. D. Usadel, Phys. Rev. E **60**, 5202 (1999).

[46] B. Koiller and M. O. Robbins, Phys. Rev. B **62**, 5771 (2000).

[47] B. Koiller and M. O. Robbins, Phys. Rev. B **82**, 064202 (2010).

[48] If the distribution of local fields in the random field Ising model is called $P(h)$, the spin-spin coupling is J, and z is the coordination number, then $q_n = \int_{-\infty}^{(2n-z)J} P(h)dh$.

[49] H. Leschhorn, T. Nattermann, S. Stepanow, and L.-H. Tang, Ann. Physik (Leipzig) **6**, 1 (1997).

[50] P. Le Doussal, K. J. Wiese, and P. Chauve, Phys. Rev. B **66**, 174201 (2002).

[51] A. Rosso, A. K. Hartmann, and W. Krauth, Phys. Rev. E **67**, 021602 (2003).

[52] P. Grassberger *et al*. (unpublished).

[53] J. Adler, Physica A **171**, 453 (1991).

[54] Bootstrap percolation on a lattice with coordination number z and with m wetted neighbors needed for support can be mapped onto a GEP with $p_k = \delta_{k,z-m}$, as seen by interchanging wetted and nonwetted sites. Notice that the same interchange was also made in [42], which is the reason why bootstrap percolation is called there an activation and not a pruning process. For completeness we point out that also heterogeneous bootstrap percolation [42] can be mapped onto GEP. The case illustrated in Fig. 1 of [42], for example, corresponds to $p_k = (1-f)\delta_{k,0} + f\delta_{k,2}$.

[55] H.-K. Janssen, J. Phys.: Condens. Matter **17**, S1973 (2005).

[56] S. Lübeck, J. Stat. Phys. **123**, 193 (2006).

[57] P. Grassberger, J. Stat. Mech. (2006) P01004.

[58] P. W. Holland and S. Leinhard, JASA **76**, 373 (1981).

[59] J. Park and M. E. J. Newman, Phys. Rev. E **70**, 066117 (2004).
[60] G. Robins, P. Pattison, Y. Kalish, and D. Lusher, Social Networks **29**, 173 (2007).
[61] S. Chatterjee and P. Diaconis, arXiv:1102.2650 (2011).
[62] J. Berg and M. Lässig, Phys. Rev. Lett. **89**, 228701 (2002).
[63] G. Bizhani *et al*. (unpublished).
[64] J. Park and S.-H. Yook, J. Stat. Mech. (2011) P08008.
[65] D. Foster, J. Foster, M. Paczuski, and P. Grassberger, Phys. Rev. E **81**, 046115 (2010).
[66] M. E. J. Newman, S. H. Strogatz, and D. J. Watts, Phys. Rev. E **64**, 026118 (2001).
[67] M. E. J. Newman, Phys. Rev. Lett. **95**, 108701 (2005).
[68] P. Grassberger, Comp. Phys. Commun. **147**, 64 (2002).
[69] R. Lipowsky, Phys. Rev. Lett. **49**, 1575 (1982).

Chapter 5

Conclusions

Complexity is usually tied to emergent behavior –features of the system that are not easily predictable by knowing the detailed mechanisms and interactions of the microscopic components. The science of complexity provides methods and models that help us to describe some of these features, without having to consider all the details of the system. Modeling systems as networks is one of these methods which simplifies systems into agents and interactions.

The science of networks which has applications in diverse disciplines from arts and humanities to life sciences, is aimed at establishing generic methods and procedures to analyze and understand complex networks in all disciplines and to serve as a bridge between our perception of complexity in different fields of study. It tries to find and understand the common characteristics of the underlying graphs in which complex systems are embedded. Some of these common features that have been discovered in the past couple of decades are broad degree distributions, the small-world property and robustness of connectivity.

In many complex networks the connectivity of the underlying graph highly affects the function, and understanding connectivity transitions in networks is an important part of prediction and controlling of many complex systems. This thesis is devoted to the study of connectivity transitions in complex networks via several percolation models. Percolation is a well developed concept in statistical physics that deals with connected clusters in graphs as links or nodes are inserted or removed. It has been applied to models on both lattices and networks. Yet the local mechanisms that lead to global connectivity in many complex systems are more complicated than the mechanisms suggested by classical percolation. Our main aim was to study variants of percolation that incorporate such features to get a more realistic picture of connectivity transitions in complex networks.

5.1 Summary

In the first part of this thesis, we developed agglomerative percolation (AP) which should apply naturally to systems where smaller parts aggregate to form larger clusters. For example groups of people join together to form communities, which then join to make larger and more complicated social structures, villages merge to make small towns which then turn into larger cities, and countries, and at the microscopic level, atoms and molecules coagulate to make larger structures of matter. In all these problems AP and its variations can serve as a model for understanding the aggregation process. In AP, in every time step a random cluster amalgamates to all its neighbors to make a larger cluster. We showed that this process leads to a continuous percolation transition, which is in many cases in a different universality class than ordinary percolation. We examined AP transitions in detail on several network models and regular lattices of different dimensions. This type of percolation is mapped to random sequential renormalization (RSR), a method that we suggested to study the renormalization group flow of networks. Compared to previous methods of renormalization for networks, RSR is computationally faster, much easier to implement, and easier to interpret. It provides a more fine-grained picture of the renormalization group flow and can capture features that were invisible to the (quasi)parallel renormalization schemes. Our results suggest that at least some of the scaling observed in previous works on self-similarity of networks is due to the AP transition rather than the fractality of the underlying graph.

The aggregation process of AP can be adapted to achieve more realistic models of cluster growth. One of the directions that one might take is to add stochasticity to the amalgamation process, namely by amalgamating the target cluster to only a fraction of its neighbors, or by assigning a probability for each invasion to succeed. Equivalently in the RSR picture, having such probabilistic coarse graining can delay the phase transition, which is particularly important in the renormalization studies of networks with broad degree distributions. In these networks the AP transition happens at the very beginning of the renormalization flow,

and causes some technical difficulties in performing finite size scaling analysis and obtaining the critical exponents from numerical simulations of finite systems. Another step to make AP more realistic is to consider other time embeddings leading to Poissonian statistics for the agglomeration events, similar to stochastic coagulation processes.

One of the main applications of percolation is in the study of epidemics and social dynamics, and correspondingly much of the studies of percolation is based on epidemic processes, where infections (or opinion spreadings) are local events and take place independent of each other. This is usually not the case in real-world systems where cooperativity plays an important role in the process of spreading. In the second part of this thesis, we studied percolation models in which the minimal assumptions of classical percolation are softened, namely explosive percolation, percolation on interdependent networks, generalizaed epidemic processes, and cooperative percolation in Hamiltonian graphs.

In explosive percolation (EP) the growth process is altered in order to delay the emergence of the percolating cluster. In every step of EP, among two candidate links one of them is chosen according to some rule which is defined to avoid the percolation transition. This modification not only delays the transition, but makes it also much sharper. We showed that in contrary to previous claims, percolation is still continuous, but exhibits unusual finite size scaling behavior.

In interdependent networks, each node has to cooperate with its corresponding nodes in the other networks in order to be a part of the epidemics or the percolating cluster. We showed that depending on the strength of this cooperation the percolation transition can switch from continuous to discontinuous. The problem of connectivity in interdependent networks is of extreme applicational interest. In infrastructural networks of power and water distribution, transportation, networks of financial institutions and global commerce, interdependencies influence the vulnerability and have to be considered in risk assessment and stability measures. We showed that the cascading events that lead to catastrophic

failures in interdependent networks, can be simplified by adapting the usual consistency equation approach in the study of epidemic spreading. We developed a general formalism for percolation in interdependent networks and solved it analytically for the Erdös Rényi model. We showed that depending on the fraction of interdependent nodes the percolation transition can switch to discontinuous. Examining the epidemics on other interdependent network models that are more applicable to real-world systems, can help to understand and regulate connectivity transitions in such systems. A further step to expand our work, is to develop models for network growth that incorporate interdependency. One way of doing so is to upgrade the current models of network growth by adding pairs of interdependent nodes instead of single ones.

In generalized epidemic processes (GEP), cooperativity is implemented by making the infection probability dependent on the number of previous attacks. On random networks, we mapped GEP to the Dodds and Watts model of complex contagion, and derived the exact solution in an easy way. On lattices, GEP is mapped to compact or fractal cluster growth in random media at zero temperature. This allows the detailed study of the depinning transition in disordered media. Our results suggest that overhangs are not negligible for pinned rough two-dimensional surfaces in three dimensions, and in fact existing theories based on single-valued height function might be irrelevant to cluster growth in isotropic media. More work needs to be done to obtain detailed conclusions in this regard. GEP has several applications in the context of cooperative phenomena in networks. Some of the problems we suggest include the study of synergy in various systems, opinion dynamics and consensus formation, and synchronicity.

Cooperativity can also be studied in equilibrium systems with finite "temperature". One such application is studied in Hamiltonian graph models, which are of long standing application in social sciences. In these models the probability distribution of a canonical ensemble of graphs is determined by a "Hamiltonian" with cooperative terms which might include the

number of two-stars (the two-star model) or triangles (the Strauss model). We showed that here as well, cooperative terms can change the transition from continuous to discontinuous. But both the two-star and the Strauss model lead to unrealistic states that do not represent any social systems. One way to generalize Hamiltonian graph models is to apply them to spatially embedded networks rather than the mean-field approach. This is more similar to social systems where spatial compartmentalization is known to be one of their main features. Another approach to obtain better models is to consider different constraints such as fixing the number of links in the network and to combine the Hamiltonians of the Strauss and the two-star models.

5.2 Applications and Outlook

A variety of real-world systems — both natural and artificial — such as human societies, infrastructural systems, networks of protein interactions in cells, and many others, are comprised of a complicated network of interwoven connections and/or interactions, that determines the characteristics and qualities of these systems. The numerosity of components and the complexity of these relations make it almost impossible to understand and predict the behavior of such systems. The science of networks helps us to get a simplified yet informative picture of complex systems using the language and methods of graph theory, statistical physics, information theory and computer science along with our knowledge on the specific system under study. Using this picture we can investigate processes and characteristics that otherwise seem to be too involved and even unpredictable.

One of these characteristics is large-scale connectivity or possibility of epidemic spreads. This can be observed in several systems and its understanding and prediction is one of the challenges of researches across various fields. Examples range from disease spreading and epidemiology to innovation diffusion and rumor (or fad) spread in social systems to cascades of failures in networks of financial institutions or large infrastructural systems.

The study of the emergence (or similarly sudden failure) of macroscopic connectivity as a result of microscopic connections (or disconnections) is the main focus of percolation theory in statistical physics.

This thesis was mainly focused on the theoretical analysis of new percolation models and suggested possible applications of them in the study of real-world complex systems. Percolation is well-studied in the past few decades, but what is less discussed is that the details of the microscopic processes that lead to macroscopic outcomes in real-world systems is more intricate, and the minimal assumptions of classical theory of percolation do not capture some of the fundamental characteristics of the system and may lead to inaccurate predictions. Cooperative behavior, inevitable and increasing interdependency between various networks in the modern world, entanglements and correlations of events that are happening at distant times and locations, are very important factors that can change the outcomes of our models drastically, and should be taken into account.

Cooperativity, agglomeration, and other concepts discussed in this thesis, depending on the context, can be translated into relevant features of the complex phenomena under investigations, and can serve as a basis for modeling. Our results on new percolation models can provide a new insight on the study of models of disease spreading (section 2.2.7) or social dynamics (sections 4.3 and 4.4) or stability of infrastructures (section 4.2), and give results that are closer to reality. Our exact solution for the problem of aggregation (section 3.2.4) can be used in the study of cluster growth with applications in chemistry, environmental and weather studies, and even star formation and cosmology. Finally our method of random sequential renormalization can serve as a theoretical tool for studying the fundamental properties and similarities of various systems.

As all theories in physics, the results of our models need to be checked against empirical data. Fortunately our growing computational power in the twenty first century has made it easy to glean and analyze large data sets of real networks. It remains for others to expand and employ our results based on the insight that the behavior of real-world complex systems provide.

Bibliography

[Achlioptas 09] D. Achlioptas, R. D'Souza & J Spencer. *Explosive percolation in random networks.* Science, vol. 323, pp. 1453–1455, 2009.

[Amit 05] D. J. Amit. Field Theory, the Renormalization Group, and Critical Phenomena. World Scientific, 2nd edition, 2005.

[Azar 99] Y. Azar, A. Z. Broder, A. R. Karlin & E. Upfal. *Balanced allocations.* SIAM J. Comput., vol. 29, pp. 180–200, 1999.

[Bader 03] G. D. Bader & C. Hogue. *An automated method for finding molecular complexes in large protein interaction networks.* BMC Bioinformatics 4 (1): 2, vol. 4, 2, 2003.

[Balthrop 04] Justin Balthrop, Stephanie Forrest, M. E. J. Newman & Matthew M. Williamson. *Technological networks and the spread of computer viruses.* Science, vol. 304, pp. 527–529, 2004.

[Barabasi 95] A.-L. Barabasi & H. E. Stanley. Fractal concepts in surface growth. Cambridge University Press, 1995.

[Barabási 99] A.-L. Barabási & R. Albert. *Emergence of scaling in random networks.* Science, vol. 286, pp. 509–512, 1999.

[Baxter 10] G. J. Baxter, S. N. Dorogovtsev, A. V. Goltsev & J. F. F. Mendes. *Bootstrap percolation on complex networks.* Phys. Rev. E, vol. 82, 011103, 2010.

[Baxter 11] G. J. Baxter, S. N. Dorogovtsev, A. V. Goltsev & J. F. F. Mendes. *Heterogeneous k-core versus bootstrap percolation on complex networks.* Phys. Rev. E, vol. 83, 051134, 2011.

[Bellac 92] Michel Le Bellac. Quantum and statistical field theory. Oxford University Press, 1992.

[Bizhani 11a] G. Bizhani, P. Grassberger & M. Paczuski. *Random sequential renormalization and agglomerative percolation in networks: Application to Erdos-Renyi and scale-free graphs.* Phys. Rev. E, vol. 84, 066111, 2011.

[Bizhani 11b] G. Bizhani, V. Sood, M. Paczuski & P. Grassberger. *Random sequential renormalization of networks: Application to critical trees.* Phys. Rev. E, vol. 83, 036110, 2011.

[Bizhani 12] G. Bizhani, M. Paczuski & P. Grassberger. *Discontinuous percolation transitions in epidemic processes, surface depining in random media and Hamiltonian random graphs.* Phys. Rev. E, vol. 86, 011128, 2012.

[Boettcher 09] Stefan Boettcher & Jessica L. Cook. *Patchy percolation on a hierarchical network with small-world bonds.* Phys. Rev. E, vol. 80, 041115, 2009.

[Boettcher 12] Stefan Boettcher, Vijay Singh & Robert M. Ziff. *Ordinary percolation with discontinuous transitions.* Nat. Commun., vol. 3, 787, 2012.

[Bogná 09] Marián Bogná, Dmitri Krioukov & K. C. Claffy. *Navigability of complex networks.* Nat. Phys., vol. 5, pp. 74–80, 2009.

[Brauer 10] Fred Brauer & Carlos Castillo-Chvez. Mathematical models in population biology and epidemiology. Springer, 2010.

[Brummitta 12] Charles D. Brummitta, Raissa M. D'Souza & E. A. Leicht. *Suppressing cascades of load in interdependent networks.* Proc. Natl. Acad. Sci., vol. 109, pp. 680–689, 2012.

[Buldyrev 10a] S. V. Buldyrev, R. Parshani, G. Paul, H. E. Stanley & S. Havlin. *Catastrophic cascade of failures in interdependent networks.* Nature, vol. 464, pp. 1025–1028, 2010.

[Buldyrev 10b] S. V. Buldyrev, R. Parshani, G. Paul, H. E. Stanley & Shlomo Havlin. *Catastrophic cascade of failures in interdependent networks.* Nature, vol. 464, pp. 1025–1028, 2010.

[Callaway 00] D. S. Callaway, M. E. J. Newman, S. H. Strogatz & D. J. Watts. *Network robustness and fragility: Percolation on random graphs.* Phys. Rev. Lett., vol. 85, pp. 5468–5471, 2000.

[Callaway 01] Duncan S. Callaway, John E. Hopcroft, Jon M. Kleinberg, M. E. J. Newman & Steven H. Strogatz. *Are randomly grown graphs really random?* Phys. Rev. E, vol. 64, 041902, 2001.

[Cardy 85] J L Cardy & P Grassberger. *Epidemic models and percolation.* J. Phys. A: Math. Gen., vol. 18, L262, 1985.

[Christensen 05] K. Christensen & N. R. Moloney. Complexity and Criticality. Imperial College Press, 2005.

[Christensen 12] C. Christensen, G. Bizhani, S-W. Son, M. Paczuski & P. Grassberger. *Agglomerative percolation in two dimensions.* Europhys. Lett., vol. 97, 16004, 2012.

[Clauset 09] A. Clauset, C. R. Shalizi & M. E. J. Newman. *Power-law distributions in empirical data.* SIAM Rev., vol. 51, pp. 661–703, 2009.

[Cohen 10] Reuven Cohen & Shlomo Havlin. Complex networks: Structure, robustness and function. Cambridge University Press, 2010.

[Csermely 09] Peter Csermely. Weak links: The universal key to the stability of networks and complex systems. Springer, 2009.

[da Costa 10] R. A. da Costa, S. N. Dogorovtsev, A. V. Goltsev & J. F. F. Mendes. *Explosive percolation Transition is actually continuous.* Phys. Rev. Lett., vol. 105, 255701, 2010.

[Daley 99] D. J. Daley & J. Gani. Epidemic modelling: An introduction. Cambridge University Press, 1999.

[Derenyi 04] I. Derenyi, I. Farkas, G. Palla & T. Vicsek. *Topological phase transitions of random networks.* Physica A, vol. 334, pp. 583–590, 2004.

[Desiderio 09] A. Desiderio & F. Maronta. *Internet and the mediterranean bottleneck.* Heartland, Eurasian Review of Geopolitics, http://temi.repubblica.it/limes–heartland/internet–and–the–mediterranean–bottleneck/1425, 2009.

[Dodds 04] P. S. Dodds & D. J. Watts. *Universal behavior in a generalized model of contagion.* Phys. Rev. Lett., vol. 92, 218701, 2004.

[Dodds 05] P. S. Dodds & D. J. Watts. *A generalized model of social and biological contagion.* J. Theor. Biol., vol. 232, pp. 587–604, 2005.

[Drossel 92] B. Drossel & F. Schwabl. *Self-organized critical forest-fire model.* Phys. Rev. Lett., vol. 69, pp. 1629–1632, 1992.

[D'Souza 07] R. M. D'Souza, P. L. Krapivsky & C. Moore. *The power of choice in growing trees.* Eur. Phys. J. B, vol. 59, pp. 535–543, 2007.

[D'Souza 10a] R. M. D'Souza & M. Mitzenmacher. *Local cluster aggregation models of explosive percolation.* Phys. Rev. Lett., vol. 104, 195702, 2010.

[D'Souza 10b] Raissa M. D'Souza & Michael Mitzenmacher. *Local cluster aggregation models of explosive percolation.* Phys. Rev. Lett., vol. 104, 195702, 2010.

[Erdös 59] P. Erdös & A. Rényi. *On random graphs.* Publicationes Mathematicae, vol. 6, pp. 290–297, 1959.

[Erdös 60] P. Erdös & A. Rényi. *On the evolution of random graphs.* Publ. Math. Inst. Hung. Acad. Sci, vol. 5, pp. 17–61, 1960.

[Erdös 61] P. Erdös & A. Rényi. *On the strength of connectedness of a random graph.* Acta. Math. Hung., vol. 12, pp. 261–267, 1961.

[Falconer 03] K. J. Falconer. Fractal geometry: Mathematical foundations and applications. Cambridge Univ. Press, 2nd edition, 2003.

[Gastner 06] M.T. Gastner & M.E.J. Newman. *The spatial structure of networks.* Eur. Phys. J. B, vol. 49, pp. 247–252, 2006.

[Goh 06] K.-I. Goh, G. Salvi, B. Kahng & D. Kim. *Skeleton and fractal scaling in complex networks.* Phys. Rev. Lett., vol. 96, 018701, 2006.

[Goltsev 06] A. V. Goltsev, S. N. Dorogovtsev & J. F. F. Mendes. *k-core (bootstrap) percolation on complex networks: Critical phenomena and nonlocal effects.* Phys. Rev. E, vol. 73, 056101, 2006.

[Grassberger 83] P. Grassberger. *On the critical behavior of the general epidemic process and dynamical percolation.* Math. Biosci., vol. 63, pp. 157–172, 1983.

[Grassberger 11] P. Grassberger, C. Christensen, G. Bizhani, S-W. Son & M. Paczuski. *Explosive percolation is continuous, but with unusual finite size behavior.* Phys. Rev. Lett., vol. 106, 225701, 2011.

[Herbut 07] Igor Herbut. A modern approach to critical phenomena. Cambridge University Press, 2007.

[Holme 11] Petter Holme & Jari Saramki. *Temporal networks.* arXiv:1108.1780v2 [nlin.AO], 2011.

[Kardar 07] Mehran Kardar. Statistical physics of fields. Cambridge University Press, 2007.

[Kim 07a] J. S. Kim, K. I. Goh, B. Kahng & D. Kim. *A box-covering algorithm for fractal scaling in scale-free networks.* Chaos, vol. 17, 026116, 2007.

[Kim 07b] J. S. Kim, K. I. Goh, B. Kahng & D. Kim. *Fractality and self-similarity in scale-free networks.* New J. Phys., vol. 9, 177, 2007.

[Kim 07c] J. S. Kim, K. I. Goh, G. Salvi, E. Oh, B. Kahng & D. Kim. *Fractality in complex networks: Critical and supercritical skeletons.* Phys. Rev. E, vol. 75, 016110, 2007.

[King 01] P. R. King, S.V. Buldyrev, N. V. Dokholyan, S. Havlin, Y. Lee, G. Paul, H. E. Stanley & N. V. Vandesteeg. *predicting oil recovery using percolation theory.* Petrol. Geosci., vol. 7, pp. S105–S107, 2001.

[King 02] P. R. King, S. V. Buldyrev, N. V. Dokholyan, S. Havlin, E. Lopez, G. Paul & H. E. Stanley. *Using percolation theory to predict oil field performance.* Physica A, vol. 314, pp. 103–108, 2002.

[Krapivski 91] P. L. Krapivski. *Aggregation processes with n-particle elementary reactions.* Phys. A: Math. Gen., vol. 24, pp. 4697–4703, 1991.

[Lau 12] H-W Lau, M. Paczuski & P. Grassberger. *Agglomerative percolation on bipartite networks: Nonuniversal behavior due to spontaneous symmetry*

breaking at the percolation threshold. Phys. Rev. E, vol. 86, 011118, 2012.

[Leicht 09] E. A. Leicht & Raissa M. D'Souza. *Percolation on interacting networks.* arXiv:0907.0894v1 [cond-mat.dis-nn], 2009.

[Leyvraz 03] F. Leyvraz. *Scaling theory and exactly solved models in the kinetics of irreversible aggregation.* Phys. Rep, vol. 383, pp. 95–212, 2003.

[Milgram 67] S. Milgram. *The small-world problem.* Psychol. Today, vol. 1, pp. 61–67, 1967.

[Motter 02] A. E. Motter & Y. C Lai. *Cascade-based attacks on complex networks.* Phys. Rev. E, vol. 66, 065102(R), 2002.

[Newman 00] M. E. J. Newman & R. M. Ziff. *Efficient Monte Carlo algorithm and high-precision results for percolation.* Phys. Rev. Lett., vol. 85, pp. 4104–4107, 2000.

[Newman 01a] M. E. J. Newman, S. H. Strogatz & D. J. Watts. *Random graphs with arbitrary degree distributions and their applications.* Phys. Rev. E, vol. 64, 026118, 2001.

[Newman 01b] M. E. J. Newman & R. M. Ziff. *Fast Monte Carlo algorithm for site or bond percolation.* Phys. Rev. E, vol. 64, 016706, 2001.

[Newman 02] M. E. J. Newman. *Spread of epidemic disease on networks.* Phys. Rev. E, vol. 66, 016128, 2002.

[Newman 10] M.E.J. Newman. Networks: An introduction. Oxford University Press, 2010.

[Onnela 07] J.-P. Onnela, J. Saramki, J. Hyvnen, G. Szab, D. Lazer, K. Kaski, J. Kertsz & A.-L. Barabsi. *Structure and tie strengths in mobile communication networks.* Proc. Natl. Acad. Sci., vol. 104, pp. 7332–7336, 2007.

[Parshani 10] R. Parshani, S. V. Buldyrev & S. Havlin. *Interdependent networks: Reducing the coupling strength leads to a change from a first to second order percolation transition.* Phys. Rev. Lett., vol. 105, 048701, 2010.

[Parshani 11] R. Parshani, S. V. Buldyrev & S. Havlin. *Critical effect of dependency groups on the function of networks.* Proc. Nat. Acad. Sci., vol. 108, pp. 1007–1010, 2011.

[Pastor-Satorras 01] R. Pastor-Satorras & A. Vespignani. *Epidemic dynamics and endemic states in complex networks.* Phys. Rev. E, vol. 63, 066117, 2001.

[Price 76] D. Price. *A general theory of biometric and other cumulative advantage processes.* J. Amer. Soc. Inform. Sci, vol. 27, pp. 292–306, 1976.

[Radicchi 08] F. Radicchi, J. J. Ramasco, A. Barrat & S. Fortunato. *Complex networks renormalization: Flows and fixed points.* Phys. Rev. Lett, vol. 101, 148701, 2008.

[Radicchi 09] F. Radicchi, A. Barrat, S. Fortunato & J. J. Ramasco. *Renormalization flows in complex networks.* Phys. Rev. E, vol. 79, 026104, 2009.

[Robins 07] G. Robins, P. Pattison, Y. Kalish & D. Lusher. *An introduction to exponential random graph (p^*) models for social networks.* Soc. Networks, vol. 29, pp. 173–191, 2007.

[Rozenfeld 10] H. D. Rozenfeld, C. Song & H. A. Makse. *Small-world to fractal transition in complex networks: A renormalization group approach.* Phys.

Rev. Lett., vol. 104, 025701, 2010.

[Sattari 12] Arsalan Sattari, Maya Paczuski & Peter Grassberger. *Comment on "Dynamic opinion model and invasion percolation"*. Phys. Rev. Lett., vol. 109, 079801, 2012.

[Schneider 11] C. M. Schneider, N. A. M. Araujo, S. Havlin & H. J. Herrmann. *Towards designing robust coupled networks*. arXiv:1106.3234v1, 2011.

[Seidman 83] S. B. Seidman. *Network structure and minimum degree*. Soc. Networks, vol. 5, pp. 269–287, 1983.

[Shao 09] Jia Shao, Shlomo Havlin & H. Eugene Stanley. *Dynamic opinion model and invasion percolation*. Phys. Rev. Lett., vol. 103, 018701, 2009.

[Simon 55] H. A. Simon. *On a class of skew distribution functions*. Biometrika, vol. 42, pp. 425–440, 1955.

[Solomonoff 51] R. Solomonoff & A. Rapoport. *Connectivity of random nets*. B. Math. Biophys., vol. 13, pp. 107–117, 1951.

[Son 11a] S-W. Son, G. Bizhani, C. Christensen, P. Grassberger & M. Paczuski. *Irreversible aggregation and network renormalization*. Europhys. Lett., vol. 95, 58007, 2011.

[Son 11b] S-W. Son, C. Christensen, G. Bizhani, P. Grassberger & M. Paczuski. *Exact solutions for mass-dependent irreversible aggregations*. Phys. Rev. E, vol. 84, 040102(R), 2011.

[Son 11c] S-W. Son, P. Grassberger & Paczuski. M. *Percolation transitions are not always sharpened by making networks interdependent*. Phys. Rev. Lett., vol. 107, 195702, 2011.

[Son 12] S.-W. Son, G. Bizhani, C. Christensen, P. Grassberger & M. Paczuski. *Percolation theory on interdependent networks based on epidemic spreading.* Europhys. Lett., vol. 97, 16006, 2012.

[Song 05] C. Song, S. Havlin & H. A. Makse. *Self-similarity of complex networks.* Nature, vol. 433, pp. 392–395, 2005.

[Song 06a] C. Song, L. K. Gallos, S. Havlin & H. A. Makse. *How to calculate the fractal dimension of a complex network: the box covering algorithm.* J. Stat. Mech., P03006, 2006.

[Song 06b] C. Song, S. Havlin & H. A. Makse. *Origins of fractality in the growth of complex networks.* Nat. Phys., vol. 2, pp. 275–281, 2006.

[Stanley 71] H. E. Stanley. Introduction to phase transitions and critical phenomena. Oxford University Press, 1971.

[Stauffer 94] D. Stauffer & A. Aharony. Introduction to Percolation Theory. Taylor & Francis, 2nd edition, 1994.

[Strauss 86] D. Strauss. *On a general class of models for interaction.* SIAM Rev., vol. 28, pp. 513–527, 1986.

[Vespignani 10] A. Vespignani. *The fragility of interdependency.* Nature, vol. 464, pp. 984–985, 2010.

[Watts 98] D. J. Watts & S. H. Strogatz. *Collective dynamics of "small-world" network.* Nature, vol. 393, pp. 440–442, 1998.

[Watts 02] D. J. Watts. *A simple model of global cascades on random networks.* PNAS, vol. 99, pp. 5766–5771, 2002.

[Wilson 71a] K. G. Wilson. *Renormalization group and critical phenomena. I. Renormalization group and the Kadanoff scaling picture.* Phys. Rev. B, vol. 4, 3174, 1971.

[Wilson 71b] K. G. Wilson. *Renormalization group and critical phenomena. II. Phase-space cell analysis of critical behavior.* Phys. Rev. B, vol. 4, 3184, 1971.

[Yook 05] S-H. Yook, F. Radicchi & H. Meyer-Ortmanns. *Self-similar scale-free networks and disassortativity.* Phys. Rev. E, vol. 72, 045105(R), 2005.

[Zangwill 01] A. Zangwill. *Statistical physics: Advances in aggregation.* Nature, vol. 411, pp. 651–652, 2001.

[Zinck 10] Richard D. Zinck, Karin Johst & Volker Grimm. *Wildfire, landscape diversity and the Drossel-Schwabl model.* Ecol. Model., vol. 221, pp. 98–105, 2010.

[Zinn-Justin 02] J. Zinn-Justin. Quantum Field Theory and Critical Phenomena. Oxford Univ. Press, 4th edition, 2002.

Appendix A

On the Inclusion of Previously Published Works

As required by the Thesis Guidelines document of July 2012, this appendix details my contributions to the previously published works in this dissertation. A summary of these publications, their connection to each other as well as the title of my thesis is given in chapters 3 and 4. Both chapters 3 and 4 includes reprints of my publications in refereed journals.

In chapter 3, sections 3.3.1 and 3.3.2 are published in Physical Review E [Bizhani 11b], and [Bizhani 11a]. I was the first author and lead researcher in both. I wrote the simulation code, analyzed the data and produced all the figures, except for sections III.I and III.J of [Bizhani 11b]. I worked out the analytical calculations in collaboration with Maya Paczuski and wrote the first draft of the manuscripts. I had primary responsibility for most of the subsequent revisions.

Section 3.3.3 is published in Europhysics Letters [Son 11a], and section 3.3.4 was published in Physical Review E [Son 11b]. I was the second author in the first paper and the third author in the second one. My main contribution was in performing the analytical calculations and interpretation of results, specially their connection to network renormalization and agglomerative percolation. I also contributed in editing the manuscripts.

Section 3.3.5 is published Europhysics Letters [Christensen 12]. I was the second author in this work and contributed in performing the computer simulations, analyzing the data, editing the manuscript and giving scaling arguments. I had the main contribution in extracting transition properties of AP on triangular lattices from simulation data.

In chapter 4, section 4.5.1 is published in Physical Review Letters [Grassberger 11]. As the third author of this paper I contributed in the analysis and interpretation of the simula-

tion results and discussions on unusual finite size scaling properties of explosive percolation.

Section 4.5.2 is published in Europhysics Letters [Son 12]. I was the second author of this paper and had extensive contribution in the mathematical formulation of the problem and the analytical solutions provided in the paper. I wrote the first draft of the analytical part and contributed in revisions of the manuscript.

Section 4.5.3 is published in Physical Review E [Bizhani 12]. I wrote the computer code for simulating percolation on Hamiltonian random graphs, and analyzed the data. I performed the analytical calculations and analyzed the results of computer simulations with Peter Grassberger, and contributed in writing and revising the paper.

All of this research was done in the collaborative environment of the Complexity Science Group. Numerous group meetings, formal and informal discussions, and contribution of all authors made it possible to prepare the project for publication in its final format. I greatly appreciate and remain grateful to all my collaborators who made this happen.